

Expression and Function of ErbB4 Splice Variants in the Central Nervous System

Dissertation zur Erlangung des Doktorgrades (Dr. rer. nat.)
der Mathematischen-Naturwissenschaftlichen Fakultät
der Rheinischen Friedrich-Wilhelms-Universität Bonn

vorgelegt von

Larissa Erben

aus Sindelfingen

Bonn 2019

Angefertigt mit der Genehmigung der Mathematisch-Naturwissenschaftlichen Fakultät der Rheinischen Friedrich-Wilhelms-Universität Bonn.

Promotionskommission:

- Erstgutachter: Prof. Dr. Andreas Zimmer
(*Institut für Molekulare Psychiatrie, Universität Bonn*)
- Zweitgutachter: Prof. Dr. Michael Pankratz
(*Life & Medical Sciences Institute, Universität Bonn*)
- Fachnahes Mitglied: Dr. Andrés Buonanno
(*National Institute of Child Health and Human Development,
National Institutes of Health, Bethesda, MD*)
- Fachfremdes Mitglied: Prof. Dr. Barbara Kirchner
(*Institut für Physikalische und Theoretische Chemie, Universität Bonn*)

Tag der Promotion: 16. Juli 2019

Erscheinungsjahr: 2019

Abstract

Neuregulins and their cognate neuronal receptor tyrosine kinase ErbB4 (avian erythroblastosis virus oncogene B4) are genetically linked with an increased risk for schizophrenia. NRG/ErbB4 signaling regulates neurodevelopment, synaptic plasticity, network activity and modulates several neurotransmitter systems. Four ErbB4 isoforms are generated by alternative splicing in the juxtamembrane (JMa and JMb) and cytoplasmic region (Cyt-1 and Cyt-2). These isoforms mediate unique downstream signaling pathways exerting divergent biological functions. Although the expression of ErbB4 variants is altered in postmortem brains of schizophrenia patients, little is known about the distribution and functions of ErbB4 isoforms in the brain. This dissertation investigates the hypothesis that ErbB4 variants are differentially expressed in the central nervous system and uniquely contribute to ErbB4's role in the brain. Using next-generation sequencing, major and rare ErbB4 variants in the mouse brain are first identified. Then, to analyze splice variants at the cellular level, a novel ultrasensitive exon-specific *in situ* hybridization approach is implemented and validated, and quantitation tools developed. I extensively describe the mRNA distribution of the four major ErbB4 variants in the mouse brain, identify spatiotemporal- and cell type-specific expression, and expand these findings to the human brain. The examination of subcellular distribution of ErbB4 protein in distinct neuronal cell types reveals that in contrast to the somatodendritic restriction of ErbB4 in cultured gamma-aminobutyric acid (GABA)ergic interneurons, ErbB4 is present on axonal projections of dopaminergic neurons, independent of the isoform. Finally, we generated isoform-specific Cyt-1 mutant mice to explore *in vivo* functions of this ErbB4 variant. Although Cyt-1 variants comprise 40% of all ErbB4 transcripts in the brain, extensive molecular, transcriptomic, neurodevelopmental, neurochemical and behavioral evaluation show modest phenotypic effects, suggesting a possible compensation throughout development or redundant functions of Cyt isoforms. These findings advance our understanding of the basic biology of ErbB4 isoforms and their pathophysiological changes in schizophrenia.

Zusammenfassung

Neureguline und ihr neuronaler Tyrosinkinase-Rezeptor ErbB4 (*avian erythroblastosis virus oncogene B4*) sind genetisch mit einem erhöhtem Risiko für Schizophrenie assoziiert. NRG/ErbB4 Signalübertragung reguliert unter anderem die Neuronentwicklung, synaptische Plastizität, Netzwerkaktivität und moduliert verschiedene Neurotransmittersysteme. Vier ErbB4 Isoformen entstehen durch alternatives Spleißen in der juxtamembranen (JMa und JMb) und zytoplasmatischen Region (Cyt-1 und Cyt-2). Diese Isoformen vermitteln spezifische Signalwege und damit unterschiedliche biologische Funktionen. Obwohl die Expression von ErbB4-Spleißvarianten in postmortalen Gehirnen von Schizophrenie-Patienten verändert ist, ist wenig über ihre Verteilung oder Funktionen im Gehirn bekannt. Diese Dissertation untersucht die Hypothese, dass ErbB4-Spleißvarianten im zentralen Nervensystem differenziell exprimiert sind und auf spezifische Weise zu den bekannten ErbB4-Funktionen beitragen. Mit Sequenziermethoden der nächsten Generation werden zunächst Haupt- und seltene ErbB4-Spleißvarianten festgelegt. Um Spleißvarianten auf zellulärer Ebene zu analysieren, wird dann eine neue ultrasensitive und Exon-spezifische *in situ* Hybridisierungsmethode etabliert und validiert, sowie quantitative Hilfsmittel entwickelt. Ich beschreibe ausführlich die mRNA Verteilung der vier ErbB4 Hauptspleißvarianten im Mausgehirn, einschließlich ihrer neuroanatomischen, zeitlichen und Zelltyp-spezifischen Expression, und erweitere diese Erkenntnisse auf das menschliche Gehirn. Die Untersuchung der subzellulären Verteilung von ErbB4 Protein in verschiedenen neuronalen Zelltypen ergibt, dass ErbB4 im Gegensatz zur somatodendritischen Beschränkung in kultivierten gamma-Aminobuttersäure (GABA)ergen Interneuronen in axonalen Fortsätzen von dopaminergen Neuronen zu finden ist; unabhängig von der Isoform. Schließlich erzeugten wir eine Isoform-spezifische Cyt-1 Mauslinie, um die *in vivo* Funktion dieser ErbB4-Spleißvariante zu charakterisieren. Obwohl Cyt-1 Isoformen 40% aller ErbB4-Transkripte im Gehirn darstellen, offenbaren die umfangreichen molekularen, transkriptomischen, entwicklungsbiologischen, neurochemischen und Verhaltensstudien kaum Phänotypen, möglicherweise als Resultat kompensatorischer Prozesse während der Entwicklung oder Redundanz von Cyt Isoformen. Diese Erkenntnisse vertiefen unser biologisches Grundlagenverständnis von ErbB4 Isoformen und ihrer pathophysiologischen Veränderungen in Schizophrenie.

Table of contents

<i>Abstract</i>	<i>I</i>
<i>Zusammenfassung</i>	<i>III</i>
<i>Table of contents</i>	<i>V</i>
1 INTRODUCTION	1
<hr/>	
<i>1.1 The psychiatric disorder Schizophrenia</i>	<i>1</i>
1.1.1 Symptoms, etiology and treatment	1
1.1.2 Pathophysiology: glutamate, GABA and dopamine neurotransmission	2
1.1.3 Association of Neuregulin and ErbB4 variants with schizophrenia	3
<i>1.2 Neuregulin/ErbB4 signaling</i>	<i>4</i>
1.2.1 The Neuregulins and ErbB receptor family	4
1.2.2 Neuregulin/ErbB4 signaling pathways	6
<i>1.3 Neuregulin/ErbB4 signaling in the central nervous system</i>	<i>8</i>
1.3.1 Expression of ErbB4 in the brain	8
1.3.2 Regulation of neurodevelopment	9
1.3.3 Regulation of cortical and hippocampal circuits	13
1.3.4 Behavioral deficits of Neuregulin and ErbB4 mutant mice	19
1.3.5 Modulation of the dopamine system	21
<i>1.4 ErbB4 isoforms</i>	<i>22</i>
1.4.1 Alternative splicing of ErbB4	22
1.4.2 Functional differences between ErbB4 isoforms	23
1.4.3 Expression and role of ErbB4 isoforms in the central nervous system	25
<i>1.5 Aims and outline of the thesis</i>	<i>26</i>
2 CHARACTERIZATION OF ERBB4 SPLICE VARIANTS IN THE CENTRAL NERVOUS SYSTEM	29
<hr/>	
<i>2.1 Introduction</i>	<i>29</i>
<i>2.2 Methods</i>	<i>31</i>
<i>2.3 Results</i>	<i>34</i>
2.3.1 Alternative splicing of ErbB4 transcripts is confined to previously characterized splice sites	34
2.3.2 Detection of rare ErbB4 splice variants in the adult mouse brain	37
2.3.3 Ratios of juxtamembrane JM _a /JM _b and cytoplasmic Cyt-1/Cyt-2 variants	37
<i>2.4 Discussion</i>	<i>37</i>
3 AUTOMATED QUANTIFICATION OF MULTIPLEX AND EXON-SPECIFIC IN SITU HYBRIDIZATION SIGNALS	41
<hr/>	
<i>3.1 Abstract</i>	<i>41</i>
<i>3.2 Introduction</i>	<i>42</i>
<i>3.3 Strategic Planning: Probe Design</i>	<i>44</i>

3.4	<i>Basic Protocol 1: Multiplex Fluorescent In Situ Hybridization (RNAscope) using Fresh-Frozen Sections</i>	46
3.4.1	Alternate Protocol 1: Use of formalin-fixed paraffin-embedded sections	52
3.4.2	Alternate Protocol 2: <i>In situ</i> hybridization in cultured adherent cells	55
3.5	<i>Basic Protocol 2: Single-Pair Probe In Situ Hybridization</i>	57
3.6	<i>Basic Protocol 3: Post-hoc immunostainings</i>	66
3.7	<i>Basic Protocol 4: Automated Quantification of Fluorescent ISH Signal using CellProfiler</i>	70
3.8	<i>Reagents & Solutions</i>	75
3.9	<i>Commentary</i>	76
3.9.1	Background Information	76
3.9.2	Critical Parameters & Troubleshooting	77
3.9.3	Understanding Results & Statistical Analyses	78
3.9.4	Time Consideration	80
4	ERBB4 ISOFORM EXPRESSION IN THE MOUSE AND HUMAN BRAIN	83
4.1	<i>Abstract</i>	83
4.2	<i>Introduction</i>	84
4.3	<i>Materials and Methods</i>	86
4.4	<i>Results</i>	88
4.4.1	Sensitivity and specificity of the novel single-pair probe ISH approach	88
4.4.2	Semi-quantitative analysis of junction-specific single-pair probe ISH	89
4.4.3	Differential expression of ErbB4 isoforms in distinct regions of the adult brain	91
4.4.4	Expression of the cleavable JMa isoform in cells of the oligodendrocyte lineage	93
4.4.5	Conservation of differential ErbB4 isoform expression in human cortex and corpus callosum	95
4.5	<i>Discussion</i>	96
4.5.1	Differential and cell-type-specific expression of ErbB4 isoforms in the adult CNS	96
4.5.2	Alterations of ErbB4 isoform expression in Scz	97
4.5.3	General considerations for the broad application of the single-pair probe ISH approach	98
4.6	<i>Supplementary Materials</i>	100
5	SUBCELLULAR EXPRESSION OF ERBB4 & ITS ISOFORMS IN DISTINCT NEURONS	117
5.1	<i>Introduction</i>	117
5.2	<i>Methods</i>	119
5.3	<i>Results</i>	125
5.3.1	Axonal expression of ErbB4 in dopaminergic neurons	125
5.3.2	None of the ErbB4 isoforms targets to axons of GABAergic interneurons	128
5.4	<i>Discussion</i>	132
6	NEURODEVELOPMENTAL, NEUROCHEMICAL AND BEHAVIORAL ANALYSES OF ISOFORM-SPECIFIC ERBB4 CYT-1 MUTANT MICE	135
6.1	<i>Abstract</i>	135

6.2	<i>Introduction</i>	136
6.3	<i>Methods</i>	138
6.4	<i>Results</i>	146
6.4.1	Generation of Cyt-1 mutant mice	146
6.4.2	Cyt-1 is expressed in cortical and hippocampal GABAergic interneurons, but dispensable for GABAergic interneuron development	148
6.4.3	Cyt-1 mutant mice do not exhibit behavioral deficits	152
6.4.4	Cyt-1 expressed in dopaminergic neurons regulates extracellular dopamine levels	153
6.4.5	Cognitive function is normal in Cyt-1 mutant mice	155
6.4.6	Cyt-1 is enriched in the medial habenula, but does not regulate habenula-associated behaviors	157
6.4.7	Gene expression analysis reveals changes in transcription factors regulating development	158
6.5	<i>Discussion</i>	160
6.5.1	Mild phenotypes in heterozygote Cyt-1 mutant mice	161
6.5.2	Developmental loss of Cyt-1 may be compensated	162
6.5.3	ErbB4 splice variants in schizophrenia	163
7	DISCUSSION & FUTURE DIRECTIONS	165
7.1	<i>Expression and subcellular targeting of ErbB4 isoforms</i>	165
7.2	<i>ErbB4 isoform function in vivo</i>	170
8	APPENDIX	173
	<i>Acknowledgments</i>	173
	<i>Eidesstattliche Erklärung</i>	175
	<i>List of abbreviations</i>	176
	<i>List of figures</i>	179
	<i>List of tables</i>	181
	<i>Reprints and Permissions</i>	182
	<i>References</i>	184

1

Introduction

1.1 The psychiatric disorder Schizophrenia

1.1.1 Symptoms, etiology and treatment

Schizophrenia is a severe psychiatric disorder affecting about 0.5-1% of the population. Symptoms are chronic and can be subdivided into three groups: positive, negative and cognitive. Most commonly known positive symptoms involve a ‘false reality’ in patients’ mind and present as hallucinations, delusions, as well as thought and movement disorders. Negative symptoms are more difficult to diagnose but precede the first psychotic episode and include symptoms such as social withdrawal, apathy, anhedonia and emotional blunting. Cognitive deficits are the most incapacitating symptoms and demonstrate as defects in attention, concentration, working memory, organized speech and critical thinking¹⁻³. Endophenotypes characteristic to schizophrenia are also observed in non-affected relatives and include deficits in sensorimotor gating, working memory, executive cognition and defects in eye movements⁴.⁵ The heterogeneity of phenotypes and similarity to other psychiatric disorders make the diagnosis challenging^{6,7}.

Schizophrenia is largely genetically pre-dispositioned with an estimated heritability of ~80%⁸; however, only a few copy number variations, chromosomal rearrangements and high penetrance rare variants have been associated with the disorder³. The risk to develop schizophrenia generally arises from a combination and functional convergence of several low penetrance common variants⁹. Genome-wide association studies (GWAS) have identified more than 100 susceptibility genes¹⁰, yet most mutations are de-novo and non-coding³. Environmental factors explain the non-heritable component of the disease and have been

associated with stress during development such as maternal malnutrition, obstetric complications and infections^{8, 11}.

To date, schizophrenia is incurable and current antipsychotic drugs are limited to controlling symptoms and preserving functionality but are accompanied by serious side effects. Most antipsychotic drugs target the dopamine system, typical antipsychotics are dopamine receptor D2 (D2DR) antagonists, whereas atypical antipsychotics also block the serotonin receptor 2A with lower incidence of extrapyramidal side effects. Clozapine is the most efficacious second-generation atypical antipsychotic; however, its use is limited due to the high risk of agranulocytosis. Therefore, other atypical antipsychotics, such as risperidone, are recommended as first-line monotherapy. Unfortunately, only a fraction of patients report favorable treatment outcomes and complete remission of their positive symptoms, while others respond poorly and continue to experience psychotic episodes and chronic symptoms – particularly treatment-resistant negative and cognitive symptoms¹²⁻¹⁴.

1.1.2 Pathophysiology: glutamate, GABA and dopamine neurotransmission

Schizophrenia is considered a neurodevelopmental disorder caused by developmental alterations that precede the onset of psychotic symptoms in the second decade of life. These developmental neurobiological deficits include abnormal neuronal migration, excessive synapse pruning, altered maturation of neuronal processes and reduced myelination¹¹. Additionally, prominent neurochemical alterations have been characterized such as changes of the neurotransmitters glutamate, gamma-aminobutyric acid (GABA) and dopamine, and are strongly implicated with the pathophysiology of schizophrenia¹⁵⁻²¹.

The glutamate hypofunction theory of schizophrenia emerged after the two non-competitive N-methyl D-aspartate (NMDA) receptor antagonists, ketamine and phencyclidine, were found to induce schizophrenia-like positive and negative symptoms, such as hallucinations and social withdrawal in healthy individuals. The reduction of NMDA receptor activity may selectively occur on GABAergic interneurons¹⁷. Consistently, GABAergic neurotransmission in schizophrenia patients is tempered. The expression of several GABAergic markers, including the rate limiting enzyme in the synthesis of GABA glutamate decarboxylase GAD67, and the calcium-binding protein Parvalbumin (PV), expressed by largest subclass of GABAergic interneurons, are reduced in postmortem brains of

schizophrenia patients²¹. However, whether the density of interneurons is reduced or if interneurons lose their GABAergic phenotype is of debate^{21, 22}. Ultimately, changes in the strength of either excitation by glutamate or inhibition by GABA result in an excitatory/inhibitory imbalance that has been proposed to be causative for patient symptoms¹⁸.

The hyperdopamine hypothesis of schizophrenia initially arose based on the observation that most effective antipsychotics block dopamine receptors, particularly D2DR. However, more recent studies indicate that although subcortical areas are hyperdopaminergic, cortical dopamine is reduced in subjects diagnosed with schizophrenia^{15, 19}. This dopamine imbalance has been associated with positive motor symptoms (nigrostriatal dopamine excess), as well as negative and cognitive symptoms (mesocortical dopamine deficiency)^{20, 23}. Importantly, the complex reciprocal interaction of the glutamate, GABA, and dopamine circuits, impedes the identification of one single causative neurotransmitter system or the assignment of particular neurochemical changes to symptoms in patients²³. Moreover, at least in a subset of patients, other neurobiological processes such as inflammation, oxidative stress and immune dysfunction contribute to the complexity of the pathophysiology of schizophrenia⁷. Importantly, transcriptome studies have also identified changes in expression of genes related to synaptic function, GABA neurotransmission, oligodendrocytes, mitochondrial and energy metabolism, immunity and developmental genes consistent with these diverse neurobiological and neurochemical changes³. Specifically, these studies have also identified a particular enrichment of aberrant alternative splicing in the schizophrenic transcriptome²⁴⁻²⁶.

1.1.3 Association of Neuregulin and ErbB4 variants with schizophrenia

Among the many risk factors for schizophrenia, polymorphisms in the genes encoding the neurotrophic factors Neuregulins (NRGs) and their cognate receptor ErbB4 (avian erythroblastosis virus oncogene B4) are associated with an increased risk for schizophrenia. *NRG1* was the first gene of the family identified as genetically linked with schizophrenia in Icelandic patients²⁷, followed by *ERBB4* in Ashkenazi Jews²⁸, and more recently *NRG3*²⁹. Most, but not all meta-analyses, GWAS and phenotype-based genetic studies in different populations, support the genetic association between NRG/ErbB4 and schizophrenia. In total, more than 40, 20 and 25 single nucleotide polymorphisms (SNPs) were identified in the genes

of *NRG1*, *NRG3* and *ERBB4*, respectively, to predispose an individual to schizophrenia^{23, 30-32}. Lastly, one study has also suggested *NRG2* as susceptibility gene for schizophrenia²⁹.

Some of the identified SNPs have been found to correlate with endophenotypes of schizophrenia in both patients and unaffected controls, such as deficits in sensorimotor gating, cognitive function, unusual thoughts in conflict-related situations and psychotic symptoms. SNPs in *NRG1*, specifically, are linked with anatomical, myelin-related defects, such as reduced volume of white and gray matter, decreased white matter integrity, increased lateral ventricles and reduced structural connectivity, whereas SNPs in *ERBB4* mainly relate to interneuron deficits and alterations in GABA levels³⁰. Most identified SNPs are non-coding and correlate with alterations in transcript levels, primarily manifesting as increased RNA and protein levels. One coding SNP in the transmembrane domain of *NRG1* type III variant has been shown to reduce the susceptibility to gamma-secretase-dependent cleavage³³, and a rare *de novo* chromosomal variant encodes a truncated potentially dominant-negative ErbB4 receptor³⁴. Considering additional gene interactions among *NRGs* and *ERBB4*, but also with other schizophrenia susceptibility genes, these findings support a crucial role of NRG/ErbB4 signaling at several levels in the etiology of schizophrenia^{23, 30, 32}.

1.2 Neuregulin/ErbB4 signaling

1.2.1 The Neuregulins and ErbB receptor family

ErbB4 is a tyrosine kinase of the ErbB receptor family which comprises three other tyrosine kinase receptors: ErbB1 (also known as epidermal growth factor receptor (EGFR)), ErbB2 and ErbB3 (Fig 1.2). ErbB receptors are type I transmembrane glycoproteins with an apparent size of ~180kDa. ErbB receptors are activated by a diverse family of EGF-like ligands that can be classified into two groups, the EGF (epidermal growth factor) and the NRG family. The former comprises EGF itself, transforming growth factor-alpha (TGF- α), heparin-binding EGF (HB-EGF), betacullin, epiregulin and amphiregulin. The EGF domain common to all ligands, is necessary and sufficient to bind and activate receptors of the ErbB family^{32, 35, 36}.

Here, I will review in depth the family of the neurotrophic NRGs that are abundantly expressed in the central nervous system (CNS). Six genes encode NRGs (NRG1-6) of which three (NRG1, NRG2, NRG3) are expressed in the brain. Alternate splicing of each NRG further

enhances the heterogeneity of one of the largest gene families. NRG1, the best-studied member of the family, is one of the largest mammalian genes and has over 30 isoforms^{32, 35}. For instance, usage of different promoters results in different N-termini classified as six major NRG1 types (I-VI). NRG1 type I (also known as neu differentiation factor (NDF), heregulin or acetylcholine-receptor-inducing activity (ARIA)), type II (also referred to as glial growth factor (GGF)) and type III (or sensory and motor neuron-derived factor (SMDF) also termed cysteine-rich domain (CRD)-NRG) are best studied^{23, 32, 37}. Although directly secreted splice variants have been described, most NRGs are synthesized as immature transmembrane proteins, or pro-NRGs. The active EGF-like moiety is exposed after proteolytic cleavage (Fig. 1.1). Different extracellular proteases have been identified to process NRGs such as ADAM17 (a disintegrin and metalloproteinase domain-containing protein 17) or TACE (tumor necrosis factor α -converting enzyme), ADAM19, BACE1 (β -site amyloid precursor protein cleaving enzyme), disintegrin and neuropsin^{30, 32, 35}. Recently, our lab has shown that in neurons activity-dependent processing of Ig-NRGs is mediated by ADAM10 (Vullhorst et al. 2019, *in revision*).

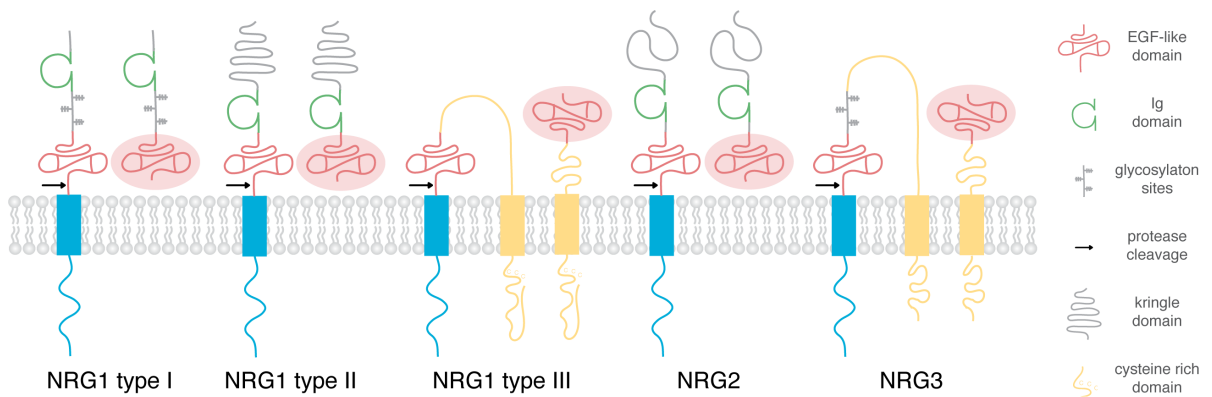


Figure 1.1 | Soluble and transmembrane Neuregulins.

Neuregulin (NRGs) are synthesized as inactive transmembrane (blue) proteins. The EGF-like domain is activated (red circle) after metalloprotease-mediated cleavage (black arrow). Soluble NRGs (NRG1 type I, NRG1 type II and NRG2) contain an immunoglobulin (Ig) domain (green) and are released after cleavage. Membrane-anchored NRGs contain a second N-terminal transmembrane domain (yellow). Scheme adapted from³⁸.

NRGs can be subdivided into two classes (Fig.1.1): soluble immunoglobulin (Ig)-NRGs (NRG1 type I, NRG1 type II, NRG 1 type IV and NRG2) and membrane-bound NRGs (NRG1 type III and NRG3). Soluble Ig-NRGs are single-pass transmembrane proteins that are diffusible after activity-dependent proteolytic cleavage. Ig-NRGs also contain an extracellular

heparin-binding immunoglobulin (Ig) domain. On the other hand, membrane-attached NRGs remain attached to the cell surface due to a second N-terminal transmembrane domain. Releasable Ig-NRGs therefore can signal in both an autocrine and paracrine manner, whereas transmembrane (TM)-NRGs are cell-contact-dependent (juxtacrine signaling)³⁷⁻³⁹. Subcellular targeting of Ig-NRGs and TM-NRGs fundamentally differs. While pro-Ig-NRGs accumulate at subsurface cisterna on the soma and proximal dendrites, processed TM-NRGs are targeted to axons and presynapses^{39, 40}. The expression of NRGs in the CNS is tightly regulated – both temporally and spatially – and differs substantially between different NRGs and NRG1 isoforms during development and in the adult brain⁴¹. Consistently, mutant mice of different NRG1 isoforms have been shown to exhibit differences in phenotypes. For instance, NRG1 type I is required for neural crest-derived sensory neurons in cranial ganglia and heart trabeculation, whereas NRG1 type III is essential for the development of Schwann cells. Taken together, this suggests largely non-overlapping distinct functions of different NRG genes and splice variants^{23, 32, 35, 38, 41}.

1.2.2 Neuregulin/ErbB4 signaling pathways

Upon ligand binding, ErbB receptors can form homo- and heterodimers (Fig. 1.2). The unique 55 amino acid EGF-domain of NRGs preferentially binds to ErbB3 and ErbB4 receptors but can build heterodimers with ErbB1 and ErbB2 to propagate signaling³⁵. ErbB2 harbors a constitutively active kinase domain, is unable to bind a ligand, and often acts as a co-receptor⁴². On the other hand, ErbB3 receptor has no kinase activity and depends on heterodimerization⁴³. ErbB4 is the only receptor that can both bind NRG and mediate downstream signaling autonomously³²; therefore I will further concentrate on reviewing the role of Neuregulin signaling through ErbB4 receptors.

As with other receptor tyrosine kinases, ligand binding induces tertiary structural changes and dimerization. Thereby, the tyrosine kinase is activated and cross-phosphorylates the dimerizing receptor. Phosphorylated sites serve as binding domains for adaptor proteins or kinases. The main downstream signaling pathways of ErbB4 are the Ras/mitogen-activated protein kinase (MAPK) and the phosphoinositide 3-kinase (PI3K)/protein kinase B (Akt) pathways³⁶ (Fig. 1.2). Both pathways regulate diverse and overlapping cellular functions. Signaling through MAPK promotes proliferation, differentiation and neuronal survival, and is

protective against oxidative stress. PI3K/Akt is also involved in cell proliferation, growth and survival, but additionally regulates nutrient uptake and metabolism, migration and autophagy⁴⁴.

Adaptor proteins such as growth factor receptor bound 2 (Grb2) and guanine nucleotide exchange factors like Son of Sevenless 1 (Sos1) are recruited to the phosphorylated tyrosine kinase receptor. Activated Sos1 induces the GDP/GTP exchange of membrane-bound Ras, which rapidly recruits accelerated fibrosarcoma (Raf) to the membrane and triggers sequential phosphorylation of Raf, MAP/Erk kinases 1/2 (Mek1/2) and extracellular signal regulated kinases 1/2 (Erk1/2, or MAPK). More than 200 downstream targets of Erk have been identified and include several transcription factors (e.g. fos, jun, myc)⁴⁴.

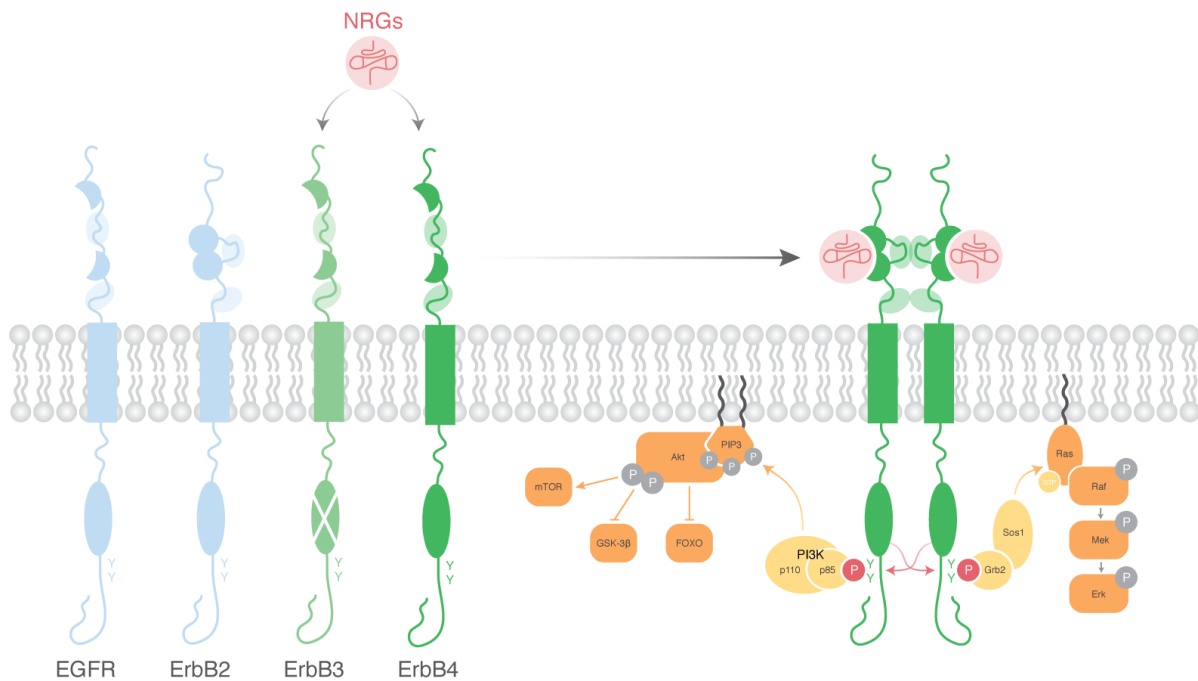


Figure 1.2 | ErbB receptor family and canonical signaling pathways.

Neuregulins (NRGs; red circle) bind to the two cysteine-rich ligand binding domains of ErbB3 and ErbB4 receptors (green). The kinase domain of ErbB3 is inactive (white cross), while the structure of ErbB2 (light blue) suggests that it does not bind any ligand. Upon ligand binding ErbB4 receptor homo- and heterodimerizes with other receptors of the ErbB family via its furin-like domains (light green). Tyrosine kinase cross-phosphorylation triggers downstream signaling pathways PI3K/Akt and MAPK. Scheme adapted after³⁶.

On the other hand, the regulatory p85 unit of PI3K binds to phosphorylated sites of the receptor via its Src homology 2 (SH2) domain, which then mediates the recruitment and activation of the p110 catalytic subunit. Activated PI3K phosphorylates phosphatidylinositol

4,5-biphosphates (PIP₂) to form phosphatidylinositol (3,4,5)-triphosphate (PIP₃). PIP₃ then binds with high affinity to the pleckstrin homology domain of protein kinase B (known as Akt). The localization of Akt at the membrane allows its phosphorylation at Thr308 and Ser472 by phosphoinositide dependent kinase 1 (PDK1) and mammalian target of rapamycin complex 2 (mTORC2), respectively. Fully-activated Akt then activates transcription factors, such as β -catenin and cAMP response element binding protein (CREB), and inhibits the inactivating enzyme glycogen synthase kinase-3 beta (GSK-3 β) and transcriptional repressors such as forkhead box transcription factors FOXO. Additionally, Akt also activates the mammalian target of rapamycin (mTOR), a key enzyme in the ribosomal protein synthesis enhancing cell growth⁴⁴.

Other ErbB4 downstream signaling pathways include janus kinase (JAK)/signal transducer and activator of transcription (STAT) and phospholipase C- γ (PLC- γ)/protein kinase C (PKC) pathways, which are particularly activated by ErbB4/ErbB1 heterodimers. Moreover, ErbB4 interacts with cyclin dependent kinase 5 (Cdk5) and the tyrosine protein kinase Fyn, protein-tyrosine kinase 2-beta (Ptk2b or Pyk2), Abelson tyrosine kinase c-Abl and c-Jun N-terminal kinase (JNK)^{32, 45}. In addition, non-canonical kinase-independent ErbB4 functions have been described⁴⁶ and the intracellular domain (ICD) of some receptor isoforms can initiate back signaling to the nucleus⁴⁷⁻⁴⁹ (see section 1.4.2). Retrograde signaling was also proposed for pro-NGF and NGF type III activated by soluble extracellular domain of ErbB4 and involves the cleavage of the intracellular domain of NGF³².

1.3 Neuregulin/ErbB4 signaling in the central nervous system

1.3.1 Expression of ErbB4 in the brain

In the CNS, ErbB4 expression is high in neurons, whereas ErbB3 expression is confined to glia and epithelial cells⁵⁰⁻⁵³. Thus, ErbB4 is the only neuronal Neuregulin receptor. ErbB4 is expressed both in the developing embryonic and adult brain^{54, 55}. In the adult neocortex, ErbB4 is expressed in scattered GABAergic interneurons with varying density across different cortical areas^{56, 57}. Importantly, it has been unambiguously shown – using a variety of approaches (immunostaining, single-cell PCR, reporter mice, conditional knock-out mice) – that ErbB4 is absent from excitatory pyramidal neurons in the cortex and hippocampus⁵⁷⁻⁶².

Among interneuron classes, ErbB4 is mainly expressed in parvalbumin (PV)-expressing interneurons, but also was described in other interneuron subtypes such as cholecystokinin (CCK)-, calretinin (CR)-, neuropeptide Y (NPY)-, vasoactive intestinal peptide (VIP)- and neuronal nitric oxide synthetase (nNOS)-positive interneurons; whereas only few somatostatin (SOM)-positive interneurons express ErbB4^{54, 59, 60, 63, 64}. Subcellular localization of ErbB4 in GABAergic interneurons has been characterized at post-and peri-synaptic clusters of excitatory synapses on soma and dendrites. ErbB4 is also present in detergent-soluble extra-synaptic fractions and intracellular^{46, 58, 65-67}. Most inhibitory axons and pre-synapses are devoid of ErbB4. However, ErbB4 has been detected on inhibitory boutons of a subset of GABAergic interneurons confined to some brain areas (e.g. CCK baskets in subiculum, frontal and entorhinal cortex)⁵⁸, and functional evidence for ErbB4 at the presynaptic Chandelier boutons has been presented^{60, 68-70}.

ErbB4 is also expressed in several subcortical regions. High ErbB4 expression was described in the medial habenula and in GABAergic neurons in the reticular thalamic nucleus and in intercalated nuclei of the amygdala^{52, 56, 57}. Almost all dopaminergic neurons in the substantia nigra compacta (SNc) and ventral tegmental area (VTA) and some serotonergic neurons in the dorsal raphe express ErbB4^{50, 53, 57}. ErbB4 is absent from norepinephrinergic neurons⁵⁷, although this view was recently challenged⁷¹. In the basal ganglia, scattered ErbB4-expressing interneurons have been described, whereas medium spiny neurons are largely ErbB4-negative^{57, 72}. Besides, ErbB4 is expressed at high levels in some hypothalamic nuclei^{50, 57} and lower ErbB4 expression levels have been described in the hindbrain, thalamus and cerebellum⁵⁷. In the latter, ErbB4 expression has been specifically demonstrated in cerebellar granule cells and Bergmann glia^{52, 72-74}. ErbB4 was detected in thalamic S100b-positive glia and in oligodendrocytes^{51, 57}. Lastly, the ErbB4 expression described in rodents is generally conserved in the developing and adult brain of both monkeys and humans^{59, 75-77}.

1.3.2 Regulation of neurodevelopment

1.3.2.1 *GABAergic interneuron migration*

Telencephalic excitatory glutamatergic and inhibitory GABAergic neurons are generated by two fundamentally distinct processes. While excitatory neurons are born in the ventricular zone of the pallium and migrate radially to form the cortical plate, cortical and hippocampal

inhibitory neurons are derived from the subventricular zone (SVZ) of the subpallial ganglionic eminences (GE) and have to undergo long-range tangential migration. Upon entering the pallium, inhibitory neuroblasts disperse, switch to radial migration and invade the cortical plate to reach their final location and integrate into cortical circuits⁷⁸. ErbB4 is expressed on progenitor cells in the SVZ of the medial ganglionic eminence (MGE) as early as embryonic day 12 (E12) in rats. Its expression is maintained on tangential migratory streams of GABAergic progenitors derived from the MGE and continued to be expressed by GABAergic interneurons after their integration into the cortical plate throughout life^{54, 55, 79}.

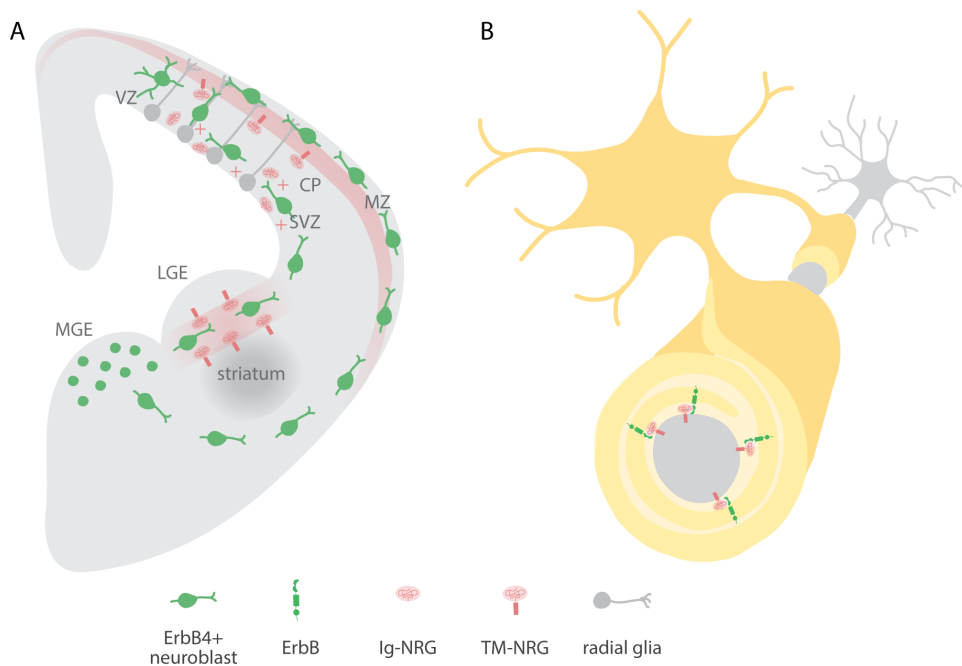


Figure 1.3 | Regulation of neurodevelopment by NRG/ErbB4.

(A) NRG/ErbB4 signaling regulates interneuron migration during embryonic development. ErbB4+ neuroblasts (green) born in the medial ganglionic eminence (MGE) migrate tangentially and invade the cortex in two streams in the subventricular zone (SVZ) and the marginal zone (MZ). Migrating interneurons pass a permissive corridor generated by the expression of NRG1 type III (red) in the lateral ganglionic eminence (LGE) and are attracted to soluble Ig-NRG (red, plus symbol) expressed in the cortex. To reach their final allocation in the cortical plate (CP) interneurons switch to radial migration, a process regulated by NRG3 (red). (B) NRG/ErbB signaling is essential for myelination by peripheral Schwann cells (adapted from³²). Axonal TM-NRG (red) initiates myelination by ErbB (green)-expressing Schwann cells. In contrast, NRG/ErbB is dispensable for central myelination by oligodendrocytes and regulates only a few aspects of oligodendrocyte development. VZ – ventricular zone.

NRG/ErbB4 signaling plays a pivotal role in regulating the migration and allocation of GABAergic interneurons^{63, 79-81} (Fig. 1.3A). Membrane-bound NRG1 type III provides a permissive corridor for migrating ErbB4-positive neuroblasts in the developing striatum,

whereas diffusible NRG1 type I in the cortex is chemoattractive⁷⁹ (a view challenged by⁸⁰) and promotes the emergence of new better-aligned branches from the leading process⁸². NRG3, likewise a membrane-bound NRG³⁹, is expressed in developing cortical plate and guides cortical interneurons to their final allocation⁸¹. In ErbB4 mutant mice, GABAergic interneurons fail to reach the developing cortex, as a consequence GABAergic interneuron numbers in the postnatal cortex and hippocampus are reduced^{63, 79, 80, 83}. Reduction of hippocampal interneurons in ErbB4 KO mice predominantly affects PV- and nNOS-expressing interneurons, whereas CCK-positive interneurons are only slightly reduced, and ErbB4-negative SOM interneurons are unaltered⁶³. ErbB4 mutant mice in which ErbB4 was conditionally removed at post-mitotic stages (by the promoters distal-less homeobox 6 (Dlx6) or LIM homeobox 6 (Lhx6) expressed in the MGE) showed no alteration in GABAergic interneuron numbers, but laminar distribution of interneurons was shifted towards upper cortical layers resembling the phenotype in NRG3 mutants^{60, 68, 81}. Deficits in interneuron numbers and placement are thought to ultimately affect the excitatory/inhibitory balance in NRG and ErbB4 mutant mice³⁸.

Adult neurogenesis occurs mainly in two brain regions: the hippocampus and the olfactory bulb (OB). Olfactory GABAergic interneurons are generated in the SVZ of the lateral ventricle. Tangentially-migrating neuroblasts to the OB form the rostral migratory stream (RMS) through which they move in organized chains⁸⁴. ErbB4 is expressed in postnatally-generated neuronal progenitors in the SVZ, migrating neuroblasts in the RMS and in GABAergic interneurons in the destined OB^{55, 72, 85}. NRG2 stimulation mediates the proliferation of neuronal progenitors in the SVZ⁸⁶ and the loss of ErbB4 alters chain migration and results in reduced number and poorly differentiated interneurons in the OB^{85, 86}. Recently, ErbB4 has also been proposed to promote survival and maturation of neuroblasts in the hippocampal subgranular zone⁸⁷.

In addition to regulating the migration of interneurons, NRG/ErbB4 also controls axonal outgrowth and guidance. Accordingly, NRG promotes axon growth and arborization of GABAergic interneurons *in vitro*^{60, 88}, and pathfinding of thalamocortical axons (TCAs) i.e. projections from the thalamus to the cortex, depends on NRG/ErbB4 as well. Reminiscent of the distinct chemoattractive properties of different NRG isoforms in the regulation of interneuron migration, soluble NRG1 type I stimulates axonal growth, and membrane-bound

NRG1 type III in the MGE allows ErbB4-expressing TCAs to pass through an otherwise non-permissive area⁸⁹.

1.3.2.2 *Oligodendrocyte differentiation and myelination*

Axons of peripheral and central neurons can either be unmyelinated or myelinated, i.e. enveloped by a multilayer myelin sheath. Myelin is generated by non-neuronal glial cells, oligodendrocytes in the CNS and Schwann cells in the peripheral nervous system (PNS) by wrapping their specialized plasma membranes around neuronal axons. Myelination provides electrical isolation and ensures fast propagation of nerve impulses. Myelin thickness is determined by the number of evenly-spaced myelin sheets around the axon and correlates with the thickness of the axon^{90, 91}. NRG/ErbB signaling regulates the development of Schwann cells, including survival, proliferation, migration and differentiation, and is indispensable for the myelination of peripheral nerves by Schwann cells^{30, 92, 93}. Importantly, axonal-derived NRG1 type III on the surface of peripheral axons dictates which nerves are myelinated⁹³ and how thick the myelin envelops⁹² (Fig. 1.3B). ErbB2/ErbB3 heterodimers on Schwann cells were identified to mediate these effects^{94, 95}. Consequently, the absence of ErbB receptors or the reduction or the complete loss of NRG1 type III result in thinner myelin and slower nerve conduction velocity^{92, 93, 95-97}.

In the CNS, myelinating oligodendrocytes express ErbB2, ErbB3 and ErbB4^{98, 99}. Based on the requirement of NRG/ErbB for myelination in the PNS, it was assumed that NRG/ErbB also plays a crucial role in oligodendrocyte development and myelination. *In vitro* as well as *ex vivo* explant studies have supported this idea and suggested that NRG promotes survival and proliferation of oligodendrocyte progenitor cells (OPCs), inhibits their differentiation and enhances myelination of mature oligodendrocytes^{94, 98-103}. *In vivo*, however, NRG/ErbB signaling has been found to be largely dispensable for the development of oligodendrocytes¹⁰⁴⁻¹⁰⁷. Thorough analyses of multiple NRG and ErbB mutant mice have determined that normal oligodendrocyte myelination in the CNS does not require NRG1, ErbB3 or ErbB4¹⁰⁴. Based on the discrepancies between *in vitro* and *in vivo* studies, neuronal activity has been suggested to be required for initiating myelination¹⁰⁴, in line with emerging evidence for activity-dependent myelination¹⁰⁸. Nevertheless, NRG/ErbB signaling regulates some aspects of glial development in the CNS. Transgenic overexpression of NRG1 can induce (hyper)myelination¹⁰⁴, while late loss of ErbB3/ErbB4 interferes with oligodendrocyte

maturation and provokes hypomyelination deficits¹⁰⁶, and early OPC migration in the optic nerve (~E16.5) is reduced in ErbB4 mutant mice but recovered perinatally¹⁰⁵. Interestingly, oligodendroglia have also been proposed to play a role in the pathophysiology of schizophrenia¹⁰⁹. Several genes associated with schizophrenia control oligodendrocyte function¹¹⁰, and schizophrenia patients suffer from dramatic white matter loss¹¹¹ that has been correlated to SNPs in ErbB4^{112, 113}.

1.3.3 Regulation of cortical and hippocampal circuits

ErbB4 in GABAergic interneurons modulates both inhibitory and excitatory circuits in the cortex and hippocampus at different levels beginning with the assembly of synapses (see Fig. 1.4). In line with the subcellular distribution of ErbB4 on GABAergic interneurons at glutamatergic postsynapses and GABAergic presynapses, ErbB4 regulates (1) glutamatergic input onto interneurons at postsynaptic densities (Fig. 1.4A, section 1.3.3.1) and (2) inhibitory synapse formation at presynaptic terminals in some subtypes (Fig. 1.4B, section 1.3.3.2). Moreover, secondary or indirect circuit effects of NRG/ErbB4 signaling affect (3) glutamatergic neurotransmission between excitatory neurons (Fig. 1.4C, section 1.3.3.3). By modulating synaptic GABAergic and glutamatergic neurotransmission, ErbB4 also regulates (4) plasticity and network activity of cortical and hippocampal circuits (Fig. 1.4.D, E, section 1.3.3.4)¹¹⁴.

1.3.3.1 *ErbB4 at glutamatergic post-synapses*

The postsynaptic density (PSD) at glutamatergic synapses serves as structural scaffold that anchors receptors, channels and signaling proteins to effectively regulate the postsynaptic response²³. The PDZ domain at the C-terminal end of the ErbB4 receptor directly interacts with proteins of the membrane-associated guanylate kinase (MAGUK) family. Its association with the postsynaptic density protein 95 (PSD-95) stabilizes the receptor at glutamatergic postsynapses on GABAergic interneurons⁶⁵⁻⁶⁷ (Fig. 1.4A). Interestingly, the interaction of ErbB4 with PSD-95 is reduced in the postmortem prefrontal cortex (PFC) of schizophrenia patients¹¹⁵. ErbB4 accumulated at glutamatergic synapses on GABAergic interneurons has been suggested to be the primary target site of NRG/ErbB4 signaling²³.

ErbB4 promotes the assembly of glutamatergic synapses onto GABAergic interneurons. In the hippocampus of null and interneuron-specific ErbB4 mutant mice, somatic vesicular

glutamate transporter 1 (vGLUT-1)-positive presynaptic boutons and postsynaptic PSD-95-labeled densities are reduced on both PV-positive basket and Chandelier cells^{60, 68, 70, 116} (Fig. 1.4A). These anatomical changes are accompanied by reduced frequency but not amplitude of miniature excitatory postsynaptic currents (mEPSCs) on GABAergic interneurons^{60, 68, 70}. In the prefrontal cortex, however, the final maturation rather than the initial formation of glutamatergic synapses on PV basket interneurons depends on ErbB4¹¹⁷. Consistent with the assembly and pruning of synapses being an early postnatal developmental process, the acute loss of ErbB4 in the adult brain neither changes the number of glutamatergic synapses on GABAergic interneurons nor the mEPSCs frequency; and the reduction of glutamatergic synapses onto GABAergic interneurons by the early loss of ErbB4 cannot be recovered by the reintroduction of ErbB4 at later stages¹¹⁸. ErbB4 on post-synapses has also been proposed to influence presynaptic differentiation by trans-synaptic interactions with NRGs or other binding partners¹¹⁹.

Post- and extra-synaptic located ErbB4 triggers the internalization of diverse receptors. For instance, ErbB4 directly interacts with the NMDA receptor subunit 2B (GluN2B) and upon NRG activation rapidly decreases its surface localization⁴⁰ (Fig. 1.4A). NRG/ErbB4 also promotes endocytosis of other neurotransmitter receptors such as alpha-7 nicotinic acetylcholine receptors ($\alpha 7$ -nAChR) and GABA A receptor alpha 1 (GABA_AR $\alpha 1$)^{46, 120, 121}, suggesting that the internalization of surface receptors is a common mechanism mediated by ErbB4⁴⁰. Moreover, NRG1 directly decreases voltage-gated sodium channels (Nav) activity, possibly through internalization, and thereby has been suggested to reduce the intrinsic excitability of hippocampal interneurons¹²⁰; however others reported increased excitability of cortical fast-spiking PV interneurons elicited by NRG due to lowering the voltage threshold for action potentials through the voltage-gated potassium channel Kv1.1¹²².

1.3.3.2 *ErbB4 at inhibitory pre-synapses*

ErbB4 has been proposed to play a role at the presynaptic terminals of inhibitory synapses of both major classes of PV interneurons, soma-innervating fast-spiking basket cells and axo-axonic interneurons also known as Chandelier cells. The presence of the receptor on these cells has however not been demonstrated unambiguously^{60, 123}. Whereas, ErbB4 on presynaptic boutons of Chandelier Cells regulating synapse development has been supported by several

reports^{60, 68-70}, the presence of ErbB4 on terminals of PV basket cells is controversial^{58, 59, 68, 117} vs.^{60, 123, 124}. Therefore, I will discuss these two interneuron classes separately.

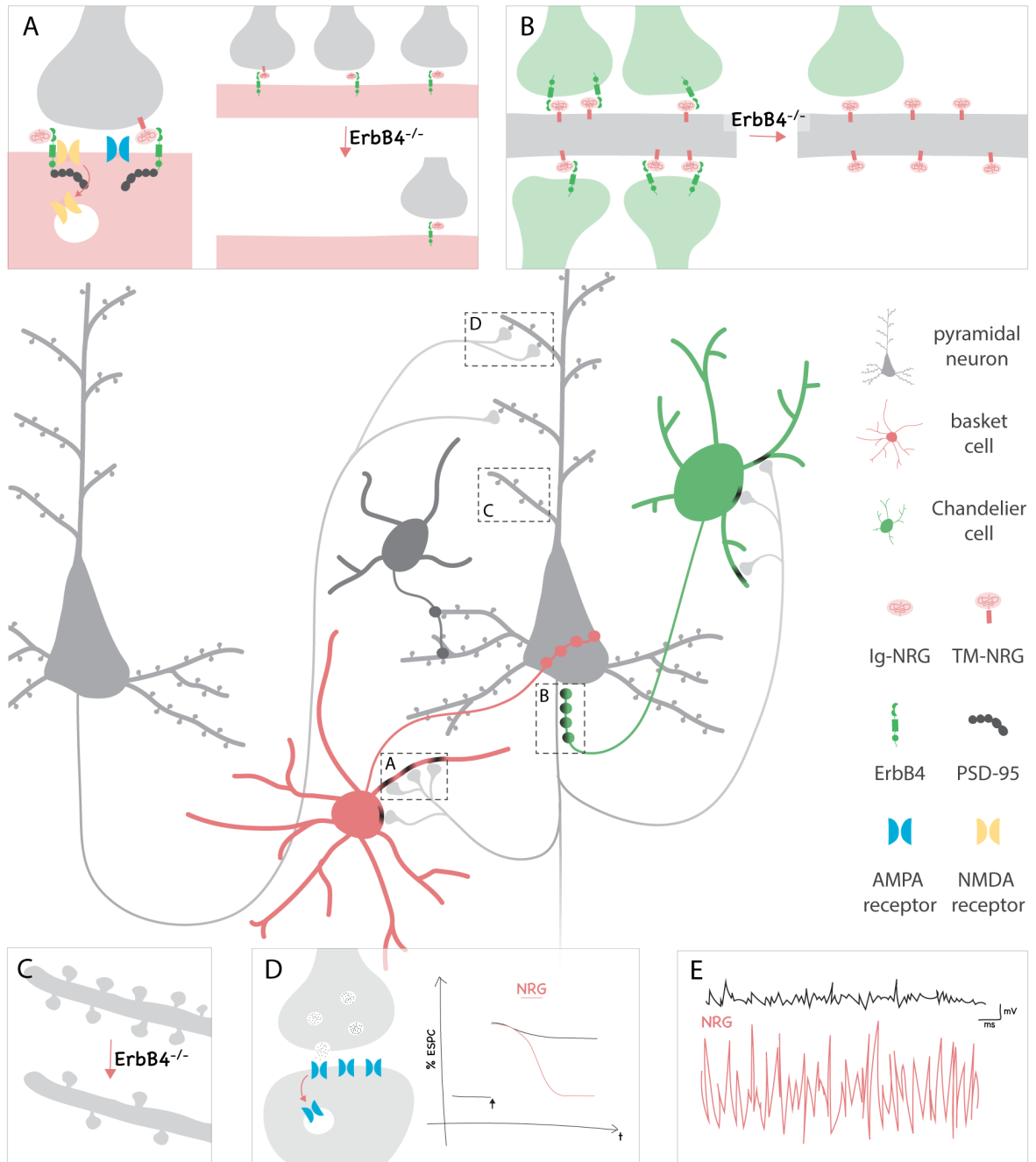


Figure 1.4 | Regulation of cortical and hippocampal circuits by Neuregulin/ErbB4 signaling.

(A) ErbB4 (green) accumulates at excitatory synapses on soma and dendrites of GABAergic interneurons and interacts with postsynaptic density protein PSD-95 (dark grey) and NMDA receptors (yellow). Endocytosis of the latter is induced by NRG stimulation (left panel). Loss of ErbB4 signaling results in a reduction of excitatory input onto GABAergic interneurons (right panel). (B) Pre-synaptic ErbB4 on Chandelier cells (green) regulates

synapse assembly. (C) Dendritic spines on pyramidal neurons are reduced in ErbB4 mutant mice. (D) NRG/ErbB4 signaling regulates long-term plasticity at Schaffer collateral CA3-CA1 excitatory synapses. NRG stimulates AMPA receptor (*blue*) internalization (left panel) and reverses long-term potentiation (right panel). (E) NRG increases the power of γ -oscillations. Main panel adapted after¹¹⁴.

First, ErbB4 cell-autonomously regulates the development of synaptic cartridges of Chandelier cells, uniquely targeting the axon initial segment (AIS) of pyramidal neurons with several boutons. ErbB4 knock-down in Chandelier cells, or interneuron-specific ErbB4 loss reduces the number and sizes of boutons (Fig. 1.4B). Concomitant with the reduction in inhibitory synapses, the frequency but not the amplitude of miniature inhibitory postsynaptic currents (mIPSCs) on postsynaptic pyramidal neurons is decreased in the hippocampus and prefrontal cortex of mutant mice, whereas release probability is unaltered^{60, 68, 70}. Elegantly designed mutant mice allowed to distinguish between developmental and adult ErbB4 function and revealed that ErbB4 is essential for the development of Chandelier cartridges but not for their maintenance. Nevertheless, mIPSC frequency is reduced in mice that lose ErbB4 postnatally^{118, 125}. Behavioral significance of decreased inhibition due to the loss of Chandelier synapses has been demonstrated in mice that lack ErbB4 specifically in late-born Chandelier Cells⁷⁰. These mice display impaired schizophrenia-relevant behaviors (locomotor activity, sensory motor gating, working memory and social novelty recognition) that are enhanced with an agonist for the GABA_A receptor subunit $\alpha 2$ enriched at the postsynaptic AIS^{70, 126}. Of note, the loss of chandelier cartridges has also been reported in the PFC of schizophrenia subjects^{127, 128}.

Second, ErbB4 on presynaptic terminals of PV basket cells has been suggested to regulate activity-dependent GABAergic neurotransmission^{61, 118, 123, 124}. While acute treatment with NRG1 does not affect basal GABAergic transmission, NRG increases evoked GABA release^{123, 129} and elicits increased inhibitory postsynaptic responses in pyramidal neurons mediated through GABA_A receptors^{61, 124}. Evoked inhibitory postsynaptic currents (eIPSCs) in pyramidal neurons are reduced in ErbB4 mutant mice and GABA release probability is compromised¹¹⁸. NRG1 suppresses the activity and firing of pyramidal neurons⁶¹, in line with increased firing rates of pyramidal neurons and decreased activity-dependent GABAergic transmission in ErbB4 mutant mice lacking ErbB4 specifically in interneurons^{68, 117}. Moreover, ErbB4 on GABAergic terminals contacting the soma of pyramidal neurons has been implicated in synaptogenesis⁶⁰ and somatic PV boutons have been reported to be reduced in ErbB4 mutant

mice¹¹⁸. Others, however, have reported no alteration in inhibitory synapses innervating the soma of pyramidal neurons^{68, 117}. Further, mIPSCs in deep layer pyramidal neurons mainly targeted by PV basket interneurons were unchanged in the medial prefrontal cortex (mPFC) of interneuron-specific ErbB4 mutant mice, suggesting that ErbB4 is dispensable for the development of GABAergic synapses of fast-spiking basket cells, in contrast to Chandelier cells^{70, 117}. Lastly, inhibitory synapses between interneurons form and mature independently of ErbB4^{116, 117}.

1.3.3.3 *Indirect effects on glutamatergic neurons*

ErbB4 is absent from pyramidal neurons^{58, 60} and deletion of ErbB4 in pyramidal neurons (using Ca^{2+} /calmodulin-dependent protein kinase II (CaMKII) or neuronal basic helix-loop-helix protein (Nex) promoter-driven Cre expression in ErbB4 floxed mice) has therefore no effects on neurotransmission, synaptic plasticity or animal behavior^{60, 62, 124}. Nevertheless, ErbB4 on GABAergic interneurons affects glutamatergic pyramidal neurons and their neurotransmission non-cell autonomously^{23, 62}. Dendritic spine morphology is regulated by ErbB4 on GABAergic interneurons. Reduced spine density in the cortex and hippocampus has been described in brain- and interneuron-specific ErbB4 mutant mice^{60, 62, 68, 118, 130}, by viral ErbB4 knockdown in slice culture¹³¹, and in the subiculum of NRG1 type III heterozygote mutants¹³² (Fig. 1.4C). The reduction of spines particularly affects mushroom-shaped spines and is prominent in proximal dendrites, but absent from distal parts of the dendrites^{68, 118}. On the other hand, in hippocampal culture chronic NRG1 treatment stimulates spine formation and enlargement¹³³. Adult spine formation or maturation are independent of ErbB4 and postnatal defects due to the developmental loss of ErbB4 are irreversible¹¹⁸. Decreased spine density in ErbB4 mutant mice has been proposed to be a compensatory effect for the hyperactivity of pyramidal neurons provoked by the GABA hypofunction³⁰. Interestingly, spine reduction has also been described in the PFC of schizophrenia patients¹³⁴. Concomitant with a reduction in spine density, reduced mEPSCs in hippocampal pyramidal neurons suggest impaired basal glutamatergic transmission at CA3-CA1 Schaffer collateral (SC) synapses in ErbB4 mutant mice^{62, 118}. However, GluN2B-mediated synaptic currents at SC are also augmented in NRG2 KO mice¹³⁵. Taken together, these findings suggest that the long-term loss of NRG/ErbB4 signaling on GABAergic interneurons also indirectly affects glutamatergic neurotransmission between pyramidal neurons.

1.3.3.4 Regulation of plasticity and network activity

Synaptic plasticity changes the strength of synapses in an activity-dependent manner and is important for learning and memory. Long-term potentiation (LTP), depotentiation or LTP reversal as well as long-term depression (LTD) bidirectionally regulate glutamatergic synapses²³. Hippocampal SC synapses have been the primary model system for LTP. Early LTP is mediated by CaMKII through the recruitment and stabilization of α -amino-3-hydroxy-5-methyl-4-isoxazolepropionic acid (AMPA) receptors (AMPA) at the synapse¹³⁶. While NRG1 does not alter basal glutamatergic neurotransmission or short-term plasticity of glutamatergic synapses, it prevents the induction of LTP at SC, and rapidly suppresses LTP in a time- and concentration-dependent manner^{65, 124, 137-141} (Fig. 1.4D). LTP depotentiation by Neuregulin is mediated by internalization of AMPAR¹³⁷, and both dopaminergic and GABAergic transmission has been suggested to play a role^{124, 138}. Importantly, LTP depotentiation induced by NRG is absent in ErbB4 mutant mice that lack ErbB4 in either all neurons or specifically in PV interneurons^{124, 139, 142}. Interestingly, these mice also exhibit enhanced LTP^{124, 139, 142}.

While the output activity of the cortical and hippocampal network is mediated by excitatory neurons, GABAergic interneurons modulate and synchronize the activity of the network. Since NRG/ErbB4 regulates the glutamatergic drive onto GABAergic interneurons, it is not surprising that this pathway also controls neuronal synchrony and oscillatory activity^{23, 114}. In hippocampal and cortical slices, NRG1 enhances the synchrony amongst pyramidal neurons and interneurons¹⁴³ and dramatically increases kainite-induced gamma oscillations important for cognition, learning and memory^{83, 144} (Fig 1.4E). Modulatory effects of NRG1 on gamma oscillations are blocked by ErbB inhibitors and are absent in ErbB4 mutant mice^{83, 144}. Gamma oscillations are overall reduced in ErbB4-deficient mice and mice that lack neuropsin, one of the NRG-converting enzymes^{83, 145}. *In vivo*, both in anaesthetized and freely moving mice, the power of gamma oscillations is however increased in mice that lack ErbB4 from interneurons or all cells^{68, 125}. In these mice, the synchrony between hippocampal and prefrontal cortical oscillations in the theta and delta range is diminished during the resting state and top-down attention^{68, 125}. Attention-associated hippocampal-prefrontal coherence is also impaired when ErbB4 activity is blocked acutely in adult mice using a chemic-genetic approach¹²⁵. Of note, the power of gamma oscillations is reduced in patients with schizophrenia^{146, 147}.

Recently, two independent studies have shown that NRG/ErbB4 signaling plays a role in critical period plasticity^{148, 149}, a window of high plasticity during development that has been extensively studied in the visual cortex. Monocular deprivation during this period enhances thalamic afferents of the open eye and attenuates the input of the deprived eye, a phenomenon described as ocular dominance plasticity. Both the initiation and the closure of the critical period concomitant with the gain and loss of plasticity, depends on the excitatory-inhibitory balance and is by large controlled by the maturation of PV interneurons that receive direct thalamic input¹⁵⁰. NRG/ErbB4 signaling on PV-positive interneurons regulates both the initiation and the closure of critical period plasticity by enhancing excitatory inputs onto PV interneurons^{148, 149, 151}. Critical period plasticity is impaired in ErbB4 mutant mice lacking ErbB4 on PV interneurons¹⁴⁹ and chronic injection of NRG1 inhibits ocular dominance plasticity during the critical period, but rescues plasticity in mice with hypoexcitable interneurons¹⁴⁸. Interestingly, the administration of ErbB inhibitors rescues ocular dominance plasticity in adult mice suffering from amblyopia induced by chronic monocular deprivation¹⁴⁸.

1.3.4 Behavioral deficits of Neuregulin and ErbB4 mutant mice

Many of the described molecular and physiological functions of NRG/ErbB4 also influence animal behavior. Interestingly, mutations in both NRG and ErbB4 cause numerous behavioral deficits that are related to psychiatric disorders. Endophenotypes for positive symptoms of schizophrenia assessed in mice are drug-induced hyperactivity and sensorimotor gating¹⁵². Particularly the prepulse inhibition (PPI) task for sensorimotor gating is a reliable translational and robust preattentive assay¹⁵³. The complexity of negative symptoms and the unique human characteristics (e.g. speech) are challenging to model accurately in an animal. Negative symptoms therefore are mainly studied using social behavior¹⁵⁴. Lastly, cognitive function can be assessed in mice by a variety of different tasks, addressing attention, working and spatial memory, as well as short- and long-term memory (e.g. using water maze, radial arm maze, Y-maze, T-maze, 5-choice serial reaction time task, conditioned fear memory and extinction, novel object recognition and delayed non-match to place tasks)¹⁵³.

Homozygous mutations of NRG1 and ErbB4 are lethal during embryonic development due to heart malformation^{155, 156}. While ErbB4 mutants could be rescued by transgenic expression of ErbB4 in the heart¹⁵⁷, NRG1 is also essential for myelination in the peripheral nervous

system and the development of the neuromuscular junction³⁷. Postnatal behavior can therefore only be investigated in heterozygous NRG1 mutants. Different NRG1 variants (type I, type III) and domains (TM, Ig or EGF domain) have been targeted by mutation and mice exhibit similar, but not completely overlapping, behavioral deficits including hyperactivity in the open field test, sensorimotor-gating impairment in PPI, latent inhibition, reduced fear conditioning, reduced working and spatial memory, and abnormal social behaviors^{27, 132, 158-164}. NRG2 mutant mice are hyperactive in a novel environment, hypersensitive to amphetamine, and express impaired PPI, working memory, anxiety and social interactions¹³⁵. Similar phenotypes have also been described for NRG3 mutants, such as novelty-induced locomotor hyperactivity, impaired PPI of the acoustic startle response, deficits in fear conditioning and impulsivity^{165, 166}. Consistent with conveying all neuronal NRG signaling, ErbB4 mutants are also hyperactive, and demonstrate reduced PPI and anxiety, as well as abnormal attention, learning, spatial/working memory and social behavior^{27, 61, 125, 130, 142}. Interestingly, many of these phenotypes have been recapitulated in ErbB4 mutant mice that lack ErbB4 specifically from PV interneurons^{61, 68, 70, 124, 142, 167}, suggesting that PV cells are the main target of NRG signaling in modulating animal behavior³⁰. The adult loss of ErbB4 resulted in comparable, albeit less severe, behavioral alterations than the complete deletion of ErbB4¹¹⁸. On the other hand, restoring ErbB4 expression in adulthood can ameliorate but not fully rescue behavioral deficits provoked by its developmental deletion¹¹⁸, suggesting a more pronounced role of NRG/ErbB4 during development than in the adult brain. Lastly, some behavioral phenotypes were ameliorated by the administration of the antipsychotic drug clozapine^{27, 130, 135, 168} and the GABA agonists diazepam⁶¹.

On the contrary, transgenic overexpression of NRG1 type I (gain of function) causes similar behavioral phenotypes compared to NRG1 heterozygote mutants (loss of function); including hyperactivity in a novel environment, reduced PPI, abnormal fear and social behavior, and impaired working memory¹⁶⁹⁻¹⁷³. Based on these contrasting observations, an inverted U-shape model emerged in which alterations (both decrease and increase) from the optimal range of NRG1 concentration or signaling alters the excitatory/inhibitory balance and impairs proper brain development and function^{30, 114, 174, 175}.

1.3.5 Modulation of the dopamine system

Most studies investigating NRG/ ErbB4 signaling have focused on the cell-autonomous role in ErbB4-expressing cortical and hippocampal GABAergic interneurons or the indirect regulation of glutamatergic synapse development and neurotransmission^{30, 114}. ErbB4 is also expressed at high levels in most dopaminergic neurons (92-99%) in the substantia nigra pars compacta (SNc) and the ventral tegmental area (VTA), but absent from dopamine neurons in the retrorubal area^{50, 52, 53, 77, 176}. Starting at E9, ErbB4 is detected in proliferating precursors in the ventral midbrain and expressed in mesencephalic dopamine neurons from E11 through adulthood. The absence of ErbB4 in brain-specific ErbB4 conditional mutant mice does not alter the development of dopamine neurons or their projections¹⁷⁶, contrary to the regulation of interneuron development by NRG/ErbB4⁷⁹. However, neuroprotective properties of NRG on dopaminergic neurons have been described both *in vitro* and *in vivo* and neurite outgrowth is stimulated by NRG *in vitro*¹⁷⁷⁻¹⁷⁹. Chronic disruption of NRG/ErbB signaling has been implicated in altered extracellular dopamine levels or dopamine content, concomitant with changes in the expression of the dopamine-synthesizing enzyme, tyrosine hydroxylase and dopamine receptors^{135, 143, 169, 178, 180-183}. Intriguingly, in ErbB4 and NRG2 mutant mice, inverse changes in basal extracellular levels are observed in the prefrontal cortex and the dorsal striatum, similar to the dopamine imbalance in schizophrenia patients^{19, 135, 184} (Skirzewski et al., *in preparation*). Moreover, acute delivery of NRG elicits the rapid increase of extracellular dopamine^{138, 185}, metabotropic glutamate receptor 1 (mGluR1)-induced striatal dopamine release depends on ErbB activation¹⁸⁶ and potassium-induced dopamine release in the mPFC is augmented in mice chronically injected with NRG1¹⁴³. On the other hand, NRG1 type II has also been described to promote dopamine uptake in cultured dopamine neurons¹⁷⁷. Neonatal chronic NRG1 treatment elevates burst firing through the disinhibition of dopamine neurons¹⁸⁷; and NRG/ErbB4 signaling modulates glutamatergic transmission in dopaminergic neurons, enhancing mGluR1-dependent long-term depression¹⁸⁸. In line with the described alterations in dopamine metabolism and firing, behaviors that involve dopaminergic signaling are impaired in these NRG and ErbB4 model mice (hedonic behavior, sensorimotor gating, working and reference memory, associative learning, social interaction and hypersensitivity to amphetamine)^{135, 143, 169, 182}; some improve after antipsychotic dopamine-targeting drug treatment^{135, 143}. Taken together, although many questions remain, evidence has emerged

implicating NRG/ErbB4 signaling in regulating dopamine homeostasis and function, positioning the pathway uniquely at the interplay between GABAergic/glutamatergic and dopaminergic neurotransmission in schizophrenia¹⁸⁹.

1.4 ErbB4 isoforms

1.4.1 Alternative splicing of ErbB4

Four alternative isoforms of the ErbB4 receptor are generated by tissue-specific alternate splicing of single exons^{190, 191} (Fig. 1.5). In the juxtamembrane (JM) region, just upstream of the region encoding the transmembrane domain, ErbB4 variants include either the JMa (exon 16b; 75bp) or the JMb exon (exon 16a; 45bp)^{190, 192, 193}. Of note, the JMb exon is upstream to the JMa exon in the ErbB4 gene (on chromosome 1 in the mouse and chromosome 2 in humans), and only separated by an 121bp intron from the latter. On the other hand, the two cytoplasmic (Cyt) ErbB4 isoforms are the result of exon skipping in the cytoplasmic tail downstream to the region encoding the kinase domain. Cyt-1 and Cyt-2 ErbB4 transcripts differ by a 48bp exon (exon 26) that is included in Cyt-1 ErbB4 variants, but absent from Cyt-2¹⁹¹. Combinatory alternative splicing at these two loci thus creates four ErbB4 receptors: JMa/Cyt-1, JMa/Cyt-2, JMb/Cyt-1 and JMb/Cyt-2.

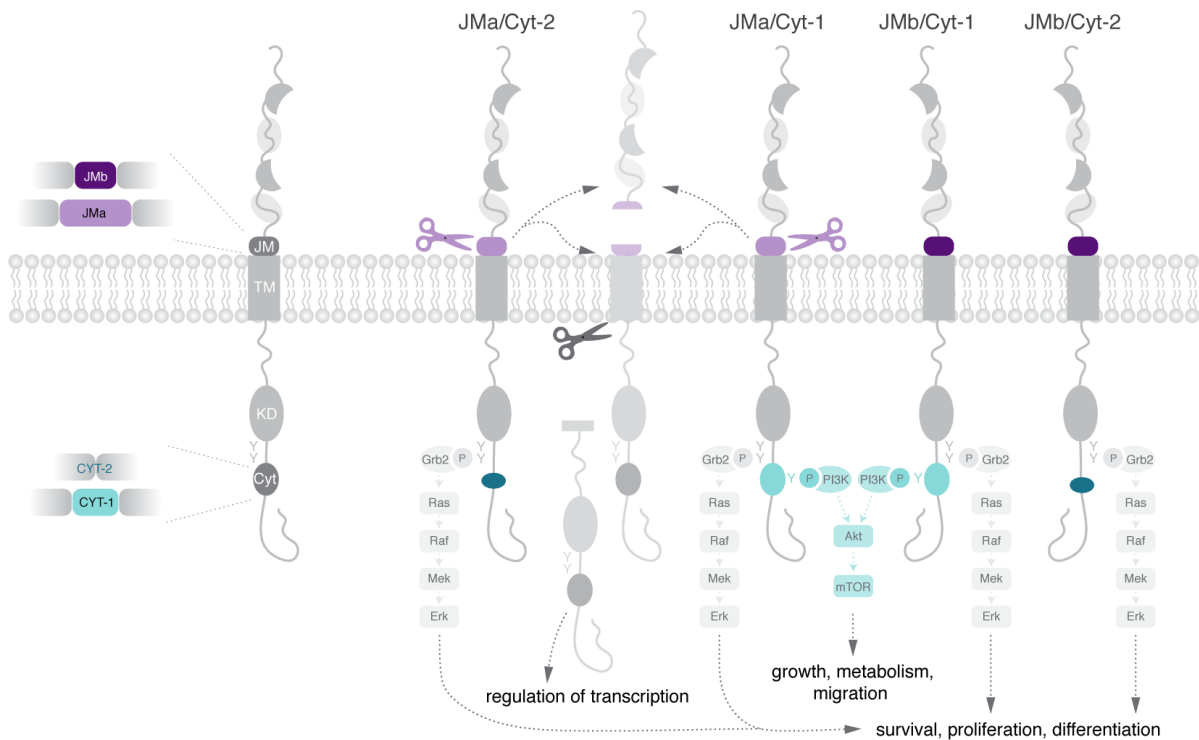


Figure 1.5 | Alternative splicing of ErbB4 and isoform-specific downstream signaling.

ErbB4 is alternatively spliced in the juxtamembrane (JM) and cytoplasmic (Cyt) region. JMa (*light violet*) and JMb (*dark violet*) exons encode juxtamembrane regions that are susceptible and resistant to metalloprotease-mediated cleavage (*light violet scissors*), respectively. Subsequent intramembrane cleavage of JMa receptors by γ -secretase (*dark scissors*) releases the intracellular domain that regulates transcription in the nucleus. The additional 48bp exon in cytoplasmic tail of Cyt-1 variants (*light turquoise*) encodes a binding domain for phosphoinositide 3-kinase (PI3K) that allows Cyt-1 receptors to activate PI3K/Akt/mTOR downstream signaling in addition to mitogen-activated protein kinase (MAPK)/Erk signaling common to all ErbB4 receptors including Cyt-2 receptors (*dark turquoise*) lacking the Cyt-1 exon. Akt – protein kinase B, Erk – extracellular signal regulated kinase, Grb2 – growth factor receptor bound protein 2, KD – kinase domain, Mek – MAPK/Erk kinase, mTOR – mammalian target of rapamycin, Raf – rapidly accelerated fibrosarcoma, TM – transmembrane. Scheme inspired by³².

1.4.2 Functional differences between ErbB4 isoforms

While the alternatively spliced exons of ErbB4 are short, ranging between 45 and 75bp, ErbB4 receptors encoded by these variants have been shown to exert fundamentally different functions in heterologous culture systems due to their unique downstream signaling mechanisms (Fig. 1.5). The juxtamembrane encoded by JMa is susceptible to metalloprotease-mediated cleavage, whereas JMb ErbB4 receptors are cleavage-resistant^{191, 194}. In heterologous cell cultures TACE and BACE1 are responsible for this cleavage releasing a 120kDa ecto-ErbB4 domain^{23, 194, 195}, calpain has been suggested to promote ischemia-induced ErbB4 breakdown¹⁹⁶ and my work has recently demonstrated that, in neuronal cultures, ADAM10 is the main secretase converting full-length ErbB4 (L. Erben *unpublished data*). Subsequent presenilin-dependent cleavage by γ -secretase within the transmembrane domain of the membrane-anchored 80kDa ErbB4 fragment releases a soluble 80kDa intracellular domain (ICD). Due to a nuclear localization signal the ErbB4 ICD is transported to the nucleus^{47, 49, 197} and possess transcriptional activity as a coactivator or corepressor by interacting with various transcription factors¹⁹⁸. For instance, ErbB4 ICD coregulates estrogen receptor α (ER α), associates with and activates STAT5A, and forms a complex with TGF-beta-activated kinase 1 and MAP3K7-binding protein 2 (TAB2) and the nuclear receptor corepressor (NCoR)^{48, 198-200}. The interaction with the coactivator Yes-associated protein (YAP) is suppressed by competitive binding of WW domain-containing oxidoreductase (WWOX)²⁰¹⁻²⁰³. Additionally, ErbB4 ICD enhances histone methylation by phosphorylating the histone methyltransferase SUV39H1²⁰⁴. Lastly, the ICD of ErbB4 also accumulates in mitochondria and acts as an apoptosis-promoting BH3-protein (B-cell lymphoma-2 homology domain 3)²⁰⁵.

The 16 amino acid sequence encoded by Cyt-1 contains binding domains for phosphoinositide-3-kinase (PI3K) and for proteins containing a WW domain (PPXY)^{191, 202}. Therefore, Cyt-1 ErbB4 receptors can directly activate PI3K/Akt signaling, whereas Cyt-2 receptors only stimulate common MAPK-mediated downstream pathways and rely on heterodimerization with ErbB3 to activate PI3K²⁰⁶ (Fig. 1.5). The presence of a third WW domain binding motif in Cyt-1 ErbB4 receptors, has been suggested to imply a stronger coupling to a subset of WW domain proteins compared to Cyt-2 receptors, particularly to a couple of E3 ubiquitin ligases (e.g. Itch (Itchy E3 ubiquitin protein ligase), Nedd4 (neuronal precursor cell expressed developmentally downregulated protein 4), WWP1 (WW domain-containing protein 1), and Nedl1 (Nedd4-like ubiquitin protein ligase 1)). Resulting mono- and poly-ubiquitinylation affects stability, endocytosis, proteasomal and lysosomal degradation and renders Cyt-1 ErbB4 receptors less stable than Cyt-2 receptors²⁰⁷⁻²¹⁰. Differences in signaling capacities also exist between the ICD of cleavable JMa/Cyt-1 and JMa/Cyt-2 receptors. Interaction of the Cyt-1-encoded ICD with the transcriptional coactivator YAP is more efficient compared to the Cyt-2-encoded ICD²⁰², and a distinct set of genes are transcriptionally regulated by the two ICDs²¹¹.

Based on the distinct downstream pathways activated by the four ErbB4 isoforms, convergent, divergent or even opposing functions have been described in heterologous and non-neuronal cell culture systems^{211, 212}. Isoform-specific functions were characterized in a variety of processes such as survival and apoptosis; chemotaxis, mobility and migration; proliferation, growth and differentiation; ubiquitination and degradation; endocytosis and subcellular localization; and phosphorylation and kinase activity itself (reviewed in²¹³). ErbB4 isoforms have been more extensively studied with regard to the proliferation and progression of different cancer types. Both up- and downregulation as well as oncogenic and tumor suppressive roles have been described and the expression of ErbB4 variants correlates with survival and the prognostic outcome of various types of cancers^{213, 214} including brain cancers²¹⁵. Lastly, the distinct activities exerted by different ErbB4 isoforms also highlight the importance for isoform-specific therapeutics to block or enhance ErbB4²¹³. A JMa-specific antibody was developed and suppresses the growth of a breast cancer cell line²¹⁶. Xenografted tumor growth has been shown to efficiently decrease by a splice-switching oligonucleotide that impedes the inclusion of the Cyt-1 exon favoring Cyt-2 variants²¹⁷.

1.4.3 Expression and role of ErbB4 isoforms in the central nervous system

In the CNS, little data is available on the expression and role of distinct ErbB4 isoforms. Analyses of ErbB4 variant expression have been confined to a few well-studied brain areas (RMS, OB, cerebellum, cortex and hippocampus). All four ErbB4 variants have been detected, with JMb (~80%) and Cyt-2 (~70%) identified as the predominant ErbB4 isoforms in the adult brain, and conserved across several species (rodents, monkeys and humans)^{59, 67, 213, 218, 219}. High expression of JMa and Cyt-1 variants, on the other hand, has been described during development and in migrating neuroblasts²¹⁹⁻²²¹. By Western blotting, the 80kDa ICD of JMa ErbB4 receptors has been detected in lysates of the cerebellum, but not in the cortex, consistent with the low expression of JMa ErbB4 in cortical tissue⁵⁸. Most of these studies were however performed by techniques (e.g. PCR approaches) that require the homogenization of the tissue and therefore do not permit the analysis of the signal distribution nor single-cell expression. To overcome this limitation one study performed laser-micro-dissection from different cortical layers of human tissue (see below)²¹⁸. Another study attempted to characterize JM variant expression in cerebellar sections using radioisotopic labeling, albeit with limited resolution, and suggested a differential expression of JM variants. JMa is preferentially expressed in cerebellar granule cells and JMb expression is high in oligodendrocytes¹⁹⁰.

Isoform-specific activities have been described by overexpression *in vitro*. In cultured neuronal progenitors, JMa/Cyt-2 and JMb/Cyt-1 ErbB4 receptor confer high migratory potential via particularly strong PI3K/Akt activation^{206, 220}. In adrenal gland pheochromocytoma PC12 cells, proliferation and neurite outgrowth is promoted by Cyt-1 and Cyt-2 ErbB4, respectively²¹³. Using transfected organotypic cultures, Cyt-1/PI3K signaling has been proposed to control the morphology and chemotaxis of migrating interneurons during embryonic development²²¹. Only one study addressed ErbB4 isoform function *in vivo*. *In utero* electroporated JMa, but not JMb-expressing ErbB4 receptors, prevented precocious astrogenesis in ErbB4 knock-out mice⁴⁸.

Interestingly, levels of ErbB4 splice variants are changed in the dorsolateral prefrontal cortex (DLPFC) of postmortem brains of schizophrenics^{28, 218, 222-224}. While changes in total expression levels of ErbB4 transcript and protein are controversial – described as either unchanged²¹⁸ or increased^{28, 222-225} – four independent studies in different ethnic populations

congruently report increased expression of the two minor JMa and Cyt-1 transcripts and concomitant reduction of JMb and Cyt-2 transcripts^{28, 218, 222-224}. Layer-specific changes were identified by laser-microdissection in layer IV of the DLPFC, where most PV-expressing basket cells reside, but not in the CR-rich layer II²¹⁸. Imbalances in ErbB4 variant expression inversely correlate with PV levels²¹⁸ and influence the severity of deficits in patients suffering from psychiatric disorders such as schizophrenia, bipolar disorder and major depressive disorder²²⁶. Inhibition of the Cyt-1 ErbB4 downstream target PI3K, itself increased in postmortem brains of patients with schizophrenia, improves amphetamine-induced hyperlocomotion and sensorimotor gating in a rat schizophrenia model²²⁴, conveying potential therapeutic value to Cyt-1/PI3K signaling.

1.5 Aims and outline of the thesis

The diverse roles of ErbB4 in regulating neurodevelopment, synaptic function and plasticity have been addressed by numerous studies and are fairly well understood (see section 1.2). However, although experiments in heterologous systems have characterized fundamentally distinct signaling mechanisms and, consequently, functions of different ErbB4 isoforms, the contribution of individual ErbB4 splice variants to ErbB4 receptor function in the CNS has been largely overlooked (see section 1.3).

Therefore, this dissertation seeks to better understand the role of ErbB4 isoforms in the brain and elaborates on the central hypothesis that ErbB4 variants are differentially expressed in the brain and encoded receptors exert unique functions. Spatiotemporal and cell type-specific regulation of ErbB4 variant expression may contribute to the variety of ErbB4 functions already described and yet to be described. ErbB4 isoforms might further diversify the potential of ErbB4 to mediate cellular mechanisms by regulating the allocation of the receptor within the cell itself. Lastly, unique downstream mechanisms of individual ErbB4 isoforms might mediate divergent biological processes, even at the same subcellular localization in the same cell. Therefore, this thesis aims to 1) characterize the expression of ErbB4 splice variants in different cell types and regions of the CNS, 2) describe subcellular distribution of ErbB4 and its isoforms in distinct neuronal cell types and 3) address the role of one ErbB4 variant (Cyt-1) *in vivo* using an isoform-specific mutant mouse.

Aim 1) Characterize the expression of ErbB4 splice variants in the CNS

Based on deficiencies in genetic labeling studies, I hypothesize that in addition to the described four main ErbB4 splice variants and a few rare variants (see below), alternate splicing also occurs in the cytoplasmic or 3' untranslated region (UTR) of the ErbB4 transcript in specific brain areas or cell types. In Chapter 2 (unpublished), using next-generation transcriptomics and PCR approaches, I therefore first examine the existence of novel variants and define the main ErbB4 splice variants in the brain to further focus on.

Common *in situ* hybridization (ISH) approaches using colorimetric, fluorescent and radioisotopic-labeled probes lack either the sensitivity or resolution to detect short sequences at cellular level. Therefore, in order to study *in situ* expression of ErbB4 splice variants, that are distinguished by short (45-75bp) single exons, I implement a sensitive, histological and quantitative approach. Chapter 3 (*Erben & Buonanno 2019*) describes the application of a novel ultrasensitive fluorescent ISH technique called BaseScope (Advanced Cell Diagnostics) and the development of an automated quantification tool for ISH signal using the open source software CellProfiler²²⁷. I then further extensively characterize and validate the sensitivity and specificity of this assay using single exon mutant mice and determine its quantitative nature and conformity to standard PCR quantitation that lacks the same single-cell resolution (Chapter 4; *Erben et al. 2018*). Finally, using these tools, I describe the expression of ErbB4 splice variants in many different brain areas and cell types of the mouse brain, as well as its relevance to the human (Chapter 4; *Erben et al. 2018*).

Aim 2) Describe subcellular targeting of ErbB4 and its isoforms in distinct neuronal cell types

Local infusion of NRG1 into the dorsal hippocampus, one of the target areas of dopamine projections, rapidly increases extracellular dopamine levels measured by reverse microdialysis¹³⁸. I conclude and hypothesize that ErbB4 mediating extracellular dopamine levels are present on axonal projections of dopamine neurons. Importantly, this is in stark contrast to the described somatodendritic restriction of the ErbB4 receptor in GABAergic interneurons⁵⁸. Using primary mesencephalic cultures and immunostainings, I confirm the presence of ErbB4 on dopaminergic axonal projections (Chapter 5; *Skirzewski et al. 2018*). Next, I ask if the targeting to axons and the difference in ErbB4 localization between

GABAergic and dopaminergic neurons is mediated by the differential targeting of ErbB4 isoforms. I address this question by viral overexpression of all four ErbB4 isoforms in cultured neurons (Chapter 5; unpublished).

Aim 3) Address the function of Cyt-1 ErbB4 in vivo using an isoform-specific mutant mouse

Cyt-1 ErbB4 transcripts comprise about 40% in the brain and ErbB4 receptors encoded by Cyt-1 uniquely activate downstream signaling through PI3K/Akt, a pathway known to regulate neuronal metabolism, neurotransmission, and neurodevelopment^{228, 229}. We therefore hypothesize that ErbB4 Cyt-1 receptors have an important role in ErbB4-mediated processes and phenotypes, and generated exon-specific mutant mice using site-specific recombination to investigate the role of Cyt-1 *in vivo*. We subject these mice to extensive molecular, behavioral, neurochemical and transcriptomic evaluation (Chapter 6; *Erben et al., in preparation*).

2

Characterization of ErbB4 splice variants in the central nervous system

This chapter is unpublished. RNA sequencing was performed in collaboration with Paul Bible and Maria Morasso (NIAMS), as well as with the NICHD Molecular Genomics Core. L.E. designed all experiments, performed experiments (except RNA sequencing), and analyzed all data.

2.1 Introduction

Before we can analyze expression and functional implications of ErbB4 splice variants in the central nervous system (CNS), we must understand how many ErbB4 splice variants exist and which are the most frequent variants in the brain. In addition to the four well characterized ErbB4 variants JMa, JMb, Cyt-1 and Cyt-2, introduced above, other less common splice variants had been described in human tissue. JMc and JMd variants lack and include both JMa and JMb exons, respectively²³⁰⁻²³² (Fig. 2.1). Due to the absence and presence of JMa-encoded sequence in JMc and JMd receptors, these isoforms are suggested to be resistant and susceptible to metalloprotease-mediated cleavage, respectively²¹³. Prevalence of both variants has been shown in the context of medulloblastoma and pilocytic astrocytoma. JMd ErbB4 has also been detected in the fetal cerebellum^{230, 232}. But no reports of JMc or JMd ErbB4 expression in normal adult tissue have been published²¹³. Moreover, an ErbB4 splice variant lacking exon 3 (del.3) producing a truncated receptor has been described in both fetal and adult human brain¹⁹³ (Fig. 2.1), but so far has not been confirmed in other species.

ErbB4 isoforms have been characterized using cloning and reverse transcription-PCR approaches confined to specific areas of the transcript^{190, 191, 193, 230, 232}; thorough splice variant

analysis using next-generation sequencing approaches across the whole ErbB4 gene has not been reported. As outlined below in detail, inconsistent labeling of ErbB4 positive cells in an ErbB4 reporter mouse line, led us to hypothesize that further uncharacterized ErbB4 splice variants – presumably in the cytoplasmic or 3' untranslated region (UTR) of the transcript – might exist, and we set out to clarify splicing of ErbB4 in the CNS by next-generation RNA sequencing.

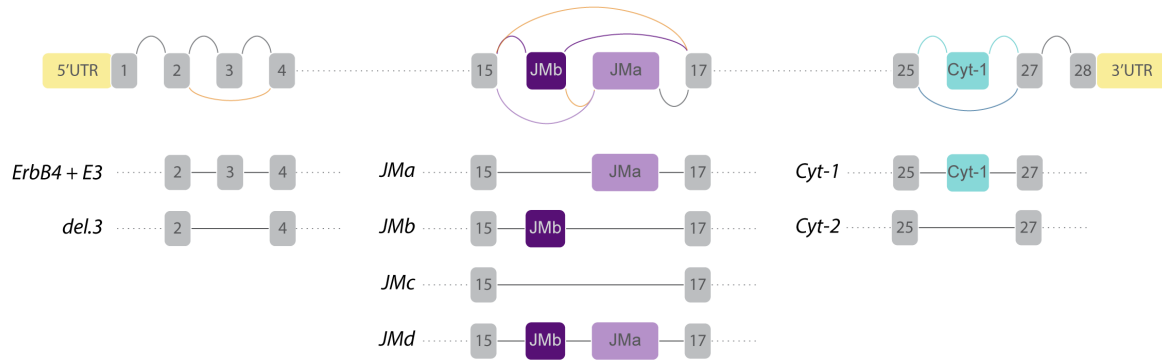


Figure 2.1 | Splicing scheme of ErbB4.

ErbB4 is encoded by a total of 29 individual exons. Alternative splicing indicated by colored connecting lines was described for exon 3 (inclusion or omission), in the juxtamembrane (JM) region for the exons JMa (light purple) and JMb (dark purple) and the cytoplasmic (Cyt) region for the Cyt-1 exon 26 (light turquoise; inclusion or omission). Note, that the JMb exon is encoded upstream to the JMa-encoding exon in the genome. Common JM splice variants are JMa (JMa exon only) and JMb (JMb exon only), whereas JMc (neither JMa nor JMb exon) and JMd (both JMa and JMb exons) are rare ErbB4 splice variants.

Inconformity of labeled cells in ErbB4 reporter mice with ErbB4-expressing cells

ErbB4::CreERT2 mice expressing inducible Cre recombinase under the control of endogenous ErbB4 promoter were generated to characterize the expression of ErbB4 in the mouse brain⁵⁷. Tamoxifen-inducible estrogen receptor (ERT2) Cre recombinase fusion protein was inserted at the 3' coding end of ErbB4, directly downstream to the stop codon of ErbB4 and separated from ErbB4 by a ribosomal 2A skip, allowing ErbB4 and CreERT2 to be expressed as separate proteins^{57, 233}. ErbB4 reporter mice were then obtained by crossing ErbB4::CreERT2 mice to Rosa::LSL-tdTomato mice and express tdTomato in ErbB4-expressing cells upon tamoxifen induction^{57, 233}. In many brain regions (e.g. cortex, hippocampus, amygdala, thalamus), ErbB4 reporter mice express tdTomato faithfully in previously characterized or co-labeled ErbB4-expressing cells^{57, 233}. However, only a fraction of dopaminergic neurons (7-22%) in the ventral tegmental area (VTA) and the substantia nigra pars compacta (SNc) was labeled by tdTomato

in these mice, in stark contrast to the previously observed 80-99% of dopaminergic neurons expressing ErbB4 mRNA^{53, 57, 77, 234}. A similar discrepancy was observed in the reticular thalamic nucleus (Rtn) that has been shown to express high levels of ErbB4^{50, 56, 123, 235}, but only a few cells in the ventral tier appeared to be positive in the reporter mice⁵⁷ (I. Karavanova *unpublished data*). While differences in the percentage of ErbB4-positive cells can result from different approaches used and ErbB4 reporter mouse might underestimate the number of ErbB4-positive cells^{57, 233}, the disparities in the VTA/SNc and Rtn are dramatic and are unlikely the result of technical limitations of the approach. Differences in ErbB4 transcription or translation particularly in these two neuronal population, could result in a lower than expected percentage of positive cells. Among other possible explanations, the usage of an alternative stop codon would affect the transcription of Cre recombinase inserted downstream to the characterized stop codon and ultimately result in the absence of tdTomato signal. Therefore, we posited that one or multiple uncharacterized alternatively spliced transcripts in the 3' region of ErbB4 exist in some cells, including dopaminergic neurons and GABAergic reticular thalamic neurons, and impede functional expression of Cre recombinase in ErbB4 reporter mice.

2.2 Methods

Animals. Adult wild-type C57BL/6J mice were purchased from the Jackson laboratories. Cyt-1 mutant mice were generated by site-specific recombination in embryonic stem cells on C57BL/6J background (see Chapter 6). Adult male and female C57BL/6J mice and wild-type (WT) littermates from heterozygote Cyt-1 mutant breeding pairs were used for ErbB4 splice variant analyses. All animals were housed on a 12–12h light-dark schedule with access to food and water *ad libitum*. Animal procedures were reviewed and approved by the NIH Animal Care and Use Committee.

RNA isolation. RNA isolation as well as downstream RNA sequencing was conducted in two cohorts. Wild-type mice (male 2-14-months-old C57BL/6J; first cohort) and wild-type littermates of Cyt-1 mutant mice (on C57BL/6J background, male and female 10-week-old; second cohort) were euthanized by an overdose of isoflurane or cervical dislocation, respectively. Brains were dissected and briefly washed with 1x RNase-free phosphate-buffered saline (PBS; Gibco, Cat No. 100010-023). 2mm-thick sections were cut using a brain matrix

(Roboz Surgical Instrument Co., Cat No. AL-1175). Micro-tissue punches (1mm diameter; Harris Micro-Punch, US Pat No. 7093508) from prefrontal cortex (PFC), dorsal hippocampus (dHpp), reticular thalamic nucleus (Rtn) and ventral tegmental area (VTA) were collected bilaterally (one punch per area and hemisphere; ~1-2mg tissue per sample) and stored at -80°C until further processing. For the first cohort, samples were pooled from 4 (PFC and dHpp samples) or 10 (Rtn and VTA samples) animals to reduce inter-sample variability. RNA was isolated using 200 and 500µl of TRI Reagent (Thermo Fisher, Cat No. AM9738) according to manufacturer's protocol, respectively. DNA was subsequently degraded using DNA-free DNA removal kit (Thermo Fisher, Cat No. AM1906). RNA yield was 4.2-8.5µg and RNA integrity was measured at an Agilent RNA 6000 Nano kit and bioanalyzer (Agilent Technologies, Cat No. 5067-1511) and ranged from 7.5 to 8.8. For the second cohort (wild-type littermates of Cyt-1 mutant mice on C57BL/6J background; 3 dHpp and 3 VTA samples), samples of three individual mice of both sexes and different collection days were pooled prior to RNA isolation. RNA was isolated using 500µl TRI Reagent Kit (Thermo Fisher, Cat No. AM9738) following manufacturer's protocol until phase separation. ~80% of the aqueous phase was then mixed with one volume of 70% ethanol and transferred to RNeasy MinElute spin column (Qiagen; Cat No. 74004) to enrich for mRNAs >200 nucleotides excluding 5.8 ribosomal RNA (rRNA), 5S RNA and transfer RNAs (tRNA). RNA was treated with DNase I and purified according to cleanup protocol from RNeasy Micro Kit (Qiagen, Cat No. 74004). RNA yield varied between 2.0 and 4.9µg for dHpp samples and 1.3-2.0µg for VTA samples. RNA integrity measured using Agilent RNA 6000 Nano Kit (Agilent Technologies, Cat No. 5067-1511) ranged between 8.7 and 9.1.

End-point reverse transcription PCR. Complementary DNA (cDNA) was synthesized in a total volume of 20µl according to manufacturer's protocol, using 1µg RNA template, 200U SuperScript IV Reverse Transcriptase (Thermo Fisher, Cat No. 18090010), 40U RNaseOUT (Thermo Fisher, Cat No. 10777019), 0.5mM dNTPs, 2.5µM random hexamers, 5mM dichlorodiphenyltrichloroethane (DDT) in SuperScript IV (SSIV) buffer for 20min at 55°C. A gene specific primer (5'-CAGCTAACTTTG-3'; Integrated DNA technologies) binding to the 3'UTR of ErbB4 was added at 0.2µM to favor amplification of the 3'UTR of ErbB4. Long template PCR was run with the Expand Long Template PCR system (Roche, Cat No. 11681834001). 18.75ng of cDNA was amplified with 11.25U of polymerase, 0.5mM dNTPs

and 0.3 μ M of each primer (primer pairs listed in Table 2.1; Integrated DNA technologies) in buffer 3, containing 2.75mM magnesium, and a total volume of 15 μ l. After two minutes of initial denaturation at 95°C, 35 cycles of 20sec denaturation at 92°C, 30sec annealing at 60.7°C and 4min elongation at 68°C were performed, before a final 7min-elongation at 68°C. 5 μ l of PCR products were separated on a 1% agarose gel in tris-acetate-EDTA (TAE; Quality Biological, Cat No. 351-008-131) buffer at 100V and visualized with ethidium bromide (Invitrogen; Cat No. 15585-011) under UV light (Azure Biosystems c150 gel documentation imaged). Gene Ruler 1kb DNA ladder (Thermo Fisher, Cat No. SM0314) was used to identify band size.

Table 2.1 | Primer pairs for end-point PCR

Forward primer	Reverse primer	Position in transcript	Amplicon size [bp]
5'-GAAGACATGATGGATGCTGAGG-3'	5'-CCACACAGAAGTGTTCCTTAGC-3'	3040 (ex25) – 4883	1843/1891
5'-CCAATGCATGACAAGCCCAAAC-3'	5'-CCACACAGAAGTGTTCCTTAGC-3'	3409 (ex27) – 4883	1474
5'-TACTGGAGAAAGGAGAGCGTCT-3'	5'-CTTGCAATCCTTCACACAGAGC-3'	2795 (ex23) – 5291	2496/2545
5'-GAAGACATGATGGATGCTGAGG-3'	5'-CTTGCAATCCTTCACACAGAGC-3'	3040 (ex25) – 5291	2251/2299
5'-CCAATGCATGACAAGCCCAAAC-3'	5'-CTTGCAATCCTTCACACAGAGC-3'	3409 (ex27) – 5291	1883
5'-GCTCTGTGTGAAGGAATGCAAG-3'	5'-TGAATTGCCTGTTCTTTCTGG-3'	5269 – 9843	4574
5'-CTAGTACATGTAGTTCGTACGG-3'	5'-CATGTAACAAAAAGGCAGAACAG-3'	7799 – 311673	3874

Sequence of primer pairs amplifying 3'terminal regions of ErbB4 transcripts. Position in transcript relative to start codon in JMa/Cyt-2 transcript, if coding sequence exon (ex) number is indicated.

RNA sequencing. For the first RNA sequencing cohort, poly-A-mRNA library was extracted from 1 μ g total RNA, fragmented and cDNA synthesized using NEBNext Ultra RNA Library Prep Kit for Illumina (New England BioLabs, Cat No. E7530). cDNA was amplified, adapter-ligated using Mondrian Ovation SP Ultralow system (NuGEN, Cat No. 0344) and sequenced on an Illumina HiSeq2000. 30-60 million 50bp paired-end reads were obtained per sample and mapped to mouse genome mm10 using Tophat (version 2.1.0) software²³⁶. Expression in rpkm (reads per kilobase of transcript, per million mapped reads) was calculated with Partek Genomics Suite (version 6.6). The library for the second sequencing cohort was constructed from 1 μ g total RNA using TruSeq Standard mRNA Library Preparation kit (Illumina, Cat No. 20020594) with polyA-enrichment. Each library was barcoded; equal amounts were combined and sequenced on an Illumina HiSeq 2500 system yielding 35-40 million paired-end reads (2x100b) per sample. Reads were aligned to the mouse genome (GENCODE mouse release

16) using RNA-STAR (version 2.6.1)²³⁷. Gene-based read quantitation was analyzed using featureCounts (version 1.6.3) with the following options (-O, -M, -g, gene_name)²³⁸. Integrative Genomics Viewer²³⁹ was used to visualize Sashimi Plots. Percent spliced in (Psi) was calculated as $\Psi = \frac{IR}{IR + ER}$, where IR is inclusion reads and ER is exclusion reads.

2.3 Results

2.3.1 Alternative splicing of ErbB4 transcripts is confined to previously characterized splice sites

In order to explore the possibility of uncharacterized alternative ErbB4 splicing in the 3' region of the gene, I isolated RNA from two brain regions with underrepresented labeling in ErbB4 reporter mice, the reticular thalamic nucleus (Rtn) and the dopaminergic ventral tegmental area (VTA), as well as from two control areas with well-characterized ErbB4 expression on GABAergic interneurons that were faithfully labeled in ErbB4 reporter mice, the prefrontal cortex (PFC) and dorsal hippocampus (dHpp). As 3' RACE (rapid amplification of cDNA ends), a common approach to identify transcript variants particularly at the 3' end of transcripts, would have been challenging due to the large size of the ErbB4 transcript (12037bp JMa/Cyt-2 variant) and the 3' untranslated region (UTR; 7855bp) itself, I resorted to end-point PCR and subsequent agarose gel analysis.

cDNA was enriched for the 3' end of ErbB4 transcripts using a mix of random hexamers and a gene-specific primer binding to the 3'UTR for reverse transcription. Multiple primer pairs designed to amplify ErbB4 transcripts spanning from exons 26, 27 or 28 into the 3'UTR were tested (see Table 2.1). Reverse primers targeting the 3'UTR were designed against evolutionary conserved regions (ECR; as defined by analysis with the ECR Browser²⁴⁰) that could potentially have functional importance (e.g. contain a coding exon). Using Expand Long template PCR, I was able to amplify fragments up to 4574bp in length. However, I did not observe shorter PCR products than those expected from the known untranslated 3'UTR, that would indicate a skipped intron and a potential new splice junction between the two primer-targeted regions (example in Fig. 2.2; see full list of successfully tested primers in Table 2.1). No differences were detected between the four brain areas analyzed. A disadvantage of this

approach is that it only allows the identification of splice junctions if a primer pair is designed to target transcribed exons before and after the putative splice junction.

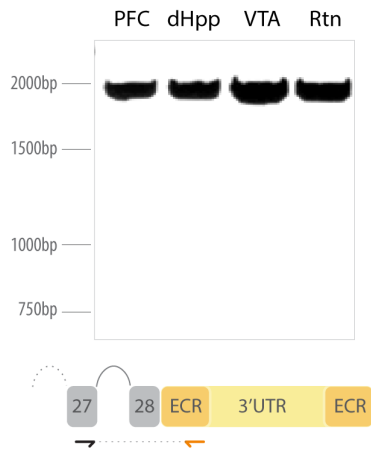


Figure 2.2 | Example of end-point PCR analysis of the 3' end of the ErbB4 transcript.

Amplification of an 1883bp region from exon 27 spanning into 3'UTR, primer location indicated in scheme. dHpp – dorsal hippocampus, ECR – evolutionary conserved region, PFC – prefrontal cortex, Rtn – reticular thalamic nucleus, VTA – ventral tegmental area.

To perform a global splice variant analysis for ErbB4, I therefore subjected the samples to whole genome RNA sequencing. Splice variant analysis of intron-spanning reads using Sashimi plots confirmed that there are no alternatively-spliced exons in the 3' region other than differential Cyt-1/Cyt-2 splicing in any of the samples analyzed (Fig. 2.3B). Next, I analyzed exon junctions across the whole ErbB4 transcript. While most identified splice junctions (total >30.000 reads for ErbB4 in all samples) either indicated conserved splice junctions or known alternatively spliced variants, occasionally, exon skipping was observed (for exon 2, 9, 15 and 19; total 7 reads from all samples) and a few reads were detected that aligned as intron-spanning reads between known exons and intronic regions within the ErbB4 gene (total 13 reads from all samples; see e.g. Fig. 2.3B third VTA sample). These reads were mostly individual events and did not reproduce between different samples. However, most intronic splice acceptor and donor sites of these intron-spanning reads were canonical (92%), likely excluding common sequencing artefacts introduced by reverse transcription or amplification²⁴¹⁻²⁴³. The low prevalence of these splice sites (<0.05%) and no reproducibility between samples suggests that these are individual mis-spliced events, errors introduced by the spliceosome without functional significance²⁴⁴, rather than uncharacterized alternative splice sites.

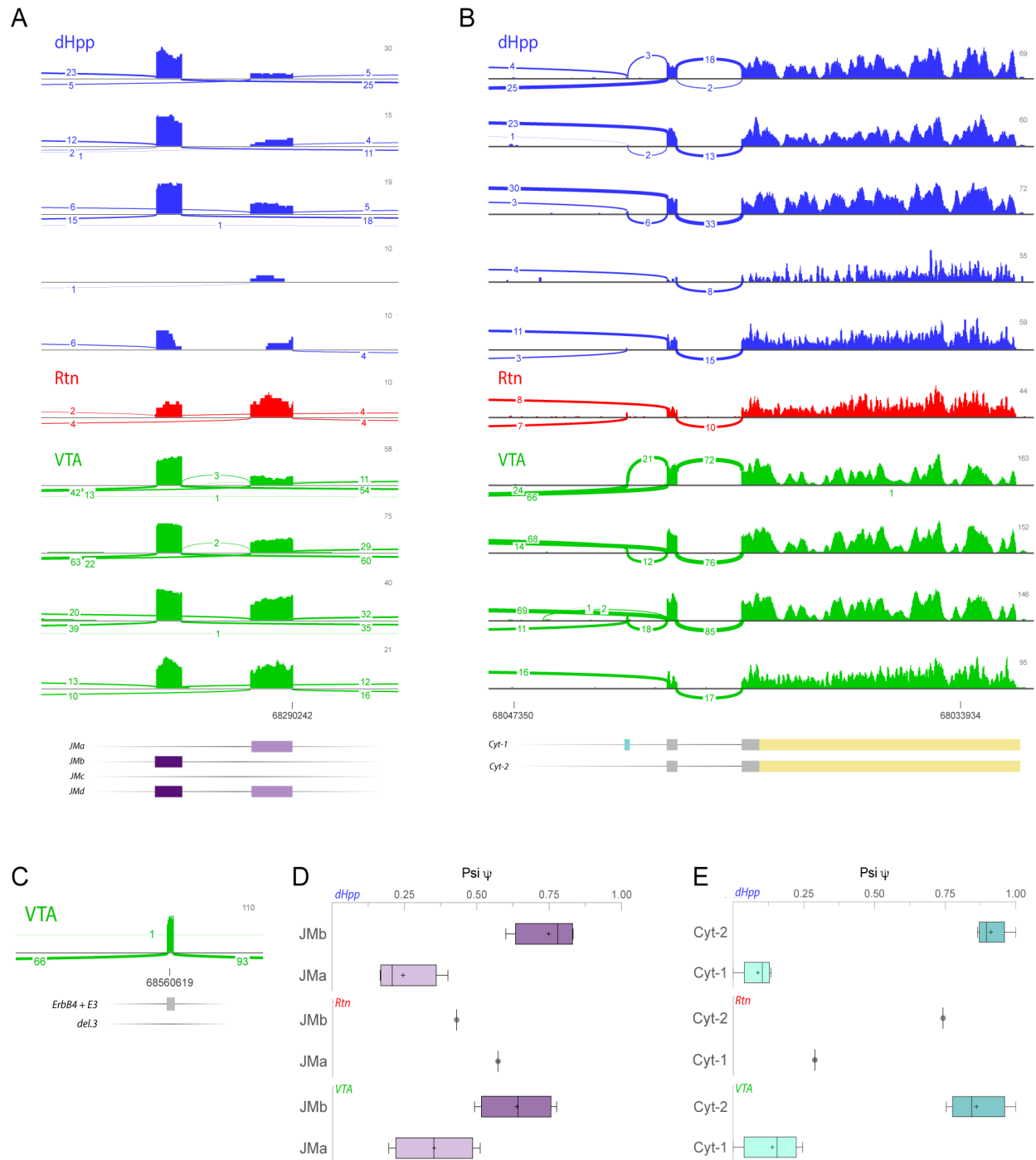


Figure 2.3 | Analysis of ErbB4 splice variants in the mouse brain by RNA sequencing.

(A, B) Sashimi plot and read densities of ErbB4 juxtamembrane exons JMa and JMb (A) and the cytoplasmic region including 3'UTR (untranslated region) (B). RNA was isolated from tissue micro-punches from dorsal hippocampus (dHpp; blue; n=5), reticular thalamic nucleus (Rtn; red; n=1) and ventral tegmental area (VTA; green; n=4) and subjected to Illumina whole genome RNA sequencing. Sashimi plot of intron-spanning reads identifies JMc and JMd ErbB4 splice variants (A) and does not suggest for alternative splicing (other than Cyt-1. Cyt-2) at the C-terminal end or 3'UTR (B). (C) Sashimi plot and read densities of ErbB4 exon 3 confirms existence of del.3 variant. Scale indicated by grey numbers in upper right corner of tracks. (D, E) Per-sliced in (Psi, Ψ) of JMa/JMb (D) and Cyt-1/Cyt-2 (E) ErbB4 splice variants in dHpp (n=4,5), Rtn (n=1) and VTA (n=4).

2.3.2 Detection of rare ErbB4 splice variants in the adult mouse brain

Interestingly, the detailed analysis of ErbB4 splice junctions revealed evidence for the previously described juxtamembrane splice variants JMc and JMd (Fig. 2.3A), that omit and include both juxtamembrane exons JMa and JMb, respectively. These variants were rare, JMc and JMd variants only accounted for about 0.5 and 0.9% of all juxtamembrane splice variants. However, to my knowledge, this is the first report of JMc and JMd variants in the adult healthy brain²¹³. Lastly, I also identified one read spanning the exon boundary exon 2/exon 4. This suggests that the del.3 variant previously described in the human brain, might also exist in the mouse brain, albeit at significant lower levels than the described (~37%) in the adult human brain¹⁹³.

2.3.3 Ratios of juxtamembrane JMa/JMb and cytoplasmic Cyt-1/Cyt-2 variants

I also explored the RNA sequencing data regarding differences in expression of the four common ErbB4 splice variants (JMa, JMb, Cyt-1 and Cyt-2) in distinct brain areas. Percent spliced in (Psi, Ψ) was calculated for the common ErbB4 splice variants JMa, JMb (Fig. 2.3D) and Cyt-1, Cyt-2 (Fig. 2.3E). No significant differences between the three brain areas analyzed (dHpp, Rtn, VTA) were detected. Cyt-2 was the prevalent isoform in all areas analyzed (dHpp $\Psi=0.91\pm 0.02$, Rtn $\Psi=0.72$, VTA $\Psi=0.86\pm 0.05$). JMb was predominant in both dHpp ($\Psi=0.74\pm 0.05$) and VTA ($\Psi=0.63\pm 0.06$), whereas more reads for the JMa than for the JMb splice variant were detected in the Rtn ($\Psi=0.57$). Of note only one Rtn sample has been tested and junction reads might not have been sufficient. In sum, ErbB4 JMa/JMb and Cyt-1/Cyt-2 ratios analyzed by RNA sequencing are similar in the dHpp and VTA.

2.4 Discussion

In conclusion, my extensive studies using end-point PCR and RNA sequencing confirmed previously reported ErbB4 splice variants and showed first time evidence for the expression of the rare ErbB4 splice variants JMc, JMd and del.3 in the adult mouse brain. No additional variants in the 3' region or elsewhere in the transcript were identified with this approach. As the detected rare ErbB4 splice variants account only for a small fraction of all ErbB4 transcripts (<1%), and JMc and JMd variants are functionally comparable to JMb and JMa variants²¹³,

respectively, I will concentrate my further analyses regarding expression and functional contribution on the four main ErbB4 splice variants: JMa, JMb, Cyt-1 and Cyt-2.

The data suggests that alternative splicing is not interfering with the expression of Cre recombinase in ErbB4 reporter mice. At this moment, we do not have a good explanation why in some neurons, most notably dopaminergic neurons and GABAergic neurons in the Rtn, the reporter mice fail to identify ErbB4-expressing cells. However, it is possible that bioavailability of tamoxifen, tdTomato protein stability, expression level, subcellular distribution of Cre recombinase or accessibility of floxed targets^{57, 233} might be different in these brain areas. Preliminary multiplex *in situ* hybridization experiments on sections from tamoxifen-injected *ErbB4::CreERT2* mice identified expression of Cre mRNA, albeit low, in ErbB4-expressing tyrosine hydroxylase-positive dopaminergic neurons in the VTA (L. Erben, *unpublished data*). While the detected Cre transcripts could be out-of-frame, tracing experiments by stereotaxic injections of Cre-dependent adeno-associated viruses (AAVs) expressing fluorescent proteins, suggest the expression of functional Cre recombinase in VTA dopaminergic neurons of *ErbB4::CreERT2* mice²⁴⁵. Therefore, recombination or stability issues of the target, tdTomato, are most conceivable. Of note, although in the Rtn and VTA the discrepancy between the reporter mice and previously observed expression levels are striking, expression is also inconsistent and underestimated in other areas. For instance, in the cortex and hippocampus, recent data suggests that almost all GABAergic interneurons are ErbB4-positive⁶⁰ (L. Erben & I. Karavanova *unpublished data*), whereas in the reporter mice only a subgroup of GAD-green fluorescent protein (GFP) cells (60-80%) were labeled with tdTomato^{57, 233}. I also observed wide-spread ErbB4 mRNA expression in the corpus callosum and choroid plexus (see Chapter 4) exceeding that detected with the reporter mice. This suggest a general underestimation of ErbB4 expression in the ErbB4 reporter mice that appears to be more severe in some brain regions than in others.

Interestingly, ratios of juxtamembrane and cytoplasmic ErbB4 splice variants were similar in the three areas analyzed. However, two important questions remain unanswered. Firstly, short-read sequencing does not allow any conclusion with regard to the combination of alternative spliced variants at the two splice sites JM and Cyt that are 1189bp apart. While tissue-specific ErbB4 isoform expression suggests that all combinations JMa/Cyt-1, JMa/Cyt-2, JMb/Cyt-1 and JMb/Cyt-2 are possible²¹³, little information is available if the regulation of

the two splice sites is coordinated or independent; or which JM/Cyt transcripts are generated in the brain. It would be interesting to perform costlier long-read RNA sequencing that allows for sequencing of up to 2000bp (Pacific Biosciences or Oxford Nanopore Technologies^{246, 247}). Alternatively, specifically designed end-point PCRs could give insights¹⁹³. Second, it is also unclear, how ErbB4 variants are distributed in distinct cell types expressing ErbB4 in the brain areas analyzed and if the two JM (JMa and JMb) and Cyt (Cyt-1 and Cyt-2) variants are co-expressed in a single cell. In the hippocampus and cortex most ErbB4 expression arises from GABAergic interneurons^{54, 58} and the detected isoform ratios should be similar in GABAergic interneurons themselves. The VTA is a heterogenous region that includes ErbB4-expressing GABAergic and dopaminergic neurons^{53, 57}. Both whole genome RNA sequencing from purified cell types (e.g. by panning or fluorescence activated cell sorting (FACS) from cell-type specific transgenic GFP mice²⁴⁸) or single-cell RNA sequencing could provide information about alternative splicing in these distinct cell types. Single-cell RNA sequencing for splice variant analyses however is technologically limited especially for low abundance transcripts²⁴³. Moreover, sequencing approaches are in general either restricted to a small brain region or only provide unspecific global information; and importantly do not maintain tissue morphology. We were interested in understanding the distribution of ErbB4 isoforms beyond a few brain areas, and therefore resorted to a novel exon-specific *in situ* hybridization approach that allows the analysis of ErbB4 splice variants at a single-cell level across the whole brain (see Chapter 3 & 4).

3

Automated quantification of multiplex and exon-specific *in situ* hybridization signals

This chapter is the peer reviewed version of the following article: Erben Larissa & Andres Buonanno (2019) Detection and Quantification of Multiple RNA Sequences Using Emerging Ultrasensitive Fluorescent In Situ Hybridization Techniques. Curr Protoc Neurosci, 87(1) which has been published in final form at <https://currentprotocols.onlinelibrary.wiley.com/doi/epdf/10.1002/cpns.63>. This article may be used for non-commercial purposes in accordance with [Wiley Terms and Conditions for Self-Archiving](#)."

Authors contributions: L.E. and A.B. designed research, L.E. performed research, L.E. analyzed the data, L.E. and A.B. wrote the paper.

3.1 Abstract

Fluorescent detection of transcripts using RNAscope has quickly become a standard *in situ* hybridization (ISH) approach in neuroscience with over 400 publications since its introduction in 2012. RNAscope's sensitivity and specificity allow the simultaneous detection of up to three low abundance mRNAs (i.e., multiplexing) in single cells and, in contrast to other ISH techniques, RNAscope is performed in 1 day. BaseScope, a newer ultrasensitive platform, uses improved amplification chemistry of single oligonucleotide probe pairs (~50 bases). This technique allows discrimination of single nucleotide polymorphisms or splice variants that differ by short exons. A present limitation of BaseScope is that expression analysis is limited to a single gene (i.e., single-plexing). This article outlines detailed protocols for both RNAscope and BaseScope in neuronal tissue. We discuss how to perform ISH experiments using either fresh-frozen or formalin-fixed paraffin-embedded sections, as well as dissociated

cultured neurons. We also outline how to obtain quantitative data from hybridized tissue sections.

3.2 Introduction

The numerous *in situ* hybridization (ISH) approaches that have been used in the field of neuroscience for the past decade were predominantly based on the use of complementary oligonucleotides or RNA probes directly labeled with radionucleotides for radioactive detection or coupled to enzymes for colorimetric detection²⁴⁹. Those approaches had limitations, such as high background, lack of sensitivity for low abundance transcripts, long turnaround times, and analysis restricted to single gene products per section. A recent advancement to circumvent these limitations has been the development of novel chemical reagents and signal amplification techniques that, due to their nature (see Fig. 3.1), are highly specific, sensitive, easy to use, and simultaneously detect expression of several genes in single cells. The technology for these products, promoted by Thermo Fisher Scientific (ViewRNA) and Advanced Cell Diagnostics (ACD; RNAscope), is based on the hybridization of ~20 “probe pair sets.” The sequential amplification via the tail region of the probe creates independent amplification branches or trees for the detection of several transcripts that are subsequently labeled with distinct fluorophores²⁵⁰. A second related recent advancement in signal amplification enhances sensitivity to the point that a single probe pair (~50 bases) can be used for detection. Using this novel ultrasensitive ISH approach, denoted as BaseScope (ACD), it is possible to investigate at the single-cell level in tissue the expression of previously undetectable RNAs that differ by short nucleotide stretches or single bases, such as splice variants that vary by short exons (<50 bases), non-coding RNAs, and single nucleotide polymorphisms^{234, 251}. Because of the extreme heterogeneity of neural cells and transcriptome complexity of the brain, and the aforementioned simplicity and fast turnaround time of RNAscope/ ViewRNA, these approaches are rapidly becoming the methods of choice to study the co-expression of genes, RNA isoforms, and polymorphism in specific neural cell types.

In this article, we describe protocols for both RNAscope (Basic Protocol 1) and BaseScope (Basic Protocol 2). These ISH assays comprise three sections: (1) pretreatment of sample depending on sample type, (2) the ISH assay itself (probe hybridization and signal amplification), and (3) detection and analysis using high-resolution fluorescent images (20 to

63x). Additionally, we provide a protocol for the combination of ISH and immunohistochemistry (Basic Protocol 3), and a detailed description of step-by-step analysis of ISH signal applicable for ISH assays beyond those described in this article (Basic Protocol 4). An overview of the protocols (Fig. 3.1) and short print-out of the protocols covered in this article (Fig. 3.2) are provided as convenient guides to users.

NOTE: All protocols using animal or human tissue must first be reviewed and approved by an Institutional Animal Care and Use Committee (IACUC) and must follow officially approved procedures for the care and use of animals.

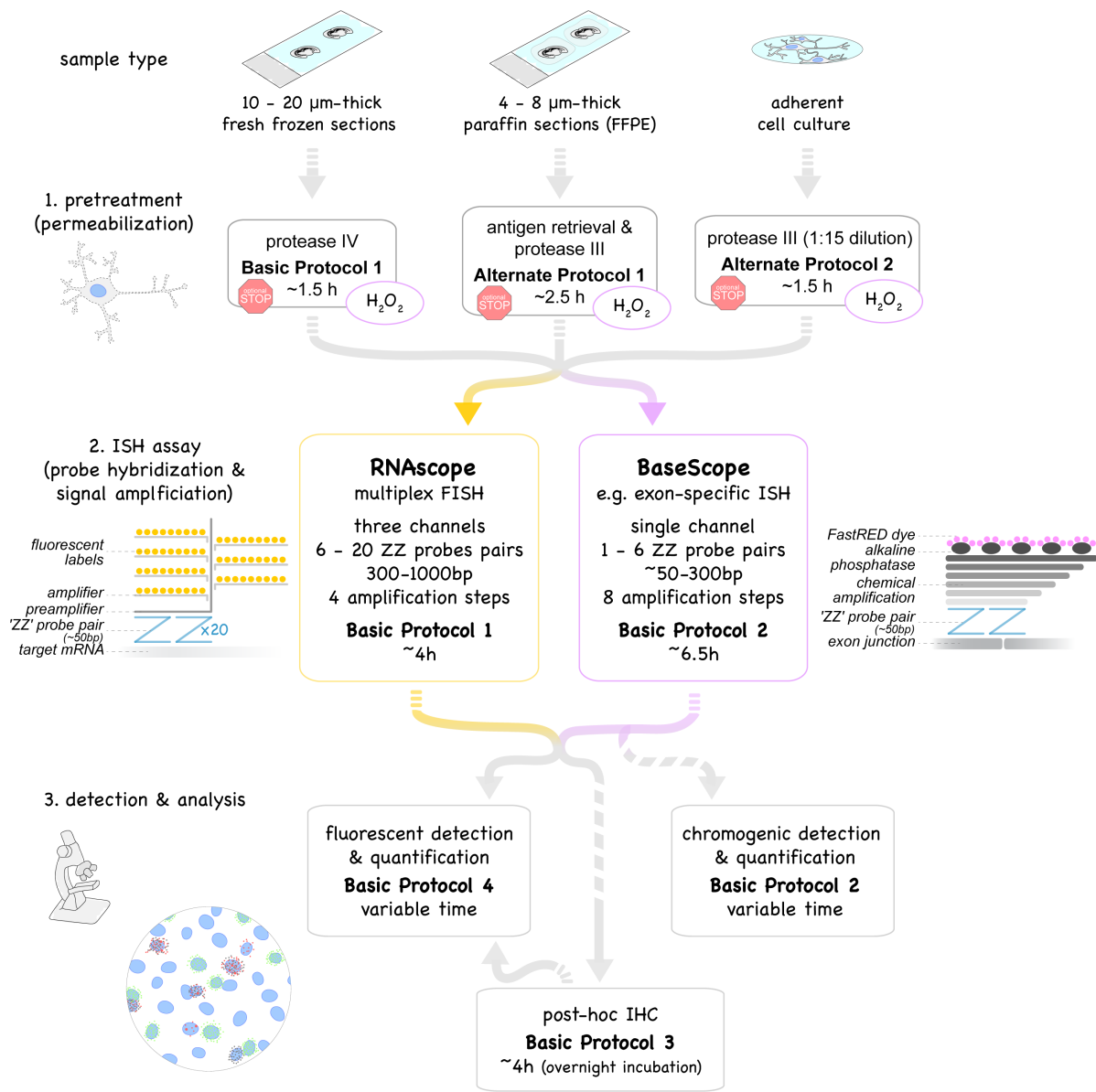


Figure 3.1 | Overview of protocols described in this article.

Multiplex fluorescent *in situ* hybridization, RNAscope (*yellow box*, Basic Protocol 1) and exon-specific *in situ* hybridization, BaseScope (*purple box*, Basic Protocol 2) use probe pairs (called “ZZ” pairs) each targeting about 50 bases of target mRNA. While RNAscope uses 6-20 ZZ pairs (targeting ~300-1000 bases), improved signal amplification allows BaseScope assays to target short RNA sequences (50-300 bases) by using only 1-6 ZZ probe pairs. Signal amplification of both assays are schematically represented and involve 4 and 8 amplification steps, respectively. Fluorescent labels in RNAscope are detected using a fluorescent microscope (Basic Protocol 1). The FastRED dye used in BaseScope and converted by alkaline phosphatase is both visible under fluorescent and light microscope (Basic Protocol 2). Both RNAscope and BaseScope are compatible with different sample types: 10-20µm thick fresh-frozen sections (Basic Protocol 1), 4-8µm thick formalin-fixed paraffin-embedded (FFPE) sections (Alternate Protocol 1) and adherent cell cultures such as neuronal cultures (Alternate Protocol 2). Pretreatment and permeabilization to allow the probes to perfuse into the tissue to the target RNA need to be adjusted accordingly. BaseScope assays require an additional pretreatment step with H₂O₂ to saturate endogenous peroxidase activity (*purple circles*). Protocols can be interrupted at optional stopping points during pretreatments (*red stop sign*). Post-assay immunostaining (Basic Protocol 3) is optional.

3.3 Strategic Planning: Probe Design

While probes are designed by the vendor, investigators need to consider a couple of important points, as discussed below, before requesting probes that are either synthesized by the vendor or purchased as an already existing probe from the catalog. First and foremost, both RNAscope and BaseScope probes need to be comprised of antisense sequences that perfectly match the RNA sequence of the species under investigation. No additional planning for channel consideration is required for single-plex BaseScope, but further steps are required to combine the different RNAscope probes effectively.

The relative abundance of the targeted RNAs, the sensitivity of the different channels, and background fluorescence need to be considered (see Fig. 3.3). Probes designed for use in Channel 1 are most sensitive, closely followed by Channel 3. Hybridization signals, which appear as dots, are also slightly larger for Channel 1 probes relative to probes on other channels. For these reasons, we regularly assign probes targeting the lower abundance transcripts – frequently our genes of interest – to Channel 1. Probes on Channel 2 show the lowest sensitivity and we therefore assign probes targeting the most abundant transcripts to this channel (e.g., cell type-specific markers). Depending on which Amplification solution 4 is used, the assignment of three different fluorophores, Alexa488, Atto550, and Atto647, can be switched between the three channels (see Fig. 3.3). Based on our experience, we recommend using AMP4B for standard applications that result in detection of Atto550 (red fluorescence) on Channel 1, Alexa488 (green fluorescence) on Channel 2, and Atto6447 (far-red fluorescence) on Channel 3. However, it is important to remember that autofluorescence from accumulated

lipofuscin granules or fixatives is most prominent in the green fluorescent range^{252, 253}. The use of tissue from younger animals ameliorates autofluorescence artifacts associated with lipofuscin accumulation²⁵⁴.

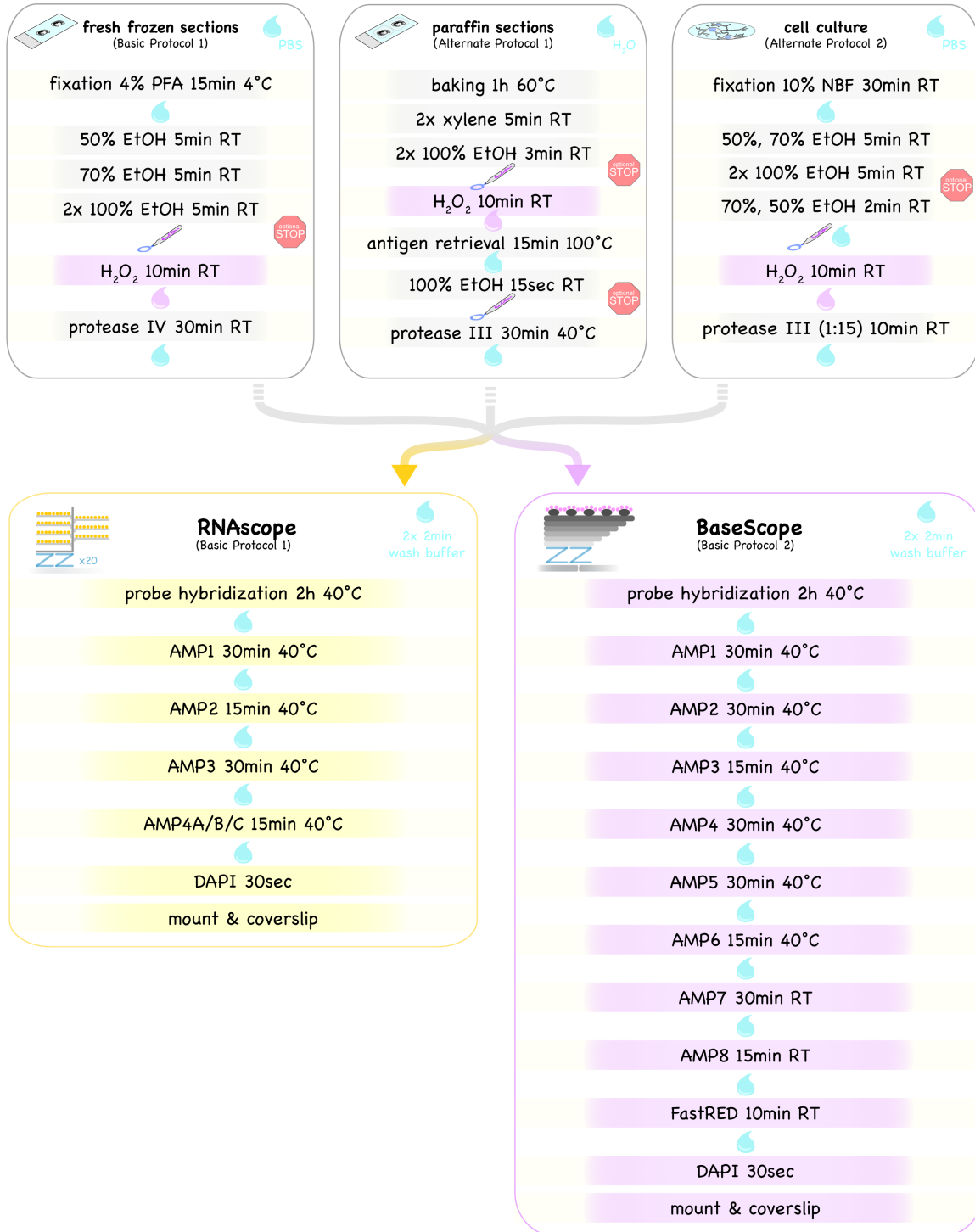


Figure 3.2 | Short print-out protocol for RNAscope and BaseScope assays on fresh-frozen and paraffin sections as well as on adherent cell culture samples.

For detailed protocols please refer to the text. Drops illustrate washing steps of varying lengths with indicated solutions, and the pen indicates the drawing of the hydrophobic barrier. The BaseScope assay requires an additional H₂O₂ pretreatment step (highlighted in *light violet* in top panels). Protocols can be paused (*red stop signs*). RT, room temperature.

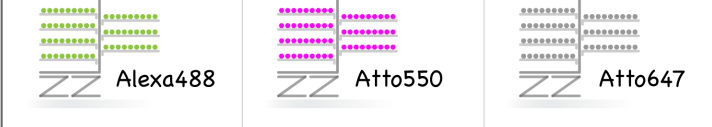
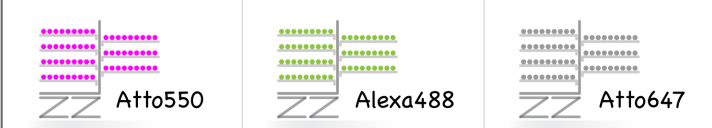

probe channel	Channel 1 (C1)	Channel 2 (C2)	Channel 3 (C3)
channel sensitivity	highest	weakest	high
cell type analysis of target gene expression	gene of interest	cell type marker 1 (e.g. vGLUT1/2)	cell type marker 2 (e.g. GAD1/2)
AMP4A			
AMP4B (recommended)			
AMP4C			

Figure 3.3 | Multiplexing of the three channels in RNAscope.

Detected fluorophores of the three channels (C1, C2, C3) can be adjusted by distinct amplification solution 4 (AMP4A, AMP4B, AMP4C). The sensitivity of the three channels is C1>C2>>C3. Therefore, we recommend examining the expression of a target gene (lowest expected expression) in different cell types using a Channel 1 (C1) probe against this gene of interest and cell type-specific marker genes in Channel 2 & 3.

3.4 Basic Protocol 1: Multiplex Fluorescent *In Situ* Hybridization (RNAscope) using Fresh-Frozen Sections

The extremely high sensitivity and specificity of RNAscope is based on the probe design and the amplification of the signal²⁵⁰. The probes for each RNA target are comprised of 6 to 20 oligonucleotide pairs that are denoted as “ZZ pairs” (each oligonucleotide is 18 to 25 bases long) and each ZZ pair is complementary to ~50 contiguous bases in the targeted RNA. The hybridized ZZ probe pairs are bound by the preamplifier via a 28-base tail region that will be used for signal amplification (see Fig. 3.1). Importantly, hybridization conditions are such that stable binding of the preamplifier requires both Z probes of a pair to hybridize adjacent RNA

sequences; off-target hybridization to non-specific RNA sequences does not result in signal amplification and therefore does not contribute to non-specific hybridization. This requirement, for the physical proximity of two specific probes to generate signal, differentiates RNAscope from other traditional ISH hybridization protocols that use either labeled single oligonucleotides or cRNAs. Following binding of the preamplifiers to each of the pairs (6 to 20 ZZ pairs per targeted RNA), signal amplification is achieved in the next steps: One preamplifier binds twenty amplifiers, and in turn, each amplifier has twenty binding sites for fluorescent labels. This sequential amplification scheme can theoretically yield an 8000-fold increase in signal per target, thus allowing detection of single transcripts. Multiplexing, ergo the simultaneous detection of several gene products, is possible because the reagents used for signal amplification in each channel are unique and are ultimately labeled with distinct fluorescent labels. Basic Protocol 1 describes the use of the RNAscope assay on 10- to 20- μ m thick fresh-frozen sections; this is the preferred type of section because of its better preservation of RNA. Examples of RNAscope on fresh-frozen sections can be found in Figures 3.4 and 3.5.

NOTE: All steps up to the probe hybridization should be performed under RNase-free conditions. Channel 1 probes are provided in dropper bottles (3ml) and serve as diluent for the other channels. Channel 2 and 3 probes are provided as a 50x stock in Eppendorf tubes (60 μ l), and are diluted 50-fold into the Channel 1 probe mix.

Materials

- RNAscope reagents (ACD):

- RNAscope® fluorescent multiplex kit (ACD, cat. no. 320851)

- Pretreatment kit (ACD, cat. no. 322380)

- 50x wash buffer (ACD, cat. no. 310091)

- Target probes in three different channels for manual RNAscope assay (C1, C2, C3 species-specific; ACD)

- *Optional:* Positive and negative probes (e.g., for mouse: 3-plex positive probe, ACD, cat. no. 320881; Polr2a-C1, Ppib-C2, Ubc-C3; 3-plex negative probe bacterial DapB, ACD, cat. no. 320871)

- *Optional:* Probe diluent (ACD, cat. no. 300041)

- 10- to 20- μ m thick fresh-frozen sections on Superfrost slides (for preparation see²⁵⁵)
- RNase AWAY (e.g., Molecular BioProducts, Thermo Fisher Scientific, cat. no. MBP#7000)
- Paraformaldehyde (PFA; e.g., 16% PFA, Electron Microscopy Sciences, cat. no. 15710)
- 100% ethanol (200 proof), 50% and 70% ethanol prepared with RNase-free water
- RNase-free water (e.g., DEPC-treated water; KD Medical, cat. no. RGF-3050)
- 1x PBS (RNase-free)
- Distilled water
- Mowiol DABCO mounting medium (aqueous; see recipe)

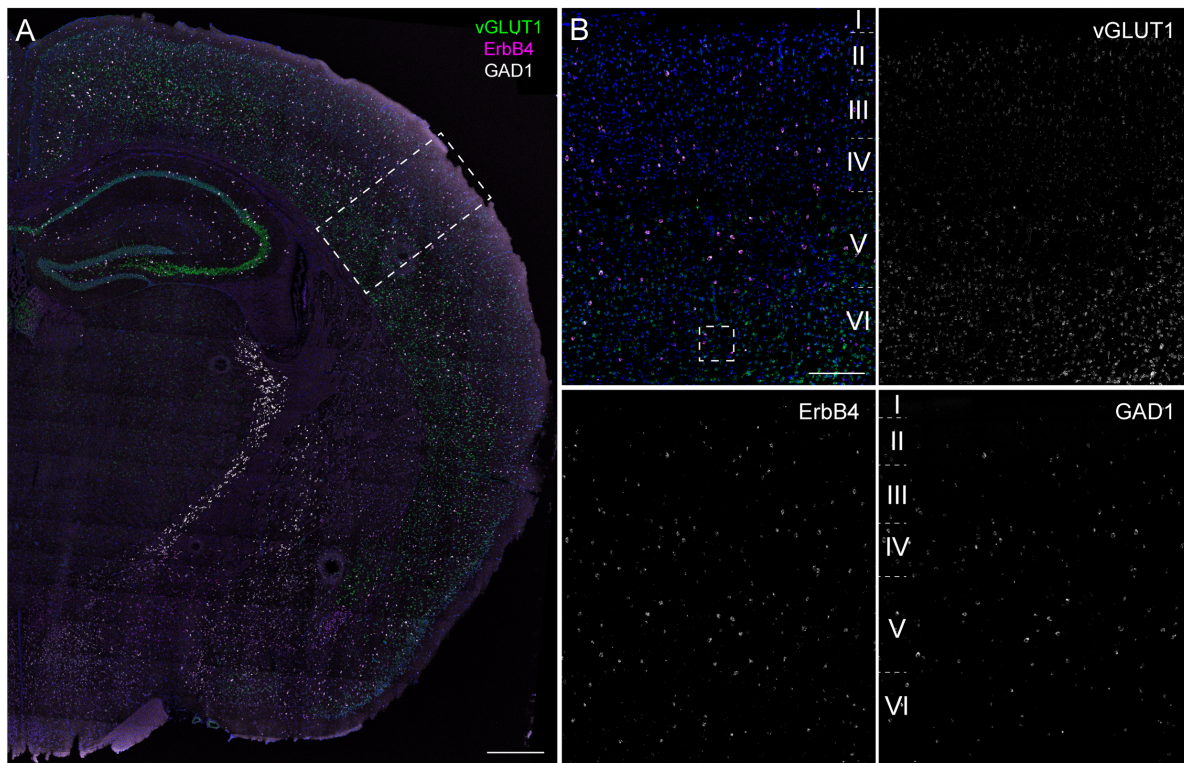


Figure 3.4 | Example for RNAscope on fresh-frozen section (Basic Protocol 1).

Expression of ErbB4 (magenta; Channel 1) was analyzed in excitatory neurons labeled by vesicular glutamate transporter 1 (vGLUT1; green; Channel 2) and in GABAergic neurons labeled by glutamate decarboxylase 1 (GAD1; white; Channel 3). (A) Overview of an adult coronal wild-type (WT; C57BL/6J) mouse brain section. (B) Magnification in the primary somatosensory cortex. Scale bars 500 μ m in A, 200 μ m in B. See Figure 3.5 for analysis.

- 8 vertical glass Coplin jars (e.g., Ted Pella, cat. no. 432-1)

- Hydrophobic barrier pen (e.g., ImmEdge hydrophobic barrier pen; Vector Laboratories, cat. no. H-4000)
- Absorbent paper (e.g., Whatman paper; GE Healthcare, cat. no. 10427804)
- Humidifying chamber (e.g., ACD, cat. no. 310012)
- Horizontal slide rack (e.g., ACD, cat. no. 310017)
- Oven (40°C; e.g., HybEZ™/ HybEZ™II Oven, 110/220 V; ACD, cat. no. 321710/20)
- Water bath (40°C)
- 1.5-ml RNase-free Eppendorf tubes
- Kimwipes (e.g., Kimtech Science Precision wipes; Kimberly-Clark Professional, cat. no. 05511)
- Cover glass (24x50 mm; e.g., Thermo Fisher Scientific, cat. no. 12-548-5M)
- Fluorescent microscope (e.g., Zeiss LSM710/780)

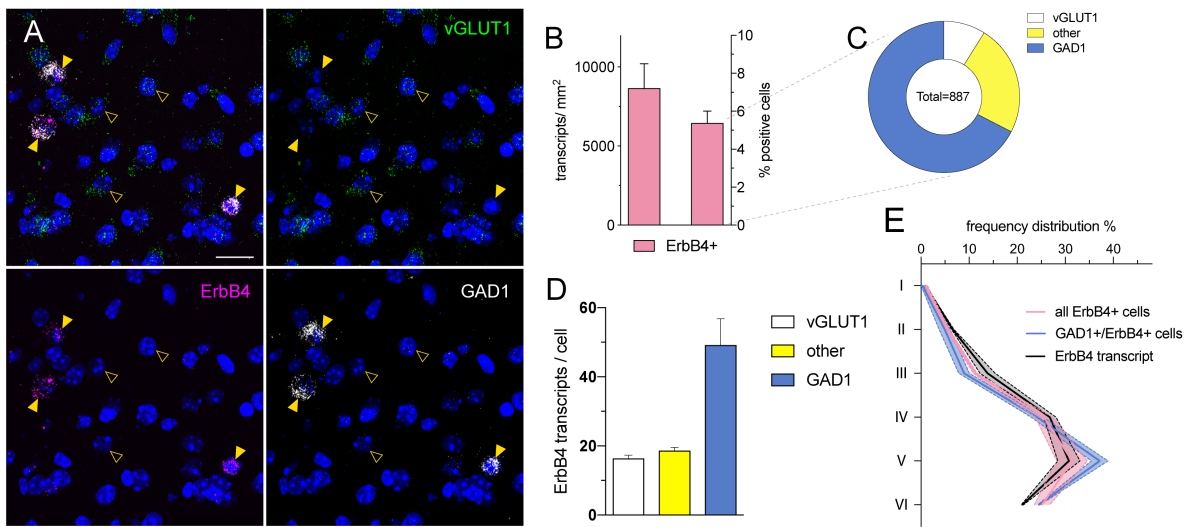


Figure 3.5 | Quantitative analysis of an exemplary RNAscope experiment.

(A) Inset for cellular resolution of ErbB4 (magenta; Channel 1) expression in the somatosensory cortex from Figure 3.4B. ErbB4 transcripts are confined to GABAergic interneurons (GAD1; white; Channel 3) in the cortex (arrowheads) and absent from glutamatergic neurons (vGLUT1; green; Channel 2; open arrowheads). (B-E) Quantification of ErbB4 expression in the somatosensory cortex using CellProfiler (see Understanding Results and Statistical Analyses; n=18429 cells; N=2 animals; bilateral). (B) ErbB4 transcript expression analyzed per area (right) and percentage of positive cells (left). (C) Fraction of ErbB4+ cells that overlap with glutamatergic (white), GABAergic (blue) signal or are none of both (yellow). (D) ErbB4 transcript levels per positive cell subdivided into the three cell populations. (E) Histogram analyses of ErbB4 expression in different cortical layers. Scale bar 20µm.

1. Prepare fresh 4% paraformaldehyde (PFA) in 1x PBS with RNase-free water and pre-chill in Coplin jar at 4°C the night before.

Alternatively, 10% normal buffered formalin can be used.

2. The day of the assay, preheat and equilibrate oven to 40°C. Assemble a humidifying chamber using absorbent paper and RNase-free water and pre-warm it in the oven.

Pretreatment of fresh-frozen sections

3. Transfer slides quickly from their slide box stored at -80°C directly into pre-chilled 4% PFA; sections should not be allowed to thaw and need to be completely submerged. Incubate 15min at 4°C.
4. Wash slides in 1x PBS at room temperature by transferring slides to a Coplin jar filled with 1x PBS. Move slides up and down five times and incubate 2min. Repeat wash once with fresh 1x PBS.
5. To dehydrate sections, transfer slides to a Coplin jar filled with 50% ethanol. Move slides up and down five times and incubate 5min at room temperature. Repeat one time in 70% ethanol and twice with fresh 100% ethanol.

Slides can be stored for up to 1 week at -20°C in 100% ethanol. Prolonged storage may result in RNA degradation and suboptimal results.

6. Carefully dry the bottom side of the slide (i.e., side without section) with a Kimwipe and using a quick flick of the wrist remove excess liquid over the tissue; air dry slides with sections facing upwards on an even surface 5min at room temperature.
7. Draw a circle or rectangle around each section with a hydrophobic barrier pen, leaving ~5mm of space between the section and the barrier, and allow barrier to completely dry before continuing (~1min).
8. Cover sections completely with protease IV pretreatment solution (provided with RNAscope pretreatment kit; e.g., 3 drops for coronal adult mouse brain section) and incubate 30min at room temperature. Cover sections with lid to avoid dust falling onto samples.
9. During incubation of the protease pretreatment, prepare probe mix:
 - a. Preheat probes 10min at 40°C in a water bath or oven.
 - b. Swirl Channel 1 probe and briefly spin down Channel 2 and Channel 3 probes.
 - c. Wipe down tubes with RNase AWAY
 - d. In an RNase-free Eppendorf tube, prepare probe mix: Drip 2 drops of Channel 1 (~50µl) per section into the tube and then mix in Channel 2 and Channel 3

probes at 1:50 (i.e., 1 μ l per section). For weaker probes, use 1.5 μ l Channel 2 or Channel 3 probes per section.

The probe mix is prepared fresh for each experiment.

10. Remove pretreatment solution by carefully blotting the side of the slide with absorbent paper and giving the slide a quick flick of the wrist. Transfer slides into a Coplin jar filled with 1x PBS at room temperature and wash by gently moving slides up and down in the solution five times then incubate 2min. Repeat wash with fresh 1x PBS.

Incubate and amplify probe

11. Remove slides from Coplin jar. Blot and remove excess 1x PBS wash from the slides as described above. Transfer each slide to a horizontal slide rack in the pre-warmed humidifying chamber, pipet onto each section ~50 μ l of probe mix (see step 9), being careful not to let the sections dry out.
12. Hybridize sections 2hr at 40°C in the sealed humidified chamber in the oven.
13. During incubation of the probes prepare 1x wash buffer:
 - a. Incubate 50x wash buffer 10min at 40°C in a water bath or oven
 - b. Prepare 1 liter of 1x wash buffer using distilled water.

After the hybridization of the probes, it is no longer necessary to continue to work under RNase-free conditions. Unused 1x wash buffer can be stored at room temperature for up to 3 months.

14. Remove excess hybridization solution as described above and transfer each slide to a Coplin jar filled with 1x wash buffer at room temperature. As before, wash sections by gently moving slides up and down five times and incubate 2min. Repeat wash once with fresh 1x wash buffer.
15. To begin amplification process, sequentially remove from each slide excess 1x wash buffer (as described in step 10) and transfer it to the humidified chamber. Completely cover each section with the Amplification solution 1 (AMP1; provided with RNAscope fluorescent multiplex kit; ~3 drops for an adult coronal mouse brain section). Incubate in the humidified chamber 30min at 40°C.
16. Wash slides twice in 1x wash buffer at room temperature, as in step 14.
17. Remove excess wash, add Amplification solution 2 (AMP2; provided with RNAscope fluorescent multiplex kit), and incubate 15min at 40°C.
18. Wash slides twice in 1x wash buffer at room temperature, as in step 14.
19. Remove excess wash, add Amplification solution 3 (AMP3; provided with RNAscope fluorescent multiplex kit), and incubate 30min at 40°C.

20. Wash slides twice in 1x wash buffer at room temperature, as in step 14.
21. To label the amplified hybridizations with fluorophores, add Amplification solution 4 (AMP4A, AMP4B, or AMP4C; provided with RNAscope fluorescent multiplex kit) and incubate 15min at 40°C.

The different AMP4 solutions assign different fluorophores to each channel (see Strategic Planning section). We recommend using AMP4B for standard applications.

22. Wash slides twice in 1x wash buffer at room temperature, as in step 14.
23. One slide at the time, counterstain cell nuclei by adding ~2 drops DAPI (provided with RNAscope fluorescent multiplex kit) and incubate 30sec at room temperature.
24. Remove excess DAPI as described above, add aqueous mounting medium (~10µl per coronal section), and add a coverslip to each slide carefully to avoid trapping air bubbles. Store slides horizontally in the dark overnight at 4°C to dry.

Detect and analyze

25. Examine dried slides within a few days of preparation on a fluorescent (confocal) microscope (magnification 20 to 63x).

The signals obtained from low abundance transcripts might be only visible at higher magnification (40 to 63x) and single dot resolution necessary for quantitative data analysis is only obtained at higher magnification (40 to 63x). Digital image analysis using a camera is highly recommended.

26. Quantify signals by simple semi-quantitative scoring of the signal (ACD), using standard free image analysis software such as ImageJ (NIH) and CellProfiler (Carpenter et al., 2006), or commercial image analysis software such as Imaris (Bitplane) or specific ISH quantification software such as HALO (Indica Labs) and Aperio (Leica).

For more details on data interpretation and signal quantification refer to Basic Protocol 4 and the Commentary section Understanding Results and Statistical Analyses.

3.4.1 Alternate Protocol 1: Use of formalin-fixed paraffin-embedded sections

The protocol described here is for ISH analysis using 4- to 8-µm thick formalin-fixed paraffin-embedded (FFPE) sections, which differs from Basic Protocol 1 (used to analyze fresh-frozen sections). Although fresh-frozen sections are generally thought to provide the highest sensitivity, because of better RNA preservation, there are instances that either experimental conditions or access to cryostats may preclude the use of fresh-frozen sections. Moreover, FFPE sections allow for consistent serial sectioning and have frequently been used

to archive human tissue because of easier long-term storage. Because the preparation of FFPE sections for RNAscope analysis requires different pretreatment steps than those described for fresh-frozen sections in Basic Protocol 1, here we provide an alternate protocol for FFPE sections. Probe hybridization and signal amplification, as well as detection, are the same as described in Basic Protocol 1. Figure 3.6A depicts an example of RNAscope on FFPE sections of embryos.

Additional Materials (also see Basic Protocol 1)

- 4- to 8- μ m thick paraffin sections on Superfrost slides (for preparation see²⁵⁶)
 - Xylene (e.g., Macron, cat. no. 8668-16)
 - *Optional*: Thermometer (100°C)
 - Drying oven (60°C)
 - Forceps
1. The day of the assay, preheat and equilibrate oven to 40°C. Assemble a humidifying chamber using absorbent paper and RNase-free water and pre-warm it in the oven.

Pretreat formalin-fixed paraffin-embedded sections

2. Bake sections 1hr in an oven at 60°C.

This can be done up to 1 week in advance and slides can be stored at room temperature with desiccants.

3. During baking of sections, prepare 1x antigen retrieval: Prepare 1x antigen retrieval from 10x stock (pretreatment II; provided with the RNAscope pretreatment kit) with RNase-free water; unused 1x antigen retrieval can be stored at room temperature for up to 3 months. On a hot plate, preheat Coplin jar filled with 1x antigen retrieval in a water-filled beaker brought to boil.

Temperature can be controlled with thermometer and should be between 98° and 102°C. Alternatively, antigen retrieval can also be performed in a preheated steamer.

4. In a fume hood, remove paraffin from sections in a Coplin jar filled with xylene. Move slides up and down five times and incubate 5min at room temperature. Repeat once with fresh xylene.
5. Transfer slides to a Coplin jar filled with 100% ethanol. Move slides up and down five times and incubate 3min at room temperature. Repeat once with fresh 100% ethanol before drying.

6. After carefully drying the bottom side of the slice (i.e., side without section) with a Kimwipe and giving the slide a quick flick of the wrist, air dry slides with sections facing upwards on an even surface 5min at room temperature.
7. With forceps, slowly place slides into preheated 1x antigen retrieval (see step 3) and incubate 15min.
8. Carefully remove slides with forceps and transfer into a Coplin jar filled with RNase-free water at room temperature. Wash sections by gently moving slides up and down five times and incubate 2min. Repeat wash once with fresh RNase-free water.

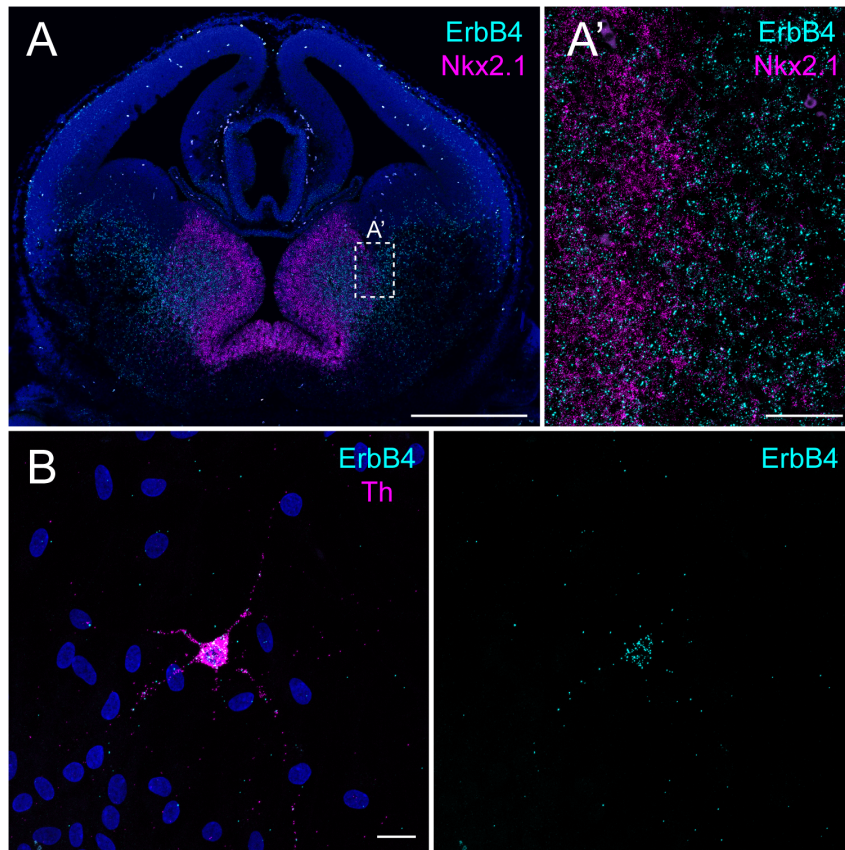


Figure 3.6 | Example for RNAscope on FFPE sections (Alternate Protocol 1) and adherent cell culture (Alternate Protocol 2).

(A) Expression of ErbB4 (C1, cyan) and Nkx2.1 (magenta, C3) on a coronal paraffin section of an E14.5 wild-type embryo. (A') Magnification at the border between the medial and lateral ganglionic eminence. (B) Expression of ErbB4 (cyan, C1) in primary cultured dopaminergic neurons (prepared as in^{234}) identified by tyrosine hydroxylase (Th, C3, magenta) at 13 days *in vitro* (DIV). Scale bars 500µm in A and 50µm in A'; 20µm in B. FFPE, formalin-fixed paraffin-embedded.

9. Transfer slides into a Coplin jar filled with 100% ethanol, incubate ~15sec, and air dry 5min as described above in step 6.

10. Draw a circle or rectangle around each section with a hydrophobic barrier pen, leaving ~5mm of space between the section and the barrier, and allow barrier to completely dry before continuing (~1min).

Optional: Dried slides can be stored overnight, and protocol continued the following day.

11. Place slides on slide rack in the pre-warmed humidifying chamber and cover completely with protease treatment III (provided with RNAscope pretreatment kit; e.g., ~3 drops per section for coronal adult mouse brain section). Incubate 30min at 40°C in the sealed humidified chamber in the oven.
12. During incubation of the protease pretreatment, prepare probe mix:
 - a. Preheat probes 10min at 40°C in a water bath or oven.
 - b. Swirl Channel 1 probe and briefly spin down Channel 2 and Channel 3 probes.
 - c. Wipe down tubes with RNase AWAY.
 - d. In an RNase-free Eppendorf tube, prepare probe mix: Drip 2 drops of Channel 1 (~50µl) per section into the tube and then mix in Channel 2 and Channel 3 probes at 1:50 (i.e., 1µl per section). For weaker probes, instead use 1.5µl of Channel 2 or Channel 3 probes per section.

The probe mix is prepared fresh for each experiment.

13. Remove pretreatment solution by carefully blotting the side of the slide with absorbent paper and giving the slide a quick flick of the wrist. Transfer each slide into a Coplin jar filled with RNase-free water at room temperature. As before, wash sections by gently moving slides up and down five times and incubating 2min. Repeat wash once with fresh RNase-free water.

Amplify, detect, and analyze

14. Continue with Basic Protocol 1, steps 11 to 26 for target probe incubation, signal amplification, and detection.

3.4.2 Alternate Protocol 2: *In situ* hybridization in cultured adherent cells

Multiplex fluorescent ISH with RNAscope can also be performed on cultured adherent cells, such as established cell lines or primary neuronal cultures. Cells need to be plated on glass coverslips or alternatively chamber slides can be used. If mitotic active cultures are used, they should be 80% to 90% confluent at the time of fixation. As in the case of fresh-frozen and FFPE sections, cell culture samples need unique pretreatment conditions for performing RNAscope. The specific steps are described below; otherwise, the protocol follows closely

Basic Protocol 1. Examples for RNAscope in primary cultured neurons are presented in Figure 3.6B.

NOTE: General handling procedure: The use of coverslips involves some handling challenges. With the exception of the RNAscope reagents, all other steps (i.e., washes, fixation, dehydration) are performed by placing the coverslips inside a multi-well cell culture dish that is shaken on a horizontal shaker. Next, transfer the coverslips onto glass slides that were previously marked with circles using the hydrophobic barrier and completely cover with RNAscope reagents. Chamber slides can be used as an alternative to coverslips; drawing of the hydrophobic barrier is difficult. However, an advantage of using chamber slides is that the procedure can be performed in Coplin jars as described earlier.

Additional Materials (also see Basic Protocol 1)

- Adherent cell cultures (e.g., dissociated neurons) on glass coverslips
 - 10% normal buffered formalin (NBF; e.g., Sigma Aldrich; cat. no. HT5011)
 - Horizontal rocking plate
 - Glass slides (75x25 mm; e.g., C&A Scientific; cat. no. 8201)
1. The day of the assay, preheat and equilibrate oven to 40°C. Assemble a humidifying chamber using absorbent paper and RNase-free water and pre-warm it in the oven.
 2. Prepare glass slides with hydrophobic barrier pen circles, with a diameter slightly exceeding the coverslip size used.

Glass slides can be washed and dried between incubations and reused. Redraw hydrophobic barrier if necessary.

Pretreat adherent cell culture sample

3. Remove cell culture medium and rinse cultures carefully with 1x PBS.
4. Replace PBS with 10% NBF and fix cultures by incubating 30min at room temperature while agitating on a horizontal shaker.

All subsequent washes should be performed while agitating on shaker.

5. Remove NBF and replace with 1x PBS for 5min at room temperature. Repeat wash once with fresh 1x PBS.
6. To dehydrate cultures, remove PBS and substitute with 50% ethanol for 5min at room temperature, then with 70% ethanol once, and twice with fresh 100% ethanol.

Fixed cultures can be stored for up to 6 months at -20°C in 100% ethanol.

7. To rehydrate culture samples, replace 100% ethanol with 70% ethanol and incubate 2min at room temperature. Repeat these steps with 50% ethanol and then wash in 1x PBS at room temperature for 10min.
8. Freshly prepare 1:15 protease III (provided with RNAscope pretreatment kit) in RNase-free 1x PBS (~100µl per 12-mm coverslip).
9. Remove coverslips one by one from cell culture plate and place cultures facing up onto the prepared glass slides that contain hydrophobic barrier circles (see step 2). Do not dry out samples. Cover immediately with prepared 1:15 dilution of protease III. Incubate 10min at room temperature. Cover sections with lid to avoid dust falling onto samples.
10. During incubation of the protease pretreatment, prepare probe mix:
 - a. Preheat probes 10min at 40°C in a water bath or oven.
 - b. Swirl Channel 1 probe and briefly spin down Channel 2 and Channel 3 probes.
 - c. Wipe down tubes with RNase AWAY.
 - d. In an RNase-free Eppendorf tube, prepare probe mix: Add 2 drops of Channel 1 (~50µl) per coverslip into the tube and then mix in Channel 2 and Channel 3 probes at 1:50 (i.e., 1µl per section). For weaker probes, use 1.5µl of Channel 2 or Channel 3 probes per section.

The probe mix is prepared fresh for each experiment.

11. Move coverslips back into culture well plate filled with 1x PBS and wash 2min at room temperature. Repeat once with fresh 1x PBS.

Amplify, detect, and analyze

12. Continue with steps 11 to 26 of Basic Protocol 1 for target probe incubation, signal amplification, and detection. Perform washes in cell culture plate and probe incubation (~50µl per 12-mm coverslip), as well as amplification steps (2 to 3 drops per 12-mm coverslip) with coverslips placed on glass slides with barrier circles to safe solutions. Mount samples on glass slides with ~10µl aqueous mounting medium per 12-mm coverslip.

3.5 Basic Protocol 2: Single-Pair Probe *In Situ* Hybridization

Single-pair probe ISH, BaseScope, is a novel approach that allows the use of a single probe pair (“ZZ”). BaseScope relies on the same probe design as RNAscope. However, due to the improved amplification chemistry, it is possible to use only a single-probe pair that hybridizes to ~50 bases of target RNA. Splice variants can be distinguished by targeting exon junctions¹⁹².

^{257, 258} (see Fig. 3.1). Other BaseScope applications include the detection of long non-coding RNAs, microRNAs, short or very similar sequences that can distinguish up to a single nucleotide, and the validation of short knockout sequences^{251, 259}. BaseScope uses 1 to 6 “ZZ” probes and is currently only a single-plex assay; ergo only one target RNA can be detected at a time. The FastRED dye used can be visualized both by fluorescence and chromogenically when counterstained with DAPI and hematoxylin, respectively (see below). In practical terms, the amplification of the signal requires more amplification steps than RNAscope (four versus eight amplification steps) and an additional peroxide (H₂O₂) treatment step (during the pretreatment) to block intrinsic enzyme activity and allow the signal detection by alkaline phosphatase. Pretreatment conditions are described here for fresh-frozen and FFPE sections, as well as for adherent cultures. A representative BaseScope experiment on FFPE sections showing the high sensitivity and specificity is shown in Figure 3.7 and an example detected with light microscopy is shown in Figure 3.8A.

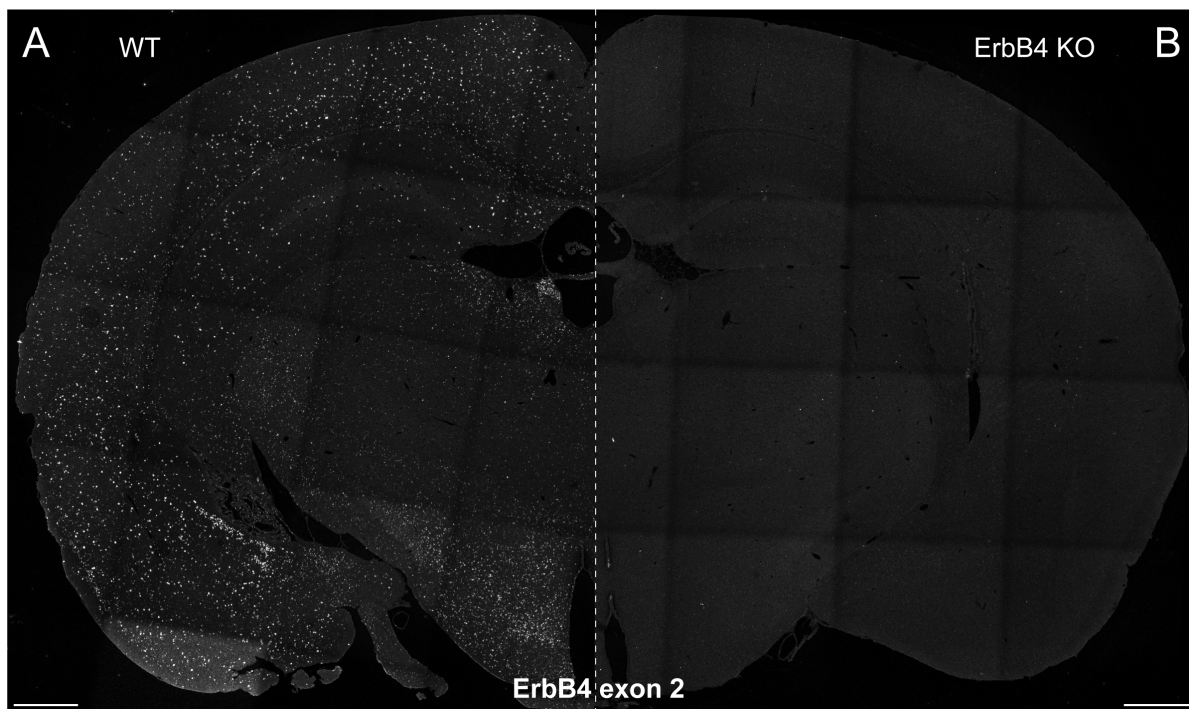


Figure 3.7 | Exon-specific BaseScope experiment on FFPE sections (Basic Protocol 2).

Exon 2 of the ErbB4 transcript was detected in coronal sections of adult C57BL/6J WT mice (**A**) but not in sections of ErbB4 mutant mice (ErbB4 KO; RRID: MGI:5318192) (**B**) that lack this exon¹⁵⁷ (for details see¹⁹²). The absence of signal in the single exon mutant confirms the high specificity of the assay. Scale bars 500µm. FFPE, formalin-fixed paraffin-embedded; WT, wild type.

NOTE: Even if reagents of RNAscope and BaseScope kits have the same name (e.g., AMP1) these reagents are not the same and not interchangeable! Only use reagents from one kit and do not mix.

Materials

- BaseScope reagents (ACD):
 - 1 to 6 ZZ target probes (ACD, C1, species-specific)
 - BaseScope™ reagent kit-RED (version 2, ACD, cat. no. 323910)
 - Pretreatment kit (ACD, cat. no. 322380)
 - 50x wash buffer (ACD, cat. no. 310091)
 - Optional:* Positive and negative probes, e.g., for mouse: Positive probes Polr2a, ACD, cat. no. 701101 (1ZZ) or 701091 (3ZZ); negative probes bacterial DapB, ACD, cat. no. 701011 (1ZZ) or 701021 (3ZZ)
- 10- to 20- μ m thick fresh-frozen sections on Superfrost slides (for preparation see²⁵⁵) or 4- to 8- μ m thick paraffin sections on Superfrost slides (for preparation see²⁵⁶) or adherent cultures on glass coverslips
- RNase AWAY (e.g., Molecular BioProducts, Thermo Fisher Scientific, cat. no. MBP#7000)
- Paraformaldehyde (PFA; e.g., 16% PFA; Electron Microscopy Sciences, cat. no.15710)
- 100% ethanol (200 proof)
- 50% and 70% ethanol prepared with RNase-free water
- RNase-free water (e.g., DEPC-treated water; KD Medical, cat. no. RGF-3050)
- 1x PBS (RNase-free)
- Distilled water
- DAPI (e.g., Invitrogen brand, Thermo Fisher Scientific, cat. no. D3571)
- Mowiol DABCO mounting medium (aqueous; see recipe)
- Xylene (e.g., Macron, cat. no. 8668-16)
- 10% normal buffered formalin (NBF; e.g., Sigma-Aldrich, cat. no. HT5011)
- Hematoxylin (e.g., Electron Microscopy Sciences, cat. no. 26030-10)
- 0.02% ammonium water (see recipe)

- Ammonium Hydroxide (e.g., Sigma-Aldrich, cat. no. 221228)
 - 12 vertical glass Coplin jars (e.g., Ted Pella, cat. no. 432-1)
 - Hydrophobic barrier pen (e.g., ImmEdge; Vector Laboratories, cat. no. H-4000)
 - Absorbent paper (e.g., Whatman paper; GE Healthcare, cat. no. 10427804)
 - Humidifying chamber (e.g., ACD, cat. no. 310012)
 - Horizontal slide rack (e.g., ACD, cat. no. 310017)
 - Oven (40°C; e.g., HybEZ™/ HybEZ™II oven, 110/220 V; ACD, cat. no.321710/20)
 - Waterbath (40°C)
 - 1.5-ml RNase-free Eppendorf tubes
 - Kimwipes (e.g., Kimtech Science Precision wipes; Kimberly-Clark Professional, cat. no. 05511)
 - Cover glass (24x50 mm; e.g., Thermo Fisher Scientific, cat. no. 12-548-5M)
 - Fluorescent microscope (e.g., Zeiss LSM710/780)
 - *Optional:* Thermometer (100°C)
 - Drying oven (60°C)
 - Horizontal rocking plate
 - Glass slides (75x25 mm; e.g., C & A Scientific, cat. no. 8201)
 - Parafilm
 - Light microscope
1. The day of the assay, preheat and equilibrate oven to 40°C. Assemble a humidifying chamber using absorbent paper and RNase-free water and pre-warm it in the oven. Depending on sample type – fresh-frozen sections (steps 2a to 12a), formalin-fixed paraffin-embedded sections (steps 2b to 16b), or adherent cell culture (steps 2c to 13c) – perform one of the following pretreatment procedures, skip steps related to pretreatment of other sample types, and continue with step 17 (probe incubation).

Pretreatment of fresh-frozen sections

- 2a. Prepare fresh 4% paraformaldehyde (PFA) with RNase-free water and pre-chill in Coplin jar at 4°C the night before.

Alternatively, 10% normal buffered formalin can be used.

- 3a. Transfer slides quickly from their slide box stored at -80°C directly into pre-chilled 4% PFA. Do not allow sections to thaw and ensure they are completely submerged. Incubate 15min at 4°C.
- 4a. Wash slides in 1x PBS at room temperature by transferring slides to a Coplin jar filled with 1x PBS. Move slides up and down five times and incubate 2min. Repeat wash once with fresh 1x PBS.
- 5a. To dehydrate sections, transfer slides to a Coplin jar filled with 50% ethanol. Move slides up and down five times and incubate 5min at room temperature. Repeat one time in 70% ethanol and twice with fresh 100% ethanol.

Slides can be stored for up to 1 week at -20°C in 100% ethanol. Prolonged storage may result in RNA degradation and suboptimal results.

- 6a. Carefully dry the bottom side of the slide (i.e., side without section) with a Kimwipe and using a quick flick of the wrist, remove excess liquid over the tissue, then air dry slides with sections facing upwards on an even surface for 5min at room temperature.
- 7a. Draw a circle or rectangle around each section with a hydrophobic barrier pen, leaving ~5mm of space between the section and the barrier, and allow barrier to completely dry before continuing (~1min).
- 8a. Cover section completely with 2 to 3 drops of H₂O₂ pretreatment (pretreatment 1 provided with pretreatment kit) and incubate 10min at room temperature. Cover sections with lid to avoid dust falling onto sections.
- 9a. Remove pretreatment solution by carefully blotting the side of the slide with an absorbent paper and giving the slide a quick flick of the wrist. Transfer slides into a Coplin jar filled with 1x PBS at room temperature, wash by gently moving slides up and down in the solution five times, and incubate 2min. Repeat wash with fresh 1x PBS.
- 10a. Remove excess PBS and cover sections completely with protease IV pretreatment solution (provided with pretreatment kit; e.g., 3 drops for coronal adult mouse brain section) and incubate 30min at room temperature. Cover sections with lid to avoid dust falling onto samples.
- 11a. During incubation with protease pretreatment, preheat BaseScope probes provided in ready-to-use dropper bottle 10min at 40°C in a water bath or oven. Swirl probe to mix
- 12a. Remove pretreatment solution and wash slides twice in 1x PBS at room temperature as described above.

Pretreatment of formalin-fixed paraffin-embedded sections

- 2b. Bake sections 1hr in an oven at 60°C.

This can be done up to 1 week in advance and slides can be stored at room temperature in the presence of desiccants.

- 3b. During baking of the sections, prepare 1x antigen retrieval: Prepare 1x antigen retrieval from 10x stock (pretreatment II; provided with the pretreatment kit) with RNase-free water. (Store unused 1x antigen retrieval at room temperature for up to 3 months.) On a hot plate, preheat Coplin jar filled with 1x antigen retrieval in a water-filled beaker brought to boil.

Temperature can be controlled with thermometer and should be between 98° and 102°C. Alternatively, antigen retrieval can also be performed in a preheated steamer.

- 4b. In a fume hood, remove paraffin from sections in a Coplin jar filled with xylene. Move slides up and down five times and incubate 5min at room temperature. Repeat once with fresh xylene.
- 5b. Transfer slides to a Coplin jar filled with 100% ethanol. Move slides up and down five times and incubate 3min at room temperature. Repeat once with fresh 100% ethanol drying.
- 6b. After carefully drying the bottom side of the slice (i.e., side without section) with a Kimwipe and giving the slide a quick flick of the wrist, air dry slides with sections facing upwards on an even surface 5min at room temperature.
- 7b. Draw a circle or rectangle around each section with a hydrophobic barrier pen, leaving ~5mm of space between the section and the barrier, and allow barrier to completely dry before continuing (~1min).

Optional: Dried slides can be stored overnight, and protocol continued the following day.

- 8b. Cover section completely with 2 to 3 drops of H₂O₂ pretreatment (pretreatment 1 provided with pretreatment kit) and incubate 10min at room temperature. Cover sections with lid to avoid dust falling onto sections.
- 9b. Remove pretreatment solution by carefully blotting the side of the slide with an absorbent paper and giving the slide a quick flick of the wrist. Transfer slides into a Coplin jar filled with RNase-free water at room temperature, wash by gently moving slides up and down in the solution five times, and incubate 2min. Repeat wash with fresh RNase-free water.
- 10b. With forceps, slowly place slides into preheated 1x antigen retrieval solution (see step 3b) and incubate 15min.
- 11b. Carefully remove slides with forceps and transfer into a Coplin jar filled with RNase-free water at room temperature. Wash sections by gently moving the slides up and down five times and incubate 2min. Repeat wash once with fresh RNase-free water.

- 12b. Transfer slides into a Coplin jar filled with 100% ethanol, incubate ~15sec, and air dry 5min as described above in step 6b.
- 13b. If necessary, reapply hydrophobic barrier.
- 14b. Place slides on slide rack in the pre-warmed humidifying chamber and cover completely with protease treatment III (provided with pretreatment kit; e.g., ~3 drops per section for coronal adult mouse brain section). Incubate 30min at 40°C in the sealed humidified chamber in the oven.
- 15b. During incubation of the protease pretreatment, preheat BaseScope probes provided in ready-to-use dropper bottle 10min at 40°C in a water bath or oven. Swirl probe to mix.
- 16b. Remove pretreatment solution and wash slides twice in RNase-free water at room temperature as described above.

Pretreatment of adherent cell culture samples

- 2c. Prepare glass slides with hydrophobic barrier pen circles with a diameter slightly exceeding the coverslip size used.

Glass slides can be washed and dried between incubations and reused. Redraw hydrophobic barrier if necessary.

- 3c. Remove cell culture medium and rinse cultures carefully with 1x PBS.

- 4c. Replace PBS with 10% NBF and fix cultures by incubating 30min at room temperature while agitating on a horizontal shaker.

All subsequent washes should be performed while agitating on shaker.

- 5c. Remove NBF and replace with 1x PBS for 5min at room temperature. Repeat wash once with fresh 1x PBS.

- 6c. To dehydrate cultures, remove PBS and substitute with 50% ethanol for 5min at room temperature, then with 70% ethanol once, and twice with fresh 100% ethanol.

Fixed cultures can be stored for up to 6 months at -20°C in 100% ethanol.

- 7c. To rehydrate culture samples, replace 100% ethanol with 70% ethanol and incubate 2min at room temperature. Repeat these steps with 50% ethanol and then wash in 1x PBS at room temperature 10min.

- 8c. Remove coverslips one-by-one from cell culture plate and place cultures face up onto the prepared glass slides that contain hydrophobic barrier circles (see preparation step 2c). Do not allow samples to dry out. Cover immediately with 2 to 3 drops of H₂O₂ pretreatment (pretreatment 1; provided with pretreatment kit) and incubate 10min at room temperature. Cover coverslips with lid to avoid dust falling onto sections.

- 9c. Move coverslips back into culture well plate filled with 1x PBS and wash 2min at room temperature. Repeat once with fresh 1x PBS.
- 10c. Freshly prepare 1:15 protease III (provided with pretreatment kit) in RNase-free 1x PBS (~100 ml per 12-mm coverslip).
- 11c. Place coverslip cultures face up onto the prepared glass slide (as described above) and cover immediately with prepared 1:15 dilution of protease III. Incubate 10min at room temperature. Cover sections with lid to avoid dust falling onto samples.
- 12c. During incubation of protease pretreatment, preheat BaseScope probes provided in ready-to-use dropper bottle 10min at 40°C in a water bath or oven. Swirl probe to mix.
- 13c. Move coverslips back into culture well plate filled with 1x PBS and wash 2min at room temperature. Repeat once with fresh 1x PBS.

Incubate and amplify probes (for all sample types)

17. Individually transfer each slide (or coverslip) to a horizontal slide rack in the pre-warmed humidifying chamber, after blotting and removing the excess wash solution from the slides as described above. Carefully cover sections with target probe (~2 drops), being careful not to let the sections dry out.
18. Hybridize sections 2hr at 40°C in the sealed humidified chamber in the oven.
19. During incubation of the probes, prepare 1x wash buffer: Incubate 50x wash buffer 10min at 40°C in a water bath or oven. Prepare 2 liters of 1x wash buffer using distilled water.

After hybridization of the probes, it is no longer necessary to continue to work under RNase-free conditions. Unused 1x wash buffer can be stored at room temperature for up to 3 months.
20. Remove excess hybridization solution as described above and transfer each slide into a Coplin jar filled with 1x wash buffer at room temperature. Wash sections by gently moving slides up and down five times and incubate 2min. Repeat wash once with fresh 1x wash buffer.
21. To begin the amplification process (amplification solutions AMP1-8 provided in BaseScope reagent kit-RED), sequentially remove from each slide excess 1x wash buffer and transfer slide to the humidified chamber. Completely cover each section with the Amplification solution 1 (AMP1; ~3 drops for an adult coronal mouse brain section). Incubate in the humidified chamber 30min at 40°C.
22. Wash slides twice in 1x wash buffer at room temperature, as in step 20.
23. Remove excess wash, add Amplification solution 2 (AMP2), and incubate 30min at 40°C.
24. Wash slides twice in 1x wash buffer at room temperature, as in step 20.

25. Remove excess wash, add Amplification solution 3 (AMP3), and incubate 15min at 40°C.
26. Wash slides twice in 1x wash buffer at room temperature, as in step 20.
27. Remove excess wash, add Amplification solution 4 (AMP4), and incubate 30min at 40°C.
28. Wash slides twice in 1x wash buffer at room temperature, as in step 20.
29. Remove excess wash, add Amplification solution 5 (AMP5), and incubate 30min at 40°C.
30. Wash slides twice in 1x wash buffer at room temperature, as in step 20.
31. Remove excess wash, add Amplification solution 6 (AMP6), and incubate 15min at 40°C.
32. Wash slides twice in 1x wash buffer at room temperature, as in step 20.
33. Remove excess wash, add Amplification solution 7 (AMP7), and incubate 30min at room temperature.
34. Wash slides twice in 1x wash buffer at room temperature, as in step 20.
35. Remove excess wash, add Amplification solution 8 (AMP8), and incubate 15min at room temperature.
36. Wash slides twice in 1x wash buffer at room temperature, as in step 20.
37. Prepare fresh FastRED solution provided with BaseScope reagent kit-RED (~60µl per coronal section). Dilute FastRED-B 1:60 in FastRED-A (e.g., 1µl FastRED-B in 60µl FastRED-A).
38. Remove excess wash buffer and cover sections completely with FastRED solution. Incubate 10min at room temperature and cover sections with lid to avoid dust falling onto sections. Remove excess FastRED solution and wash slides twice for 2min in tap water, as described in step 7a.

The FastRED dye used in the BaseScope assay is visible both in fluorescent and light microscopes. For fluorescent visualization use DAPI (outlined below, step 39); for chromogenic detection, sections need to be counterstained with hematoxylin (skip to step 40).

Counterstaining with DAPI

39. One slide at the time, counterstain cell nuclei by carefully adding DAPI (1µg/ml in PBS; ~100µl) and incubate 30sec at room temperature. Remove excess DAPI as described above. Proceed to step 45 for mounting.

Counterstaining with hematoxylin

40. Prepare 50% hematoxylin staining solution by mixing equal amounts of hematoxylin with distilled water in a Coplin jar.

41. Move slides into Coplin jar filled with 50% hematoxylin and incubate 2min at room temperature; sections will turn purple.
42. Immediately wash slides in tap water by moving slides up and down. Repeat washes with fresh tap water until the water becomes clear.
43. One-by-one incubate slides ~15sec in 0.02% ammonia water. Move slides up and down five times then place into fresh tap water; sections are observed turning blue.
44. Replace with fresh tap water and wash 2min at room temperature. Remove excess solution.
45. Add aqueous mounting medium (~10 μ l per coronal) and add a coverslip to each slide, while being careful to avoid trapping air bubbles. Store slides horizontally in the dark overnight at 4°C to dry.

Detect and analyze

46. Examine dried slides within a few days of preparation on a fluorescent (confocal) microscope for DAPI-counterstained sections and on a light microscope for hematoxylin-counterstained sections (magnification 10 to 40x).

Digital image analysis using a camera is highly recommended. For automated signal quantification, a magnification of at least 20x is recommended.

47. Quantify signals by simple semi-quantitative scoring of the signal (ACD), using standard free image analysis software such as ImageJ (NIH) and CellProfiler (Carpenter et al., 2006), or commercial image analysis software such as Imaris (Bitplane) or specific ISH quantification software such as HALO (Indica Labs) and Aperio (Leica). In the case of hematoxylin-counterstain samples, Spotstudio (ACD) software can be used to analyze specifically bright-field single-plex data.

For more details of data interpretation and signal quantification refer to Basic Protocol 4 and the Commentary, Understanding Results and Statistical Analyses section.

3.6 Basic Protocol 3: Post-hoc immunostainings

In situations when it is important to identify cell types expressing the RNA of interest, the multiplexing nature of RNAscope is advantageous over BaseScope. Nevertheless, BaseScope can be combined with immunohistochemistry (IHC) to identify different cell types expressing the RNA of interest; immunostaining is also compatible with RNAscope. In our experience, the combination of BaseScope or RNAscope with immunohistochemistry only succeeds when the ISH is performed first, as the immunostaining interferes with the specificity and sensitivity of the ISH. However, this approach is challenging, as the success of the ISH depends on proper

permeabilization to allow the probes to access the target RNAs and changing the conditions results frequently in off-target signal or reduced sensitivity. The permeabilization is mainly achieved using proteases, which in turn can destroy antigens of the antibodies used in the immunostaining. In our hands, only about 10% of the antibodies tested were compatible with performing ISH using protease digestion, largely independent of section type and corresponding pretreatment conditions. This success rate is consistent with reports from others [dual *in situ* hybridization-immunohistochemistry (ISH-IHC); ACD]. In general, we had better success with antibodies against membrane-bound proteins than soluble proteins. If the combination with immunostaining is necessary, it may require a large number of different antibodies to identify one that is compatible with ISH.

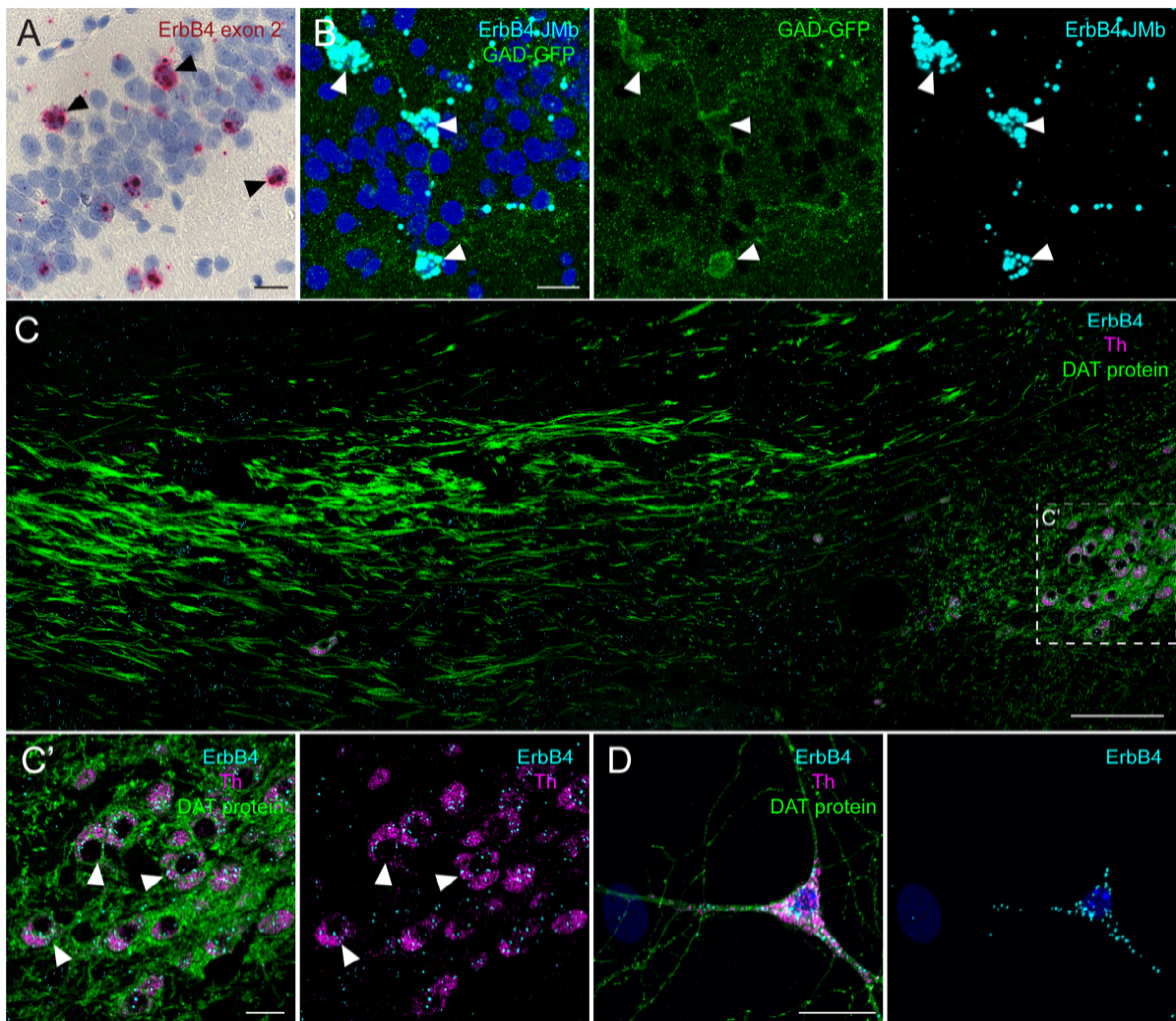


Figure 3.8 | Examples for chromogenic BaseScope detection (Basic Protocol 2) and ISH-IHC combination (Basic Protocol 3).

(A) Hippocampal section of an adult WT mice, labeled using BaseScope for ErbB4 with a single-probe pair targeting the exon boundary exon 1/exon 2. The section was counterstained with hematoxylin and signal detected with light microscopy. Arrowheads indicate ErbB4+ GABAergic interneurons. (B) Detection of one of the four ErbB4 splice variants (JMb; *cyan*) by BaseScope in GABAergic interneurons (GAD-GFP; *green*; arrowheads) in a section of an adult GAD-GFP mouse (kindly provided by Dr. Yuchio Yanagawa). GFP signal was amplified after the ISH assay with an anti-GFP antibody (NeuroMab; N86/8; RRID: AB_10671444). (C) ISH for ErbB4 (C1; *cyan*) and Th (C3; *magenta*) was combined with IHC with an antibody against DAT (*green*; SantaCruz, sc-32258; RRID: AB_627400) in a sagittal FFPE section from an adult WT mouse; depicted substantia nigra compacta (SNc) on the left and dopaminergic medial forebrain bundle. (C') Magnification of ErbB4-expressing dopaminergic neurons (*arrowheads*) in the SNc. (D) In primary mesencephalic cultures (DIV8; prepared as in²³⁴), DAT (*green*) immunostaining was performed post-hoc to RNAscope for ErbB4 (C1; *cyan*) and Th (C3; *magenta*). Scale bars 100µm in B, 20µm in other panels. Abbreviations: ISH-IHC, in situ hybridization-immunohistochemistry; GFP, green fluorescent protein; FFPE, formalin-fixed paraffin-embedded; WT, wild type.

However, we established a post-hoc immunohistochemistry protocol using cell-type-specific transgenic green fluorescent protein (GFP) mice that allows for easy identification of cell-type-specific expression if transgenic GFP mice are available. GFP expression was destroyed and could not be observed directly after the ISH protocol but performing a post-hoc immunostaining using antibodies against GFP restored the signal. Of note, not all GFP antibodies tested retrieved the GFP expression. Here, we describe a BaseScope/RNAscope-immunohistochemical protocol using a mouse monoclonal anti-GFP antibody from NeuroMab (clone N86/8; University of California, Davis). The protocol follows the ISH protocols for RNAscope (Basic Protocol 1) or BaseScope (Basic Protocol 2), but before counterstaining for DAPI continues with the post-hoc immunostaining. An example on sections of transgenic GFP mice is represented in Figure 3.8B. Figure 3.8C, D show examples of ISH-IHC combination with an antibody against the dopamine transporter DAT (clone 6-5G10; SantaCruz; sc-32258; 1:200; RRID: AB_627400), where the epitope is not destroyed by the pretreatment.

Another combinatory approach useful in neuroscience is to combine retrograde tracing with RNAscope and BaseScope. In this case, fluorescent ISH can be coupled with fluorescent RetroBeads or cholera toxin that are transported retrogradely because the fluorescent properties of these markers are not lost during sample preparation.

Additional Materials (see also Basic Protocols 1 and 2)

- *In situ* hybridization prepared samples (see Basic Protocol 1 or Basic Protocol 2)

- Blocking solution: 10% normal donkey/ goat serum (e.g., Sigma-Aldrich, cat. no. D9663), 0.3% Triton X-100 (diluted from 10% Triton X-100, e.g., Thermo Fisher Scientific, cat. no. 28314) in 1x PBS
- Mouse monoclonal anti-GFP antibody (clone N86/8; NeuroMab, UC Davis, cat. no. 73-131; RRID: AB_10671444)
- Anti-mouse fluorescent-conjugated secondary antibody (e.g., donkey-anti mouse Alexa488; Invitrogen brand, Thermo Fisher Scientific, cat. no. A-21202; RRID: AB_141607)

In situ hybridization

1. Use samples from transgenic GFP mice that were hybridized as described in Basic Protocol 1 or Basic Protocol 2 (see Fig. 1). Perform all steps up to counterstaining with DAPI before proceeding with the immunostaining (e.g., steps 1 through 22, Basic Protocol 1, RNAscope; or steps 1 through 38, Basic Protocol 2, BaseScope).

Post-hoc immunostaining

2. Immediately following ISH, place sections in blocking solution 1hr at room temperature.

This is performed on the slide rack in the humidifying chamber.

3. Slide by slide, remove excess solution and replace with 1 μ g/ml mouse monoclonal anti-GFP antibody (clone N86/8, NeuroMab) in blocking solution. Place back in humidifying chamber and incubate overnight at 4°C.
4. Wash sections in 1x PBS plus 0.25% Triton X-100 (diluted from commercial 10% Triton X-100) for 10min at room temperature. Repeat twice with fresh wash buffer; the washes can be performed in Coplin jars.

The washes with Triton X-100 might dissolve the hydrophobic barrier pen. In this case the pen needs to be carefully reapplied without letting sections dry out.

5. One-by-one remove excess solution, place slide in humidifying chamber, and cover with secondary antibody solution (e.g., 1 μ g/ml anti-mouse A488 in blocking solution). Incubate in the dark (closed humidifying chamber) for 2hr at room temperature.
6. Wash sections in 1x PBS 10min at room temperature. Repeat twice with fresh wash buffer.
7. One slide at the time, counterstain cell nuclei by covering sections with DAPI, either from RNAscope kit or 1 μ g/ml in 1x PBS (Invitrogen) and incubate 30sec at room temperature.
8. Remove excess DAPI as described above, add aqueous mounting medium (~10 μ l per coronal section) and add cover slip to each slide; be careful to avoid trapping air bubbles. Store slides horizontally in the dark overnight at 4°C to dry.

Detect and analyze

9. Examine dried slides within a few days of preparation on a fluorescent (confocal) microscope (magnification 20 to 63x). The signals obtained from low abundance transcripts might be only visible at higher magnification (40 to 63x).

Digital image analysis using a camera is highly recommended. Signal can be quantified and analyzed as described in Basic Protocol 4 and the Commentary, Understanding Results and Statistical Analyses section.

3.7 Basic Protocol 4: Automated Quantification of Fluorescent ISH Signal using CellProfiler

It is often desirable to support qualitative image data with quantitative analysis to describe reproducibility between samples and distribution within the data or area analyzed, and to compare different signals and samples statistically. Automated quantification of the signal is an objective and accurate way to analyze the data. Different software, both commercial (HALO, Aperio, Spotstudio, Imaris) and freeware (ImageJ, CellProfiler), are available (see Table 3.1) and custom-made programs can be written for analysis²⁶⁰. The general principles used by all software are similar (see Fig. 9); i.e., the signal is filtered by intensity above a background threshold and this signal is assigned to cells that are designated as an area around the DAPI (or hematoxylin) nuclear staining to account for somatic localization of RNA transcripts. While commercial software is user friendly, it is expensive and often limited to certain applications. Therefore, we have routinely analyzed RNAscope and BaseScope data using the module-based free open-source software CellProfiler²²⁷ and below provide a step-by-step explanation of how to use our custom-made pipeline (see Fig. 3.9).

Table 3.1 | Software to Analyze ISH Signal.

software	source	website	chromogenic/ fluorescent analysis	download	RRID
HALO	Indica Labs	http://www.indicalab.com/products/multiplex-fish/ http://www.indicalab.com/products/sish-dual-cish-quantification/	both		
Aperio	Leica	https://www.leicabiosystems.com/digital-pathology/analyze/ish-fish/	both		
Spotstudio	Advanced Cell Diagnostics	https://acdbio.com/rnascope-spotstudio-software	chromogenic only		
Imaris	Bitplane	http://www.bitplane.com/imaris	both		SCR_007370
ImageJ/ Fiji	NIH	http://fiji.sc	both	http://fiji.sc/#download	SCR_002285
CellProfiler	Broad Institute	http://cellprofiler.org	both	https://cellprofiler.org/releases/	SCR_007358

Abbreviations: ISH: *in situ* hybridization; RRID: Research Resource Identifiers; NIH: National Institutes of Health.

As an example, we are using RNAscope data from Figure 3.5 that corresponds to hybridization of ErbB4 transcripts expressed in vGLUT1+ pyramidal neurons and GAD1+ GABAergic interneurons in the adult mouse brain cortex. The example image shown in Figure 3.9A was taken at 63x magnification. Of note, for single-dot resolution and successful performance of the quantification with these pipelines, magnification of at least 40x for RNAscope and 20x for BaseScope is required. Pipelines (macros) for RNAscope and BaseScope analysis similar to that used for this example are freely available on the website of CellProfiler (http://cellprofiler.org/examples/published_pipelines; see¹⁹²).

NOTE: The pipeline settings described in this protocol are optimized for this example only and will need to be adjusted for individual experiments depending on microscope magnification and settings, RNAscope probes, and the sample itself (e.g., age, section type, brain area analyzed). When setting up a pipeline, we recommend adjusting the pipeline with a variety of small cropped areas (similar to the example image in Fig. 9A) across the entire region of interest and different samples in the test mode before running the entire data set in the background mode (“Hide All Windows on Run”).

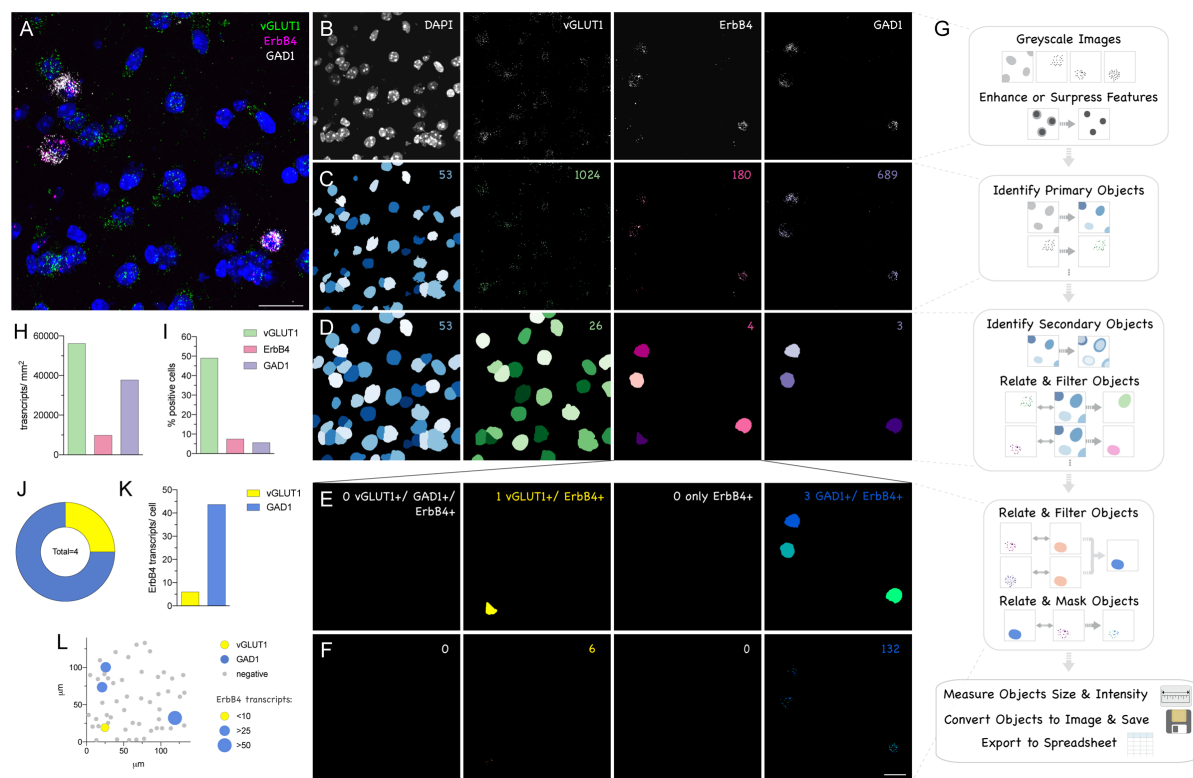


Figure 3.9 | Quantification of multiplex fluorescent ISH signal (e.g., RNAscope) with CellProfiler.

(A) Original RNAscope image analyzing ErbB4 expression (C1, *magenta*), in vGLUT1 (C2, *green*) and GAD1 (C3, *white*) positive neurons in the somatosensory cortex (see Fig. 5). (B) For analysis with CellProfiler the image is split into individual fluorescent channels and converted to grayscale. (C) Objects, “nuclei” (*blue*) and “dots” in each channel (*green, magenta, purple*) are identified using the module “IdentifyPrimaryObjects” by intensity and size. (D) “Cells” (*blue*) are computed by increasing the size of the nuclei (“IdentifySecondaryObjects”). Cells positive for one of the signals are subsequently filtered based on the related number of dots. (E) Double- and triple-positive cells were analyzed for the subpopulation of ErbB4+ cells by filtering: Triple-positive cells (NA), vGLUT1+ and ErbB4+ cells (*yellow*), only ErbB4+ (NA) and GAD1+ and ErbB4+ (*blue*). (F) ErbB4 expression levels of these subpopulations were obtained after masking the signal on these different cell types. (G) Schematic overview of CellProfiler pipeline used. (H) Transcript expression levels analyzed per area for vGLUT1 (*green*), ErbB4 (*magenta*), and GAD1 (*purple*). (I) Percentage of positive cells relative to all cells. (J) Subpopulations of ErbB4+ cells: Double-positive for ErbB4 and vGLUT1 (*yellow*), and for ErbB4 and GAD1 (*blue*). (K) ErbB4 transcripts expressed in these subpopulations. (L) Representation of the original image with ErbB4+/ vGLUT1+ in yellow, ErbB4+/ GAD1+ in blue, and ErbB4- in gray. The size of the symbols represents ErbB4 transcript levels in each individual cell. Numbers in the right upper corner indicate the number of objects identified (B-F). Scale bars 20µm.

Materials

- Computer
- ImageJ or Fiji (<http://fiji.sc/#download>)
- CellProfiler (<https://cellprofiler.org/releases/>)

- Digital images of fluorescent ISH (e.g., RNAscope, see Basic Protocol 1 or BaseScope, see Basic Protocol 2)

File input

1. Split different fluorescent channels (DAPI, green, red, far-red) of a multi-channel image using image-manipulating software (e.g., ImageJ) and save individually as.tiff files (recommended format).

CellProfiler recognizes the different channels of an image by the name of the file (e.g., contains C1 for DAPI, C2 for green, C3 for red, C4 for far-red).

2. Import image set (all channels of one image) into CellProfiler by simple drag-and-drop.
3. With the module “ColorToGray”, convert image to grayscale (if not already pre-converted in ImageJ), see Figure 3.9B.
4. *Optional:* Enhance intensity features relative to the background with the module “EnhanceOrSuppressFeatures”, which can help to identify objects.

We recommend enhancing the RNAscope signal with the feature “Speckle”. The size of the “Speckles” is in pixel units, as are all subsequent objects, and therefore depends on the resolution of the image.

Object identification

This is the key of the pipeline to identify both the RNAscope signal as well as DAPI-positive nuclei using the module “IdentifyPrimaryObjects” (Fig. 3.9C). Objects are identified by intensity threshold that can be a manual value (not recommended), based on a previous measurement or an algorithm. The signal can be additionally restricted in size (in pixels). Finally, clumped objects can be distinguished by shape or intensity.

5. Measure background intensity of DAPI channel using the module “MeasureImageIntensity”.
6. Use the module “IdentifyPrimaryObjects” to identify DAPI-positive nuclei.

We recommend identifying “nuclei” based on the previous measured mean intensity of background. The size filter of the objects in our example was 50 to 300 pixels and declumping for nuclei was done based on shape.

7. Identify RNAscope signal/ dots of one channel (e.g., green) using the same module. For dot identification in each channel both previous measurements or algorithm work generally well.

For our example, we used the global Otsu algorithm, size exclusion of 2 to 20 pixels and distinguished clumped objects by intensity.

- Repeat identification of objects for each RNAscope channel (e.g., red and white equals far-red) signal using the module “IdentifyPrimaryObjects” as described in step 7.

Identify cells and filter for single, double, and triple positive cells

- Enlarge the size of the nuclei using the module “IdentifySecondaryObjects”. This accounts for the somatic accumulation of RNAs. Use function “Distance – N” to increase the object size by a certain number of pixels until colliding with another object (Fig. 3.9D).

We typically call these objects “cells.” In our example the nuclei were expanded by 25 pixels.

- Relate the RNAscope signal (“children”) for one channel (e.g., green) to the cell (“parent”) with the module “RelateObjects”.
- Repeat step 10 for the remaining RNAscope signals (e.g., red and white channel).
- Filter positive cells for one channel (e.g., green) based on the number of dots assigned to this cell using the module “FilterObjects”. The threshold needs to be set based on expression levels of each probe to exclude false-positive cells.

In our example, we were using a minimum of 10 dots for vGLUT1 (green), 5 dots for ErbB4 (red), and 25 dots for GAD1 (white).

- Repeat step 12 for the remaining channels (e.g., red and white).
- Relate RNAscope signals (“RelateObjects”) to the newly identified cell population (e.g., red cells) and filter (“FilterObjects”) into double-positive (e.g., “red and green cells,” “red and white cells”) and triple positive (green, red, and white) as in steps 10 to 13.

In our example, we analyzed the population of ErbB4+ cells (red cells) for co-expression of one of the other markers (Fig. 3.9E).

Analyze transcript expression levels

- Re-relate signals back to the newly identified objects (single, double, and triple positive cells) using the “RelateObjects” module as described in steps 10 and 11 to identify single-cell expression levels.
- Mask RNAscope signal with the positive cells to sort for transcripts expressed in the positive cells using the “MaskObjects” module (see Fig. 3.9F).

Measurements and data export

- Optional:* Use modules “MeasureObjectSizeShape” and “MeasureObjectIntensity” to measure size and intensity of objects.

18. *Optional*: With the module “ConvertObjectsToImage”, convert objects to an image for subsequent export using the module “SaveImages”. This can serve as a quality control, when the pipeline is run in the background mode.
19. Export your data in csv format with the module “ExportToSpreadsheet”. The summary analysis is stored in the file titled “_Image”, whereas details about each individual object are found in the respective files (see Fig. 3.9G).

Data representation: Typical values obtained with this analysis are: Expression levels per area (Fig. 3.9H; area measured, e.g., in ImageJ), percentage of positive cells per all cells analyzed (Fig. 3.9I), subpopulations of positive cells (Fig. 3.9J), and the average transcript expression level in different cell populations (Fig. 3.9K). Another advantage of this analysis is that values per individual object are exported. This information allows one to determine: Expression levels per cell, x or y positions of each cell, size, and intensity of each signal. This data can be used to plot the expression in one (e.g., cortical layer, see Fig. 3.5E) or two dimensions (Fig. 3.9L). In addition, the expression per cell data can be plotted either as a histogram/frequency distribution or cumulative probability to determine the cut-off between background and signal (see Erben et al., 2018).

3.8 Reagents & Solutions

Ammonium water, 0.02% (w/v)

For the preparation of 50ml:

- In a fume hood, add 33 μ l of 30% ammonium hydroxide (e.g., Sigma-Aldrich, cat.no. 221228) to 50ml of distilled water in a Coplin jar.
- Seal with Parafilm and mix by inverting five times.
- *Prepare fresh for each experiment.*

Mowiol DABCO mounting medium

For preparation of 25 ml:

- In a 50-ml Falcon tube, add slowly (over hours) 2.4 g Mowiol (Calbiochem, cat. no. 3475904) to 6 g glycerol while mixing. Add 6 ml of water and mix at room temperature overnight.
- Add 12ml of 0.2M Tris·HCl (pH 6.8) and warm up in a water bath (beaker) on a hot plate to 50°C while stirring.
- After Mowiol is dissolved, add 0.625 g DABCO (Sigma-Aldrich, cat. no. D2522) to 2.5% w/v.

- Clarify solution by centrifugation at 5000x g for 15min.
- Aliquot supernatant and freeze at -20°C for up to 6 months.
- Before use, warm up briefly to 37°C. Store and use aliquot at 4°C.

3.9 Commentary

3.9.1 Background Information

In situ hybridization (ISH) is a widely used technique to analyze gene expression. The high specificity and reproducibility of ISH techniques that allow multiplexing, such as RNAscope and ViewRNA, can be used to determine developmental and cellular patterns of protein expression before resorting to the more complicated immunological approaches. Expression of non-coding RNAs can also be analyzed by ISH²⁶¹. In recent years numerous advancements in high throughput RNA sequencing from tissues and even from single cells has led to the identification of numerous neuronal subtypes, usually categorized by the neurotransmitter they synthesize, and a better understanding of the dynamic changes in transcriptomes during development and in disease²⁶²⁻²⁶⁴. These methods are extremely powerful for rapidly identifying biomarkers and differentially expressed genes. However, in contrast to ISH approaches, these methods fail to provide the expression of genes in single cells in the context of intact tissue. This is one reason that ISH approaches, like RNAscope, are frequently used to validate and supplement RNAseq data^{260, 265-267}. Next-generation ISH techniques, such as BaseScope, are also useful to complement transcriptome sequencing data that identifies short RNA sequences, splice variants, and single nucleotide polymorphisms. Whereas quantitative real time reverse transcription (RT)-PCR is a faster and more quantitative method than BaseScope to analyze relative levels of distinct RNA splice variants, it also lacks cellular resolution in tissue. Importantly, we recently have shown that semi-quantitative analysis of splice variants using BaseScope provides similar results to quantitative real time RT-PCR, but with the added advantage of studying splice variants with cellular resolution in intact tissue^{192, 258}.

3.9.2 Critical Parameters & Troubleshooting

Preparing sections

A critical parameter for successful results is the overall quality of the sections, as regards the preservation of RNA, cell morphology, and tears or wrinkles; see general recommendations for high-quality tissue section preparation^{255, 256}. Avoid moisture and freeze-thawing cycles that are permissive for RNase activity and use RNase-free equipment and solutions where indicated. To reduce or avoid detachment of sections, which most commonly occurs during antigen retrieval, use charged Super-frost slides and increase the baking time. When using paraffin-embedded tissue, it is important to use fresh ethanol and xylene with agitation to fully remove paraffin; otherwise, residual wax can result in unspecific staining.

Reducing edge artifacts and background

To avoid edge artifacts and background, keep sections from drying out, unless where it is specified in the protocol. To avoid these problems, it is important to ensure that the humidifying tissue and the hybridization chamber used throughout the procedure remain moist at all times; preferably, use RNase-free water. In addition, to reduce the risk of sections drying out we recommend: (1) work on a single slide at a time, (2) maintain a manageable number of slides processed in a single experiment, (3) submerge every section with reagent on a slide before proceeding to the next slide, and (4) do not skimp on reagents; always use sufficient amounts to completely submerge each section (see also²⁶⁸).

Optimization of conditions

Follow the protocols with regards to incubation times and temperatures during probe hybridization and amplification, as these have been optimized for each reagent. On the other hand, pretreatment conditions may need to be optimized if samples are not properly prepared or fixed using other protocols (e.g., human tissue). In these cases, run preliminary assay(s) with negative and positive controls to evaluate morphology and staining. If the signals are weak, but the morphology of tissue is well preserved as indicated by strong nuclear staining, this could suggest that probe accessibility is impaired due to over fixation or underdigestion. To address this point, pretreatment conditions can be adjusted as follows: Increase incubation time in target retrieval by increments of 5min and/ or increase digestion time with protease treatment

by increments of 10min. On the other hand, if the preservation of morphology is poor (weak nuclear stain) and either high background staining or non-uniform signals are observed, it could suggest that tissue sections could have been over digested or under fixed. To address this point, decrease incubation times incrementally or dilute the protease²⁶⁸.

Control probes and slides

Positive and negative control probes (see protocols) and slides (e.g., mouse 3T3 pellet, ACD, cat. no. 310023) are available from the vendor and can help to evaluate signal-to-noise and trouble-shoot conditions. In cases where no signal is detected we direct the reader to follow the workflow suggested by the vendor (see recommended workflow in²⁶⁸). Once RNAscope and BaseScope are successfully set up, the hybridization of a well-known distinctively expressed gene can also be used as reference (e.g., GAD1/2, vGLUT1/2, TH). The signal should be positive in expected areas, but low/ no signal should be observed where the gene is not expected to be expressed. The best negative control is a transgenic mouse that lacks the transcript. However, the transgene needs to lack the whole target sequence (in the case of RNAscope ~1000 bases), otherwise residual transcript might result in signal.

3.9.3 Understanding Results & Statistical Analyses

There are important differences between RNAscope and BaseScope that affect the interpretation of results; therefore, we begin by separately discussing these differences below. Under optimal conditions, RNAscope has single molecule resolution and one dot represents one transcript²⁵⁰. The number of dots therefore equals the number of transcripts expressed. However, the size and intensity of dots, which can vary between channels and the number of fluorescent labels and probe pairs bound to a transcript, are not related to the number of transcripts. A single dot per cell in RNAscope, especially when observed in only a few cells (<10%), is considered background (see Scoring Guidelines in²⁶⁸). Most house-keeping and cell marker genes are expressed at high levels (>10 dots per cell), to the extent that in some cases it is difficult to resolve single dots (clusters).

In contrast to RNAscope, which uses fluorescent labels, BaseScope uses an enzymatic dye reaction to amplify the signal and results in bigger dot sizes that sometimes fuse. In addition, the single-probe pair used in BaseScope cannot guarantee the same single transcript resolution,

as compared to the six to twenty “ZZ” probes used in RNAscope. However, because the detection threshold in BaseScope is higher, in some cases single dots might represent actual signal and cannot be discarded as background in absence of additional evaluation. We have previously evaluated the background signal of BaseScope in single exon mutant mice and rarely observed cells that were positive for a single dot¹⁹². Finally, due to short target sequences in BaseScope, variability in hybridization efficiency can be observed between different probes targeting distinct transcripts or regions within a transcript. These differences originate from variations in nucleotide sequences and accessibility of the transcript (e.g., protein binding target sequence), and are not observed in RNAscope that targets longer sequences (~1000 bases)^{192, 251}.

Considering these general differences in the nature of the hybridization signal, the overall evaluation and quantification approaches are similar for RNAscope and BaseScope. The vendor suggests a simple semi-quantitative scoring to evaluate the ISH staining. A score from 0 to 4 is assigned depending on the average expression levels per cell (0: <1 dot per 10 cells; 1: 1 to 3 dots per cell; 2: 4 to 9 dots per cell; 3: 10 to 15 dots per cell; 4: >15 dots per cell) and can be compared to the expression levels of control genes (see Scoring Guidelines in²⁶⁸). While this method is helpful to quickly evaluate the overall hybridization success between samples and batches, it carries little quantitative information.

Automated quantification results in less subjective quantitative data. Software specialized for ISH analysis (HALO, Aperio, Spotstudio) is available but similar analysis can be achieved using generic image analysis software (e.g., Imaris) and open-source software (e.g., ImageJ, CellProfiler; see Table 3.1). Basic Protocol 4 outlines step-by-step how to apply a freely available custom-made CellProfiler pipeline to analyze multiplex fluorescent ISH data.

The described quantification approach can encounter a couple of issues that originate from the nature of the ISH technique itself. In brain areas where cells are very dense (e.g., hippocampal pyramidal cell layers), single-cell quantification can be difficult. Distinguishing single nuclei is not always possible, and even if successful, transcripts from one cell can often overlap with the next cell area, resulting in false positive cells. Similarly, RNA transcripts that are transported into neuronal dendrites or axons^{269, 270} are likely to be incorrectly assigned to the wrong cell. These shortcomings are common to all ISH techniques and practically cannot

be avoided unless, at a single-cell level, an entire cell and/ or neuron and its processes are counter labeled (e.g., filled with fluorophore). However, the transport of transcripts corresponds to a small fraction of the transcriptome and in most brain areas single-cell quantification works extremely well.

For statistical analyses, multiple samples hybridized under the same conditions and imaged with the same parameters need to be compared. However, in histological analyses, such as ISH approaches, small sample numbers (n=2 to 4 animals; n=1 to 3 sections) are generally sufficient for statistical analyses^{192, 260, 271}. Even with small sample numbers thousands of cells are analyzed in one region of interest, resulting in robust data. It is important to note that if different samples (e.g., animals) are compared, it is best to hybridize and analyze all samples at the same time to avoid inter-assay variability. If this is not possible because of a large number of samples, samples should be randomized (e.g., one control sample and one knock-out or treatment sample at a time) and imaging parameters kept identical.

3.9.4 Time Consideration

A major advantage of multiplex (RNAscope) and single-plex (BaseScope), relative to other ISH techniques (i.e., using radioactivity), is their extremely fast turnaround time. The approaches are standardized for optimal signal detection and do not have varying developing times, as ISH techniques using radioactive labels and colorimetric substrates. In addition, the probes are custom made, designed, and generated by the vendor. Therefore, the hands-on time consists only of the ISH assay itself and the subsequent analysis. Depending on the sample type, pretreatment varies between ~1.5 and 2.5hr (see Fig. 3.1). There are optional stopping points during the pretreatment to split the assay into 2 days. The ISH assay needs to be completed in one session and takes 4hr for RNAscope and 6.5hr for BaseScope. Slides are dried overnight and can be imaged with a microscope the next day or within a few days. The time for detection and analysis varies depending on the application, from brief examination to overview scanning and detailed quantification with statistical analysis. If a post-hoc immunostaining is desired (Basic Protocol 3) an additional hour for blocking the day of the ISH assay needs to be considered with an overnight incubation and three additional hours the following day.

The use of ISH assays described in this article is relatively simple and does not pose major safety considerations (i.e., radiation exposure and contamination). Therefore, the intrinsic properties of these assays make them amenable not only to trained scientists but also to inexperienced trainees.

4

ErbB4 isoform expression in the mouse and human brain

This chapter presents an extended version of the publication: Erben Larissa, Ming-Xiao He, Annelies Laeremans, Emily Park & Andres Buonanno (2018) A novel ultrasensitive in situ hybridization approach to detect short sequences and splice variants with cellular resolution. Mol Neurobiol, 55(7):6169-6181. Added sections are emphasized in dark grey italics.

Authors contributions: L.E. and A.B. designed research, MX.H., A.L., E.P. designed & provided reagents, L.E. performed research, L.E. analyzed the data, L.E. and A.B. wrote the paper.

4.1 Abstract

Investigating the expression of RNAs that differ by short or single nucleotide sequences at a single-cell level in tissue has been limited by the sensitivity and specificity of *in situ* hybridization (ISH) techniques. Detection of short isoform-specific sequences requires RNA isolation for PCR analysis – an approach that loses the regional and cell-type-specific distribution of isoforms. Having the capability to distinguish the differential expression of RNA variants in tissue is critical because alterations in mRNA splicing and editing, as well as coding single nucleotide polymorphisms, have been associated with numerous cancers, neurological and psychiatric disorders. Here we introduce a novel highly sensitive single-probe colorimetric/fluorescent ISH approach that targets short exon/exon RNA splice junctions using single-pair oligonucleotide probes (~50bp). We use this approach to investigate, with single-cell resolution, the expression of four transcripts encoding the Neuregulin (NRG) receptor ErbB4 that differ by alternative splicing of exons encoding two juxtamembrane (JMa/JMb) and two cytoplasmic (CYT-1/CYT-2) domains that alter receptor stability and signaling

modes, respectively. By comparing ErbB4 hybridization on sections from wild-type and ErbB4 knockout mice (missing exon 2), we initially demonstrate that single-pair probes provide the sensitivity and specificity to visualize and quantify the differential expression of ErbB4 isoforms. Using cell-type-specific GFP reporter mice, we go on to demonstrate that expression of ErbB4 isoforms differs between neurons and oligodendrocytes, and that this differential expression of ErbB4 isoforms is evolutionarily conserved to humans. This single-pair probe ISH approach, known as BaseScope, could serve as an invaluable diagnostic tool to detect alternative spliced isoforms, and potentially single base polymorphisms, associated with disease.

4.2 Introduction

Alternative mRNA splicing increases the functional complexity of the genome, with >90% of all human multi-exon genes being differentially spliced²⁷². In the central nervous system (CNS) alternative splicing is tightly regulated in a spatiotemporal manner, as well as by neuronal activity^{248, 273, 274}. Different mRNA isoforms encode for ion channels, neurotransmitter receptors, adhesion molecules, and signaling proteins with distinct functional properties^{32, 275-277}. Splicing abnormalities are observed in different cancers and neurological diseases^{24, 278}, but are particularly abundant in psychiatric disorders, such as affective and addictive disorders, schizophrenia (Scz) and autism spectrum disorders²⁶. In the postmortem brain of Scz patients, splice variant expression of many at-risk alleles is altered²⁵; including those that encode: trophic factors^{31, 279-284}, neuronal migration and adhesion proteins^{285, 286}, structural components of myelin and synapses^{287, 288} and isoforms associated with dopaminergic, GABAergic and glutamatergic neurotransmission and signaling²⁸⁹⁻²⁹³.

The NRG/ErbB4 signaling pathway, which is reported to be associated with a risk for Scz^{27, 28, 294, 295}, and its endophenotypes⁴, regulates neuronal differentiation, migration and plasticity in the CNS^{30, 35, 38}. Alternative splicing of two exons encoding the extracellular juxtamembrane (JM) domain JMa (75bp exon) or JMb (45bp exon), and the inclusion or exclusion of a 48bp exon in the cytoplasmic (CYT) domain, generates four ErbB4 receptor isoforms: JMa/CYT-1, JMa/CYT-2, JMb/CYT-1 and JMb/CYT-2 (Fig. 4.1;^{190, 191}). ErbB4 transcript levels comprising JMa and CYT-1 exons are increased in the dorsolateral prefrontal cortex (DLPFC)

of Scz subjects^{28, 218, 222, 223}, and single nucleotide polymorphisms in ERBB4 correlate with changes in receptor isoform expression and risk for Scz^{28, 222, 223}.

The four ErbB4 isoforms differ functionally. JM_a-containing ErbB4 isoforms, but not JM_b variants, are susceptible to extracellular metalloprotease-mediated cleavage followed by gamma-secretase intramembranous cleavage that releases a transcriptionally-active intracellular domain (ICD) to regulate gene expression^{47, 48, 190, 194, 203}. CYT-1-containing isoforms encode a site for phosphatidylinositol 3-kinase recruitment that increases the downstream signaling capacities of CYT-1 variants^{191, 203}.

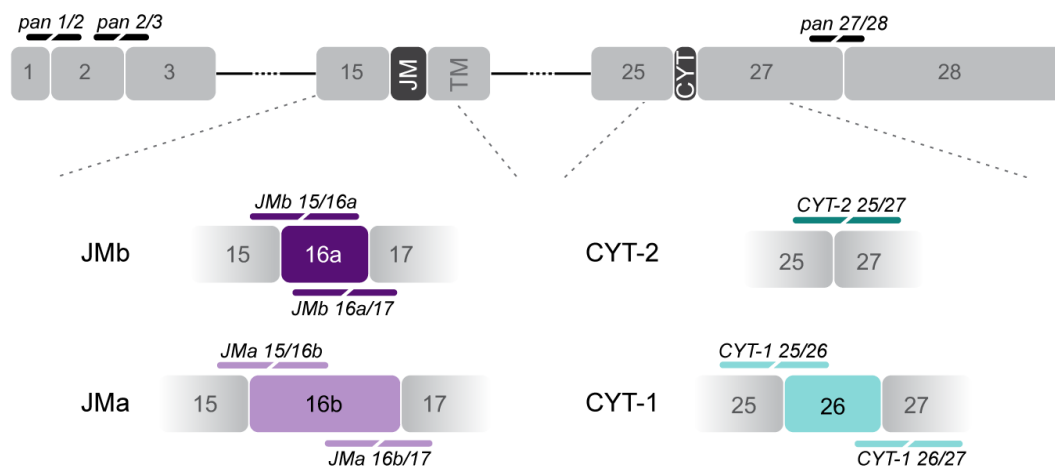


Figure 4.1 | Scheme summarizing ErbB4 isoforms and single-pair probe design.

ErbB4 isoforms are generated by alternative splicing of exons encoding the extracellular juxtamembrane domain, resulting in mutually exclusive JM_a (exon 16b, light purple, 75bp) or JM_b (exon 16a, dark purple, 45bp) isoforms, and by inclusion or exclusion of exon 26 encoding a region of the cytoplasmic domain giving rise to CYT-1 (light cyan, 48bp) and CYT-2 (dark cyan) isoforms, respectively. Single-pair probes targeting all ErbB4 isoforms (pan 1/2, pan 2/3 and pan 27/28) are illustrated in black, whereas isoform-specific single-pair probes targeting splice junctions are color-matched with their respective isoforms. JM: juxtamembrane region; TM: transmembrane domain; CYT: cytoplasmic region.

Because of the different functions imparted by distinct splice variants, in this case ErbB4, it is critically important to identify the cells that express distinct isoforms. Whereas quantitative real-time PCR (qRT-PCR) and RNA sequencing (RNAseq) can be designed to detect specific RNA splice variants with high sensitivity in different brain regions, these methodologies require the disruption of dissected tissue to isolate RNA. The technical requirements of RNA isolation come at the expense of losing *in vivo* cell-type-specific resolution of splice variant expression. Traditionally, *in situ* hybridization (ISH) using radioactively- and fluorescently-labeled complementary RNA probes have provided the sensitivity to detect abundant

transcripts at cellular level, but fail to unambiguously identify cells expressing rare splice variants. Recent advances in ISH using multiple non-radioisotopic oligonucleotide probe pairs targeting a single transcript, combined with chemical signal amplification^{250, 296}, enable specific and sensitive co-detection of rare transcripts (known as “multiplexing”²⁹⁷). However, the optimal target lengths of these probes (>300bp) exceed the size of most alternative spliced variants. Due to these limitations, in the present study we implement a novel ISH approach based on an ultrasensitive amplification chemistry that allows the specific detection of mRNA exon junctions by a single pair of 18-25bp anti-sense oligonucleotide probes targeting adjacent mRNA sequences; hereafter denoted as “single-pair probe”.

4.3 Materials and Methods

For further details see Supplemental Information.

Animals and Human Brain Samples. Homozygous ErbB4 knock-out (KO) mice lacking exon 2¹⁵⁷ will be hereafter designated as ErbB4- Δ 2 KO mice. CNP-GFP²⁹⁸, NG2-GFP²⁹⁹ and wild-type (WT) C57BL/6J mice were obtained from the Jackson Laboratory. GAD67-GFP mice³⁰⁰, were a kind gift from Yuchio Yanagawa (Gunma University, Japan). All procedures were approved by the NIH Animal Care and Use Committee. Ground frozen human brain samples from four male adult control individuals were obtained from the Human Brain Collection Core (National Institute of Mental Health, NIMH).

ISH. The novel single-pair probe ISH approached used here (BaseScope, Advanced Cell Diagnostics, Newark, CA) is based on the well-established multiplex fluorescent ISH RNAscope[®] (Advanced Cell Diagnostics²⁵⁰). The high specificity and sensitivity of both ISH technologies are reached by a unique probe design using ‘ZZ’ probe pairs and signal amplification, respectively. Advances in signal amplification over RNAscope[®] allow for the use of a single-pair probe in the BaseScope assay, consisting of a pair of 18-25bp oligonucleotide sequences. To detect exon junctions, one oligonucleotide probe hybridizes to target sequences across the exon junction and the other probe to an immediately adjacent region. Targeted sequences of customized junction-specific ErbB4 ISH probes are listed in Table 4.1 and schematically illustrated in Fig. 4.1. RNAscope[®] probes were ErbB4 (Mm-ErbB4; Cat No. 318721), GAD-2 (Mm-GAD2-C2; Cat No. 415071-C2) and MAG (Mm-MAG-C3; Cat No. 446451-C3), *ErbB3* (Mm-ErbB3-C2; Cat No. 441801-C2), *PECAM-1*

(*Mm-Pecam1-C3*; Cat No. 3176721-C3) and *PDGFRb* (*Mm-Pdgfrb-C3*). Briefly, BaseScope ISH assay was performed on 8µm-thick formalin-fixed paraffin-embedded sections of ten-week old adult mice; prepared as described by³⁰¹. Briefly, sections were deparaffinized in xylene, endogenous peroxidase activity was blocked by H₂O₂ treatment (10min at RT) and sections were permeabilized by antigen retrieval (15min at 100°C) and a protease mixture (30min at 40°C). Probes were bound by incubation for 2h at 40°C, chemically amplified, and then labeled by fluorophores (multiplex ISH) or alkaline phosphatase conversion of FastRED dye (single-pair probe ISH).

Table 4.1 | Exon junction-specific single-pair probes for the detection of distinct ErbB4 isoforms

Probe name	Exon junction	Specificity	Target sequence (5' → 3')
JMa* 15/16b	E15/E16b	JMa	CCAGGG / GTGTAACGGTCCCCTAGTCATGACTGCATTACTACCC
JMa* 16b/17	E16b/E17	JMa	GGACGGGCCATTCCACTTTACCACAACACGCTAG / AACTCCAC
JMb* 15/16a	E15/E16a	JMb	CCCAGGG / GTGCATAGGTTCAAGCATTGAAGACTGCATCGGC
JMb* 16a/17	E16a/E17	JMb	GTTCAAGCATTGAAGACTGCATCGGCCTGACGGATAG / AACTCCAC
CYT-1 25/26	E25/E26	CYT-1	CATCTACACATCCAGAACAAGAATTGACTCCAATAGG / AGTGAAATTGGAC
CYT-1 26/27	E26/E27	CYT-1	CCATGTCCGGGA / AATCAGTTTGTGTACCAAGATGGGGGCTTT
CYT-2 25/27	E25/E27	CYT-2	CCATCTACACATCCAGAACAAGAATTGACTCCAATAGG / AATCAGTTTGT
pan 1/2	E1/E2	All isoforms	TCTCAGTCAG / TGTGCGCAGGAACAGAGAACAACTGAGCTCTCTCT
pan 2/3	E2/E3	All isoforms	GAGACAACCGGGACCTCTCCTTCCTGCGG / TCTATCCGAG
pan 27/28	E27/E28	All isoforms	GCATGACAAGCCCAAACAAG / AATATCTGAATCCTGTGGAAGAGAACC
<i>JMa</i> 2pairs	<i>E15/E16b & E16b/E17</i>	<i>JMa</i>	<i>CACCCAGGG / GTGTAACGGTCCCCTAGTCATGACTGCATTACTACCATGGACGGGCCATTC CACTTTACCACAACACGCTAG / AACTCCACTGAT</i>

Name of ErbB4 single-pair probes correspond to the number of the targeted exon/exon junctions. All target sequences correspond to sense strand and exon junctions are indicated by the dash. *Juxtamembrane exons JMa and JMb are numbered for convenience as exon 16b and 16a, respectively, which correspond to exon 16 and 15b in²¹³.

Immunostainings. Post-hoc immunohistochemistry immediately following ISH was performed as previously published³⁹ using 1µg/mL mouse monoclonal anti-GFP (isotype IgG2a, clone N86/8; NeuroMab, Davis CA).

qRT-PCR. RNA was isolated from micro-dissected ROI of ten-week-old male WT mice or ground human brain tissue using TRIreagent Kit (ThermoFisher, Waltham MA). cDNA was synthesized with random hexamers from 1µg RNA using SuperScriptIV Reverse Transcriptase

(ThermoFisher). Quantification of ErbB4 isoforms was performed as described³⁰² using TaqMan assays (ThermoFisher).

Imaging and Quantification. FastRED fluorescent signal was excited at 530nm and analyzed at 20x magnification. Unbiased automated signal detection and quantification was performed using CellProfiler²²⁷. Intensity threshold was determined based on background intensity in ErbB4- Δ 2 KO sections and dot diameter threshold (≥ 3 pixels) based on mean dot diameter in WT sections. Dots/ area, percentage of positive cells and average number of dots/ cell were calculated.

Statistical Analysis. All data represent the mean \pm SEM and statistical significance was set at $p < 0.05$. Statistical analyses were performed using one-way ANOVA and Tukey's multiple comparison test. Statistical analyses are tabulated in Supplemental Tables.

4.4 Results

4.4.1 Sensitivity and specificity of the novel single-pair probe ISH approach

Initially, to determine if single-pair BaseScope probes targeting exon junctions provide the necessary sensitivity to detect ErbB4 transcripts, we hybridized sections of WT mice with two independent "panErbB4" single-pair probes that target mRNA junctions between exons 1/2 (pan 1/2) and exons 2/3 (pan 2/3) that are present in all receptor isoforms (see Fig. 4.1). The amplified signal was detected following alkaline phosphatase and FastRED staining using fluorescence (Fig. 4.2A-C) and bright-field microscopy (Fig. 4.2D), or following horseradish peroxidase and diaminobenzidine treatment (Fig. 4.2E; Suppl. Fig. 4.8). In hippocampal sections from WT mice, both panErbB4 single-pair probes labeled scattered cells (Fig. 4.2A-E). This pattern is consistent with the expression pattern of ErbB4 obtained by 20 probe pairs in multiplex fluorescent ISH (Suppl. Fig. 4.8N), the restricted expression of ErbB4 in GABAergic interneurons (Suppl. Fig. 4.8O) and its absence in pyramidal neurons⁵⁸.

To validate the specificity of the single-pair probes, we used as negative controls sections from ErbB4- Δ 2 KO mice that lack exon 2¹⁵⁷, and targeted the upstream and downstream junctions of exon 2 with probes pan 1/2 and pan 2/3, respectively. In contrast to the high cellular ErbB4 expression in hippocampal interneurons of WT mice (Fig. 4.2A-E), the signal

was absent in the ErbB4- Δ 2 KO (Fig. 4.2F-J, Suppl. Fig. 4.8). In summary, these results show the sensitivity and specificity of single-pair probes to visualize exon junctions.

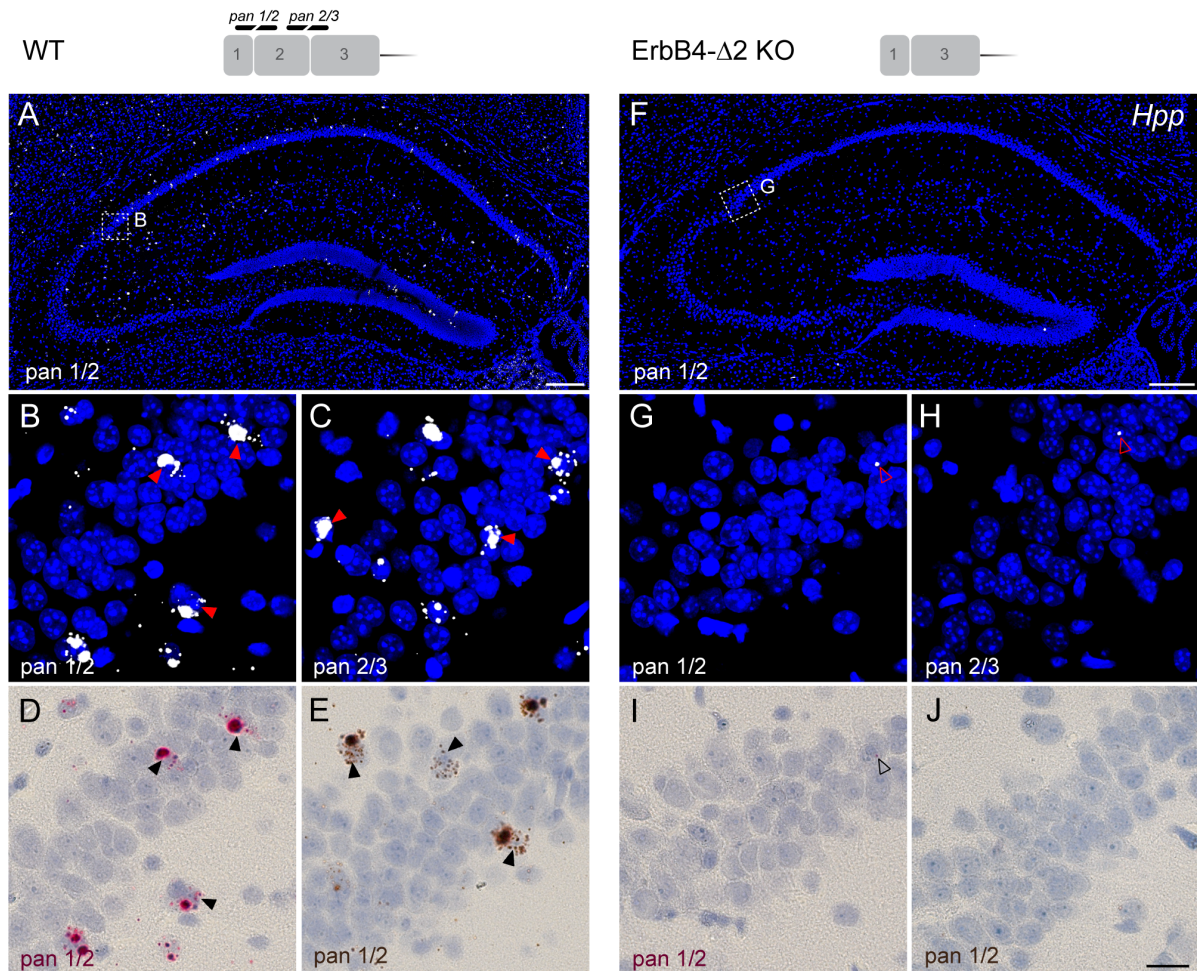


Figure 4.2 | Single-pair probes targeting unique exon junctions are specific and sensitive.

The specificity and sensitivity of single-pair probes targeting exon-exon boundaries were determined by hybridizing sections from WT (A–E) and ErbB4- Δ 2 KO mice (F–J). Probes targeting the exon 1/2 (pan1/2; A, B, D, E) or exon 2/3 (pan 2/3; C) junctions – common to all ErbB4 isoforms – labeled scattered cells in the WT hippocampus (arrowheads). (F–J) By contrast, neither probe generated signals in sections from ErbB4- Δ 2 KO mice (background signal marked by open arrowheads). (B, G) Magnified insets in panels A and F are from area CA2. Signal can be detected by alkaline phosphatase and FastRED visible both in fluorescence (A–C, F–H) and bright field microscopy (D, I) or horseradish peroxidase and diaminobenzidine (E, J). in Scale bars: A, F 200 μ m; J 20 μ m.

4.4.2 Semi-quantitative analysis of junction-specific single-pair probe ISH

To complement our qualitative analysis, we wrote a pipeline (macro) for the open-source software CellProfiler²²⁷ that allows for the unbiased quantification of signals. The pipeline, which is available online, identifies fluorescent FastRED signals above threshold and assigns

them to the closest DAPI-positive nuclei. The results are exported in Excel-format (for details see Supplemental Information). Using this approach on sections from WT mice, we found that ErbB4 expression is uniformly high in the medial habenula (mHab; Fig. 4.3A) and that its overall regional levels are low in the hippocampus (Hpp; Fig. 4.3B), consistent with prior studies^{52, 57}. Despite the low regional expression in the hippocampus, signals on sections from WT mice were dramatically higher than in sections from ErbB4-Δ2 KO mice using probes that target either boundary of the deleted exon 2 (Fig. 4.3B,C; $p < 0.0001$). Background levels in ErbB4-Δ2 KO (see open arrowheads in Fig. 4.2G,H,I) consisted mainly of single dots (Fig. 4.3D), whereas all probes targeting distinct ErbB4 exon boundaries on sections from WT mice were expressed notably above these background levels.

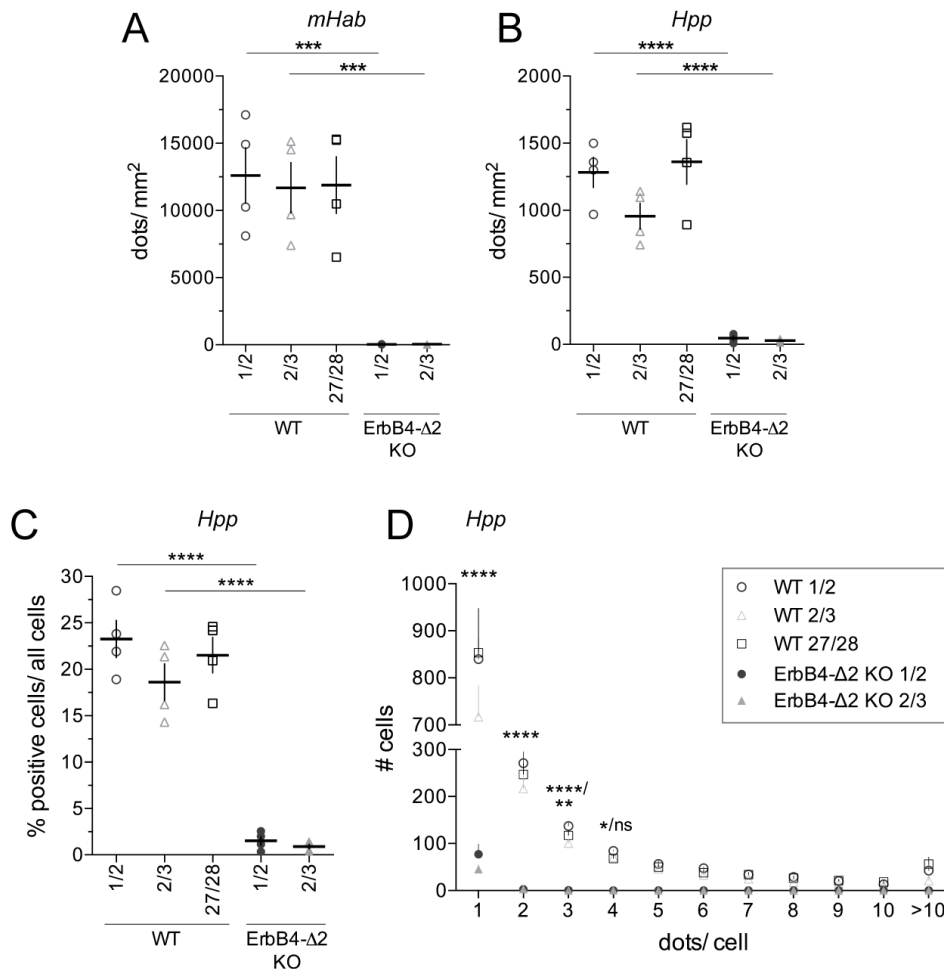


Figure 4.3 | Detection levels for independent probes targeting distinct exon junctions are similar and differ markedly from background in ErbB4-Δ2 KOs.

In situ hybridization signals of single-pair probes pan1/2 and pan 2/3 are significantly lower in sections from ErbB4-Δ2 KO mice compared to WT mice in the (A) medial habenula (mHab) and (B) hippocampus (Hpp) (n=4;

one-way ANOVA, see Suppl. Table 4.3) and did not differ among pan 1/2, pan 2/3 and pan 27/28 probes in sections from WT mice. (C) Percentage of positive cells relative to all cells in WT hippocampus (CA1–CA3). (D) Histogram distribution of dots/ positive cell detected with single-pair panErbB4 probes in hippocampal CA1–CA3 on sections from WT and ErbB4-Δ2 KO mice. Significance shown for comparisons between WT 1/2 vs. KO 1/2 and WT 2/3 vs. KO 2/3, respectively (n=4; two-way ANOVA, see Suppl. Table 4.6). Adjusted p values according to Tukey’s multiple comparison test: *p<0.05, **p<0.01, ***p<0.001, ****p<0.0001.

Expression analysis at a cellular level in the hippocampus indicate that approximately 20% of cell nuclei are labeled by single-pair panErbB4 probes (Fig. 4.3C), as was expected from the known restricted expression of ErbB4 in cortical and hippocampal GABAergic interneurons (Fig.S1; ⁵⁸). *While single-pair probes detecting all ErbB4 transcripts are sensitive enough to label similar numbers of positive cells compared to the 20 probe pairs in multiplex ISH (Suppl. Fig. 4.12B), they do not possess single transcript resolution and transcript levels per cell are lower (Supple. Fig. 4.12C; Suppl. Table 4.8). However, the detection of the low-expressed splice variant ErbB4 JMa could be improved by hybridizing two probe pairs to the 75bp exon (Suppl. Fig. 4.12D-G; Suppl. Table 4.9). Lastly, although hybridization efficiencies of small single-pair probes could theoretically vary depending on the targeted RNA sequence or be hindered by binding proteins or secondary structure, signals from single-pair probes targeting the 5’ end (pan 1/2, pan 2/3) and the 3’ end (pan 27/28; Suppl. Fig. 4.8M) of the ErbB4 mRNA coding sequences were not different (Fig. 4.3A-D; Suppl. Table 4.3-4.4). Moreover, signals from single-pair probes targeting either 5’ or 3’ boundaries of each alternatively spliced exon did not differ (Fig. 4.4; Suppl. Table 4.4), indicating sensitivities of single-pair probes are generally comparable; therefore, all subsequent analyses were performed with probes targeting the 5’ upstream exon boundaries of alternatively spliced exons.*

4.4.3 Differential expression of ErbB4 isoforms in distinct regions of the adult brain

Next, we used single-pair probes targeting JMa/JMb and CYT-1/CYT-2 exons to analyze ErbB4 isoform distribution in the adult mouse hippocampus. We found that the non-cleavable juxtamembrane isoform JMb (>85%) and the cytoplasmic isoform CYT-2 (~70%) are the predominant isoforms (Fig. 4.4J), consistent with qRT-PCR data (Suppl. Fig. 4.9A). As in the hippocampus, JMb and CYT-2 also are the predominant ErbB4 isoforms in most brain areas, including the retrosplenial cortex and the reticular thalamic nucleus (Suppl. Fig. 4.10). In stark contrast, in the corpus callosum, where total ErbB4 expression is relatively low compared to

the aforementioned regions^{52, 57}, JMa (~75%) and CYT-1 (~55%) represent most of the receptor isoforms (Fig. 4.5). This novel observation is consistent with qRT-PCR using microdissected corpus callosal-enriched tissue (Suppl. Fig. 4.9B); a similar expression pattern is found in the thalamus (Suppl. Fig. 4.11); and *JMa*, but not *CYT-1*, was the predominant splice variant in the choroid plexus of the third ventricle (Suppl. Fig. 4.13). Interestingly, although in the corpus callosum the percentage of cells expressing JMa is higher than those expressing JMb (Fig. 4.5F; $p=0.0382$), we observed higher JMb/cell than JMa/cell (Fig. 4.5G; $p=0.0006$). Based on the varying expression patterns of JMa/JMb in the corpus callosum, we hypothesized that different cell-types in the corpus callosum express distinct ErbB4 JM isoforms.

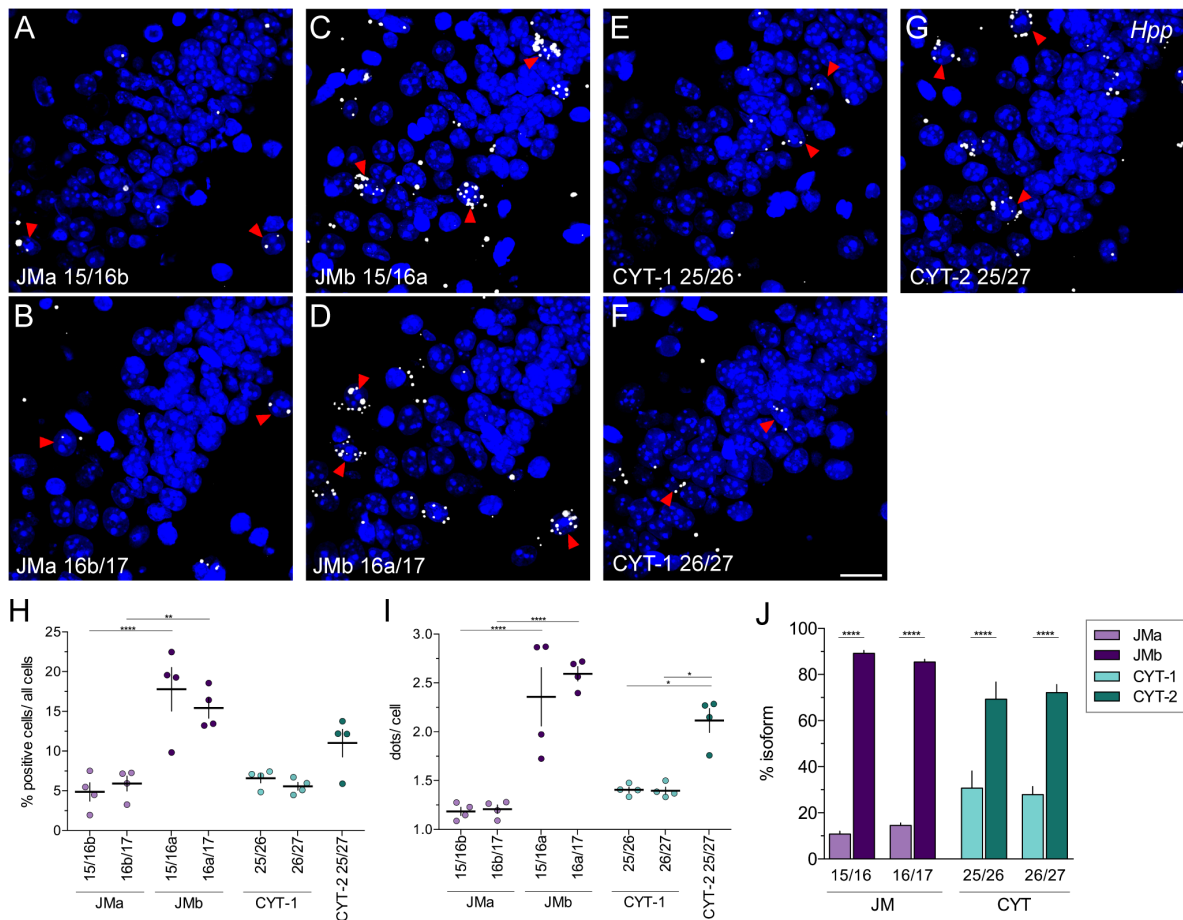


Figure 4.4 | JMb- and CYT-2-containing transcripts are the major ErbB4 isoforms expressed in adult hippocampus.

(A-G) Hybridization of ErbB4 isoform-specific single-pair probes in hippocampal CA2 area of WT mice. Arrowheads indicate examples of positive cells. (H,I) Percentages of positive cells/total cells and average dots/cell in hippocampal CA1-CA3 areas were quantified for each isoform-specific probe using CellProfiler. Results

derived with probes targeting the same isoform were not significantly different (n=4; one-way ANOVA, see Suppl. Table 4.4). (*J*) Relative abundance of JMa/JMb (purple) and CYT-1/CYT-2 (cyan) isoforms in the hippocampus (n=4; one-way ANOVA, see Suppl. Table 4.4). Adjusted p values according to Tukey's multiple comparison test: **p<0.01, ****p<0.0001. Scale bar: 20 μ m.

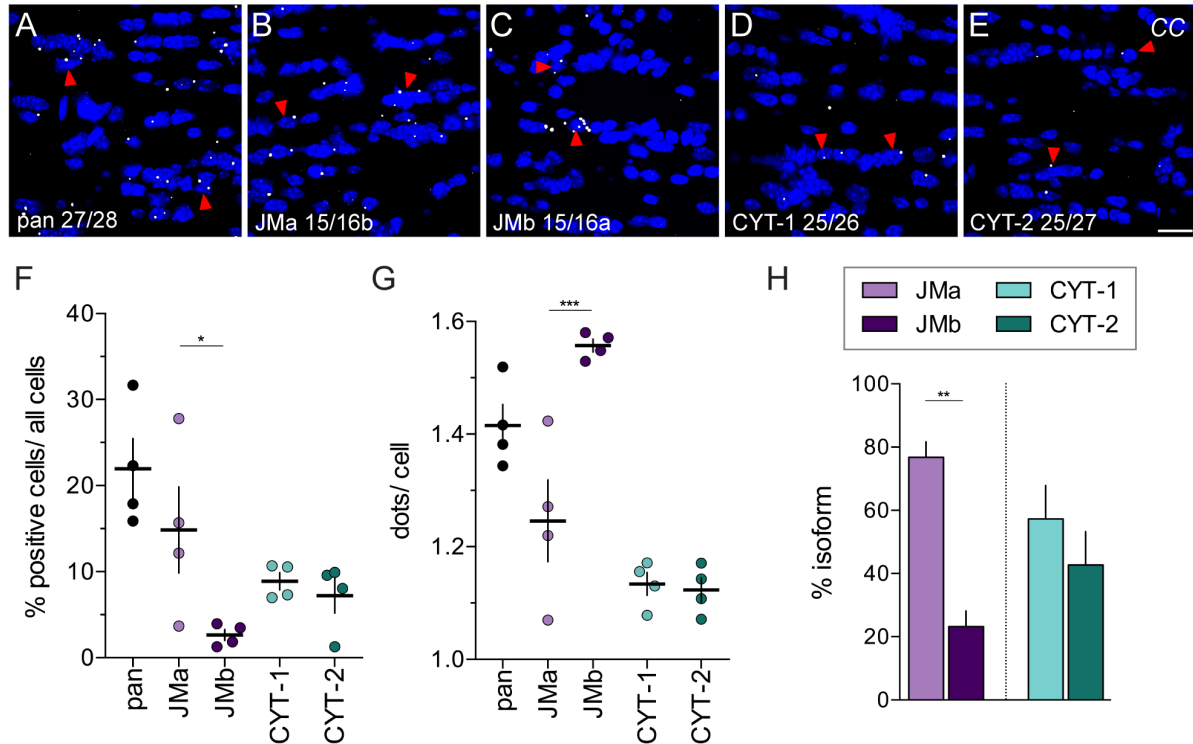


Figure 4.5 | Pattern of ErbB4 JMa and CYT-1 isoform expression in the corpus callosum differ markedly from other brain areas.

(A-E) Representative *in situ* hybridization images hybridized with pan and isoform-specific probes in the corpus callosum (CC). Arrowheads indicate representative positive cells. The (F) percentage of positive cells, (G) average number of dots/ positive cell and (H) relative expression levels of ErbB4 JMa/JMb and CYT-1/CYT-2 isoforms were quantified using CellProfiler (n=4; one-way ANOVA, *p<0.05, **p<0.01, ***p<0.001, see Suppl. Table 4.5). Scale bar: 20 μ m.

4.4.4 Expression of the cleavable JMa isoform in cells of the oligodendrocyte lineage

To investigate the aforementioned hypothesis, we began by using multiplex fluorescent ISH (RNAscope) to analyze the cell-type specific expression of ErbB4 in the corpus callosum and found that both GAD2-positive GABAergic neurons and MAG-positive oligodendrocytes express the receptor (Fig. 4.6A). Interestingly, oligodendrocytes comprised the majority (~85%) of ErbB4-expressing cells, but express lower amounts of ErbB4 than GABAergic neurons (Fig. 4.6B,C; p=0.0034).

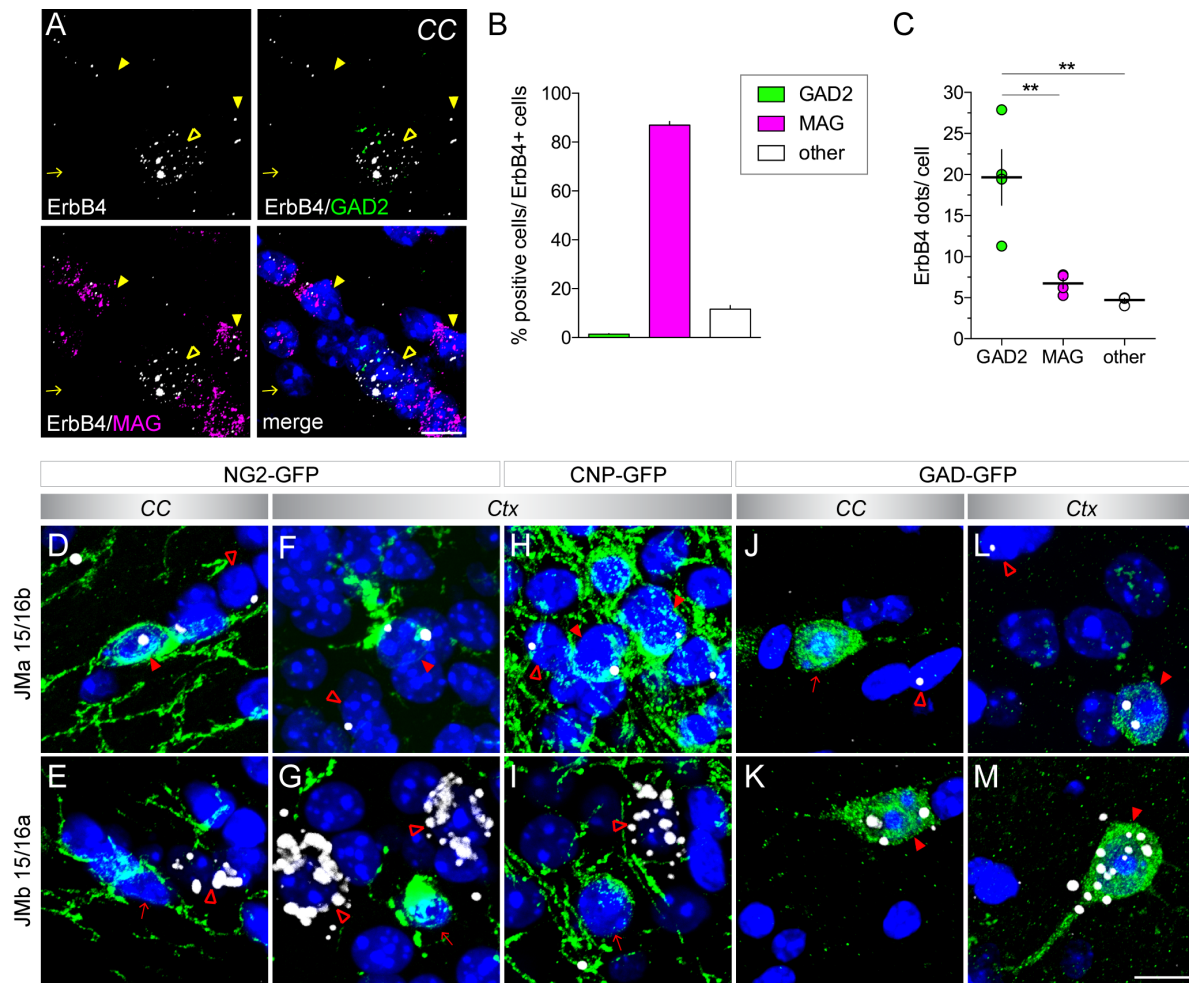


Figure 4.6 | Oligodendrocytes and GABAergic neurons in the corpus callosum express different ErbB4 juxtamembrane isoforms.

(A) Multiplex fluorescent *in situ* hybridization shows that ErbB4 (white) is expressed in both GAD2-positive GABAergic neurons (green; open yellow arrowheads) and MAG-positive oligodendrocytes (magenta; yellow arrowheads) in the corpus callosum (arrow ErbB4-negative cell). Note that dots are smaller compared to single-pair probe ISH, as signals are not enzymatically amplified. (B,C) Quantification of data shown in A (n=4). (B) The majority of ErbB4+ cells in the corpus callosum co-expresses the oligodendrocytes marker MAG (86.95 ± 1.54%), whereas a small fraction is positive for the GABAergic marker GAD2 (1.40 ± 0.23%); 11.65 ± 1.48% of ErbB4+ cells were not labeled with either marker. (C) However, GABAergic neurons express higher levels of ErbB4 per cell than oligodendrocytes (19.65 ± 3.39 dots/ cell vs. 6.73 ± 0.61 dots/ cell, p=0.0034; GAD2 vs. other 4.72 ± 0.23 dots/ cell, p=0.0013n=4; MAG vs. other p=0.7614; F(2,9)=16.53, p=0.001; one-way ANOVA; Tukey's multiple comparisons test: **p<0.01). (D-M) Isoform-specific *in situ* hybridization using probes JMa 15/16b (D,F,H,J,L) and JMb 15/16a (E,G,I,K,M) was combined with post-hoc immunohistochemistry for GFP (green) on sections from NG2-GFP (D-G), CNP-GFP (H,I) and GAD-GFP (J-M) transgenic mice. JM isoforms (white) were detected on GFP+ cells (red arrowheads), as well as on GFP negative cells (open red arrowheads) in the corpus callosum (CC) and the cortex (Ctx). Arrows depict GFP+ cells negative for JM probes. Note that the detection of JM isoforms in the corpus callosum of CNP-GFP mice was not possible because of the high density of GFP+ myelin sheaths²⁹⁸. Scale bar: 10 μm.

A present limitation of the novel single-pair probe ISH approach described here, in contrast to the multiplex system, is that its amplification chemistry is limited to one fluorescent/colorimetric channel per section and, does not allow for the simultaneous detection of independent probes with distinct fluorophores (e.g. ErbB4 exon-specific single-pair probe and cell marker probe such as MAG). To circumvent this limitation, first we had to develop a post-hoc immunohistochemical protocol because most of antibody cell markers tested were not compatible with the fixation and latter permeabilization protocol (i.e., protease treatment) necessary for ISH – even on fresh frozen sections that allow for milder pretreatment conditions than formalin-fixed paraffin sections. However, we identified a GFP antibody that is compatible with this ISH procedure and has the advantage that it is of broad use for other studies. Next, to unambiguously determine the cell-type expressing JMa transcripts, we used transgenic mice expressing GFP under specific promoters for GABAergic neurons (GAD) or for precursor (NG2) and mature (CNP) oligodendrocytes (details see Materials and Methods). Interestingly, we found that ErbB4 JMa isoforms are expressed in NG2+ oligodendrocyte precursor cells (OPCs) in the corpus callosum and cortex (Fig. 4.6D,F), as well as in CNP-GFP+ oligodendrocytes in the cortex (Fig. 4.6H); JMb isoforms were not detected in neither of these cell-types (Fig. 4.6E,G,I). Consistent with our hypothesis, GABAergic neurons in the corpus callosum and neocortex expressed high levels of JMb (Fig. 4.6K,M), but low amounts of JMa isoforms (Fig. 4.6J,L). Taken together, these findings confirm that the cleavable juxtamembrane isoform JMa is the major, if not the sole, juxtamembrane isoform expressed in cells of the oligodendrocyte lineage, whereas JMb transcripts are predominant in GABAergic neurons.

4.4.5 Conservation of differential ErbB4 isoform expression in human cortex and corpus callosum

Finally, to evaluate the relevance of the cell-type-specific expression of ErbB4 JM isoforms in humans, we analyzed the relative abundance of ErbB4 isoforms in the cingulate cortex and corpus callosum by qRT-PCR from human RNA samples. As in the adult mouse, ErbB4 JMb and CYT-2 were the major ErbB4 isoforms in the human cingulate cortex (~80% and ~70%, respectively; Fig. 4.7A). Importantly, in the corpus callosum JMa was predominant (~70%) and equal amounts of CYT were detected (Fig. 4.7B). This suggests that the cell-type-specific

ErbB4 isoform expression is conserved from mouse to human, and that cleavable JMa ErbB4 is the predominant ErbB4 isoform in human oligodendrocytes.

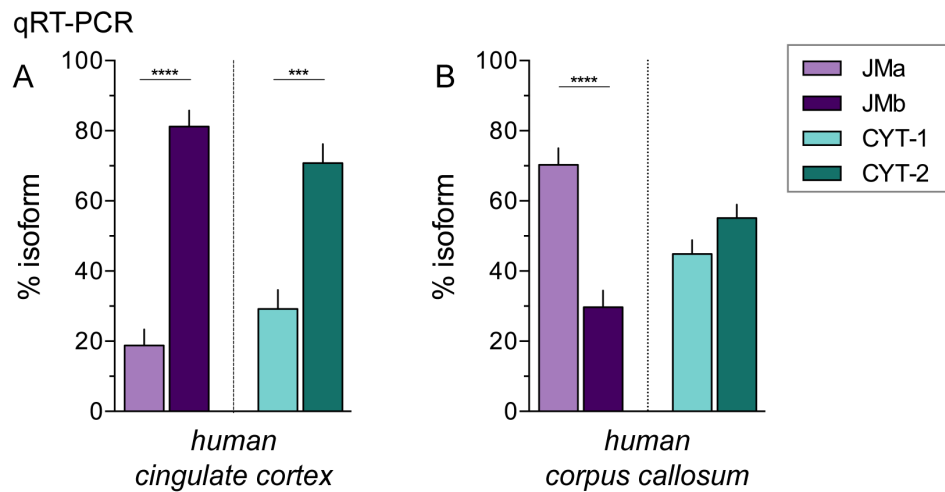


Figure 4.7 | Distinct patterns of ErbB4 JM and CYT isoforms in the grey and white matter are conserved between humans and mice.

Relative abundance of JMa/JMb (purple) and CYT-1/CYT-2 (cyan) isoforms in the adult human cingulate cortex (A) and corpus callosum (B) was determined by TaqMan qRT-PCR (n=4; one-way ANOVA, see Suppl. Table 4.7). Adjusted p values according to Tukey's multiple comparison test: ***p<0.001, ****p<0.0001.

4.5 Discussion

Here, we demonstrate the use of a novel sensitive non-radioisotopic ISH approach, called BaseScope, to analyze exon junctions in tissue sections at a single-cell level that has universal applicability to study short RNA sequences - including splice variants in the brain and other tissues. We carefully validate the sensitivity and specificity of junction-specific probes used for this ISH approach, and show that single-pair probes are generally comparable. Moreover, the semi-quantitative results obtained are consistent with established isoform analyses using TaqMan qRT-PCR. By using this novel ISH approach that provides cellular resolution, we identified differential regional ErbB4 isoform expression in the adult mouse brain that is conserved in humans, and that results from the predominant cell-type-specific expression of juxtamembrane isoforms in neurons (JMb) and cells of the oligodendrocyte lineage (JMa).

4.5.1 Differential and cell-type-specific expression of ErbB4 isoforms in the adult CNS

Our analyses identified ErbB4 transcripts harboring the JMb and CYT-2 exons as the two major isoforms in most adult mouse brain areas (e.g. hippocampus, cortex, reticular thalamic

nucleus); in line with other studies analyzing ErbB4 isoform expression in the different brain areas across species - including humans^{63, 67, 190, 191, 213, 218, 232}; but see²²³. Taking advantage of the expression overview of ErbB4 isoforms by single-pair probe ISH, we identified brain regions where – although generally low – ErbB4 JMa and CYT-1 isoforms comprise most ErbB4 expressed, namely the corpus *callosum*, *thalamus* and *choroid plexus*. Of note, the exclusive detection of JMa ErbB4 isoforms in the oligodendrocyte lineage (Fig.6) is entirely consistent with a recent study that found this distribution of ErbB4 by using RNAseq from cell-sorted brain cells²⁴⁸. The fact that JMa, but not JMb, isoforms are cleaved by metalloproteases, which is a requirement for intramembranous gamma-secretase cleavage that releases a transcriptionally active ICD^{47, 190, 203}, raises the possibility that NRG/ErbB4 signaling uniquely regulates oligodendrocyte maturation through ErbB4-dependent transcriptional mechanisms. Consistent with the expression of ErbB4 in oligodendrocytes, previous studies have reported a role of NRG/ErbB signaling in glial development and myelination^{92, 104, 105, 180}. *NRG has been proposed to cross the blood brain barrier (BBB) of adult mice by receptor-mediated transport^{303, 304} and to decrease BBB permeability^{305, 306}. In the choroid plexus which forms the blood-cerebrospinal fluid (CSF) barrier, high expression of ErbB4⁵⁷ - particularly the JMa variant - suggests that ErbB4 could play a role in maintaining and regulating the blood-CSF barrier and that this regulation could be transcriptional via the ICD of ErbB4. However, our preliminary multiplex ISH data shows the absence of both ErbB3 and ErbB4 from endothelial cells in the BBB and blood-CSF barrier in the healthy adult mouse (Suppl. Fig. 4.13), which previously were suggested to mediate effects on the BBB via ErbB2 and ErbB3 after proinflammatory stimulation³⁰⁵⁻³⁰⁷. This discrepancy may indicate that ErbB expression may be activated under certain conditions in endothelial cells³⁰⁸ and further studies need to be conducted to elucidate the role of the detected ErbB4 JMa in the choroid plexus, presumably expressed by the choroidal epithelium.*

4.5.2 Alterations of ErbB4 isoform expression in Scz

Whereas JMa and CYT-1 are the minor ErbB4 isoforms in the adult brain (this study; ^{190, 191}), they have been repeatedly reported to play an important role during neurodevelopment^{219, 221, 309} and higher expression of JMa and CYT-1 ErbB4 isoforms has been reported in postmortem DLPFC of Scz patients independently by several groups^{28, 218, 222, 223}. This is

interesting considering the increased expression of disease-associated genes in neurodevelopmental disorders during fetal development^{310, 311} and high NRG1 expression at ages with highest risk for Scz onset^{312, 313}. Further it raises the question whether the increased expression of JMa and Cyt-1 isoforms in the DLPFC of Scz results from alterations in the expression or number of cells from the oligodendrocyte lineage and/or a switch in ErbB4 isoform expression in GABAergic neurons. A proposed role of oligodendrocytes and myelination deficits associated with Scz has been emerging (see³¹⁴). An ErbB4 SNP was shown to affect brain white matter integrity¹¹³, subcortical white matter is lost in Scz patients^{109, 315}, and genes related to oligodendrocyte function have been associated with Scz^{110, 112}. These observations are interesting in the context of our novel finding that OPCs and oligodendrocytes express predominantly or exclusively the ErbB4 JMa isoform. On the other hand numerous postmortem studies implicate alterations in GABAergic neurons in the DLPFC and hippocampus of persons with Scz^{316, 317}, where a reduction of GABAergic neuron markers³¹⁸ in particular those associated with fast-spiking interneurons^{319, 320}, has been frequently reported. Interestingly, the changes have been proposed to occur in specific subtypes of interneurons^{218, 222}. Future studies, using ErbB4 isoform-specific single-pair probes reported here, will be important to investigate ErbB4 JMa/JMb and CYT-1/CYT-2 ratios in postmortem human brains of Scz patients and controls to precisely identify the cell-type(s) that underlie the changes in ErbB4 isoforms. Because in addition to ErbB4 the alternative splice variants of many at-risk genes are frequently aberrant in Scz²⁵ and affective, addictive and autism spectrum disorders²⁶, single-pair probe ISH at a cellular level could generally advance our understanding of isoform changes in psychiatric disorders.

4.5.3 General considerations for the broad application of the single-pair probe ISH approach

This study is the first to analyze exon junctions using a fluorescent ISH assay. This approach is not limited to splice variants studies, but could be generally used to analyze short mRNA sequences (e.g. pre-miRNAs and snoRNAs), highly homologous transcripts and circular RNAs, as well as point mutations. In addition, the freely-available automated analytic tool developed here renders this ISH approach a valuable semi-quantitative tool to analyze expression at a single-cell level, which complements other quantitative methodologies such as

qRT-PCR and RNAseq analysis to study splice variants. However, single-probe ISH (BaseScope) has the added benefit of post-assay analyses in morphological conserved tissue. Using post-hoc immunohistochemical analysis following hybridization of single-pair probes on sections of transgenic mice, we show how to overcome the current single-plex platform limitation to identify the cell-types expressing specific splice variants. Of note, the anti-GFP antibody used herewith is one of few antibodies (<10%) compatible with protease permeabilization.

Altogether, the advances of this novel ISH approach in analyzing short sequences and isoforms at cellular resolution in the tissue environment by far outweigh a few limitations or difficulties of this technology that merit to be mentioned. Probes targeting highly abundant transcripts tend to produce signal accumulations (clumps) during the enzymatic conversion of FastRED (see Fig. 4.2B-E; Suppl. Fig. 4.8). As shown earlier (Figs. 4.3, 4.4), in our experience hybridization efficiencies between unrelated single-pair probes are in general extremely similar but on occasion, as was the case of CYT probes, can give weaker signals relative to the panErbB4 or juxtamembrane single-pair probes (compare Fig. 4.3A, 4.4H); the differences observed could have resulted from intrinsic differences of the targeted mRNA sequences (i.e., looping). Therefore, quantification using this novel single-pair ISH should be considered carefully. Nevertheless, the relative signals for CYT-1/CYT-2 isoforms were conserved as confirmed by qRT-PCR analysis (Fig. 4.4J, Suppl. Fig. 4.10A), supporting the semi-quantitative nature of this approach.

Taken together, our study underscores the important and unique utility of this novel single-pair probe ISH technique to investigate, with cellular resolution in tissues, the expression of short and highly homologous RNA sequences. As discussed above, whilst BaseScope should be considered as semi-quantitative approach, it can be used to complement other traditionally used methodologies like qRT-PCR and RNAseq. Its numerous applications render the single-pair probe ISH as an indispensable tool to advance studies on mRNA regulation and complexity, and their association with numerous neurological and psychiatric diseases.

4.6 Supplementary Materials

Supplemental Materials and Methods

Animals. Homozygous ErbB4 knock-out (KO) mice lacking exon 2 were rescued from embryonic lethality by transgenic ErbB4 overexpression in the heart¹⁵⁷, and will be hereafter designated as ErbB4-Δ2 KO mice. CNP-mEGFP, hereafter referred to as CNP-GFP²⁹⁸ (<https://www.jax.org/strain/026105>), NG2-mEGFP/ Cspg4-mEGFP, hereafter referred to as NG2-GFP²⁹⁹ (<https://www.jax.org/strain/022735>), and wild-type (WT) C57BL/6J mice (<https://www.jax.org/strain/000664>) were obtained from the Jackson Laboratory (Bar Harbor, ME). GAD67-GFP mice, hereafter referred as GAD-GFP mice³⁰⁰, were a kind gift from Yuchio Yanagawa (Gunma University, Japan). Mice were kept on a 12-12h light-dark schedule with access to food and water *ad libitum* and handled in accordance with the National Institutes of Health (NIH) Animal Welfare guidelines. All animal procedures were approved by the NIH Animal Care and Use Committee. Ground human brain samples from four male adult control individuals (age 44-53) were obtained from the Human Brain Collection Core at NIMH.

Tissue preparation for *in situ* hybridization. Ten-week-old adult mice of both sexes were transcardially perfused with 4% paraformaldehyde (Electron Microscopy Sciences, Hartfield PA) in 0.1 M PBS, pH 7.4. Dissected brains were post-fixed overnight in 10% neutral buffered formalin (Sigma-Aldrich, St. Louis MO) at 4°C. Tissue was embedded in paraffin after ethanol dehydration steps followed by xylene. Serial coronal paraffin sections (8 μm) were mounted on Superfrost slides (Daigger, Vernon Hills IL) and baked for 10 min at 70°C. *For the preparation of fresh frozen sections, the brain of a P17 C57BL/6J mouse was dissected, coronally trimmed, immediately frozen on dry ice and attached to the object holder with OCT (Optimal cutting temperature; Sakura Finetek, Torrance CA) compound. 12 μm-thick fresh frozen sections were prepared using a Leica Cryostat (Cryostat & object temperature -18°C).*

In situ hybridization (ISH). The novel junction-specific ISH approach, known as BaseScope, is based on the same principles than the well-established multiplex fluorescent ISH RNAscope^{®250} (Advanced Cell Diagnostics, Newark, CA). The high specificity of both ISH technologies is achieved from the unique design of probes, called ‘ZZ’ probe pairs, consisting of two 18-25bp antisense probes, a spacer region and a 14bp tail that is necessary for signal amplification. The tail region is recognized by a preamplifier that can only bind if both ‘Z’

probes in a pair are hybridized directly adjacent to each other, suppressing off-target non-specific hybridization and thus resulting in extremely low background²⁵⁰. The sensitivity of BaseScope is increased by several amplification steps generating an amplification ‘tree’. The additional enzymatic and amplification steps in BaseScope ISH allow the use of a single ‘ZZ’ probe pair, instead of the 6-20 ‘ZZ’ probe pairs necessary in RNAscope, for signal detection. It is these properties that make BaseScope suitable to detect short nucleotide sequences, such as exon junctions, to analyze expression of alternative spliced transcripts. BaseScope probes are comprised of 18-25bp oligonucleotide sequences designed by a proprietary algorithm to meet required melting temperature for assay hybridization conditions and to avoid cross-hybridization. One oligonucleotide probe hybridizes target sequences across the exon junction and the other probe to immediately adjacent region. Targeted sequences of customized junction-specific ErbB4 ISH probes are listed in Table 4.1 and schematically illustrated in Fig. 4.1. RNAscope[®] probes were ErbB4 (Mm-ErbB4; Cat No. 318721), GAD-2 (Mm-GAD2-C2; Cat No. 415071-C2), MAG (Mm-MAG-C3; Cat No. 446451-C3), *ErbB3* (Mm-ErbB3-C2; Cat No. 441801-C2), *PECAM-1* (Mm-Pecam1-C3; Cat No. 3176721-C3) and *PDGFRb* (Mm-Pdgfrb-C3). RNAscope[®] was performed on 8 μ m-thick paraffin sections (Fig. 4.6) and on 12 μ m-thick fresh frozen sections (Suppl. Fig. 4.13) following manufacturer’s protocol. BaseScope ISH assays was performed on 8 μ m-thick formalin-fixed paraffin embedded (FFPE) sections. Briefly, FFPE sections were incubated for 1h at 60°C, subsequently deparaffinized by two washes in xylene for 5 min at room temperature (RT), and washed twice for 3 min in ethanol. To quench endogenous peroxidase activity, dried sections were incubated with H₂O₂ treatment for 10 min at RT. Target retrieval at 100°C for 15 min was found to be optimal for adult mouse brain sections, followed by treatment with Protease III for 30 min at 40°C. After pretreatment, sections were thoroughly washed and incubated with probes for 2 h at 40°C. For multiplex fluorescent ISH, sections were incubated with amplification solutions (AMP) as follows: AMP1, 30 min at 40°C; AMP2, 15 min at 40°C; AMP3, 30 min at 40°C; and AMP4B, 15 min at 40°C. For FastRED detection of junction-specific ISH, sections were incubated as follows: AMP0, 30 min at 40°C; AMP1, 15 min at 40°C; AMP2, 30 min at 40°C; AMP3, 30 min at 40°C; AMP4, 15 min at 40°C; AMP5, 30 min at RT; AMP6, 15 min at RT; and FastRED (60:1 mixture of FastRED A and B solution), 10 min at RT. Sections were washed thoroughly twice for 2 min in-between steps with washing buffer. Sections were

counterstained with DAPI (1 µg/mL in PBS; Thermo Fisher, Waltham MA) for 30 sec and mounted with Mowiol-DABCO. Sections shown in Fig. 4.2D,I and Suppl. Fig. 4.8C,D,I,J were additionally counterstained with hematoxylin (Electron Microscopy Sciences).

Immunostainings. Post-hoc GFP immunohistochemistry (IHC) was performed immediately following ISH as previously published³⁹. Briefly, sections were washed three times in 0.1 M PBS for 5 min each and blocked with 10% normal donkey or goat serum (Sigma-Aldrich) in 0.1 M PBS with 0.3% Triton X-100 (ThermoFisher) for 1h at RT. Sections were incubated with 1µg/mL mouse monoclonal anti-GFP (isotype IgG2a, clone N86/8; NeuroMab, Davis CA) in blocking solution overnight at 4°C. Following three washes with 0.1 M PBS + 0.25% Triton X-100, sections were incubated with donkey anti-mouse Alexa488 secondary antibody (Invitrogen A-21202, Thermo Fisher) in blocking solution for 2h at RT. Samples were extensively washed with 0.1 M PBS, counterstained with DAPI and mounted with Mowiol-DABCO.

Quantitative Real-Time PCR (qRT-PCR). RNA was isolated from micro-dissected tissue from hippocampus, thalamus and corpus callosum of five ten-week-old male WT mice, and from micro-dissected ground tissue of human cingulate cortex and corpus callosum from four individuals using the TRI Reagent Kit (Thermo Fisher). cDNA synthesis was synthesized in a total volume of 20µl according to manufacturer's protocol, using 1 µg RNA template, SuperScript IV Reverse Transcriptase (Thermo Fisher) and random hexamers for 20 min at 55°C. qRT-PCR of ErbB4 isoforms was performed using custom-made TaqMan assays (Thermo Fisher). Flanking primers and TaqMan probes were as follows (all sequences correspond to the sense strand):

Table 4.2 | TaqMan probes

Assay	Primers	<i>Mouse</i>		<i>Human</i>	
		Primers	TaqMan probe	Primers	TaqMan probe
JMa	5'CCACCCTTGCCA TCCAAA3'	FAM- ATGGACGGGCCATTCCACTTT ACCA-MGB	FAM- ATGGACGGGCCATTCCACTTT ACCA-MGB	5'CCACCCATGCCA TCCAAA3'	FAM- ATGGACGGGCCATTCCACTTT ACCA-MGB
JMb	5'CCAATGACTCCG GCTGCAATCA3'	FAM- TTCAAGCATTGAAGACTGCAT CGGCCTGAC-MGB	FAM- TTCAAGCATTGAAGACTGCAT CGGCCTGAC-MGB	5'CCAATTACTCCA GCTGCAATCA3'	FAM- CTCAAGTATTGAAGACTGCAT CGGCCTGAT-MGB
CYT-1	5'CAACATACCTCC TCCCATCTACAC3'	FAM- TGAAATTGGACACAGCCCTCC TCCTG-MGB	FAM- TGAAATTGGACACAGCCCTCC TCCTG-MGB	5'CAACATCCCACC TCCCATCTATAC3'	FAM- TGAAATTGGACACAGCCCTCC TCCTG-MGB
CYT-2	5'GCATTCTTGTT GTGTAGCAA3'	FAM- AATTGACTCCAATAGGAATCA GTTTGTGTACCAAGAT-MGB	FAM- AATTGACTCCAATAGGAATCA GTTTGTGTACCAAGAT-MGB	5'ACACTCCTTGTT CAGCAGCAA 3'	FAM- AATTGACTCGAATAGGAACC AGTTTGTATACCGAGAT-MGB
β -actin	5'ATCTGGCACCAC ACTTTCTACAAT3' 5'CCGTCTCCGGAG TCCATCA3'	VIC- TGACCCAGATCATGTTTGAGA CCTTCAACAC-MGB	VIC- TGACCCAGATCATGTTTGAGA CCTTCAACAC-MGB	5'ATCTGGCACCAC ACTTTCTACAAT3' 5'CCGTCTCCGGAG TCCATCA3'	VIC- TGACCCAGATCATGTTTGAGA CCTTCAACAC-MGB

1ng cDNA was amplified using 0.25 μ M isoform-specific FAM-labeled TaqMan probes and 0.9 μ M corresponding primers (Thermo Fisher) in a total volume of 10 μ l total volume using TaqMan universal PCR Master Mix (Thermo Fisher). As reference, β -actin was detected with a custom-made VIC®-labeled probe. Cycling was performed in 384-well plates using a QuantStudio 6 Thermocycler (Thermo Fisher) and the following parameters: 2min at 50°C and 10min at 92°C, followed by 40 cycles of 15s at 95°C, 1min at 60°C (for JM probes) or 65°C (for CYT probes). Standard curves (1fg–1ng) of cloned DNA for ErbB4 JMa/CYT-1 and JMb/CYT-2, as well for β -actin, were run beforehand to verify that sample values were in the linear range and that PCRs showed similar efficiency between isoform-specific assays. As negative controls, 100 pg DNA of non-matching isoforms were included to demonstrate assay specificity.

Imaging and Quantification. FastRED fluorescent punctuate signal (syn: “dots” and “puncta”) was analyzed on a Zeiss LSM710 confocal microscope at 20x and 63x magnifications using a 530 nm laser. Bright-field images were taken on a Zeiss Axiovert200 with an Axio Cam HRc at 63x magnification. For visualization, images were adjusted for overall brightness and contrast using Image J (<http://imagej.nih.gov/ij/>); fluorescent signal were converted into gray scale. For quantification, areas of interest were imaged in Z across the whole thickness of the section at 20x magnification and 1024x1024 resolution. Due to smaller puncta size, multiplex

fluorescent ISH analysis (Fig. 4.6A) was performed on images acquired at 63x magnification. Image stacks were projected in Z using the maximum intensity method and then converted to RGB format or single channel images in case of the multiplex fluorescent ISH. ROIs were manually defined and measured using Image J; area size did not differ between groups analyzed (see Suppl. Tables 4.3-4.5). Quantification was performed using CellProfiler²²⁷, the pipelines (macros) are available at the provider's homepage (cellprofiler.org/examples/published_pipelines). Intensity threshold was set based on the mean background intensity in all ErbB4- Δ 2 KO sections and defined as 10x mean intensity. Then, dot diameter threshold was set as ≥ 3 pixels based on the mean dot diameter from all WT hippocampi analyzed (3.9 pixels); these settings were found to faithfully identify dots as manually verified in a subset of ROIs from both WT and ErbB4- Δ 2 KO sections. Percentage of positive cells ((positive cells/ all cells) x 100), average number of dots/ area (in mm²) or dots/ cell were calculated. For multiplex fluorescent ISH, percentage of ErbB4-positive cells also positive for GAD2 or MAG ((marker/ ErbB4+ cells) x 100) and ErbB4 dots/ cell was calculated (Fig. 4.6B,C). Overlapping neighboring cells were excluded from the analysis. Hippocampal dentate gyrus was excluded from quantification of cellular analyses because the density of granule cells prevented accurate designation of DAPI-labeled nuclei.

Statistical Analysis. Population (n) in all analyses was defined as number of animals/humans analyzed. For histological analyses (Fig. 4.2-4.5), four 10-week old mice were analyzed per group (WT: 4 males; ErbB4- Δ 2 KO: 2 males and 2 females), a population size consistent with earlier studies⁶³. ROIs were analyzed bilaterally on one brain section and cellular analyses comprised, depending on cell density, between 750 cells and 15,000 single cells per animal and ROI. All data represent the mean \pm SEM and statistical significance was set at $p < 0.05$. Statistical analyses were performed with Graph Pad Prism 6 using one-way ANOVA and Tukey's multiple comparison test. Statistical significance (p values) are stated in the text; all values (including means \pm SEM, degrees of freedom and multiple comparisons) are listed in Suppl. Tables 4.3-4.7. Two-way ANOVA analysis was used for the dots/ cell histogram distribution analysis shown in Fig. 4.3D (see Suppl. Table 4.6).

Supplemental Figures

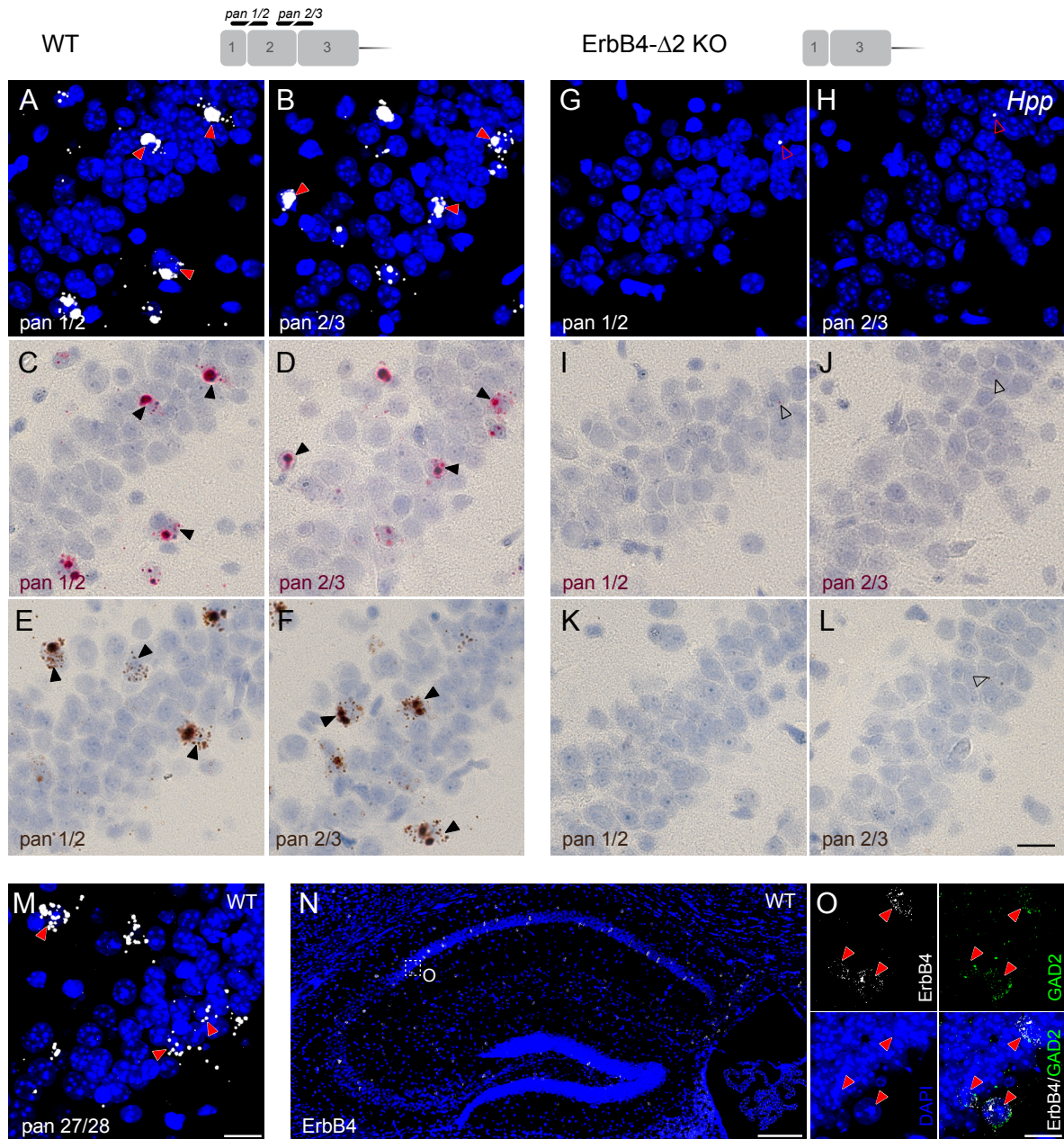


Figure 4.8 | Visualization of exon-specific and multiplex ISH signal by fluorescent and chromogenic dyes in hippocampal GABAergic interneurons.

Hybridization of single-pair probes targeting exon 2 (*pan 1/2* and *pan 2/3*) in sections from WT (**A-F**) and ErbB4-Δ2 KO mice (**G-L**) was visualized using alkaline phosphatase and FastRED in fluorescence (**A,B,G,H**) or bright field microscopy (**C,D,I,J**) or horseradish peroxidase and diaminobenzidine (**E,F,K,L**). (**M**) Hybridization with probe *pan 27/28* targeting the 3' end of ErbB4 transcripts showed essentially the same pattern (*arrowheads* – positive cells; *open arrowheads* - background signal). (**N,O**) Multiplex fluorescent ISH (20 probe pairs) shows that (**O**) ErbB4 (*white*) is expressed in scattered cells in the hippocampus that correspond to GAD2-positive (*green*) GABAergic neurons (*arrowheads*). Note that more transcripts are detected by the multiplex fluorescent

ISH due to the increased sensitivity resulting from multiple probe pairs. Differences in dot sizes between the two assays are attributed to the differences in detection methodology (i.e. catalytic in the new junction-specific assay vs. fluorescent in the multiplex fluorescent ISH assay). Scale bars: N 200 μm ; L,M,O 20 μm .

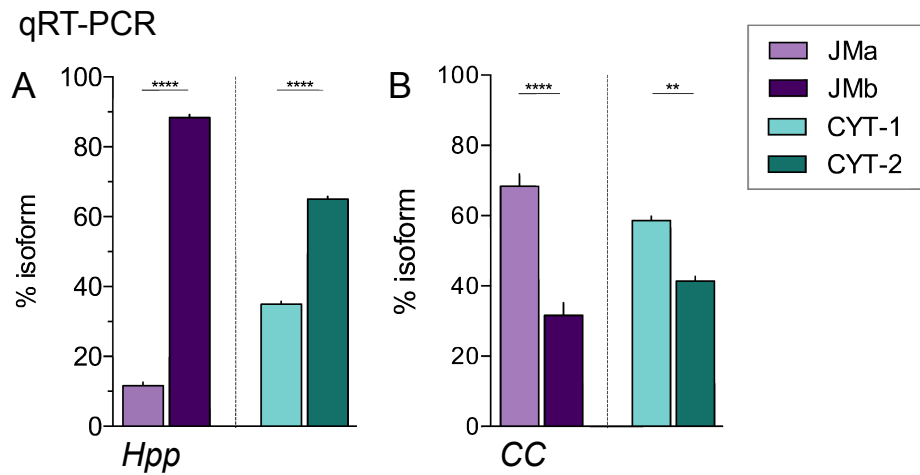


Figure 4.9 | TaqMan qRT-PCR analysis of ErbB4 isoforms in the adult mouse hippocampus (Hpp) and corpus callosum (CC).

Relative abundance of JMa/JMb (purple) and CYT-1/CYT-2 (cyan) isoforms was analyzed in the micro-dissected tissue of adult mouse hippocampus (A) and corpus callosum (B) by TaqMan qRT-PCR (n=5; one-way ANOVA, see Suppl. Tables 4.4-4.5). Adjusted p values according to Tukey's multiple comparison test: **p<0.01, ****p<0.0001 (Tukey's multiple comparison test).

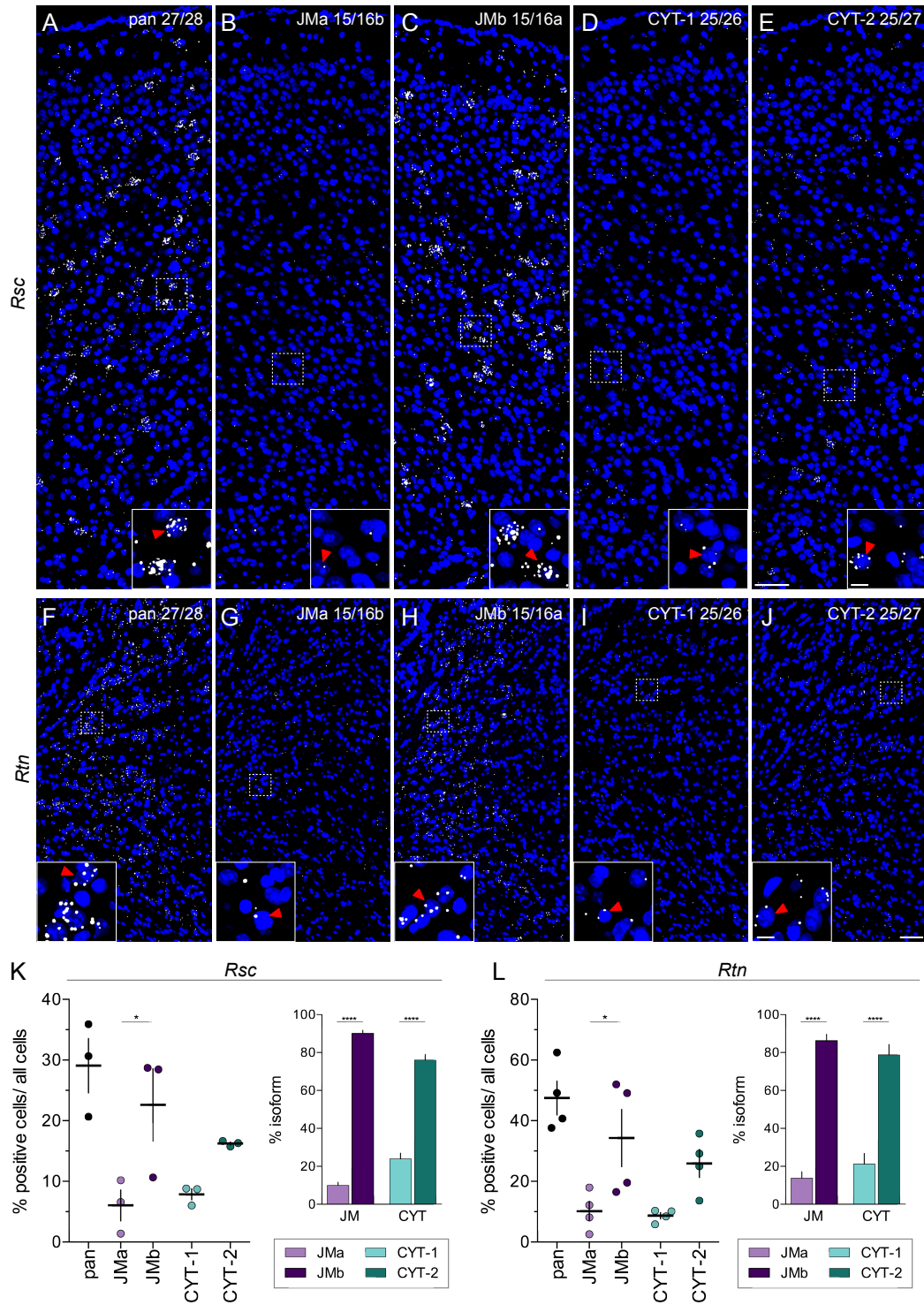


Figure 4.10 | *ErbB4* isoform expression pattern in the retrosplenial cortex and the thalamic reticular nucleus are similar to the hippocampus.

Representative images of pan and isoform-specific *ErbB4* single-pair probe hybridizations in (A-E) the retrosplenial cortex (*Rsc*) and in (F-J) the thalamic reticular nucleus (*Rtn*); boxed areas are magnified in the insets shown on the bottom right of each panel. Representative positive cells are indicated (arrowheads). (K,L)

Percentages of positive cells and relative expression of ErbB4 JMa/JMb and CYT-1/CYT-2 isoforms are quantified in the (K) Rsc (n=3) and (L) Rtn (n=4; one-way ANOVA; *p<0.05; see also Suppl. Table 4.5). Scale bars: 50 μ m (overviews); 10 μ m (insets).

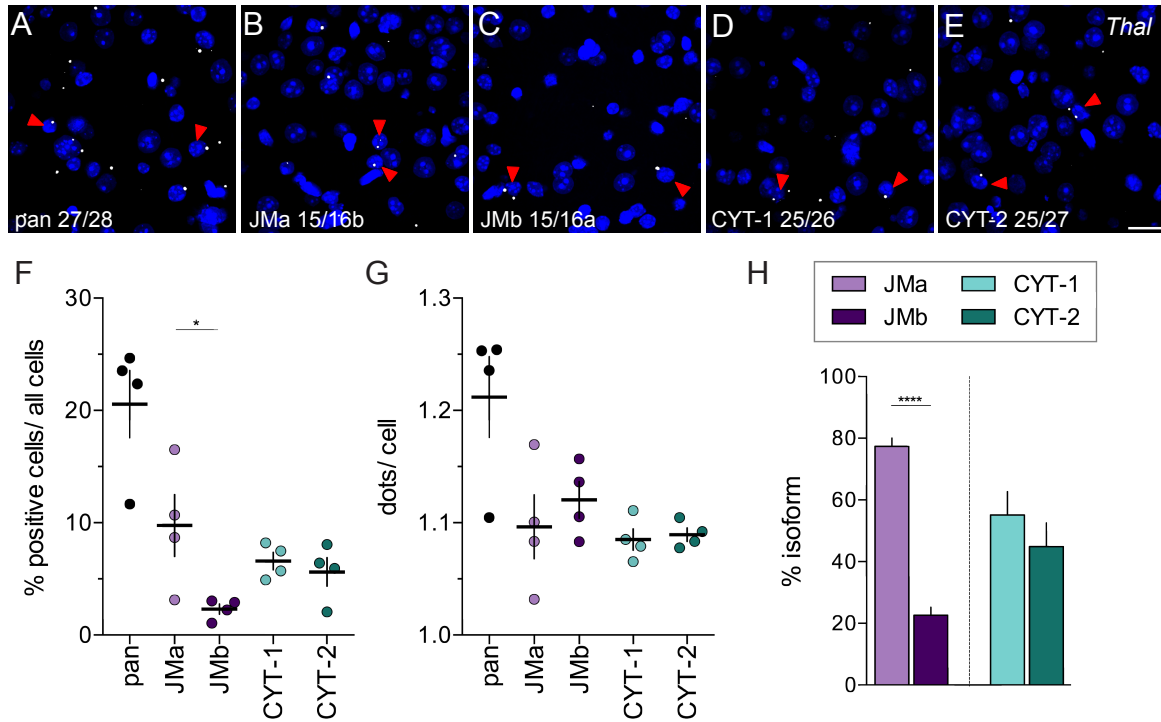


Figure 4.11 |As in the corpus callosum, JMa and CYT-1 isoforms are the major ErbB4 variants expressed in the thalamus.

(A-E) Representative *in situ* hybridization images hybridized with pan and isoform-specific single-pair probes in the medial thalamus (*Thal*). Arrowheads indicate representative positive cells. The (F) percentage of positive cells, (G) average number of dots/ positive cell and (H) relative expression levels of ErbB4 JMa/JMb and CYT-1/CYT-2 isoforms were quantified using CellProfiler (n=4; one-way ANOVA, *p<0.05, ***p<0.001, see also Suppl. Table 4.5). Scale bar: 20 μ m.

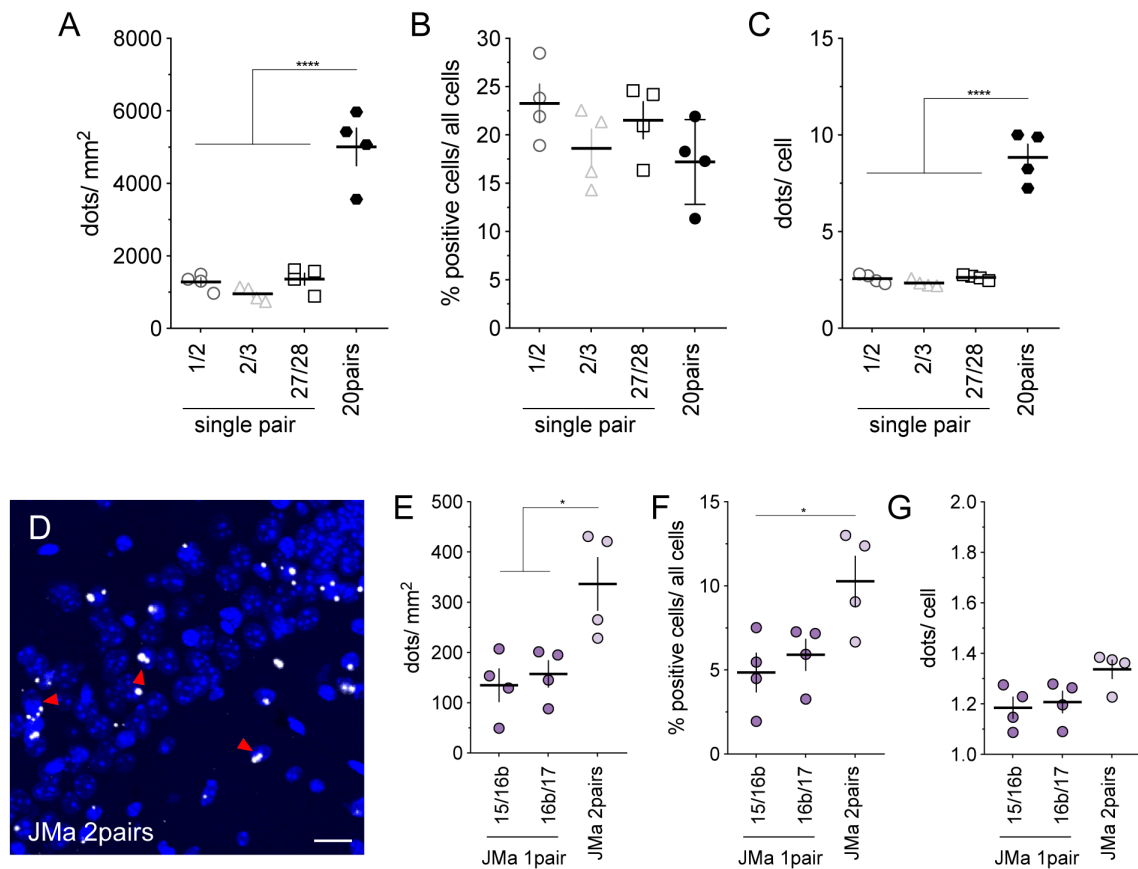


Figure 4.12 | Detection of low-abundant transcripts is increased when using multiple probe pairs.

(A-C) Comparison of the sensitivity between single-pair probes and 20 probe pairs targeting ~1000bp used in multiplex ISH. The percentage of positive cells detected with single-pair probes targeting exon junctions 1/2, 2/3 or 27/28 common for all *ErbB4* transcripts (see Fig.1) is comparable to 20 probe pairs used in multiplex ISH (B; see Fig.S1) when analyzed on hippocampal sections of WT mice, but signals per area (A) and transcripts per cell (C) are lower ($n=4$; one-way ANOVA; **** $p<0.0001$; see also Suppl. Table 4.8). (D-G) The 75bp *JMa* exon allows for the use of two probe pairs targeting both exon junctions and enhancing transcript detection. (D) Representative hybridization (white) of the two probe pairs targeting the *JMa* exon (*JMa* 2pairs) in the CA2 region of the hippocampus (red arrowheads indicate positive cells). (E-G) Compared to probes targeting a single exon junction (see Fig.4) more signal is detected per area (E), more positive cells are detected (F) and transcript detection in positive cells is slightly increased (G; $n=4$; one-way ANOVA; * $p<0.05$; see also Suppl. Table 4.9). Scale bar: 20 μm .

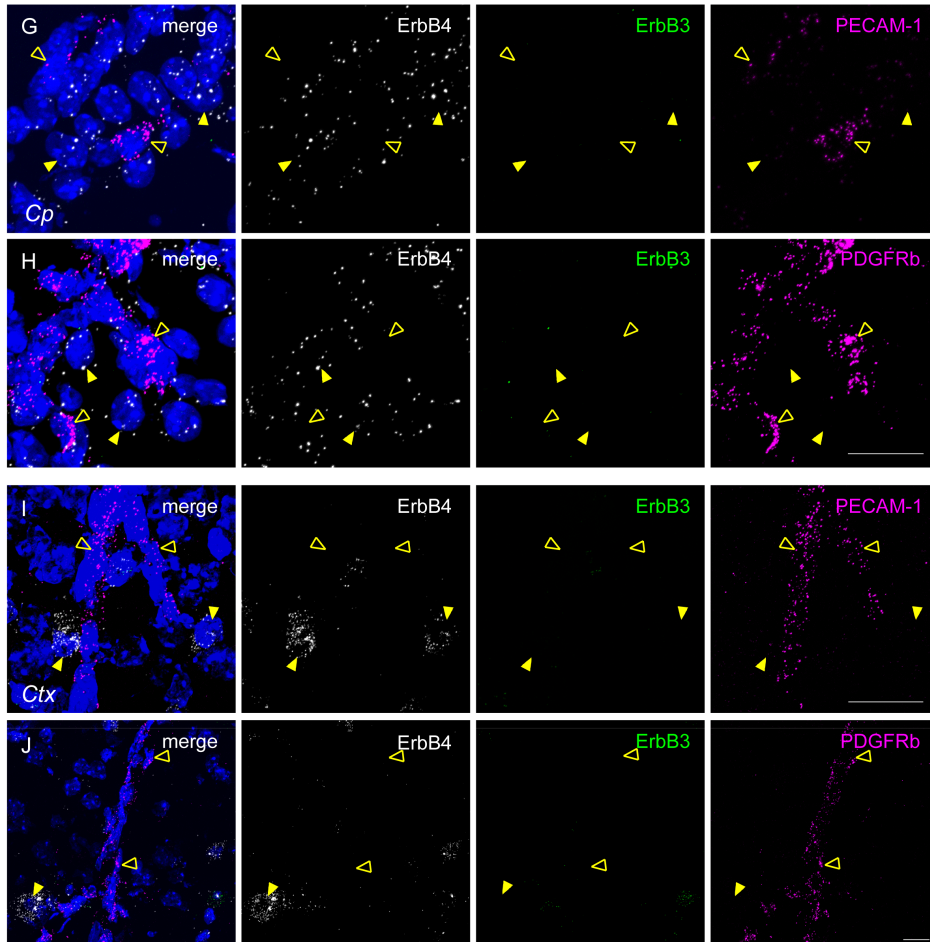
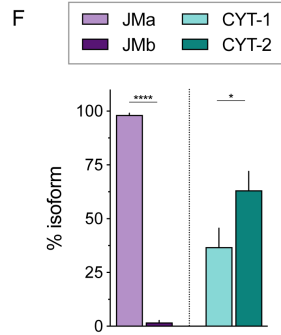
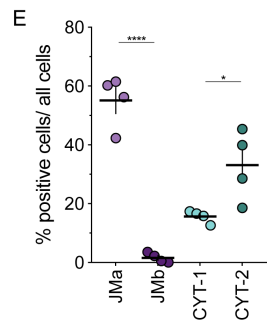
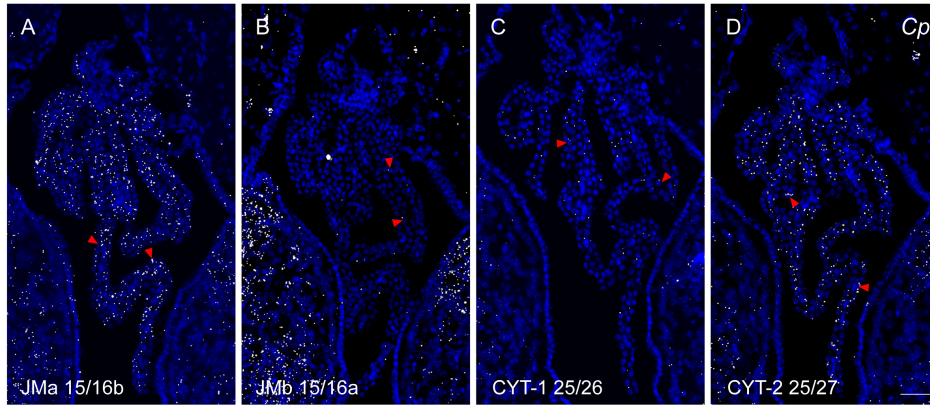


Figure 4.13 | *In the choroid plexus, ErbB4 JMa is the predominant juxtamembrane splice variant.* (A-D) Representative *in situ* hybridization images hybridized with isoform-specific single-pair probes in the choroid plexus (Cp). Arrowheads indicate representative positive cells. (E) The percentage of positive cells, and (F) relative expression levels of ErbB4 JMa/JMb and CYT-1/CYT-2 isoforms quantified with CellProfiler (n=4; one-way ANOVA, *p<0.05, ****p<0.0001, see also Suppl. Table 4.10). (G-J) Preliminary results of multiplex fluorescent ISH on fresh-frozen sections of adult WT mice show the absence of ErbB3 (green) and ErbB4 (white) in PECAM-1 (platelet and endothelial cell adhesion molecule-1)-positive endothelial cells (magenta; F,H) and PDGFRb (platelet derived growth factor receptor beta)-positive pericytes (magenta; G,I) in the choroid plexus as well as cortical (Ctx) microvessels forming the blood-brain barrier (H,I), suggesting expression of ErbB4 in the choroid plexus is confined to the choroidal epithelium. Arrowheads label ErbB4-positive cells, open arrowheads indicate endothelial cells and pericytes. Scale bars: 50 μ m in D, 20 μ m in H-J.

Supplemental Tables

Table 4.3 | **Quantification and statistical analysis of ErbB4 expression in the medial habenula (mHab) and the hippocampus (Hpp) using pan ErbB4 single-pair probes.**

ROI	probes	WT			ErbB4- Δ 2 KO		one-way ANOVA	Statistics	
		pan 1/2	pan 2/3	pan 27/28	pan 1/2	pan 2/3		WT vs. ErbB4- Δ 2 KO (pan 1/2; pan 2/3)	WT 1/2 vs 2/3; 1/2 vs 27/28; 2/3 vs 27/28
mHab	area [mm ²]	0.1780 \pm 0.0043	0.1687 \pm 0.0085	0.1704 \pm 0.0081	0.1616 \pm 0.0184	0.1724 \pm 0.0259	F(4,15)=0.1518 p=0.9593	N/A	N/A
	dots/ mm ²	12603.9 \pm 2069.3	11694.3 \pm 1878.5	11894.0 \pm 2110.9	30.3 \pm 11.0	41.6 \pm 12.6	F(4,15)=17.73 p<0.0001	p=0.0004*** p=0.0008***	p=0.9934 p=0.9975 p>0.9999
Hpp	area [mm ²]	4.56 \pm 0.30	4.61 \pm 0.31	4.42 \pm 0.35	4.65 \pm 0.54	4.55 \pm 0.55	F(4,15)=0.0423 p=0.9962	N/A	N/A
	dots/ mm ²	1282.1 \pm 112.3	955.3 \pm 96.6	1360 \pm 166.3	45.8 \pm 16.3	27.9 \pm 7.0	F(4,15)=42.92 p<0.0001	p<0.0001**** p<0.0001****	p=0.1944 p=0.9799 p=0.0753
Hpp w/o DG	area [mm ²]	3.26 \pm 0.19	3.33 \pm 0.21	3.13 \pm 0.22	3.24 \pm 0.41	3.21 \pm 0.42	F(4,15)=0.0543 p=0.9939	N/A	N/A
	dots/ mm ²	1439.4 \pm 103.0	1046.5 \pm 108.2	1482.7 \pm 179.9	38.6 \pm 13.1	23.1 \pm 7.1	F(4,15)=48.25 p<0.0001	p<0.0001**** p<0.0001****	p=0.1100 p=0.9982 p=0.0652 p=0.2557
	% ErbB4+	23.27 \pm 2.0	18.61 \pm 1.99	21.52 \pm 1.91	1.51 \pm 0.49	0.89 \pm 0.26	F(4,15)=51.26 p<0.0001	p<0.0001**** p<0.0001****	p=0.9249 p=0.6774 p=0.2264 p=0.8748 p=0.1090
	dots/ cell	2.57 \pm 0.12	2.34 \pm 0.08	2.64 \pm 0.06	N/A	N/A	F(2,9)=2.90 p=0.1068	N/A	

Values represent the mean \pm SEM of analyzed areas, dots/ area and percentage of ErbB4-positive cells in sections of WT and ErbB4- Δ 2 KO mice. *p<0.05, **p<0.01, ***p<0.001, ****p<0.0001 (n=4; one-way ANOVA with Tukey's multiple comparison test). N/A: not applicable.

Table 4.4 | Quantification and statistical analysis of ErbB4 expression in the adult hippocampus (Hpp) using isoform-specific single-pair probes.

ROI	probes	JMa 15/16b	JMa 16b/17	JMb 15/16a	JMb 16a/17	CYT-1 25/26	CYT-1 26/27	CYT-2 25/27	one-way ANOVA	JMa 15/16b vs. 16b/17; JMb 15/16a vs. 16a/17; CYT-1 25/26 vs. 26/27	JMa vs. JMb (15/16; 16/17)	CYT-1 vs. CYT-2 (25/26; 26/27)
Hpp w/o DG	area [mm ²]	3.22 ± 0.35	3.48 ± 0.24	3.14 ± 0.35	3.55 ± 0.24	3.29 ± 0.25	3.12 ± 0.23	3.31 ± 0.23	F(6,21)=0.3391 p=0.9083	N/A	N/A	N/A
	dots/ mm ²	143.5 ± 34.2	166.6 ± 29.0	1192.6 ± 244.9	995.3 ± 108.8	223.4 ± 30.2	205.3 ± 30.2	566.9 ± 104.7	F(6,21)=15.28 p<0.0001****	p>0.9999 p=0.8637 p>0.9999	p<0.0001**** p=0.0005****	p=0.3426 p=0.2882
	% ErbB4+	4.86 ± 1.16	5.91 ± 0.93	17.78 ± 2.75	15.42 ± 1.28	6.57 ± 0.58	5.55 ± 0.49	11.00 ± 1.75	F(6,21)=12.76 p<0.0001****	p=0.9985 p=0.9088 p=0.9987	p<0.0001**** p=0.0026**	p=0.3670 p=0.1669
	dots/ cell	1.19 ± 0.04	1.21 ± 0.04	2.36 ± 0.30	2.59 ± 0.07	1.41 ± 0.03	1.40 ± 0.04	2.28 ± 0.12	F(6,21)=20.94 p<0.0001****	p>0.9999 p=0.8481 p>0.9999	p<0.0001**** p<0.0001****	p=0.0120* p=0.0108*
Hpp	area [mm ²]	4.44 ± 0.51	4.83 ± 0.38	4.40 ± 0.50	4.93 ± 0.40	4.56 ± 0.39	4.38 ± 0.34	4.61 ± 0.37	F(6,21)=0.2666 p=0.9464	N/A	N/A	N/A
	dots/ mm ²	135.0 ± 32.8	157.4 ± 26.3	1103.3 ± 227.4	907.8 ± 103.2	208.7 ± 32.6	185.4 ± 18.5	511.4 ± 86.7	F(6,21)=15.21 p<0.0001****	p>0.9999 p=0.8193 p>0.9999	p<0.0001**** p=0.0006***	p=0.3905 p=0.3095
	% isoform	10.79 ± 1.24	14.51 ± 1.10	89.21 ± 1.24	85.49 ± 1.10	30.70 ± 7.44	27.87 ± 3.54	7.44 ± 72.13 ± 3.54	F(7,24)=59.15 p<0.0001****	p=0.9981 p=0.9981 p=0.9997	p<0.0001**** p<0.0001****	p<0.0001**** p<0.0001****
	qRT-PCR % isoform	11.65 ± 0.94		88.35 ± 0.94		34.96 ± 0.80		65.04 ± 0.80	F(3,16)=1495 p<0.0001****	N/A	p<0.0001****	p<0.0001****

Relative isoform expression levels of JM and CYT isoforms (% isoform) in the Hpp (w/ or w/o the dentate gyrus (DG)), as determined by ISH and qPT-PCR. Values represent the mean ± SEM (n=4) of analyzed areas, dots/area and percentage of ErbB4-positive cells, as well as dots/cell (analysis only performed for on hippocampus w/o DG). *p<0.05, **p<0.01, ***p<0.001, ****p<0.0001 (n=4; one-way ANOVA with Tukey's multiple comparison test). N/A: not applicable.

Table 4.5 | Quantification and statistical analysis of ErbB4 isoform expression in various adult brain region using isoform-specific single-pair probes.

ROI	probes	pan 27/28	JMa 15/16b	JMb 15/16a	CYT-1 25/26	CYT-2 25/27	one-way ANOVA	JMa vs. JMb	CYT-1 vs. CYT-2
Rsc	area [mm ²]	2.36 ± 0.15	2.28 ± 0.15	2.24 ± 0.12	2.40 ± 0.13	2.38 ± 0.13	F(4,10)=0.2492 p=0.9037	N/A	N/A
	dots/ mm ²	2870.6 ± 638.0	2105.9 ± 673.3	256.7 ± 107.0	393.7 ± 72.17	1224.3 ± 62.47	F(3,8)=6.172 p=0.0178*	p=0.0218*	p=0.3801
	% ErbB4+	29.07 ± 4.48	6.05 ± 2.55	22.61 ± 5.98	7.86 ± 0.91	16.24 ± 0.26	F(3,8)=5.483 p=0.0242*	p=0.0301*	p=0.3374
	dots/cell	2.53 ± 0.10	1.20 ± 0.06	2.29 ± 0.35	1.43 ± 0.05	2.15 ± 0.11	F(3,8)=7.985 p=0.0086**	p=0.0152*	p=0.0998
	% isoform	N/A	9.93 ± 1.69	90.07 ± 1.69	23.94 ± 3.06	76.06 ± 3.06	F(3,8)=249.5 p<0.0001****	p<0.0001****	p<0.0001****
Rtn	area [mm ²]	0.654 ± 0.067	0.692 ± 0.128	0.590 ± 0.099	0.807 ± 0.124	0.669 ± 0.128	F(4,15)=0.5026 p=0.7344	N/A	N/A
	dots/ mm ²	3410.4 ± 760.2	364.9 ± 110.0	2445.3 ± 805.9	276.0 ± 44.3	1135.0 ± 225.3	F(3,12)=5.642 p=0.0120*	p=0.0205*	p=0.5015
	% ErbB4+	47.48 ± 5.56	10.19 ± 3.25	34.29 ± 9.42	8.68 ± 1.04	25.88 ± 4.64	F(3,12)=5.061 p=0.0171*	p=0.0408*	p=0.1776
	dots/ cell	2.05 ± 0.26	1.11 ± 0.04	1.80 ± 0.33	1.10 ± 0.01	1.41 ± 0.07	F(3,12)=3.714 p=0.0424*	p=0.0621	p=0.5812
	% isoform	N/A	13.77 ± 3.37	86.23 ± 3.37	21.24 ± 5.57	78.76 ± 5.57	F(3,12)=67.30 p<0.0001****	p<0.0001****	p<0.0001****
Thal	area [mm ²]	5.65 ± 0.30	5.44 ± 0.59	5.55 ± 0.56	5.27 ± 0.39	5.55 ± 0.32	F(4,15)=0.1055 p=0.9788	N/A	N/A
	dots/ mm ²	703.4 ± 111.8	284.3 ± 84.6	73.4 ± 12.9	184.5 ± 22.6	156.6 ± 33.4	F(3,12)=3.380 p=0.0543	p=0.0364*	p=0.9744
	% ErbB4+	20.57 ± 3.00	9.75 ± 2.76	2.30 ± 0.45	6.58 ± 0.77	5.62 ± 1.27	F(3,12)=3.751 p=0.0413*	p=0.0268*	p=0.9726
	dots/ cell	1.21 ± 0.04	1.10 ± 0.03	1.12 ± 0.02	1.09 ± 0.01	1.09 ± 0.01	F(3,12)=0.8241 p=0.5055	p=0.7643	p=0.9980
	% isoform	N/A	77.41 ± 2.66	22.59 ± 2.66	55.10 ± 7.62	44.90 ± 7.62	F(3,12)=15.90 p=0.0002***	p<0.0001****	p=0.6018
CC	area [mm ²]	0.330 ± 0.024	0.363 ± 0.275	0.344 ± 0.029	0.347 ± 0.021	0.346 ± 0.027	F(4,15)=0.2049 p=0.9317	N/A	N/A
	dots/ mm ²	1063.6 ± 162.2	632.8 ± 231.6	147.6 ± 27.4	312.6 ± 49.2	259.7 ± 71.1	F(3,12)=2.800 p=0.0854	p=0.717	p=0.9900
	% ErbB4+	21.95 ± 3.51	14.84 ± 5.0	2.64 ± 0.62	8.89 ± 1.00	7.21 ± 2.02	F(3,12)=3.34 p=0.0562	p=0.0382*	p=0.9722
	dots/ cell	1.42 ± 0.04	1.25 ± 0.07	1.56 ± 0.01	1.13 ± 0.02	1.12 ± 0.02	F(3,12)=25.93 p<0.0001****	p=0.0006***	p=0.9973
	% isoform	N/A	76.80 ± 4.94	23.20 ± 4.94	57.32 ± 10.59	42.68 ± 10.59	F(3,12)=7.535 p=0.0043**	p=0.0030**	p=0.6075
	qRT-PCR % isoform	N/A	68.33 ± 3.56	31.67 ± 3.56	58.62 ± 1.29	41.38 ± 1.29	F(3,16)=38.25 p<0.0001****	p<0.0001****	p=0.0017**

Values represent the mean ± SEM (n=3, 4) of analyzed areas, dots/ area, percentage of ErbB4-positive cells, dots/ positive cell and relative isoform expression (% isoform) in the retrosplenial cortex (Rsc), reticular thalamic nucleus (Rtn), thalamus (Thal) and corpus callosum (CC) hybridized with pan and isoform-specific single-pair ErbB4 probes. Relative isoform expression in the CC was additionally performed by qRT-PCR using TaqMan probes. One-way ANOVA was performed to compare isoform expression (except for area) was performed and adjusted p values of Tukey's multiple comparison test are listed, *p<0.05, **p<0.01, ***p<0.001, ****p<0.0001. N/A: not applicable.

Table 4.6 | Histogram distribution of number of cells with same amount of dots in hippocampus of WT and ErbB4-Δ2 KO mice.

Dots/ cell	WT			ErbB4-Δ2 KO		Statistics (two-way ANOVA: F(40,165)=41.03, p<0.0001****)	
	pan 1/2	pan 2/3	pan 27/28	pan 1/2	pan 2/3	WT vs. ErbB4-Δ2 KO (pan 1/2; pan 2/3)	WT 1/2 vs 2/3; 1/2 vs 27/28; 2/3 vs 27/28
1	839.75 ± 46.11	717.50 ± 66.25	835.50 ± 94.03	77.25 ± 21.26	45.25 ± 9.13	p<0.0001**** p<0.0001****	p<0.0001**** p=0.9847 p<0.0001****
2	271.00 ± 24.18	217.00 ± 26.52	246.75 ± 23.67	3.00 ± 1.68	3.5 ± 1.32	p<0.0001**** p<0.0001****	p=0.2412 p=0.8863 p=0.7869
3	137.25 ± 7.18	101.00 ± 8.85	117.50 ± 11.49	1.00 ± 0.58	0.25 ± 0.25	p<0.0001**** p=0.0016**	p=0.6382 p=0.9430 p=0.9700
4	84.00 ± 2.35	70.50 ± 4.13	68.25 ± 6.50	0.00 ± 0.00	1.00 ± 0.41	p=0.0137* p=0.0653	p=0.9857 p=0.9747 p>0.9999
5	56.75 ± 6.64	46.25 ± 4.21	50.25 ± 4.96	0.50 ± 0.29	0.00 ± 0.00	p=0.2046 p=0.3110	p=0.9945 p=0.9992 p=0.9999
6	47.25 ± 3.33	32.75 ± 2.50	38.00 ± 6.49	0.25 ± 0.25	0.00 ± 0.00	p=0.3796 p=0.7213	p=0.9813 p=0.9966 p=0.9996
7	34.00 ± 2.42	24.75 ± 5.12	34.00 ± 5.02	0.50 ± 0.50	0.00 ± 0.00	p=0.7039 p=0.8786	p=0.9966 p>0.9999 p=0.9966
8	29.00 ± 2.35	18.00 ± 2.16	26.50 ± 2.72	0.25 ± 0.25	0.00 ± 0.00	p=0.8072 p=0.9589	p=0.9934 p>0.9999 p=0.9976
9	20.25 ± 1.32	14.50 ± 2.22	21.50 ± 2.22	0.00 ± 0.00	0.00 ± 0.00	p=0.9379 p=0.9813	p=0.9995 p>0.9999 p=0.9989
10	13.50 ± 4.91	10.25 ± 2.39	18.25 ± 4.09	0.00 ± 0.00	0.00 ± 0.00	p=0.9857 p=0.9950	p>0.9999 p=0.9998 p=0.9981
>10	42.25 ± 3.38	21.50 ± 10.18	56.50 ± 14.44	0.25 ± 0.25	0.25 ± 0.25	p=0.4966 p=0.2046	p=0.9324 p=0.9825 p=0.6684

Mean values ± SEM are tabulated for the number of cells with between 1 and >10 dots/cell. Adjusted p values are listed, *p<0.05, **p<0.01, ***p<0.001, ****p<0.0001 (n=4; two-way ANOVA with Tukey's multiple comparison test).

Table 4.7 | ErbB4 isoform expression in human cingulate cortex and corpus callosum.

ROI	JMa	JMb	CYT-1	CYT-2	one-way ANOVA	JMa vs. JMb	CYT-1 vs. CYT-2
Cingulate cortex	18.81 ± 4.60	81.19 ± 4.60	29.22 ± 5.34	70.78 ± 5.34	F(3,12)= 37.21 p<0.0001****	p<0.0001****	p=0.0004***
Corpus callosum	70.29 ± 4.73	29.71 ± 4.73	44.92 ± 3.86	55.08 ± 3.86	F(3,12)= 15.64 p=0.0002***	p=0.0001***	p=0.3824

Relative abundance of ErbB4 isoforms in the human cingulate cortex and corpus callosum analyzed by TaqMan qRT-PCR. Values represent the mean ± SEM. Adjusted p values are listed, *p<0.05, **p<0.01, ***p<0.001, ****p<0.0001 (n=4; one-way ANOVA with Tukey's multiple comparison test).

Table 4.8 | Quantification and statistical analysis of ErbB4 expression in the hippocampus (Hpp) comparing single-pair probes to probes using 20 pairs.

ROI	probes	single-pair probe			20 pairs	Statistics	
		pan 1/2	pan 2/3	pan 27/28	pan	one-way ANOVA	1pair vs 20pairs 1/2; 2/3; 27/28
Hpp	area [mm ²]	4.56 ± 0.30	4.61 ± 0.31	4.42 ± 0.35	4.71 ± 0.41	F(3,12)=0.121 8 p=0.9455	N/A
	dots/ mm ²	1282.1 ± 112.3	955.3 ± 96.6	1360 ± 166.3	5007 ± 516.0	F(3,12)=46.30 p<0.0001	p<0.0001**** p<0.0001**** p<0.0001****
Hpp w/o DG	area [mm ²]	3.26 ± 0.19	3.33 ± 0.21	3.13 ± 0.22	3.37 ± 0.25	F(3,12)=0.221 9 p=0.8793	N/A
	dots/ mm ²	1439.4 ± 103.0	1046.5 ± 108.2	1482.7 ± 179.9	5181 ± 577.3	F(3,12)=38.77 p<0.0001	p<0.0001**** p<0.0001**** p<0.0001****
	% ErbB4+	23.27 ± 2.0	18.61 ± 1.99	21.52 ± 1.91	17.20 ± 2.19	F(3,12)=1.845 p=0.1928	p=0.2013 p=0.9591 p=0.4632
	dots/ cell	2.57 ± 0.12	2.34 ± 0.08	2.64 ± 0.06	8.85 ± 0.67	F(3,12)=84.72 p=0<0.0001	p<0.0001**** p<0.0001**** p<0.0001****

Values represent the mean ± SEM of analyzed areas, dots/ area and percentage of ErbB4-positive cells analyzed with single-pair probes and 20 probe pairs in WT sections. *p<0.05, **p<0.01, ***p<0.001, ****p<0.0001 (n=4; one-way ANOVA with Tukey's multiple comparison test). N/A: not applicable.

Table 4.9 | Quantification and statistical analysis of ErbB4 JMa expression in the hippocampus (Hpp) comparing probes using one or two probe pairs, respectively.

ROI	probes	JMa 15/16b	JMa 16b/17	JMa 2pairs	one-way ANOVA	15/16b vs. 2pairs; 16b/17 vs. 2pairs
Hpp	area [mm ²]	3.22 ± 0.35	3.48 ± 0.24	3.22 ± 0.30	F(2,9)=0.238 7 p=0.7925	N/A
	dots/ mm ²	143.5 ± 34.2	166.6 ± 29.0	348.3 ± 47.10	F(2,9)=8.921 p=0.0073**	p=0.0097** p=0.0188*
Hpp w/o DG	% ErbB4+	4.86 ± 1.16	5.91 ± 0.93	10.28 ± 1.48	F(2,9)=5.634 p=0.0259	p=0.0280* p=0.0727
	dots/ cell	1.19 ± 0.04	1.21 ± 0.04	1.34 ± 0.04	F(2,9)=4.079 p=0.0548	p=0.0628 p=0.1146
Hpp	area [mm ²]	4.44 ± 0.51	4.83 ± 0.38	4.52 ± 0.45	F(2,9)=0.213 5 p=0.8118	N/A
	dots/ mm ²	135.0 ± 32.8	157.4 ± 26.3	336.5 ± 52.33	F(2,9)=8.110 p=0.0097**	p=0.0128* p=0.0240*

Values represent the mean ± SEM (n=4) of analyzed areas, dots/ area and percentage of ErbB4-positive cells, as well as dots/cell. *p<0.05, **p<0.01, ***p<0.001, ****p<0.0001 (n=4; one-way ANOVA with Tukey's multiple comparison test). N/A: not applicable.

Table 4.10 | Quantification and statistical analysis of ErbB4 splice variants in the choroid plexus (Cp).

ROI	probes	JMa 15/16b	JMb 15/16a	CYT-1 25/26	CYT-2 25/27	one-way ANOVA	JMa vs. JMb	CYT-1 vs. CYT-2
Cp	area [mm ²]	0.059 ± 0.019	0.064 ± 0.020	0.068 ± 0.018	0.066 ± 0.018	F(3,12)=0.045 8 p=0.9863	N/A	N/A
	dots/ mm ²	4712 ± 775.8	105 ± 66.39	1026 ± 198.0	2227 ± 484.0	F(3,12)=18.10 p<0.0001****	p<0.0001****	p=0.3153
	% ErbB4+	55.07 ± 4.41	1.57 ± 0.81	15.63 ± 1.05	33.10 ± 5.98	F(2,9)=5.634 p=0.0259		p=0.0280* p=0.0727
	dots/ cell	1.54 ± 0.15	1.14 ± 0.14 [#]	1.27 ± 0.15	1.31 ± 0.06	F(3,11)=1.687 p=0.2270	p=0.1971	p=0.9953
	% isoform	98.18 ± 0.90	1.82 ± 0.90	36.82 ± 8.81	63.18 ± 8.81	F(3,12)=42.47 p<0.0001****	p<0.0001****	p=0.0492*

Values represent the mean ± SEM (n=4). *p<0.05, ****p<0.0001 (n=4; one-way ANOVA with Tukey's multiple comparison test). N/A: not applicable. #: One sample did not show any expression of JMb in the choroid plexus and therefore was excluded from the 'dots per positive cell' analysis (n=3 for JMb).

5

Subcellular expression of ErbB4 & its isoforms in distinct neurons

Section 5.3.1 'Axonal expression of ErbB4 in dopaminergic neurons' is part of the publication: Miguel Skirzewski, Irina Karavanova, Alon Shamir, Larissa Erben, Jennie Garcia-Olivares, Jung Hoon Shin, Detlef Vullhorst, Veronica A. Alvarez, Susan G. Amara and Andres Buonanno (2018) ErbB4 signaling in dopaminergic axonal projections increases extracellular dopamine levels and regulates spatial/working memory behavior. Mol Psychiatry (23), 2227-2237.

L.E. designed and performed research, analyzed data for data shown in section 5.3.1 and all other unpublished sections of this chapter if not otherwise stated.

5.1 Introduction

ErbB4 function on GABAergic interneurons has been extensively studied. Limited attention has been dedicated on the other hand to its expression on dopaminergic neurons and the role of NRG/ErbB4 signaling in the dopamine system (see Introduction 1.3.5). Interestingly, previous studies from our lab have suggested, that NRG/ErbB4 regulates dopamine levels in the dorsal hippocampus, a target area of long-projecting dopaminergic neurons. Direct infusion of NRG1 by reverse microdialysis into the dorsal hippocampus of behaving rats, rapidly increases the extracellular dopamine concentration that lasts for about 15min¹³⁸. Conversely, the administration of ErbB inhibitors results in a small but significant reduction of extracellular dopamine levels¹⁸⁹. Moreover, dopamine neurotransmission is also required to mediate the modulatory effects of NRG on LTP reversal and augmentation of γ -oscillations in the dorsal hippocampus. Both have been shown moreover to depend on dopamine receptor D4 (D4DR)^{138, 321, 322}. Since in slice recordings axonal dopamine terminals are separated from their somas, we hypothesize that ErbB4 receptors mediating the modulatory

effects of NRG on LTP and γ -oscillations by potentially increasing extracellular dopamine levels is present locally on dopaminergic fibers.

Importantly, this proposed axonal expression of ErbB4 on dopaminergic neurons is in stark contrast to the confined somatodendritic localization of ErbB4 on most GABAergic interneurons including PV basket cells^{58, 59}. The presence of ErbB4 on presynaptic boutons has been suggested for the interneuronal subclass of PV+ Chandelier cells based on the observed reduction of inhibitory cartridges upon loss of ErbB4^{60, 68-70}. In hippocampal cultures, despite the development of GABAergic synapses at the AIS³²³, as well as in immunohistochemistry, ErbB4 has not been detected on PV+ boutons with antibodies specific for ErbB4, but *in vivo* was found on a few CCK+ synapses (<9%) confined to a few brain areas^{58, 59}. While the presynaptic localization in both dopaminergic neurons and Chandelier cells needs still to be confirmed, an interesting model emerges, in which in some neuronal cell types ErbB4 expression is strictly restricted to the dendrites and cell body (most GABAergic interneurons, e.g. PV basket cells), whereas in other neurons in addition to the somatodendritic compartment ErbB4 is also located to axonal projections and synaptic terminals (e.g. dopaminergic neurons, Chandelier cells).

Differential subcellular targeting of protein isoforms to neurites (dendrites and axon) has previously been demonstrated, e.g for the voltage-gated potassium channel Kv3.1 isoforms Kv3.1a and Kv3.1b³²⁴ and protein phosphatase 1 (PP1) variants PP1 β and PP1 γ ³²⁵. Interestingly, targeting differs also between N-terminal isoforms of NRG1. While the TM-NRG NRG1 type III localizes to axons, the soluble Ig-NRG isoforms NRG1 type I and type II are restricted to the soma and proximal dendrites³⁹. Moreover, isoform-specific localization also arises from spatial restriction of mRNA variants and subsequent local translation. In particular, variants at the 3' end of the transcript have been identified to regulate neurite localization. Gene distal alternative last exons and long 3'UTR variants are frequently enriched in the neuropil³²⁶⁻³²⁸. Therefore, I hypothesize that ErbB4 isoforms regulate the differential localization in distinct neuronal cell types. One (or several) ErbB4 isoforms might be anterogradely transported into axons. These splice variants could be specifically expressed in some neuronal types (i.e. Chandelier cells and dopaminergic neurons) but not in others (i.e. most classes of GABAergic interneurons). Our current understanding of ErbB4 variant

expression only suggests that there are no fundamental regional differences in JM and Cyt expression between the dorsal hippocampus, cortex and the VTA, namely in all areas ErbB4 receptors are predominantly JMb and Cyt-2 isoforms (see chapter 2 & 4). Moreover, all ErbB4 variants have been detected in GABAergic interneurons (see Chapter 4, L. Erben *unpublished data*) and both Cyt variants have been detected in dopaminergic neurons (see Chapter 6). However, it remains unclear which variants are co-expressed in a single cell and if a subset of dopaminergic neurons and GABAergic interneurons (i.e. Chandelier cells) preferentially expresses one splice variant. On the other hand, differences in subcellular localization and trafficking of ErbB4 isoforms indeed have been previously described in non-neuronal cells. In fibroblast-like COS-7 (CV-1 origin with SV40) kidney cells, Cyt-2 receptors have been suggested to be endocytosis-impaired, whereas Cyt-1 ErbB4 were present on intracellular vesicles²⁰⁷. Surface distribution including targeting to neuronal neurites has not been interrogated.

Here, to address if ErbB4 is present on axonal projections of dopaminergic neurons, I perform immunocytochemistry on primary mesencephalic tissue cultures to visualize endogenous receptors. Next, the subcellular localization of the four ErbB4 isoforms (JM_a/Cyt-1, JM_a/Cyt-2, JM_b/Cyt-1 and JM_b/Cyt-2) is tested by viral transduction in cultured hippocampal GABAergic interneurons and subsequent immunostainings specific for the exogenous overexpressed receptor.

5.2 Methods

Animals. Full ErbB4 knock-out (KO) mice, lacking the second exon have been described previously¹⁵⁶. Embryonic lethality of ErbB4-KO was rescued by transgenic ErbB4 overexpression in the heart (ErbB4^{MHC-ErbB4})¹⁵⁷, heart-rescued ErbB4-KO mice are hereafter referred to as ErbB4-KO. ErbB4-KO mice were backcrossed to C57BL/6J for >15 generations. Control adult wild-type C57BL/6J mice were purchased from the Jackson laboratories and Sprague Dawley rats from Charles River. Animals of both sexes were used for primary tissue culture. All animals were housed on a 12–12h light-dark schedule with access to food and water *ad libitum*. Animal procedures were reviewed and approved by the NIH Animal Care and Use Committee.

Primary neuronal cultures. Dissociated hippocampal neurons were prepared from E19 Sprague Dawley rat embryos by the biologist in the laboratory, Irina Karavanova. Hippocampi were dissected in dissection buffer (1x HBSS (Gibco, Cat No. 14185-052), 10mM HEPES pH7.3 (Gibco, Cat No. 15630-080), 1x Penicillin/Streptomycin (Pen/Strep; Gibco, Cat No. 15140122)), trypsinized with 0.25% trypsin (Gibco, Cat No. 15090-046) for 15min at 37°C, and carefully triturated in neurobasal medium (Gibco, Cat No. 15170-064) supplemented with 1x B27 supplement (Gibco, Cat No. 17504-044), 1x Pen/Strep, 0.5mM glutamine (Gibco, Cat No. 25030-149) and 0.0125mM glutamate. 42.500 neurons were plated per 24well onto poly-D-lysine (PDL; Sigma-Aldrich, Cat No. P7405-5mg)-covered (100µg/mL) 12mm coverslips (#1; Carolina Assistant-Brand, Cat No. 41001112). Half of the medium was changed every week starting on day 6 in vitro (DIV6). Feeding medium does contain all components of the plating medium but glutamate. Primary mouse mesencephalic cultures were grown on a layer of rat cortical astrocytes. Cortices were dissected from E19 rat embryos in dissection medium (1x HBSS, supplemented with 20mM sucrose (Sigma-Aldrich, Cat No. S7903), 28mM dextrose (Sigma-Aldrich, Cat No. G5767) and 4.2mM sodium bicarbonate (Sigma-Aldrich, Cat No. S5761)) and trypsinized with 0.25% trypsin in the same buffer for 15min at 37°C. Cells were triturated in advanced DMEM/F12 medium (Gibco, Cat No. 12634-010) supplemented with 10% heat-inactivated fetal bovine serum (FBS; Gibco, Cat No. 16140-063), 2mM GlutaMAX (Gibco, Cat No. 35050-061), 10µg/mL gentamicin (Gibco, Cat No. 15170-064) and plated in Nunc tissue culture flasks (Thermo Fisher Scientific, Cat No. 156499). At DIV7, neurons and oligodendrocytes were shaken off, astrocytes trypsinized and plated onto PDL-covered (100µg/mL) coverslips at a density of 50.000-100.000 cells per 24 well. Astrocytes were arrested with 10µM Floxuridine (FUDR; Sigma-Aldrich, Cat No. F0503) at confluency and mouse mesencephalic cultures plated on top of the astrocytic layer within 1-3 days. The mesencephalic area was dissected from E15 C57BL/6J and ErbB4-KO mouse embryos in dissociation medium, trypsinized in 0.25% trypsin at 37°C for 5min and triturated in culture medium (advanced DMEM/F12 (Gibco, Cat No. 35050-061), 1x N2 (Gibco, Cat No. 17502-048), 200mM GlutaMAX and 2% heat-inactivated FBS, supplemented with 10µg/mL gentamicin and 10µM FUDR). 50.000 cells were plated per 24 well and 10ng/ml basic fibroblast growth factor (bFGF, R&D Systems, Cat No.4114-TC) added. Half medium changes were performed once a week starting on DIV3.

Cloning of ErbB4 isoforms. Gateway entry vector pENTR223.1 encoding mouse ErbB4 JM_a/Cyt-2 was purchased from Imagenes and a stop codon inserted at the end of the coding sequence. G-block cloning strategy was used to clone all other ErbB4 isoforms. Restriction enzymes EcoRI and KpnI (New England BioLabs, Cat No. R3101 & R3142) were used to insert 561bp Cyt-1 G-block (Integrated DNA Technologies) sequence to obtain pENTR223.1_mErbB4_JM_a/Cyt-1. pENTR223.1_mErbB4_JM_b/Cyt-2 was cloned with BsaBI (New England BioLabs, Cat No. R0537) and EcoRI and 909bp JM_b G-block from dam^r/dcm^r pENTR223.1_mErbB4_JM_a/Cyt-2. Finally, pENTR223.1_mErbB4_JM_b/Cyt-1 was cloned from JM_b/Cyt-2 plasmid using EcoRI, KpnI and Cyt-1 encoding G-block as described above. Successful cloning was confirmed by DNA sequencing (Macrogen). pAAV Gateway destination vector was generated by Detlef Vullhorst by inserting a Gateway conversion cassette into pAAV(MCS) (Agilent, AAV Helper-Free System, Cat No. 240071) and replacing the cytomegalovirus (CMV) promoter by an human synapsin I (hSynI) promoter for confined neuronal expression. Gateway cloning (Gateway LR clonase II, ThermoFisher, Cat No. 11791100) was used according to manufacturer's protocol to shuttle ErbB4 coding sequences into destination pAAV-hSynI vector. Successful recombination was confirmed by SacI (New England BioLabs, Cat No. R3156) restriction digest and plasmid DNA was prepared using Qiagen Plasmid Midi kit (Qiagen, Cat No. 12145) for AAV transfection

Preparation of adeno-associated viruses (AAV). AAV-293HEK (human embryonic kidney) cells (Agilent, Cat No. 240073) grown in DMEM (Gibco; Cat No. 105690-010)/10% FBS were used for AAV production. Cells between passages 3-5 were plated in 15cm dishes (2 dishes per AAV preparation; Falcon, Cat No. 353025). At 60-70% confluence, a complete medium change was performed 2h prior to transfection. Per 15cm dish, 6.6µg pHelper (Agilent, AAV Helper-Free System, Cat No. 240071), 4.4µg pAAV-RC1 (Cell Biolabs, Cat No. VPK-421) and 4.4µg recombinant pAAV-hSynI-ErbB4 transfer plasmid (1:1:1 mass ratio) were mixed with 60µl polyethyleneimine (1mg/mL; Polysciences Inc., Cat No. 23966) in 500µl DMEM medium without serum. After 10min incubation the DNA was added to the cells. Cells were fed with fresh medium after 48h and harvested 72h by scraping into 2mL (per dish) gradient buffer (150mM NaCl, 10mM MgCl₂, 10mM Tris-Cl, pH 7.6). Cells were lysed by four freeze-thaw cycles with intermediate trituration through a 23-gauge needle. DNA was degraded with 250U benzonase (Sigma-Aldrich, Cat No. E1014) per preparation (~5mL) for 1h at 37°C with

occasional agitation. The lysate was cleared by centrifugation at 3000g for 15min at 4°C and the supernatant layered on top of an iodixanol gradient (Sigma-Aldrich, Cat No. D1556; 15%, 25%, 40% and 58% (v/v) in gradient buffer) in a Beckman quick seal centrifuge tube (Beckman, Cat No. 344326). The remaining volume was filled with gradient buffer and the tubes sealed without trapping an air bubble. Ultracentrifugation was done at 48,000rpm in a type 70Ti fixed angle rotor (Beckman) for 2h at 18°C. AAV was collected from the 40% iodixanol layer, aliquoted and stored at -80°C for long-term storage or at 4°C for immediate use. 4µl of each AAV1-hSynI-ErbB4 were transduced into primary hippocampal neurons and expression verified by Western using rabbit monoclonal Ab10 antibody⁵⁸ with an apparent mass of ~180kDa. For immunostaining in hippocampal cultures, 0.25µl of AAV was mixed into the cell culture medium at DIV10-DIV13.

Immunocytochemistry. Immunostaining was performed at DIV10 for mesencephalic cultures and at DIV20-DIV27 for hippocampal cultures. Cultures were fixed for 15min at RT in 4% paraformaldehyde (PFA; Electron Microscopy Sciences, Cat No. 15710), 4% sucrose in PBS pH-7.4. After extensive washes with PBS, cells were blocked and permeabilized with 2-3% normal donkey serum (NDS; Sigma-Aldrich, Cat No. D9663)/0.1% TX-100 (Thermo Fisher Scientific, Cat No. 28314) in PBS (blocking solution) and incubated overnight with primary antibodies (rat monoclonal anti-DAT (1:200; sc-32258 Santa Cruz, TX), mouse monoclonal anti-parvalbumin (isotype IgG1, 1:1000, Sigma, Cat No. P3088), mouse monoclonal anti-ankyrinG (1:500-1000; clone N106/36 (isotype IgG2a) or clone N106/65 (isotype IgG2b), NeuroMab), guinea pig anti-tau (1:10000; Synaptic Systems, Cat No. 314004) or guinea pig anti-microtubule associated protein (MAP2; 1:2000; Synaptic Systems, Cat No. 188004), and rabbit monoclonal anti-ErbB4 antibodies (clone mAb-6⁵⁸, undiluted hybridomas supernatant or at 1µg/mL of affinity-purified antibody; clone mAb-10⁵⁸ at 1µg/mL)) at 4°C in blocking solution. After extensive washing in PBS, cells were incubated with secondary antibodies (all 1:1000; goat anti-mouse IgG1-A488 (Life technologies, Cat No. A21121), goat anti-mouse (IgG2a or IgG2b)-A647 (Life technologies, Cat No. A21241/21242), donkey anti-rat A488 (Invitrogen, Cat No. A21208), donkey anti-rabbit-DL549 or -Cy3 (Jackson ImmunoResearch Labs, Cat No. 111-485-144/ 711-165-153) and goat anti-guinea pig biotin conjugate (Life technologies, Cat No. A18779)) for 1h at RT in blocking solution. For biotin streptavidin conjugation, if applicable, cells were washed with PBS and incubated with streptavidin-pacific

blue (1:1000, Life technologies, Cat No. S11222) for 1h at RT in blocking solution. Washed coverslips were mounted on slides using Mowiol (Calbiochem, Cat No. 3475904)/DABCO (Sigma-Aldrich, Cat No. D2522) mounting medium and analyzed on a LSM710 confocal microscope at 63x magnification (Zeiss). Images were adjusted for overall brightness and contrast and mean fluorescent intensity was analyzed in manually-defined region of interest (ROI) based on PV, MAP2 and ankyrin G staining in ImageJ. Neurite expression was assessed in the first 200-400 μ m of one randomly-chosen neurite and confined to a single branch. Neurite enrichment was calculated as the ratio between mean fluorescent intensity in the axon and dendrite, normalizing for the total expression level per neuron. Somatic fluorescent ErbB4 expression was normalized to the average intensity in each experiment.

Brain membrane fractionation. Dorsal striatum was dissected from eight male rats (13-weeks old) yielding in 600mg tissue, immediately homogenized in 20 volumes of cold fractionation buffer (320mM sucrose, 10mM HEPES pH7.4, 1x protease inhibitor (cOmplete protease inhibitor cocktail, Roche, Cat No. 11697498001)) using at first a glass-glass Dounce homogenizer with a tight plunger (A), then a glass-Teflon homogenizer rotating at 900rpm on ice. Brain membrane fractionation was performed as briefly described⁴⁰. Briefly, nuclei and unbroken cells were removed by centrifugation for 10min at 1,000g. Supernatant (S1) was centrifuged for 20min at 10,000g to obtain crude membrane pellet (P2) which was washed by resuspending in 10 volumes of fractionation buffer, homogenizing and centrifugating. After resuspending P2 in 5 volumes RIPA (radioimmunoprecipitation assay buffer; 50mM Tris-Cl pH7.5, 150mM NaCl, 1x protease inhibitor) the protein concentration was determined from a 20-fold dilution using Bradford assay (Bio-Rad, Cat No. 500-0006) against bovine IgG standard curve (Bio-Rad, Cat No. 500-0208). 5mg protein was aliquoted, pelleted by centrifugation for 10min at 10,000g and resuspended in 1mL oxygenated Ringer's solution (120mM NaCl, 5.6mM KCl, 2.2mM CaCl₂, 1mM MgCl₂, 25mM NaHCO₃, 5.5mM HEPES, 10mM glucose, pH7.4). P2 membranes were incubated with 12.5nM NRG2-ECD (extracellular domain; Genscript, custom-made in baculovirus), 12.5 μ M PD158780 (Calbiochem, Cat No. 171179-06-9), both or under control conditions for 15min at 37°C. Samples were precipitated for 10min at 10,000g and solubilized in 1mL cold RIPA buffer containing 1% TritonX-100 and phosphatase inhibitor cocktail III (Calbiochem, Cat No.

524627). After incubation for 30min at 4°C on rotarod, soluble and insoluble P2 were separated by centrifugation at 32,000g for 20min (Beckman tabletop centrifuge TLS55.1).

Immunoprecipitation. ErbB4 immunoprecipitation was performed from soluble (sol) P2 fraction (see above). Resuspended insoluble fraction served as negative control (ins). Soluble fractions were pre-cleared with 50µl equilibrated protein A-agarose (Pierce, Cat No. A20421) for 1h at 4°C with agitation. ErbB4 and interacting proteins were immunoprecipitated with 10µg monoclonal rabbit anti-ErbB4 antibody (mAb10⁵⁸) overnight at 4°C. As negative control 10µg normal rabbit IgG (nrbIgG; Santa Cruz Biotechnology, Cat No. sc2027) was used. 50µl equilibrated protein A-agarose was added and samples incubated for 1h at 4°C with agitation. Input and flow-through control were collected, agarose-beads washed in RIPA buffer containing 1% Triton X-100 and proteins eluted in 100µl RIPA buffer supplemented with 1x non-reducing LDS (lithium dodecyl sulfate) sample buffer (Thermo Fisher, Cat No. 84788, final concentration 1x) and 5% β-mercaptoethanol (Sigma-Aldrich, Cat No. M3148). Samples were 10-times enriched compared to input and were denatured for 10min at 80°C for ErbB4 Western Blotting, whereas samples for DAT immunoblots were incubated at RT. Western Blotting was performed as described below.

Microdissected protein samples. For immunoblotting, tissue was dissected from 9-week old male C57BL/6J and ErbB4 KO mice (n=3/genotype). Briefly, mice were euthanized by cervical dislocation, the brain was dissected and washed with cold PBS. Microdissection of the dorsal striatum was performed using 25-gauge needles in dissection buffer (20mM sucrose, 8mM D-glucose, 4mM NaHCO₃ in 1x HBSS) under a dissecting microscope from 2mm-thick coronal sections cut with the help of a brain matrix. Samples were immediately homogenized using a hand-held Ultraturrax with a 5mm probe in 300µl of cold RIPA buffer and further processed by Detlef Vullhorst. Homogenates were incubated on ice for 5-10min and centrifuged at 5,000rpm for 5min. Protein concentration was measured from 1:20 dilutions of the supernatant using Bradford assay against bovine IgG standard curve, ranged between 5-7mg/mL and was adjusted with RIPA buffer to 1mg/mL. 1x non-reducing LDS and β-mercaptoethanol (final concentration 5%) were added. Importantly, for successful DAT immunoblot with rat monoclonal anti-DAT antibody (clone 6-5G10; Santa Cruz Biotechnology, Cat No. sc-32258,) samples were not heated.

Western Blotting. 15µl of protein sample were loaded on 4-15% acrylamide gradient gels (Mini-PROTEAN TGX, Bio-Rad, Cat No. 456-1086), stacked at 80V and separated at 120V in Tris/Glycine buffer (BioRad, Cat No. 161-0732). Proteins were transferred onto nitrocellulose membrane using 7-min turbo transfer (Bio-Rad, Cat No.170-4270). The membrane was blocked for 1h at RT with 3% BSA (bovine serum albumin, Sigma-Aldrich, Cat No. A7906) in TBST (1x tris-buffered saline (Quality Biology, Cat No. 351-086-131) + 0.05% Tween 20 (BioRad, Cat No. 161-0781)) and incubated with primary antibodies over night at 4°C. After extensive washes in TBST (5x 10min) the membrane was incubated with secondary horseradish peroxidase (HRP)-conjugated antibodies (1:2000-1:10000; Jackson Immuno Research; anti-rat-HRP, Cat No. 712-035-150; anti-rabbit-HRP, Cat No. 211-032-171) in 5% (w/v) milk in TBST for 1h at RT. Blots were extensively washed in TBST and signals detected using chemiluminescence (Western Lightning Plus-ECL, Perkin Elmer, Cat No. NEL120E001EA) in a ChemiDoc MP imager (Bio-Rad, Universal Hood III). Densiometric analysis was performed using Image Lab software (Bio-Rad). For repeated analysis with other antibodies, the membrane was stripped for 15min at RT (Restore Western Blot Stripping Buffer, Thermo Fisher Scientific, Cat No. 21059), extensively washed with TBST and blocked with 3% BSA/TBST. Primary antibodies were analyzed in the following order: monoclonal rat anti-DAT antibody (1µg/mL, clone 6-5G10; Santa Cruz Biotechnology, Cat No. sc-32259), rhodamine conjugated anti-tubulin-rhodamine (1:5000, Bio-Rad, Cat No. AbD22584), monoclonal rabbit anti-ErbB4 (mAb10⁵⁸; 2µg/mL). Of note, the fluorescent detection of the house-keeping gene tubulin does not require stripping.

Statistical Analysis. All data represent the mean ± SEM and statistical significance was set at p<0.05. Outliers (ROUT, Q=1%) were excluded from analyses and statistical analysis was performed using Graph Pad Prism 8, unpaired non-parametric t-test (Fig. 5.2) and one-way ANOVA with Tukey's multiple comparison test (Fig. 5.3).

5.3 Results

5.3.1 Axonal expression of ErbB4 in dopaminergic neurons

To explore the subcellular localization of ErbB4 protein in dopaminergic neurons, I cultured primary mesencephalic cells. Consistent with mRNA detection (Fig. 5.1A), ErbB4

receptor protein was found to be expressed in cultured DAT-positive primary midbrain neurons. Interestingly, in contrast to the somatodendritic pattern of ErbB4 immunoreactivity previously reported for GABAergic interneurons⁵⁸, ErbB4 in dopaminergic neurons was found not only on somata and dendrites but also on axonal projections co-labeled with ankyrinG and tau antibodies (n=9; Fig. 5.1.A). Importantly, immunoreactive puncta for ErbB4 were absent from cultured DAT-positive neurons from ErbB4-KO mice, showing the specificity of the antibody (n=10; Fig. 5.1B).

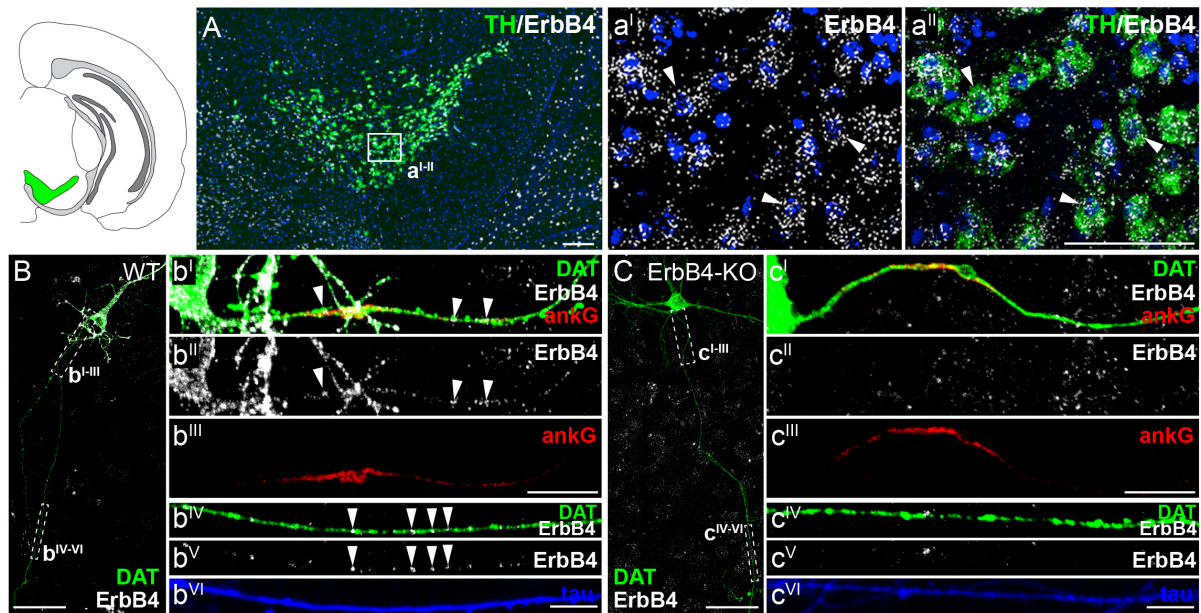


Figure 5.1 | ErbB4 mRNA and protein is expressed in soma and axons of midbrain dopaminergic neurons. (A) Double-fluorescence *in situ* hybridization (RNAscope) for ErbB4 (white) and TH (green) transcripts in midbrain coronal sections from wild-type C57BL/6J mice; anatomical region corresponds to area highlighted in green in the adjacent scheme. The boxed area in (A) is enlarged in the two panels on the right (*a'*-*a''*) to visualize the numerous dopamine (DA) neurons abundantly expressing ErbB4 transcripts (arrowheads); nuclei were labeled by DAPI (blue). Panel A was generated by Irina Karavanova. (B, C) Representative immunofluorescence images of dissociated primary midbrain neurons isolated from (B) wild-type C57BL/6J or (C) ErbB4-KO mice. (*b'*-*b''''*) Higher magnification of the area demarked in (B) show that ErbB4 receptor puncta (arrowheads) distribute on the cell soma and along DAT-positive axonal processes that are positive for the axon hillock marker Ankyrin G (ankG). (*b'*-*b''*) A second magnified area from the same neuron shows ErbB4 immunoreactive puncta along a more distal DAergic Tau-positive axonal process. The immunoreactivity for the receptor is specific, because the somatic (C) and axonal (*c'*-*c''*, *c'*-*c''*) puncta are absent from DAT-positive mesencephalic neurons isolated from ErbB4 KO mice. For panels (B) and (C), 9 DAT-positive neurons from C57BL/6J WT and 10 DAT-positive neurons from ErbB4-KO mice were analyzed in two independent cell culture preparations, respectively. Scale bars: 200µm in A, *a'*-*a''*, 100µm in B, C, 10µm in *b'*-*b''*, *c'*-*c''*.

In Skirzewski et al. (2018), we went on to show that ErbB4 present on axonal projections mediates rapid increases of extracellular dopamine after local NRG1 infusion into dopamine

target areas. NRG-induced dopamine accumulation was absent in mice lacking ErbB4 on dopamine neurons (Th-Cre; ErbB4^{fl/fl}), but not in mice where ErbB4 was ablated from PV interneurons (PV-Cre; ErbB4^{fl/fl}). Importantly, the development of dopamine terminals in general was not impaired in Th-Cre; ErbB4^{fl/fl} mice as potassium-induced depotentiation efficiently release dopamine. Increases in dopamine levels elicited by NRG stimulation can be due to an augmentation of dopamine release and/ or a reduction in dopamine clearance. Using fast-scan cyclic voltammetry, we found that NRG has no effect on electrically evoked dopamine release in the striatum. Uptake assays of [³H] in differentiated LUHMES (Lund Human Mesencephalic) cells³²⁹, however, suggested that NRG increases dopamine levels – at least partially – by attenuating dopamine re-uptake via DAT. Besides, basal dopamine levels are imbalanced in dopamine target areas of Th-Cre; ErbB4^{fl/fl}. Increased levels are detected in the mPFC and dorsal hippocampus, but hypodopaminergia in the striatum; reminiscent, but opposite to the dopamine imbalance in schizophrenia subjects¹⁹. Consistent with the hyperdopaminergic state in the mPFC and the hippocampus, Th-Cre; ErbB4^{fl/fl} mice showed deficits in spatial reference and working memory. Interestingly, behavioral deficits in mice that lack ErbB4 in dopaminergic (Th+ neurons) and PV interneurons are complementary and additive when compared to phenotypes observed in null ErbB4 mutants lacking ErbB4 from all cells²³⁴.

We then further followed up on how NRG/ErbB4 mediates reduced dopamine uptake through DAT. NRG/ErbB4 may alter the surface localization of DAT, as other channels and receptors endocytosed upon ErbB4 activation, some via direct interaction with ErbB4^{40, 46, 121}. However, immunoprecipitation experiments from rat striatal tissue, did not suggest an interaction between ErbB4 and DAT (Fig. 5.2.A), which was supported by the fact that ErbB4 and DAT puncta are rather exclusive than overlapping in immunocytochemistry (see Fig. 5.1). We also did not find any evidence for NRG-mediated DAT internalization addressed by surface biotinylation in HEK293 cells stably expressing DAT²³⁴ (D. Vullhorst *unpublished data*). And lastly, DAT protein levels were not altered in the dorsal striatum of ErbB4 KO mice (Fig. 5.2B). Taken together, this suggests that DAT regulation by ErbB4 is not mediated by a direct interaction and independent of alterations in DAT surface expression.

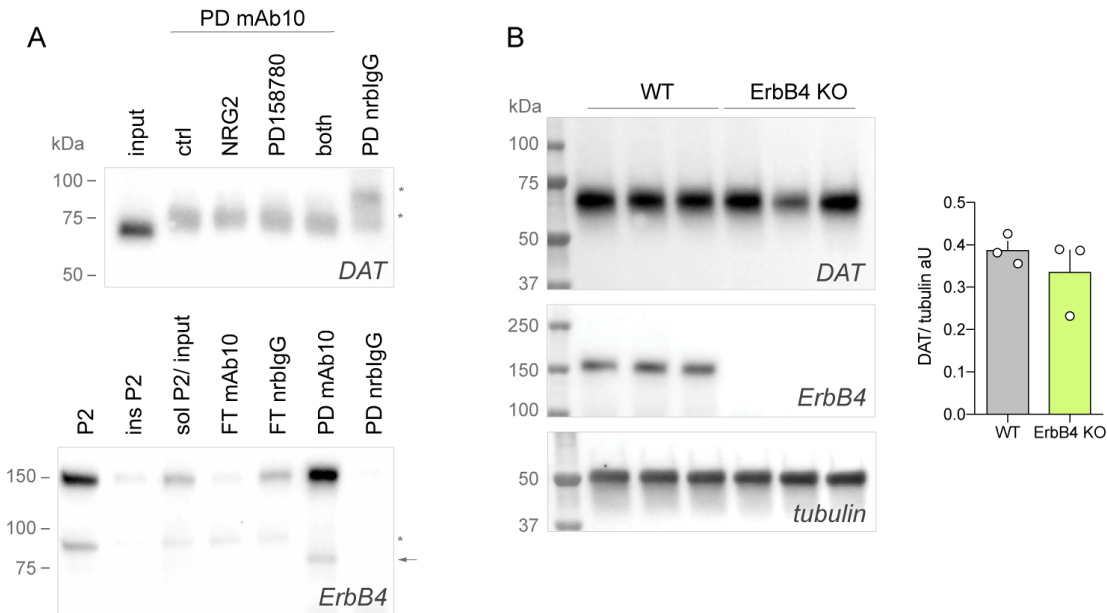


Figure 5.2 | *ErbB4* does not interact with *DAT*, and *DAT* expression is not altered in *ErbB4* knock-out (KO) mice.

(A) Immunoprecipitation of ErbB4 using monoclonal rabbit anti-ErbB4 antibody did not reveal an interaction with DAT (*upper panel*), although ErbB4 was successfully enriched in pull-down (PD) samples (*lower panel*). * – unspecific bands, arrow highlights 80kDa intracellular ErbB4 domain. (B) DAT protein is unaltered in ErbB4 KO mice in the dorsal striatum. Western blot signal (*left panel*) was quantified using densitometric quantification (*right panel*). DAT signal normalized to the house-keeping gene tubulin was not different between age-mapped WT (wild-type; *grey*) and ErbB4 KO mice (*green*; n=3, Mann-Whitney test, p>0.9999). Of note, ErbB4 KO sample #2 was dissected from a slightly more anterior region yielding in lower DAT expression. aU – arbitrary units, both – NRG2 & PD158780, ctrl – control, FT – flow-through, ins – insoluble in 1% Triton X-100, nrbIgG – normal rabbit IgG, sol – soluble, P2 – crude membrane pellet, PD – pull-down.

5.3.2 None of the ErbB4 isoforms targets to axons of GABAergic interneurons

As ErbB4 targets to axons of dopamine neurons, but not of GABAergic interneurons, I next assessed if the axonal targeting of the ErbB4 receptor is mediated by a particular isoform and analyzed the subcellular distribution of overexpressed ErbB4 isoforms in cultured GABAergic interneurons using immunocytochemistry. In accordance with previous reports⁵⁸, endogenous ErbB4 expression was confined to the somatodendritic compartment of PV interneurons in primary rat hippocampal cultures; and ErbB4 was not detected on axonal projections, identified by the AIS marker ankyrinG, and on PV+ boutons (Fig. 5.3A). On somas and dendrites of GABAergic interneurons, ErbB4 accumulated in surface clusters (puncta) that previously were characterized as excitatory post-synapses⁶⁶. To define the subcellular localization of each individual ErbB4 isoform, I overexpressed the four major ErbB4 isoforms

(JMa/Cyt-1, JMa/Cyt-2, JMb/Cyt-1 and JMb/Cyt-2) by viral induction. An antibody against ErbB4 (mAb6) that does not recognize the endogenous rat protein⁵⁸ (Fig. 5.3B) was used to visualize exogenous mouse ErbB4 receptor. In contrast to transfection approaches that resulted in neurotoxic expression levels of ErbB4 (data not shown), moderate overexpression was achieved by viral infection and resulted in distribution of ErbB4 similar to the endogenous protein (e.g. ErbB4 clusters on the cell surface), validating adequate expression levels. Interestingly, ErbB4 was restricted to a small fraction of neurons, some co-expressing the interneuronal marker PV, suggesting that transduced ErbB4 specifically accumulates in GABAergic interneurons.

Expression of ErbB4 was then further analyzed in PV interneurons, the main subclass of GABAergic interneurons expressing ErbB4⁶⁰. The receptor accumulated at higher levels when the two cleavage-resistant ErbB4 isoforms JMb/Cyt-1 (B1) and JMb/Cyt-2 (B2) were overexpressed compared to JMa/Cyt-1 (A1) and JMa/Cyt-2 (A2) ErbB4 receptors that are susceptible to metalloprotease-mediated cleavage (Fig. 5.3G; n=13-14 neurons/group, normalized mean fluorescent intensity: A1 0.62 ± 0.06 , A2 0.70 ± 0.08 , B1 1.17 ± 0.08 , B2 1.32 ± 0.17 ; Tukey's multiple comparisons test A1 vs. B1 $p=0.0047^{**}$, A1 vs. B2 $p=0.0001^{***}$, A2 vs. B1 $p=0.0282^*$, A2 vs. B2 $p=0.0011^{**}$). On the other hand, nuclear localization of the ICD of JMa receptors was not detected under these normal culture conditions.

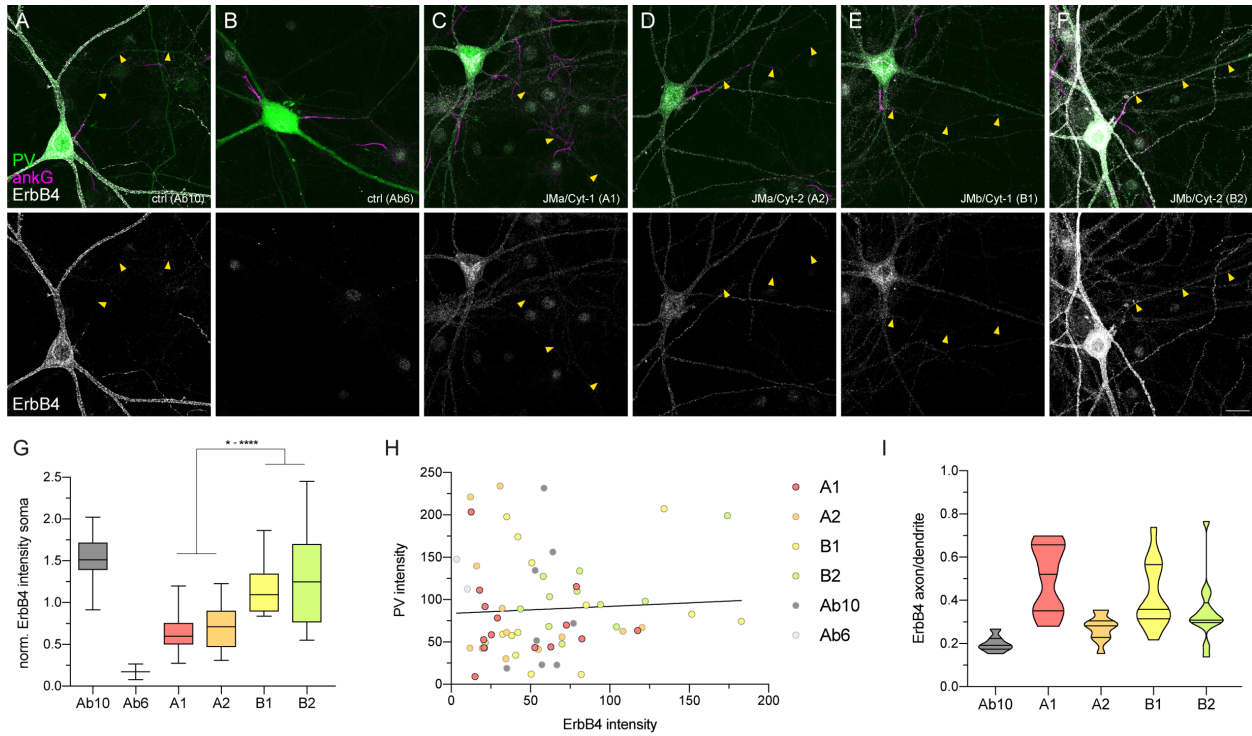


Figure 5.3 | Subcellular targeting of ErbB4 isoforms in hippocampal PV interneurons.

(A-F) Representative images of endogenous and exogenous ErbB4 expression in cultured rat hippocampal PV interneurons at DIV27 show absence in axonal projections (yellow arrowheads). (A) Endogenous expression was visualized with rabbit monoclonal antibody mAb10. (B) Rabbit monoclonal antibody mAb6 is blind to the endogenous rat protein⁵⁸, (C-F) but recognizes viral transduced mouse ErbB4. (G) Cleavage-resistant ErbB4 isoforms JMb/Cyt-1 (B1) and JMb/Cyt-2 (B2) are expressed at higher levels than cleavable isoforms JMa/Cyt-1 (A1) and JMa/Cyt-2 (A2) and in the soma of PV interneurons as assessed by normalized mean fluorescent intensity (n=2-8 control neurons/group, n=13-14 transduced neurons/group, N=3 independent cultures, one-way ANOVA, $F(5,57)=12.15$, $p<0.0001$ ****). (H) Somatic PV and ErbB4 intensity do not correlate ($R^2=0.0032$). (I) Subcellular distribution of ErbB4 isoforms in PV interneurons measured as fluorescent intensity ratio between axon and dendrite (n=7-14 neurons/group, N=3 cultures; one-way ANOVA, $F(4,53)=8.541$, $p<0.0001$ ****). Scale bar 20 μ m.

NRG/ErbB4 signaling was suggested to regulate the excitation and maturation of PV interneurons^{148, 149}. Expression of PV itself is activity-dependent and increases during maturation of the neuron³³⁰. Varying expression levels of PV and ErbB4 prompt me to test if the expression intensity of PV is regulated by the expression level of ErbB4. *In vitro* somatic PV intensity does however not correlate with the expression of ErbB4 (n=63 neurons, Fig. 5.3H). Importantly, regardless of the transduced isoform, subcellular localization of the ErbB4 was restricted to the soma and dendrites of PV interneurons (Fig. 5.3C-F). Only in a few cells, that expressed particularly high levels of transduced ErbB4, a few dim puncta were observed in the axon beyond the AIS (see Fig. 5.3F), but absent from distal parts of the axon and

presynaptic boutons. This is consistent with the observation that endogenous protein in some cases (36%) is found up to four cell diameters into the axon, but never more distal⁵⁸. The distribution of ErbB4 in neurites (ratio axon/dendrites) was similar to endogenous expression (Fig. 5.3I), albeit a bit increased due to higher background under overexpressing conditions and different antibodies used. Of note, fluorescent intensity analysis of ErbB4 in the axonal compartment was likely generally overestimated owing to background staining and overlap with other transduced neurons and dendrites. This probably also resulted in the varying and increased axonal/ dendritic ratios observed for the JMa/Cyt-1 isoform with low overall expression (see Fig. 5.3I), as immunofluorescent images do not show any axonal ErbB4 (Fig. 5.3C). In sum, none of the ErbB4 isoforms is targeted to axons when expressed at physiological levels. The analyses moreover did not reveal any substantial differences in subcellular distribution of ErbB4 isoforms in GABAergic PV interneurons. I therefore concluded that restriction of ErbB4 to the somatodendritic compartment in hippocampal GABAergic interneurons is independent of the isoform and that differences in distinct targeting of ErbB4 in GABAergic and dopaminergic neurons is rather due to divergent protein trafficking in these neuronal types than to the isoform expressed.

Lastly, I also intended to address the subcellular localization of ErbB4 isoforms in dopaminergic neurons by immunocytochemistry of transduced primary mesencephalic cultures of ErbB4 KO mice. However, I was confronted with technical difficulties, as the cultured dopaminergic neurons did not transduce well with the same ErbB4-expressing AAV 1 virus or the synthetic serotype AAV-DJ. With 3.9kb coding sequence, pAAV-hSynI-ErbB4 is at the packing limit of ~5kb of AAVs and I reasoned that the titer could be too low to successfully transduce dopaminergic neurons that represent only about 5% of cells in these mixed mesencephalic culture conditions while infecting efficiently GABAergic interneurons in hippocampal cultures (10-20% of cells). Therefore, I plan to revisit the transduction of ErbB4 in dopaminergic neurons using a high capacity AAV vector generated by Detlef Vullhorst in the laboratory. This pAAV-hSynI Gateway vector additionally lacks the β -globin intron and the polyadenylation signal of human growth hormone was replaced by the shorter corresponding signal from the human simplex virus thymidine kinase gene (HSV-TK) reducing the size to 899bp flanking sequence between the inverted terminal repeats (ITR) after Gateway recombination. To achieve higher titers, we also reached out to commercially produce

and purify these AAVs. Alternatively, it is also possible that ErbB4 overexpression is not tolerated well by dopamine neurons compared to GABAergic interneurons.

5.4 Discussion

In conclusion, I provided first-time evidence for the axonal localization of ErbB4 receptors in cultured dopaminergic neurons (Fig. 5.1). Axonal targeting in dopamine neurons is in stark contrast to the somatodendritic expression of ErbB4 on most GABAergic interneurons (Fig. 5.3). Moreover, none of the four ErbB4 isoforms when overexpressed is transported into axonal projections of cultured GABAergic. Taken together, I concluded that axonal targeting in different neuronal types is likely independent of the ErbB4 isoform, and rather due to differences in trafficking mechanisms between these neurons resulting in different localization of the same receptor.

Axonal transport has been mainly studied in hippocampal cultures due to the relative homogeneity, ease of overexpression and suitability for live-cell imaging. On the other hand, biochemical studies are frequently conducted in cortical cultures with higher cell densities³³¹. But only a few studies have addressed axonal transport in dopamine neurons^{332, 333} and the transport of dopamine-relevant cargos such as Parkinson's disease-causing α -synuclein are predominantly analyzed in other systems including hippocampal cultures³³⁴. Further, comparative studies addressing the transport of one cargo or protein in different cell culture systems have rarely been performed³³⁵. In general, polarized transport has been found to be cargo-specific³³⁶, and previously described to differ for protein isoforms^{39, 324, 325}. To my knowledge, trafficking of the same protein to different compartments in distinct neuronal cell types has not been reported yet. One study suggested that both GABA and glutamate can be similarly anterogradely transported in inhibitory and excitatory neurons³³⁵. Besides, the transport of synaptic vesicles depends on kinesin-3 (KIF1A, Unc104) in both *Caenorhabditis elegans* posterior deirid (PDE) dopamine neurons and in rat hippocampal culture³³⁷. Similar trafficking mechanisms for GABA and glutamate transporter are supported by the colocalization of vesicular GABA transporter (vGAT) and the two vesicular glutamate transporters vGLUT1/vGLUT2 in both excitatory and inhibitory synapses^{338, 339}. However, vGLUT2 and vesicular monoamine transporter 2 (VMAT2) target to different microdomains of rodent mesoaccumbens axons³⁴⁰.

If a protein is located to the axonal compartment is regulated at the AIS and the adjacent pre-axonal exclusion zone (PAEZ). The dense cytoskeleton in these areas limit lateral diffusion, vesicular carriers with axonal proteins interact with specific adaptors and microtubules, and freely pass this filter, whereas somatodendritic carriers are blocked^{331, 341}. In principle, the axonal localization of the same protein in one neuronal class but not in others, can be possibly attributed to two scenarios (1) a more stringent filter at the AIS/PAEZ in some neuronal cell types that restricts the protein to the somatodendritic compartment, and/or (2) the expression of specific transport proteins e.g. adaptor proteins or kinesins in only some neuronal cell types that allow for the axonal transport. While the first scenario is a rather passive retention from the axon, the second consists of active transport. In GABAergic neurons, in which ErbB4 was overexpressed to particularly high levels, a few dim ErbB4 puncta were observed beyond the AIS, but never in distal parts or presynaptic boutons. This suggests that the diffusion barrier at the AIS was saturated by the high expression levels and as a result ErbB4 receptor 'leaked' into the proximal axon but was not actively transported to more distal parts, portend to the second scenario. On the other hand, ErbB4 may be retained from the axons of GABAergic interneurons, but a more relaxed filter in long-projecting dopamine neurons allows the receptor to be transported into distal parts of the axon. However, this is purely speculative, and it will be interesting to see, if in the future comparative studies elucidate divergent and/or convergent trafficking mechanism of the same cargos in distinct neuronal cell types. If polarized transport differs between neuronal cell types is a very interesting but fundamental important question at the intersection between molecular biology and neuroscience that has been largely overlooked. Transport studies in dopamine neurons are particularly challenging as they only represent a fraction (<5%) of cells in primary mesencephalic cultures³⁴² and dopaminergic cell lines such as LUHMES cells do not specify neurites³²⁹.

While in GABAergic interneurons, none of the overexpressed ErbB4 isoforms located into axonal projections, it remains unclear if only a few or all ErbB4 isoforms are present in axonal projections of dopaminergic neurons. Preliminary experiments using multiplex fluorescent ISH, RNAscope, in primary dopaminergic neurons cultured in microfluidic chambers suggested that the protein and not the mRNA of ErbB4 is transported to the axon of dopaminergic neurons (L. Erben *unpublished data*). We are continuing to pursue the

overexpression of ErbB4 variants in primary mesencephalic cultures using commercially produced viruses. Of note, dopamine levels in target areas as well as cognitive function in Th-Cre; ErbB4^{fl/fl} was rescued by the viral overexpression of Cre-dependent ErbB4 JMb/Cyt-2 receptors injected into the midbrain²³⁴, suggesting that at least JMb/Cyt-2 receptors do localize to axonal projections and are able to regulate extracellular dopamine levels.

Lastly, it remains unresolved how ErbB4 modulates DAT activity to increase extracellular dopamine levels after NRG stimulation. While the DAT blocker GBR increases dopamine in the medium of LUHMES cell culture and occludes further NRG1-mediated increase, the uptake of DA is only attenuated about 20% by NRG1 stimulation²³⁴, suggesting that other mechanisms than the blockage of dopamine re-uptake are involved. Here, we could not present any evidence for a direct interaction between DAT and ErbB4 or NRG/ErbB4-mediated DAT endocytosis. Moreover, striatal DAT expression was unaltered in ErbB4 KO mice, suggesting that longer time scale transcription or translation of DAT are also independent of ErbB4. In contrast DAT was reported to be increased in the striatum, nucleus accumbens and cortex of transgenic mice expressing a dominant-negative ErbB4 variant in oligodendrocytes¹⁸⁰. These discrepancies may arise as dominant negative ErbB4 may also interfere with ErbB3 and ErbB2 signaling. Besides, DAT mediating the reuptake of dopamine, DAT independently mediates DA release. DA efflux via DAT can be elicited Ca²⁺-independent by NMDA and triggered by G_q-protein coupled receptors. Both pathways activate protein kinase C (PKC) that has been shown to phosphorylate DAT, activating outward flux and inhibiting at the same time inward flux³⁴³. PKC is downstream to ErbB4 receptor^{36, 45}. On the other hand, Gβγ subunits have been shown to inhibit DAT activity³⁴⁴ and amphetamine-induced DA efflux depends on Ca²⁺/calmodulin-dependent protein kinase-II (CaMKII)³⁴³. Although surface localization of DAT is unchanged after NRG stimulation, the transporter may be redistributed on the surface by NRG/ErbB4. DAT has been shown previously to be recruited to PKC-rich lipid drafts which could affect efflux³⁴⁵. Therefore, NRG/ErbB4 signaling besides attenuating dopamine uptake via DAT, could at the same time also regulate DAT-mediated dopamine efflux. Further studies will be necessary to clarify this hypothesis and signaling mechanisms.

6

Neurodevelopmental, neurochemical and behavioral analyses of isoform-specific ErbB4 Cyt-1 mutant mice

This chapter presents an extended version of a manuscript currently in preparation: Larissa Erben, Marie Cronin, Ricardo Murphy, Miguel Skirzewski, Irina Karavanova, Detlef Vullhorst, Steven Carroll & Andres Buonanno (in preparation). Added sections are emphasized in dark grey italics.

Authors contributions: L.E., M.S. & A.B. designed research, I.K., D.V., S.C. & A.B. designed & generated mutant mouse, L.E., M.C., R.M. & M.S. performed research, L.E., M.C. & M.S. analyzed the data, L.E. wrote the manuscript.

6.1 Abstract

The Neuregulins and their cognate neuronal tyrosine kinase receptor ErbB4 are associated with schizophrenia and the expression of the four ErbB4 splice variants is altered in postmortem brains of schizophrenia patients. Although ErbB4 mutant mice display a vast variety of phenotypes, including altered GABAergic migration, dopamine imbalances and impairments in behavioral tasks with relevance to schizophrenia, the contribution and function of individual ErbB4 splice variants in the central nervous system remains completely elusive. Here, we generated splice variant-specific mutant mice that lack the Cyt-1 exon, one of two cytoplasmic ErbB4 splice variants. Cyt-1 is increased in schizophrenia and encodes a receptor uniquely able to activate PI3K/Akt pathways over Cyt-2 ErbB4 receptors. Loss of Cyt-1 during development did not affect GABAergic interneuron development or show deficits in locomotor activity, anxiety, sensorimotor gating or cognitive behaviors. However, extracellular dopamine in the medial prefrontal cortex are increased in heterozygote Cyt-1 mutants that also exhibit

mild phenotypes. Taken together, we conclude that ErbB4 Cyt-1 receptor is largely dispensable for CNS development and function *in vivo*.

6.2 Introduction

The psychiatric disorder schizophrenia affects about 1% of the population and is characterized by positive (hallucinations, delusions), negative (social withdrawal, lack of motivation) and cognitive (attention and working memory deficits) symptoms. However, the pathophysiology of this heterogenous disease remains poorly understood despite the identification of many genetic risk factors^{3, 7}. The neurotrophic factors Neuregulins (NRGs) and their cognate neuronal tyrosine kinase receptor ErbB4 are genetically linked to schizophrenia and its endophenotypes^{4, 27, 28, 30, 31}. Remarkably, mice with mutations in NRG1, NRG2, NRG3 or ErbB4 exhibit schizophrenia-related behavioral phenotypes including hyperactivity, sensorimotor gating deficits, reduced anxiety, cognitive and social impairments^{61, 132, 135, 142, 165}. NRG/ErbB4 signaling is best characterized in the cortex and hippocampus, where ErbB4 expression is confined to GABAergic interneurons^{58, 60}. Among others, NRG/Erb4 regulates interneuron migration and allocation^{79, 81} and as a consequence, GABAergic interneurons are reduced in the cortex and hippocampus of ErbB4 mutant mice^{63, 79}. NRG/ErbB4 also regulates glutamatergic and GABAergic synapse development and neurotransmission^{60, 68, 70, 117, 123} and modulates synaptic plasticity^{65, 124, 137, 175}, critical period plasticity^{148, 149} and network activity^{83, 322, 346}. Moreover, ErbB4 is also expressed on dopaminergic neurons^{50, 53} and recently has been shown to play an important role in regulating dopamine homeostasis and cognitive function^{138, 234}. Interestingly, conditional ErbB4 mutant mice that lack ErbB4 in tyrosine hydroxylase-expressing neurons including dopaminergic neurons (Th-Cre; ErbB4^{fl/fl}) exhibit an imbalance of basal extracellular dopamine levels in distinct projection areas²³⁴, reminiscent of the described hyperdopaminergic state in dorsal striatum but hypodopaminergic state in the prefrontal cortex of patients^{19, 184}.

Four ErbB4 isoforms are generated by alternative splicing of single exons at two loci. At the juxtamembrane (JM), JM_a and JM_b variants arise by the inclusion of exon 16b and 16a, respectively, and regulate the receptor's susceptibility to metalloprotease- and subsequent γ -protease-mediated cleavage and therefore its transcriptional potential^{147, 48, 190, 194, 203}. In the cytoplasmic (Cyt) region of the receptor, inclusion or omission of the 48bp exon 26, generates

Cyt-1 and Cyt-2 variants, respectively¹⁹¹. The additional 16 amino acid-sequence in the Cyt-1 ErbB4 receptor encodes both a binding domain for phosphatidylinositol-3-kinase (PI3K) and a recognition motif for WW domain proteins (PPXY)^{191, 202}. As a result, Cyt-1-containing ErbB4 receptors can directly stimulate PI3K and Akt phosphorylation^{191, 212}, whereas Cyt-2 ErbB4 receptors rely on the heterodimerization with ErbB3 to activate PI3K²⁰⁶. The presence of a third WW domain binding motif in the Cyt-1 ErbB4 receptor implies a stronger coupling of a subset of WW domain proteins such as ubiquitin ligases which render Cyt-1 ErbB4 less stable compared to Cyt-2 ErbB4 receptors²⁰⁷⁻²¹⁰.

Both convergent and divergent functions have been described for the cytoplasmic ErbB4 isoforms Cyt-1 and Cyt-2^{211, 212}. In heterologous and non-neuronal cell cultures isoform-specific functions were described in survival and apoptosis, chemotaxis, mobility and migration, proliferation, growth and differentiation, ubiquitination and degradation, endocytosis and subcellular localization, as well as phosphorylation and kinase activity (reviewed in²¹³). Moreover, proliferation, progression and prognostics of different cancer types depend on the ErbB4 Cyt isoform expressed (e.g. mammary gland cancer³⁴⁷⁻³⁴⁹, ovarian adenocarcinoma³⁵⁰, medulloblastoma²¹⁵, colorectal cancer³⁵¹, bladder cancer³⁵², malignant melanoma³⁵³). In the central nervous system (CNS), Cyt-2 is the predominant ErbB4 isoform in most brain areas^{192, 213, 218}. However, few studies have addressed the different roles and contributions of ErbB4 isoforms to the characterized modulations by ErbB4 and phenotypes observed in ErbB4 mutant mice. In cultured neuronal progenitors, isoform-specific migratory activity has been described^{206, 220, 354}, in PC12 (adrenal gland pheochromocytoma) cells, proliferation and neurite outgrowth is promoted by Cyt-1 and Cyt-2 ErbB4, respectively²¹³ and ErbB4/PI3K signaling was proposed to control interneuron migration *in vivo*²²¹. Interestingly, in the postmortem dorsolateral prefrontal cortex (DLPFC) of schizophrenia patients, ErbB4 Cyt-1 variants and the downstream target PI3KCD are increased compared to healthy controls^{28, 218, 222-224}. Moreover, inhibition of PI3K, improves amphetamine-induced hyperlocomotion and sensorimotor gating in a rat schizophrenia model²²⁴.

ErbB4 Cyt-1 variants constitute about 40% of ErbB4 receptor in the adult brain and are increased in postmortem brains of schizophrenia. However, how ErbB4 Cyt-1 receptors are contributing to ErbB4 receptor functions in the CNS and which are its implications in the pathophysiology of schizophrenia, remains completely elusive. In order to better understand

the role of ErbB4 Cyt-1 receptors in the brain, we generated ErbB4 Cyt-1 mutant mice by site-specific recombination to remove the Cyt-1 cassette (exon 26) and subjected these mice to an extensive evaluation of developmental, neurochemical, behavioral and expression studies.

6.3 Methods

Animals & generation of Cyt-1 KOs. Mice were kept on a 12-12h light-dark schedule with access to food and water *ad libitum*. All studies were conducted in female and male mice. Animals were handled in accordance with the NIH Animal Welfare guidelines and all animal procedures were approved by the NIH Animal Care and Use Committee. The Cyt-1 targeting construct, harboring loxP sites flanking ErbB4 exon 26, was generated by “recombineering” using vector pL253³⁵⁵ (Fig. 6.1A). Site-specific recombination of the *erbb4* locus and generation of conditional Cyt-1 mutant mice was performed at the Transgenic & Genetically Engineered Models Core of the University of Alabama at Birmingham. Successfully targeted and PCR-validated embryonic stem (ES) cells derived from C57BL/6J mice were injected into blastocysts from albino C57BL/6J mice (JAX stock # 000058). Chimeric offspring was bred with albino C57BL/6J mice; only black F1 mice were used for further breeding. Mice were then crossed to FLP deleter strain B6;SJL-Tg(ACTFLPe)9205Dym/J (JAX stock # 003800) to remove the FRT site-flanked neomycin cassette used for ES cell selection. Null (germline) Cyt-1 mutant mice, hereafter referred as Cyt-1 mutant mice, were generated by crossing floxed Cyt-1 mice to mice expressing Cre recombinase under the control of ubiquitously active EIIa promoter (also on C57BL/6 background; JAX stock # 003724). Heterozygous Cyt-1 knockout mice were used for breeding and yielded normal litter sizes ($6.4 \text{ pups} \pm 0.11$, N=2 cohorts, n=648 mice; compared to C57BL/6J $6.2 \pm 0.2 \text{ pups}$ ³⁵⁶), balanced sexes ($52.9 \pm 1.29\%$ males, N=2 cohorts, n=648 mice), and Mendelian genotype frequencies ($24.5 \pm 0.03\%$ +/+, $50.3 \pm 1.47\%$, $25.1 \pm 1.44\%$, N=2 cohorts, n=648 mice). Routine genotyping was performed by PCR using forward primers 5'-AGTTTCCTTATTCCTAGCTCTCC-3' and 5'-TGTCTTAGATGTCTGTAACCTGG-3' and reverse primer 5'-GATGATCCAGCAATGCTACCCTC-3' at 60°C annealing for 20s and 72°C elongation for 10s. Primer binding sites are schematically illustrated in Fig. 6.1A and representative genotyping results are shown in Fig. 6.1B. Cyt-1 mutant mice were crossed to GAD67-GFP mice (kindly provided by Dr. Yuchio Yanagawa; Gunma University, Japan) to analyze

GABAergic interneuron density by immunohistochemistry in GFP+/- animals (denominated as Cyt-1 KO; GAD-GFP mice, see below). Adult wild-type C57BL/6J mice were purchased from the Jackson laboratories *and bred overnight to obtain timed pregnancy*.

Isoform-specific in situ hybridization (ISH). Exon-specific ISH (BaseScope version 1 & 2; Advanced Cell Diagnostics) was performed on serial 8µm-thick coronal formalin-fixed paraffin-embedded sections of eight-to-eleven-week-old adult mice (C57BL/6J or Cyt-1 homozygote/ heterozygote mutants and control littermates; both sexes) *and E14.5 C57BL/6J embryos (sex undetermined)* according to the vendor's protocol and as previously described^{192, 357}. Custom-made ErbB4 Cyt-1 and Cyt-2 probes are targeting exon junctions 25/26 (5'-CATCTACACATCCAGAACAAGAATTGACTCCAATAGG/AGTGAAATTGGAC-3') and 25/27 (5'-CCATCTACACATCCAGAACAAGAATTGACTCCAATAGG/AATCAGTTTGT-3') of ErbB4 transcripts, respectively. Briefly, paraffin sections were deparaffinized with xylene and pretreated with hydrogen peroxide (10min at RT), antigen retrieval (15min at 100°C) and proteases (protease III, 30min at 40°C). Probes were incubated for 2h at 40°C, signal was chemically amplified with 7/8 amplification steps (BaseScope version 1/2) and subsequently detected using alkaline phosphatase and FastRED dye. For post-hoc immunostaining sections were immediately subjected to antibody staining with rat anti-dopamine transporter (DAT) antibody (clone 6-5G10; Santa Cruz; sc-32258; 1:200) and secondary donkey-anti-rat-Alexa488 (1:1000, Invitrogen, Thermo Fisher) as described in detail in³⁵⁷ using standard immunofluorescence histochemistry (IHC) protocol (see below).

Immunofluorescence histochemistry (IHC). Immunostaining of 50µm-thick free-floating sections of postnatal day 30 (P30) Cyt-1 KO; GAD-GFP and heterozygote/control littermates (n=4, both sexes) was performed as previously described³⁹. Briefly, mice were transcardially perfused with 4% paraformaldehyde (PFA) in 0.1M PBS, pH 7.4. Dissected brains were post-fixed overnight in the same fixative at 4°C and 50µm-thick sequential sections cut on a vibratome. Sections were blocked in 10% normal donkey serum, 0.3% Triton X-100 in 0.1M PBS for 1h at RT and incubated with primary antibodies in blocking solution overnight at 4°C. Following three 10-min washes in 0.1M PBS with 0.25% Triton X-100, secondary antibodies were incubated in blocking buffer for 2h at RT. Samples were extensively washed with 0.1M

PBS, counterstained with DAPI and mounted with Mowiol-DABCO. As primary antibodies rat monoclonal anti-GFP (clone GF090R, Nacalai Tesque, Japan; 1:2000) and and visualized with donkey secondary antibodies (Invitrogen, Thermo Fisher & Jackson Immuno Research). For GABAergic interneuron densities, bilateral cortical analyses were performed at the three different bregma levels ($\sim+0.26$, -0.46 , -1.22), and bilateral hippocampal analyses at four different bregma levels (~-1.22 , -1.82 , -2.46 , -3.08). Damaged sections were excluded from analysis.

Image analysis. FastRED ISH signal were analyzed fluorescently at 20x magnification using Zeiss LSM710/800 confocal microscopes. Unbiased automated quantitative analysis of maximum intense projections obtained from Z-stack images was performed using CellProfiler²²⁷ as previously described¹⁹² and explained in detail in³⁵⁷. For ISH-IHC analyses (Fig. 6.5D,E) $>30\%$ overlap of the cell with DAT staining was defined as positive dopaminergic neuron. Similarly, IHC in GAD-GFP mice was analyzed using 10x magnification at a Zeiss LSM800 confocal microscope. Density of GABAergic interneurons was analyzed from maximum intense projections using a custom-made CellProfiler pipeline identifying GAD-GFP+ cells (size $>25/50\mu\text{m}^2$ SSCtx/Hpp, threshold= $1.5 \times$ median background intensity) and filtering by eccentricity (>0.94). Hippocampal subregions and cortical layers were defined based on morphology, DAPI stain and interneuron density. Injection sites in floxed Cyt-1 mutant mice were evaluated using 10x magnification using Zeiss LSM 710. In all analyses, analyzed areas were not different between transcripts and/or genotype or group.

Quantitative reverse-transcription PCR (qPCR). Real-time qPCR using TaqMan probes was performed as previously described¹⁹². Briefly, RNA was isolated from whole brain of ten-week-old Cyt-1 KO mice, and their heterozygote and control littermates ($n=3/\text{genotype}$; both male and female), from microdissected embryonic/perinatal/postnatal pallial/cortical and subpallial/striatal tissue (C57BL/6J; $n=3-4/\text{time-point}$; both male and female, sex undetermined until P10) and from micro-dissected mesencephalic tissue of three-month old floxed Cyt-1 mice injected with AAV (see below; $n=3/\text{group}$; both male and female) using TRI Reagent (Thermo Fisher). cDNA was synthesized from $1\mu\text{g}$ RNA (500ng RNA only for samples used in RNA sequencing, see below) using SuperScript IV Reverse Transcriptase (Thermo Fisher) and random hexamers for 20min at 55°C . Gene expression was subsequently

assessed using TaqMan universal PCR Master Mix (Thermo Fisher), 0.25 μ M FAM/VIC-labeled TaqMan probes, and 0.9 μ M corresponding primers from 2.5-5ng cDNA in a total volume of 10 μ l. Cycling was performed in 384-well plates using a QuantStudio 6 Thermocycler (Thermo Fisher) and the following parameter: 2min at 50°C and 10min at 92°C, followed by 40 cycles of 15s at 95°C, 1min at 65°C (for Cyt probes) or 60°C (for all other probes). Custom-made isoform-specific ErbB4 TaqMan probes (Thermo Fisher) were FAM-ATGGACGGGCCATTCCACTTTACCA-MGB for JMa, FAM-TTCAAGCATTGAAGACTGCATCGGCCTGAC-MGB for JMb, FAM-TGAAATTGGACACAGCCCTCCTCCTG-MGB for Cyt-1 and FAM-AATTGACTCCAATAGGAATCAGTTTGTGTACCAAGAT-MGB for Cyt-2. Flanking primers used were 5'-CCACCCTTGCCATCCAAA-3' and 5'-CCAATGACTCCGGCTGCAATCA-3' for JM isoforms, and 5'-CAACATACCTCCTCCCATCTACAC-3' and 5'-GCATTCCTTGTGTGTAGCAAA-3' for Cyt isoforms. ErbB3 (Thermo Fisher, Mm01159999_m1) and ErbB4 (Thermo Fisher, Mm01256793_m1) TaqMan probes are catalog probes and standard TaqMan assays (all Thermo Fisher) for Nkx2.1 (Mm00447558_m1), Nr2f2 (Mm00772789_m1), Slc5a7 (Mm00452075_m1), Rin1 (Mm00455104_m1), Dbh (Mm00460472_m1), Dlx6 (Mm01166201_m1), Slc17a7 (Mm00812886_m1), Foxg1 (Mm02059886_s1), Ngb (Mm00452101_m1) and Vip (Mm00660234_m1) were analyzed to confirm differential expressed genes identified in the RNA sequencing study. Normalization was done in all cases using a VIC-labeled TaqMan probe for GAPDH (Thermo Fisher, Mm9999915_g1). Standard curves (10ag–1ng) of cloned DNA for ErbB4 JMa/Cyt-1 and JMb/Cyt-2 and of synthesized DNA fragments for ErbB3, confirmed linearity and showed similar efficiency for isoform-specific assays. Assay specificity was tested using 100pg DNA of non-matching ErbB4 isoforms or ErbB receptor.

RNA sequencing. For RNA sequencing and post-hoc qPCR analysis, RNA was isolated from dorsal hippocampal (Hpp) and the ventral tegmental area (VTA) micropunches (bilateral ~1 μ g per animal) from 10-week old Cyt-1 mutant mice, heterozygote and control littermates of both sexes. Three samples of both sexes were pooled prior to RNA isolation using TRI Reagent (Thermo Fisher) and purification with RNeasy Micro Kit (Qiagen). RNA yield varied between 1.3-4.9 μ g and RNA integrity measured using Agilent RNA 6000 Nano Kit (Agilent

Technologies) ranged between 8.7 and 9.1. RNA sequencing library was constructed from 1µg total RNA using TruSeq Standard mRNA Library Preparation kit (Illumina) with polyA-enrichment. Each library was barcoded; equal amounts were combined and sequenced on an Illumina HiSeq 2500 system (Illumina) yielding an average of 38.2 million paired-end reads (2x100b) per sample. Reads were aligned to the mouse genome (GENCODE mouse release 16) using RNA-STAR (version 2.6.1; ²³⁷). Sample gene expression was quantitated using subread featureCounts (version 1.6.3) against GENCODE mouse release 16 with the following options (-O, -M, -g, gene_name; ²³⁸) and differential expression was tested across defined conditions using DESeq2 (v1.16.1; ³⁵⁸). Gene ontology analysis was done using gProfiler³⁵⁹ and splice variant analyses performed in the Integrative Genomics Viewer²³⁹ with the Sashimi plot function. Expression of genes identified as differentially expressed (adjusted p<0.05) was analyzed by TaqMan qPCR (see above). Three pooled samples were analyzed by RNA sequencing, four pooled samples by TaqMan qPCR.

Dopamine (DA) measurements. Measurements of basal extracellular DA levels in the medial prefrontal cortex (mPFC) of freely moving mice (n=6-7/genotype, both sexes, 2.5-4 months old) were performed by no-net flux (NNF) microdialysis approach as previously described ³⁶⁰. Briefly, counterbalanced unilateral stainless-steel guide shafts (21-gauge, 6mm-long) were chronically implanted into the mPFC (AP: 2.0mm, L:0.3mm, V:0.3 mm with respect to bregma, midsagittal sinus and brain surface³⁶¹). After one-week post-operative recovery, mice underwent NNF procedure by lowering a laboratory-made microdialysis probe through the implanted guide shaft as previously described ³⁶². The tip of the microdialysis probe consisted in a 2mm-long cellulose hollow fiber (18kDA MWCO, SpectrumLabs Inc) protruding from the tip of the guide shaft. Artificial cerebrospinal fluid (aCSF; 136mM NaCl, 3.7mM KCl, 2.2mM CaCl₂, 1mM MgCl₂, and 10mM NaHCO₃ at pH 7.4) was continuously perfused through the microdialysis probe at a flow rate of 1µl/min during 2 hours before sample collection. Five different DA standard concentrations (0, 0.5, 1.0, 1.5, and 2.0nM) were randomly perfused through the microdialysis probe during 60min and duplicate samples of 30min each standard were collected in 10µl of 100mM HCl + 1mM EDTA to prevent catecholamine degradation. Samples were immediately frozen and stored at -80°C until posterior analysis no further than a week. Probe placements were verified by Nissl staining in 50µm thick vibratome sections (Fig. 6.6G) and animals with misplaced probes excluded from

analysis. An autosampler (high performance liquid chromatography (HPLC) autosampler INSIGHT, Eicom) injected DA standards and samples into an isocratic HPLC system coupled to amperometric detection as described by the manufacturer (HTEC-510, Eicom). A regression curve was built up per genotype by subtracting the area under the curve of the corresponding standard (IN) minus the area under the curve of the dialysate sample (OUT) at this particular concentration of DA standard. The equation of each regression curve allowed us to estimate the NNF DA concentration for each animal ($y=0$).

Battery of behavior tests. Behavioral testing of adult Cyt-1 mutant mice (3-7 months old; both sexes) was conducted in the following sequence: open field, elevated plus maze, prepulse inhibition and separately Y-maze, followed by Barnes maze testing. Different cohorts were tested and behaved similarly. Behavioral testing was performed during the light period of the day and all apparatuses were cleaned with 70% ethanol between trials. Tracking in the open field, elevated plus maze, Y-maze, and Barnes maze was conducted with ANY-maze software. The experimenter was blind to the genotypes.

Open Field: Locomotor activity was tested in an open field assay (white chamber, 40cm x 40cm x 30cm, center defined as 28cm x 28cm, 70-80lux in the perimeter, 80-90lux in the center). Mice (n=12-14/genotype) were habituated to the testing environment for 30min prior to testing. Mice were permitted to freely explore the maze for 30min. Center time and traveled distance were analyzed.

Elevated plus maze: The elevated plus maze test for anxiety-like behavior was tested in a plus-shaped white plastic apparatus (30cm x 5cm arms) consisting of two closed arms (18cm-high black walls, 60-70lux) and two open arms (130-140lux) which stood 40cm above the ground. Cyt-1 mutant mice and heterozygote and control littermates (n=11-14/genotype) were habituated for 30min to the room. Mice were permitted to explore the maze for 5min and time spent in the open and closed arms was analyzed.

Prepulse inhibition (PPI): Startle response and prepulse inhibition testing was conducted using a standard startle response system (SR-LAB). Cyt-1 mutant mice (n=17-18/genotype) were acclimated to a 65dB background noise in the plexiglas tube of the testing chamber for 5min on three consecutive days. Startle response in arbitrary units was determined by pseudo-random presentations of tones ranging from 70 to 120db, in 5db increments (5 tones each) and

normalized to the average of 120db pulses of the cohort. During PPI testing on the following day, the animals were presented with a pseudorandom sequence of 20ms prepulse tones (PP; 66, 70, 74, 78dB; 12 times each) and 40ms 120dB pulse pairings with variable inter-trial interval between 5 to 20s. A 120db no prepulse (NPP) presented 28 times was used to calculate percentage of prepulse inhibition of startle response as $(\text{average startle to NPP} - (\text{average startle to PP}) / \text{average startle to NPP}) * 100$.

Y-maze: Working memory of Cyt-1 mutant mice (n=12-14/genotype) was tested in a Y-Maze apparatus (30cm x 18cm x 9.5cm three-arm maze with opaque tan walls, 50lux). Mice were habituated for 30min to the testing environment and then permitted to explore the maze for 5min. Novel arm entries were identified manually as entries into the third arm different from the current and previously explored arm and percentage of alternation was calculated.

Barnes maze: Barnes maze spatial learning and memory test was conducted as previously described²³⁴. The edge of the round elevated apparatus (Stoelting, 90cm diameter, 800lux, 90cm above ground) is marked by 20 open holes (~10cm diameter) with a hidden escape chamber placed underneath of one of the holes (target, 0) and the rest of the holes were labeled as +1 to +10, and -1 to -9. The edges of the maze were covered with a wall providing spatial cues and 85db background white noise was played during all phases of the test. The conducted Barnes Maze consisted of three phases: training, probe test, and new escape test. During the training, mice (n=8-11/genotype) were allowed to explore the maze. The trail ended when the animal entered the escape chamber, the noise switched off automatically and aversive light was blocked. The mouse was held in the chamber for 1min. Mice that could not locate the chamber within 3min were manually guided to the escape hole. Training was conducted over four days (4 trials per day). Mice that failed to escape the maze in more than one trial on the fourth day of training were excluded from analysis. On the fifth day, the escape chamber was removed, and mice were tested for 90 s (probe test). Latency to escape and time in the correct zone were recorded in ANY-maze, target hole nose pokes and errors defined as non-target nose pokes were quantified by hand-scoring of collected videos. 48h after the probe test, mice were re-introduced to the testing apparatus in which the escape chamber has been moved from its original position to hole +8 (new target test). Mice were permitted to explore the maze until they located the new escape for up to 3min, at which point they were guided to the new escape

(see learning phase). Four subsequent trials were performed and latency to escape and errors were quantified as described above.

Progressive Ratio: A progressive ratio task was used to test mice ($n=11-16$) for their motivation and willingness to work for palatable food rewards³⁶³. Mice were kept at 85% free-feeding body weight and conditioning performed in sound-attenuated operant chambers (ENV-300; Med Associates). Briefly, chambers were equipped with two nose-poke apertures on either side of the reward magazine dispensing palatable pellets (14mg dustless precision pellets, Bioserv), a house light that turned on (5s) during reward delivery, and a fan that provided white noise and ventilation during the experiment. One nose-poke aperture was set as active and the other as inactive, with the locations counterbalanced across animals. Nose poking in the active aperture resulted in the delivery of one reward pellet, while responses in the inactive port were recorded but had no consequence. Prior to the start of conditioning, mice were habituated to retrieve rewards delivered at variable interval schedule (range 5-100s) for 30min and nose poke responses had no consequence. Then, mice were trained in a fixed ratio 1 (FR1) schedule of reinforcement where each nose poke in the active aperture resulted in the delivery of one reward. We considered mice to have reached a stable performance when thirty food pellets were collected under a 30min-long session during three consecutive days. Then, mice were progressively transferred to FR3 (three responses in active aperture – one reward) and FR5 (five responses in active aperture – one reward) schedules following the same criteria performance as FR1. Finally, a progressive ratio 7 (PR7) schedule was used to test for motivation to work for rewards. PR7 schedule consisted in record the total number of rewards collected (breaking point) and number of nose pokes in the active/inactive holes in a 3h-long test or until 60min of inactivity occurred (no recorded nose-poke), where the number of nose pokes in the active aperture to obtain a reward progressively increased by 7 (7, 14, 21, 28, 35, etc.) with each subsequent pellet delivered.

Locomotor activity in homecage: Mice ($n=5-8$) were independently located in a home cage (19.4cm x 18.1cm x 39.8cm) with regular bedding, free access to food and water, and regular 12h light/dark schedule for 96 hours. To continuously record their horizontal locomotor activity, each home cage with one single mouse was placed in a square frame with infrared beams (43cm x 43cm; Columbus Instruments).

Experimental Design & Statistical Analyses. All data represent the mean \pm SEM and statistical significance was set at $p < 0.05$. Outliers (ROUT, $Q=1\%$) were excluded from data analyses. Statistical analyses were performed using one-way ANOVA and Tukey's multiple comparisons test (Fig. 6.1D-H; Fig. 6.4G,H, Fig. 6.6F, Fig. 6.7A,D,E, Fig. 6.8D), Mann-Whitney test for comparison of two groups only (Fig. 5.2E,F, Fig. 6.6C,E, Fig. 6.8C) and two-way ANOVA and Tukey's multiple comparison test for comparisons of multiple variables (Fig. 6.4I-L, Fig. 6.5A-C, Fig. 6.7B,C,F,G, Fig. 6.8E) in Graph Pad Prism 8.

6.4 Results

6.4.1 Generation of Cyt-1 mutant mice

The lack of knowledge about ErbB4 Cyt-1 *in vivo* function prompt us to generate Cyt-1 knockout mice that specifically lack the Cyt-1 exon (exon 26) (see Materials & Methods, Fig. 6.1A). Successful ablation of Cyt-1 and flanking genomic sequence was confirmed by PCR from genomic DNA (Fig. 6.1B). Cyt-1-containing ErbB4 transcripts were absent in the brain as shown by exon-specific *in situ* hybridization¹⁹² (ISH; BaseScope; Fig. 6.1C,D, % Cyt-1, $+/+$ $28.63 \pm 0.98\%$, $+/-$ $18.9 \pm 2.86\%$ $-/-$ $2.36 \pm 0.44\%$), TaqMan quantitative PCR (Fig. 6.1E, % Cyt-1, $+/+$ $38.66 \pm 2.11\%$, $+/-$ $20.712 \pm 1.42\%$, $-/-$ $0.00 \pm 0.00\%$; $n=3$, one-way ANOVA $F(2,6)=174.4$, $****p < 0.0001$) and RNA sequencing analyses (data not shown). Interestingly, Cyt-1 transcript levels were reduced to approximately half in heterozygote littermates compared to control littermates (Fig. 6.1D,E), suggesting that each ErbB4 allele contributes equally to ErbB4 expression. Moreover, as expected, all ErbB4 transcripts were 'forced' to splice as Cyt-2 transcripts in Cyt-1 mutant mice. Cyt-2 transcripts were augmented (% Cyt-2/GAPDH, $+/+$ $0.46 \pm 0.004\%$, $+/-$ $0.52 \pm 0.010\%$, $-/-$ $0.62 \pm 0.031\%$; $n=3$, one-way ANOVA, $F(2,6)=18.13$, $p=0.0029$), as total ErbB4 expression remained unchanged (Fig. 6.1G; % ErbB4/GAPDH, $+/+$ $2.85 \pm 0.09\%$, $+/-$ $2.90 \pm 0.08\%$, $-/-$ $2.82 \pm 0.05\%$; $n=3$, one-way ANOVA, $F(2,6)=0.2687$, $p=0.7731$). Splicing at the second alternative splice site in the JM also was largely unaffected by the loss of Cyt-1 (Fig. 6.1F, % JMa, $+/+$ $18.16 \pm 0.70\%$, $+/-$ $18.97 \pm 0.52\%$, $-/-$ $21.27 \pm 0.78\%$; $n=3$, one-way ANOVA $F(2,6)=5.725$, $*p=0.0407$), providing for the first time evidence that splicing of ErbB4 at the two loci (JM and Cyt) is regulated independently.

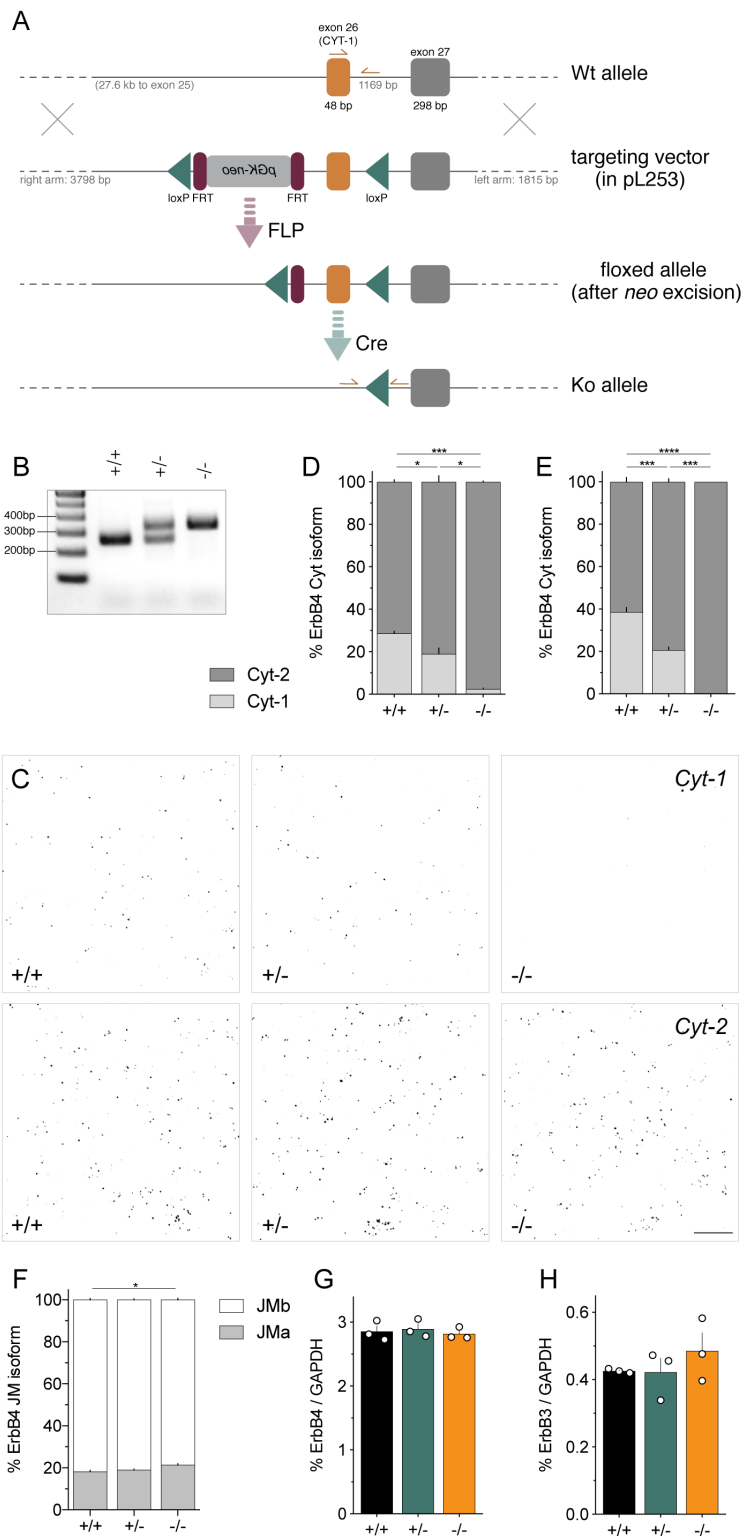


Figure 6.1 | Generation and validation of isoform-specific ErbB4 Cyt-1 knock-out mice by transcript analyses. (A) Scheme illustrating strategy to generate Cyt-1 mutant mice (details see methods). Exon 26 (orange), encoding the Cyt-1 cassette, was targeted by site-specific recombination in C57BL/6J embryonic stem cells to insert flanking loxP sites (green). Subsequently, the FRT-pGK-neo-FRT (magenta) selection cassette was removed in

mice harboring the targeted allele by crossing to a FLP deleter strain. The Cyt-1 exon was then ablated in germline by crossing to mice expressing Cre recombinase under the control of ubiquitously active EIIa promoter. **(B)** Representative genotyping results using primers indicated in A. **(C)** Isoform-specific ISH shows absence of Cyt-1 transcript in Cyt-1 homozygote (-/-) mutant mice and reduction of Cyt-1 transcript in heterozygote (+/-) mutant mice compared to control littermates. Examples from mesencephalic ventral tegmental area (VTA). **(D)** Quantification of data shown in C (n=3; one-way ANOVA, *p<0.05, ***p<0.001). **(E-H)** TaqMan qPCR analyses from whole brain (n=3/genotype). **(E)** Cyt-1 transcript was absent in Cyt-1 mutant mice (-/-) and reduced to approximately half in heterozygote (+/-) compared to control littermates (+/+). Expression of JM ErbB4 splice variants **(F)**, and total ErbB4 **(G)** and ErbB3 **(H)** expression levels were unchanged (n=3; one-way ANOVA, *p<0.05, ***p<0.001, ****p<0.0001). Scale bar 50µm.

Lastly, we addressed expression of ErbB3, as ErbB4 Cyt-2 receptor is able to activate PI3K through ErbB3/ErbB4 heterodimers²⁰⁶. ErbB3 expression is unchanged in Cyt-1 mutant mice (Fig. 6.1H; % ErbB3/GAPDH +/+ 0.426 ± 0.004%, +/- 0.423 ± 0.042%, -/- 0.485 ± 0.054%; n=3, one-way ANOVA, F(2,6)=0.8039, p=0.4906). Finally, Cyt-1 mutant mice were viable, had normal litter sizes (6.4 pups ± 0.11, N=2 cohorts; C57BL/6J 6.2 ± 0.2 pups³⁵⁶) and no obvious anatomical, developmental or behavioral deficits.

6.4.2 Cyt-1 is expressed in cortical and hippocampal GABAergic interneurons, but dispensable for GABAergic interneuron development

Cortical and hippocampal GABAergic interneurons express high levels of ErbB4^{58, 60, 63}. ErbB4 functions on GABAergic interneurons have been extensively studied and identified to regulate many aspects of GABAergic and glutamatergic neurotransmission, directly or through indirect circuit effects, respectively¹²⁴. In order to address if ErbB4 Cyt-1 may be involved in the modulation on GABAergic interneurons, we characterized the expression of Cyt-1 and Cyt-2 ErbB4 splice variants in the adult mouse hippocampus (Hpp) and somatosensory cortex (SSCtx) using exon-specific ISH. Both Cyt variants were detected in a scattered pattern well-known for GABAergic interneurons^{54, 56} (Fig. 6.2A-D). Consistent with previous reports^{59, 192, 213, 218}, Cyt-1 ErbB4 variants contributed ~40% of total ErbB4 in both areas (Fig. 6.2E,F; Hpp: Cyt-1 40.83 ± 0.9215%, Cyt-2 59.17 ± 0.9215%, n=4; Mann-Whitney test, p=0.0286; SSCtx: Cyt-1 37.28 ± 1.276%, Cyt-2 62.72 ± 1.276%, n=4; Mann-Whitney test, p=0.0286). This suggest that a significant portion of ErbB4 signaling in cortical and hippocampal GABAergic interneurons is mediated through ErbB4 Cyt-1 receptors and we next sorted to address in which processes regulated by ErbB4, Cyt-1 receptors are involved.

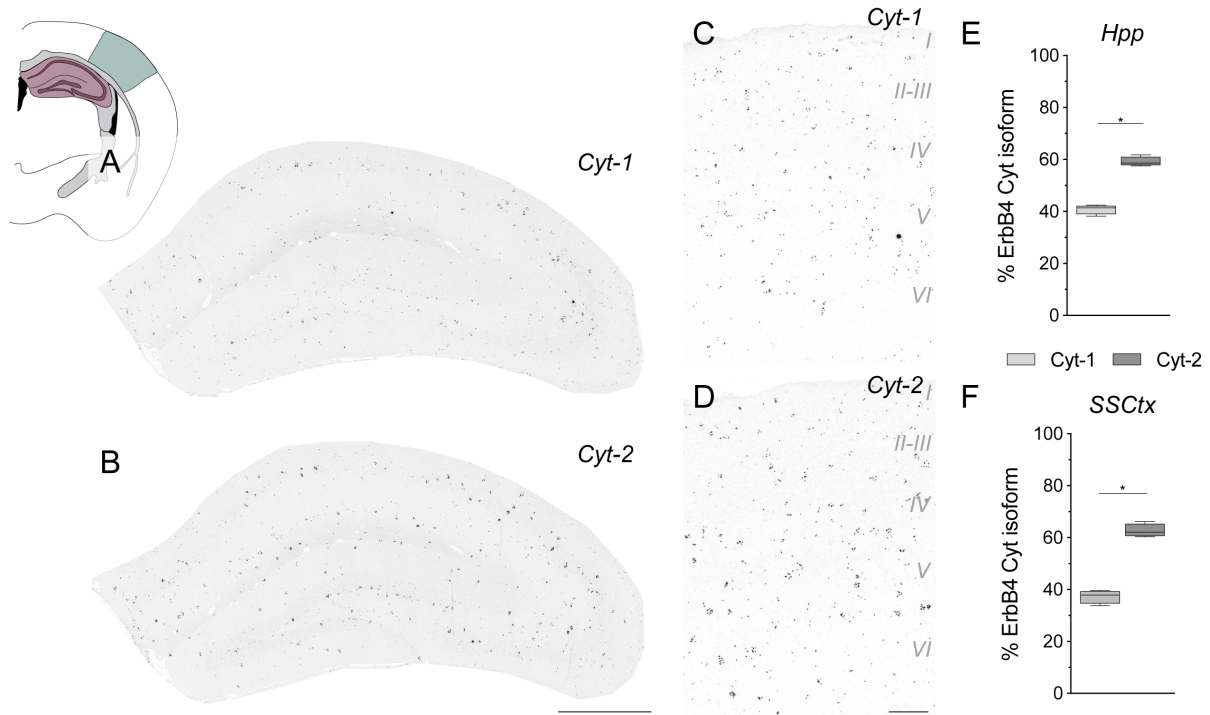


Figure 6.2 | Expression of ErbB4 Cyt variants in hippocampal and cortical interneurons.

(A-D) Exon-junction-specific ISH for Cyt-1 and Cyt-2 ErbB4 splice variants on sections of C57BL/6J mice. (A,B) Representative expression of Cyt-1 and Cyt-2 in the dorsal mouse hippocampus (red area in scheme; A,B) and primary somatosensory cortex (barrel field, green area in scheme; C,D). (E,F) Quantitative analysis of Cyt splice variant expression in the hippocampus (Hpp; E) and the primary somatosensory cortex (SSCtx; F; * $p < 0.05$; $n = 4$; Mann-Whitney test). Scale bars 500 μ m in B, 100 μ m in D.

During neurodevelopment, ErbB4 is expressed on tangentially migrating GABAergic neuroblasts⁵⁴ and loss of ErbB4 results in the reduction of cortical and hippocampal interneurons in the adult as GABAergic neuroblasts fail to enter the developing cortex^{63, 79}. ErbB4 Cyt-1 was previously reported to be expressed at particularly high levels in the ganglionic eminences, the origin of interneurons²²⁰, as well as in migrating GABAergic interneurons itself during both embryonic and postnatal development^{219, 221}. Moreover, phosphorylation of Y1056 in the Cyt-1 encoded region was proposed to regulate directionality and polarity of migrating interneurons²²¹. We first analyzed the expression of Cyt variants during development using exon-specific ISH and qPCR. Cyt-1 transcripts were present on tangentially migrating interneurons entering the cortical plate (Fig. 6.3A). Moreover, Cyt-1 transcripts are relatively high expressed (40-60%) at all embryonic and perinatal time-points analyzed (E11.5-P10) compared to postnatal (P30) expression (~30%) in both pallial/cortical

and subpallial/striatal tissue (Fig. 6.3C). Of note, *Cyt-1* expression peaked at birth (P0), particularly in the cortex, when interneurons are allocated in the cortical plate³⁶⁴.

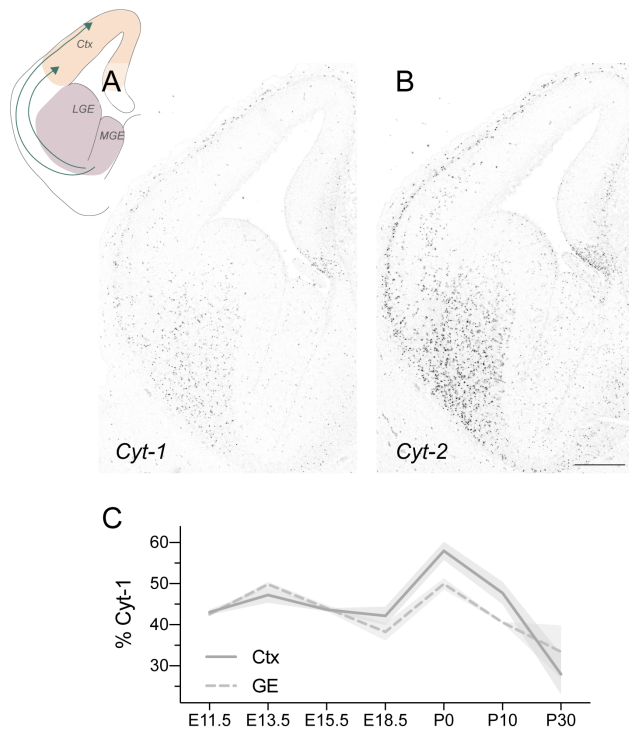


Figure 6.3 | Expression of Cyt transcripts during development.

(A,B) ISH for *Cyt-1* (A) and *Cyt-2* (B) transcripts on a coronal section of E14.5 WT (C57BL/6J) embryos detects migrating interneurons from the ganglionic eminences invading the cortical plate in two streams in the marginal zone and subventricular zone (green arrows in scheme). (C) *Cyt-1* expression (% of Cyt transcripts) analyzed by TaqMan qPCR in pallial/cortical (Ctx; orange area in scheme) and subpallial/striatal (GE; magenta area in scheme) across different time points during embryonic, perinatal and postnatal development (n=3-4/time-point). Scale bar 200 μ m. LGE – lateral ganglionic eminence, MGE – medial ganglionic eminence.

We hypothesized that *Cyt-1* transcripts are involved in regulating interneuron migration and particularly their cortical allocation, and that potential deficit in tangential migration of GABAergic interneurons in *Cyt-1* mutant mice could manifest in reduced interneuron numbers or altered distribution of interneurons in the postnatal cortex and hippocampus. To evaluate, GABAergic interneuron density and position, we crossed *Cyt-1* mutant mice to transgenic GAD-GFP mice, that express GFP under the control of the GABAergic marker GAD1 (glutamate decarboxylase). To our surprise, the number of GABAergic interneurons was unchanged compared to heterozygote and control littermates both in the SSCtx and the dorsal Hpp of young adult *Cyt-1* mutant mice (Fig. 6.4; GAD-GFP cells in Hpp: *Cyt-1* +/+ 180.8 \pm 7.73 cells/mm², *Cyt-1* +/- 178.1 \pm 8.21 cells/mm², *Cyt-1* -/- 180.1 \pm 3.54 cells/mm²; n=4, one-way ANOVA, F(2,9)=0.04186, p=0.9592; in SSCtx: *Cyt-1* +/+ 407.7 \pm 10.71 cells/mm², *Cyt-1* +/- 385.5 \pm 7.10 cells/mm²; *Cyt-1* -/- 392.0 \pm 11.99 cells/mm²; n=4, one-way ANOVA F(2,9)=1.264, p=0.3283). Taken together, we conclude that *ErbB4* *Cyt-1* variants are dispensable for interneuron migration and allocation in contrast to previous suggestions²²¹.

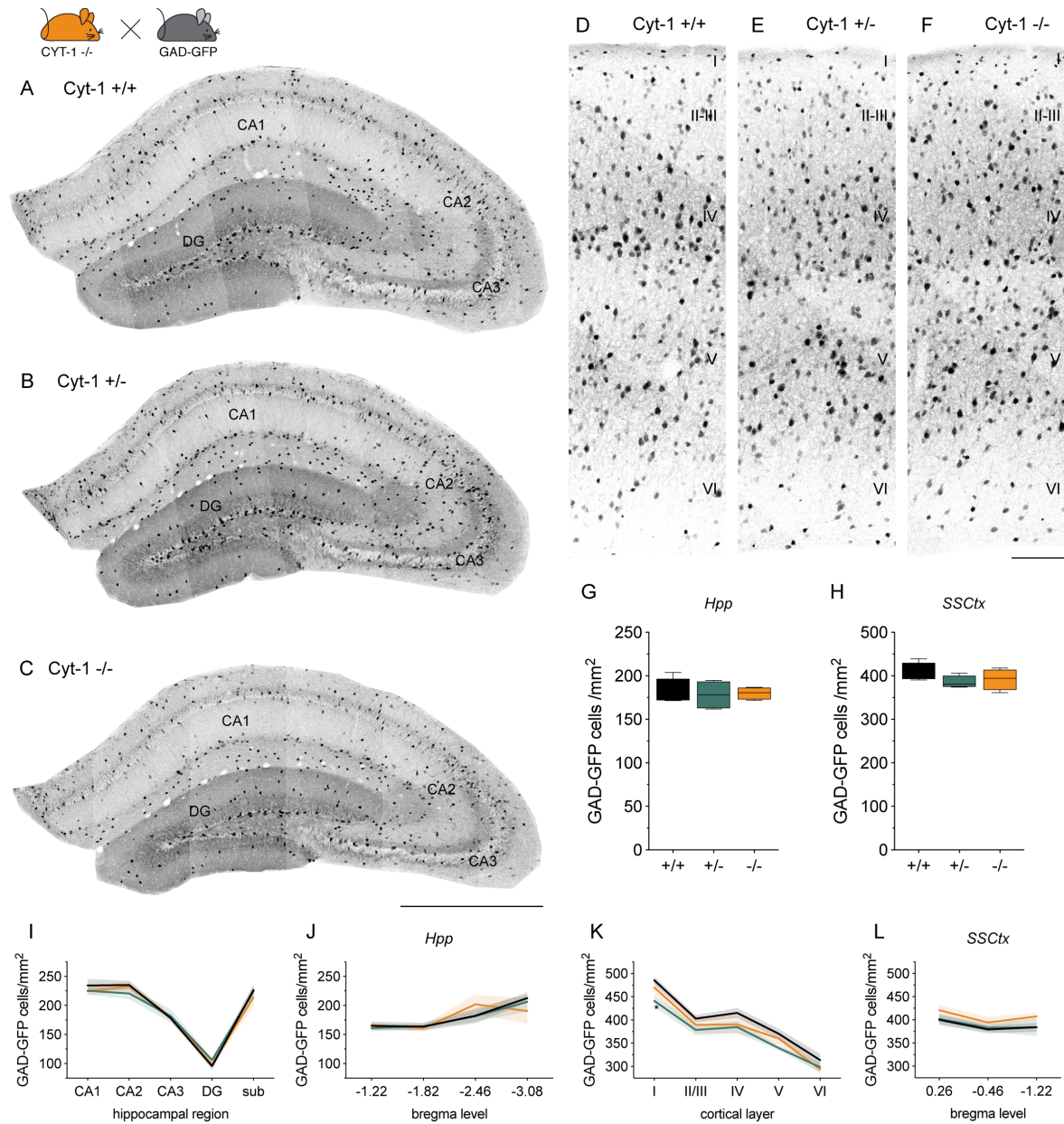


Figure 6.4 | GABAergic interneurons in the hippocampus and primary somatosensory cortex are unaltered in *Cyt-1* mutant mice.

(A-H) Analysis of GABAergic interneurons in the hippocampus and primary somatosensory cortex of *Cyt-1* mutant mice (-/-), heterozygote (+/-) and control (+/+) littermates crossed to GAD67-GFP mice at P30. Representative GFP-positive interneurons in the dorsal hippocampus (A-C) and the somatosensory cortex (D-F). (G,H) Quantification of GABAergic interneurons in the hippocampus (Hpp; G) and the somatosensory cortex (SSCtx; H) and (I-L) subregion-, layer-specific and rostro-caudal analyses (n=4; two-way ANOVA, *p=0.0325 in K +/- vs. +/+ in layer I). Scale bars 500µm in C, 100µm in F. DG – dentate gyrus, sub – subiculum

6.4.3 Cyt-1 mutant mice do not exhibit behavioral deficits

Behavioral abnormalities pertinent to schizophrenia have been described in null ErbB4 mutant mice¹⁴² and many are recapitulated in mice in which ErbB4 was conditionally ablated from parvalbumin (PV)-expressing interneurons (PV-Cre; ErbB4^{fl/fl})^{61, 142}, one of the major GABAergic interneuron classes expressing ErbB4^{58, 60, 63}. For instance, both null ErbB4 mutant and PV-Cre;ErbB4^{fl/fl} mice affecting all ErbB4 splice variants respond with locomotor hyperactivity to novelty and exhibit impaired sensorimotor gating and reduced anxiety^{61, 142, 167}. To determine if ErbB4 Cyt-1 receptor is contributing to these phenotypes, we subjected Cyt-1 mutant mice to a battery of behavioral tests previously shown to be regulated by ErbB4 in interneurons. Contrary to our expectations, Cyt-1 mutant mice traveled similar distances in the open-field test with a trend to hypoactivity and faster habituation (Fig. 6.5A; n=10-14/genotype, total distance traveled +/+ 101.7 ± 6.2m, +/- 91.3 ± 3.8m, -/- 85.6 ± 2.4m, one-way ANOVA, F(2,34)=2.905, p=0.0684, Tukey's multiple comparisons test +/+ vs. -/- p=0.0646). Of note, heterozygote Cyt-1 mutant mice were hypoactive when across all time points compared to their control littermates (Fig. 6.5A; distance traveled in 5min time blocks, two-way ANOVA, F(10,215)=0.5155, p=0.8783; Tukey's multiple comparisons main column effect +/+ vs. +/- *p=0.0135, +/+ vs. -/- p=0.683, +/- vs. -/- p=0.8703). In the elevated plus maze, Cyt-1 mutant mice have unaltered anxiety levels, i.e. spent similar time in the open and closed arms of the elevated plus maze (Fig. 6.5B, n=11-14/genotype, two-way ANOVA, F(2,69)=0.1420, p=0.8679, open +/+ 27.04 ± 3.87s, +/- 28.59 ± 6.41s, -/- 25.07 ± 4.36s, closed +/+ 194.5 ± 9.82s, +/- 187.8 ± 9.81s, -/- 189.7 ± 11.21s). And finally, sensorimotor gating in the prepulse inhibition (PPI) task appeared normal in Cyt-1 mutant mice compared to control and heterozygote littermates (Fig. 6.5C, n=17-18/genotype, two-way ANOVA, F(6,100)=0.1108, p=0.9951; Tukey's multiple comparisons test main column effect +/+ vs. +/- p=0.6833, +/+ vs. -/- p=0.9859, +/- vs. -/- p=0.5836). However, male heterozygote Cyt-1 mutant mice exhibit an increased startle response manifesting in an ameliorated PPI compared to their female counterparts and male control littermates, homozygote Cyt-1 mutants have an intermediate phenotype (two-way ANOVA, Tukey's multiple comparisons test main column effect, startle response F(55,555)=1.131, p=0.2490, +/+ male vs. +/- male ****p<0.0001, +/+ male vs. -/- male ****p<0.0001, +/- male vs. -/- male *p=0.0297, +/- male vs. +/- female ****p<0.0001, -/- male vs. -/- female ***p=0.0001; PPI F(15,180)=0.2669, p=0.9974, +/+

male vs. +/- male * $p=0.0269$, +/- male vs. +/- female **** $p<0.0001$). We also observed general sexual dimorphism in the total distance traveled and center time in the open-field task ($n=5-8$ /sex and genotype, one-way ANOVA, distance traveled, sex $F(1,33)=5.781$, * $p=0.0220$, center time, sex $F(1,33)=8.949$, ** $p=0.052$), as well as in the time spent in the closed arms of the elevated plus maze ($n=5-8$ /sex and genotype, one-way ANOVA, sex $F(1,63)=6.875$, * $p=0.0109$) consistent with previous reports suggesting increased locomotor activity, but increased anxiety in female mice^{163,365}. Taken together, Cyt-1 mutant mice show no behavioral impairments in tasks related to ErbB4 in interneurons.

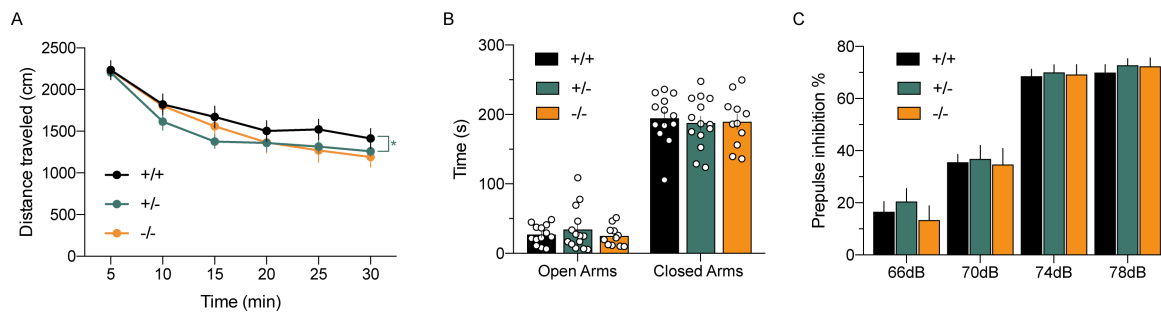


Figure 6.5 | Schizophrenia-related behaviors are unchanged in Cyt-1 mutant mice.

Cyt-1 mutant mice (-/-; orange) do not exhibit deficits in the (A) open field, (B) elevated plus maze, and (C) prepulse inhibition compared to heterozygote (+/-; green) and wildtype (+/+; black) littermates ($n=12-18$ /genotype; two-way ANOVA, * in A Tukey's multiple comparisons test main column effect +/+ vs. +/- * $p=0.0135$).

6.4.4 Cyt-1 expressed in dopaminergic neurons regulates extracellular dopamine levels

ErbB4 is expressed in dopaminergic neurons in the substantia nigra compacta (SNc) and the VTA. Recently, ErbB4 on axonal projections of dopaminergic neurons has been shown to rapidly increase extracellular dopamine levels after NRG1 infusion in projecting areas^{138,234}. Moreover, conditional Th-Cre; ErbB4^{fl/fl} mutant mice exhibit increased basal extracellular dopamine levels in the prefrontal cortex and dorsal hippocampus, but a reduction in dopamine in the striatum²³⁴. Changes in dopamine levels were accompanied by cognitive deficits in spatial working and reference memory²³⁴. To address a potential role of ErbB4 Cyt-1 in the regulation of dopamine function, we analyzed expression of ErbB4 Cyt splice variants by splice variant-specific ISH in the VTA and found that ErbB4 Cyt-1 contributes about 20% to ErbB4 expressed in this area (Fig. 6.6C; Cyt-1 $19.86 \pm 1.83\%$, Cyt-2 $80.14 \pm 1.83\%$, Mann-Whitney test, $n=4$, * $p=0.0286$). Since ErbB4 is expressed on both dopaminergic and

GABAergic neurons in this area^{53, 57}, we asked if there is a cell-type specific preference of Cyt variant expression and performed isoform-specific ISH with post-hoc immunohistochemical identification of dopaminergic neurons as previously described^{192, 357}. Both ErbB4 Cyt variants are expressed in dopaminergic and non-dopaminergic, presumably GABAergic, neurons (Fig. 6.6D). While, as expected, more ErbB4 Cyt-2 positive cells and higher Cyt-2 expression per cell compared to Cyt-1 are detected (data not shown), the percentage of Cyt-expressing cells that are dopaminergic are similar (Fig. 6.6E; % DA/Cyt, Cyt-1 $39.27 \pm 0.46\%$, Cyt-2 $39.27 \pm 1.53\%$, $n=3$, Mann-Whitney test, $p>0.9999$), suggesting that dopaminergic and GABAergic neurons express similar ratios of Cyt splice variants.

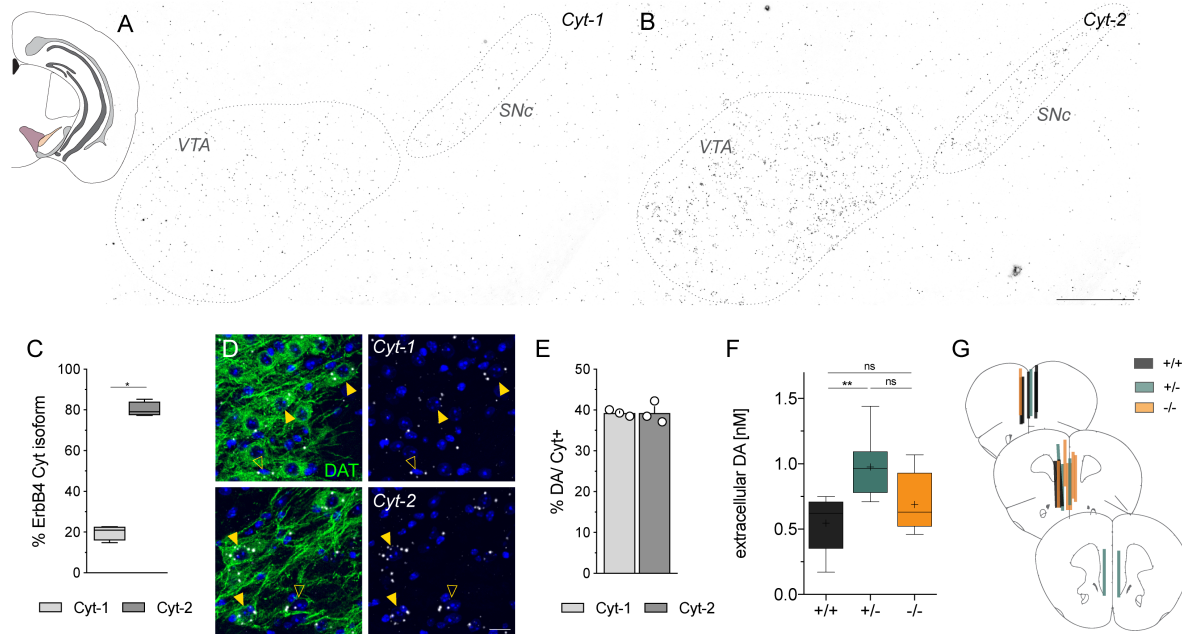


Figure 6.6 | ErbB4 Cyt variants in the ventral tegmental area (VTA).

(A,B) Representative expression of Cyt-1 and Cyt-2 ErbB4 variants in the VTA analyzed by exon-junction-specific ISH on sections of C57BL/6J mice. **(C)** Quantitative analysis of Cyt splice variant expression in the ventral tegmental area and substantia nigra compacta ($*p<0.05$; $n=4$; Mann-Whitney test). **(D)** Dopaminergic (dopamine transporter (DAT)-positive, green, arrowhead) and non-dopaminergic cells (open arrowhead) express Cyt ErbB4 variants (white) in the VTA. **(E)** Portion of dopaminergic Cyt-positive cells ($n=3$; Mann-Whitney test). **(F)** Extracellular dopamine (DA) levels were analyzed by unilateral no net-flux microdialysis in the medial prefrontal cortex (mPFC) of freely moving Cyt-1 mutant mice ($-/-$; orange), heterozygote ($+/-$; green) and control littermates ($+/+$; black; $n=6-7$; one-way ANOVA, $**p<0.01$). **(G)** Placement of 2mm-long microdialysis probes in the mPFC at bregma levels +2.22mm, +1.98mm and +1.78mm were evaluated in 50 μm -thick sections using Nissl staining. Scale bars 200 μm in B, 20 μm in D.

To evaluate the role of ErbB4 Cyt-1 in modulating extracellular dopamine levels, we performed no-net flux microdialysis in the medial prefrontal cortex (mPFC) of freely moving

Cyt-1 mutant mice. To our surprise Cyt-1 heterozygote, but not homozygote mutant mice have increased basal extracellular dopamine levels in the mPFC (Fig. 6.6F; $+/+$ $0.546 \pm 0.080\text{nM}$, $+/-$ $0.977 \pm 0.103\text{nM}$, $+/+$ $0.689 \pm 0.085\text{nM}$, $n=6-7/\text{genotype}$, one-way ANOVA, $F(2,17)=5.863$, $*p=0.0116$). In sum, Cyt-1 is expressed in dopaminergic neurons in the VTA albeit at lower levels than in the cortex and regulates some aspects of dopamine homeostasis as Cyt-1 heterozygote mutants exhibit increased extracellular dopamine concentration in the mPFC.

6.4.5 Cognitive function is normal in Cyt-1 mutant mice

The alterations in extracellular dopamine levels in the mPFC in heterozygote mutant mice prompt us to investigate cognitive functions in Cyt-1 mutant mice found to be impaired in null ErbB4 and Th-Cre; ErbB4^{fl/fl} mutants²³⁴. We subjected the mice to a Y-maze task for spontaneous alternation and spatial working memory, as well as to a Barnes maze test for learning abilities and spatial reference memory. Novel arm preference in the Y-maze (Fig. 6.7A) was unaltered in Cyt-1 mutant mice compared to their littermate controls ($n=12-14/\text{genotype}$, % alternation $+/+$ $51.64 \pm 1.75\%$, $+/-$ $48.65 \pm 2.44\%$, $+/+$ $50.07 \pm 2.04\%$, one-way ANOVA, $F(2,360)=0.4$, $p=0.6193$), of note alternation was overall lower in female than in male mice as reported previously³⁶⁶ (two-way ANOVA, $F(1,33)=6.619$, $*p=0.0148$). Next, we tested acquisition and recall of spatial reference memory in the Barnes maze. Cyt-1 mutant mice learned the task equally as their heterozygote and control littermates, as expressed by similar latency to escape (Fig. 6.7B; $n=8-11/\text{genotype}$, two-way ANOVA, $F(6,108)=0.9364$, $p=0.4721$) and number of errors committed during the four day training phase (Fig. 6.7C, $n=8-11/\text{genotype}$, two-way ANOVA, $F(6,107)=0.9876$, $p=0.4375$). Cyt-1 mice performed similar to their heterozygote and control littermates in the probe test ($n=8-11/\text{genotype}$, number of errors, Fig. 6.7D, $+/+$ 17.5 ± 3.5 , $+/-$ 24.8 ± 3.5 , 20.8 ± 3.8 , one-way ANOVA, $F(2,27)=0.9498$, $p=0.3994$; time in correct zone Fig. 6.7E, $+/+$ $33.6 \pm 4.7\text{s}$, $+/-$ $36.0 \pm 3.0\text{s}$, $-/-$ $37.4 \pm 3.4\text{s}$, one-way ANOVA, $F(2,27)=0.2508$, $p=0.7799$; number of nose pokes per hole, Fig. 6.7F, two-way ANOVA, $F(38,540)=0.6784$, $p=0.9298$, Tukey's multiple comparisons test main column effect, $+/+$ vs. $+/-$ $*p=0.0242$, $+/+$ vs. $-/-$ $p=0.6638$, $+/-$ vs. $-/-$ $p=0.1344$). Finally, we tested cognitive flexibility and perseverance by moving the escape target in the Barnes maze to a new location. Cyt-1 mutant mice adapted equally to the new paradigm as heterozygote and control

littermates indicated by similar latencies to escape (Fig. 6.7G, $n=8-11/\text{genotype}$, two-way ANOVA, $F(6,106)=0.4240$, $p=0.8616$) and errors committed over the four trials (Fig. 6.7H, $n=8-11/\text{genotype}$, two-way ANOVA, $F(6,105)=1.799$, $p=0.1063$). Interestingly, consistent with change in dopamine in the heterozygote Cyt-1 mutant mice, heterozygote mice made more mistakes in the first trial (Fig. 6.7H, $n=8-11/\text{genotype}$, Tukey's multiple comparisons test, # errors in trial 1 $+/+$ 20.25 ± 8.03 , $+/-$ 32.91 ± 1.17 , $-/-$ 16.45 ± 3.04 , $+/+$ vs. $+/-$ $*p=0.0472$, $+/+$ vs. $-/-$ $p=0.7523$, $+/-$ vs. $-/-$ $**p=0.0027$). Taken together, cognitive function in Cyt-1 heterozygote and homozygote mutant mice was largely unaffected.

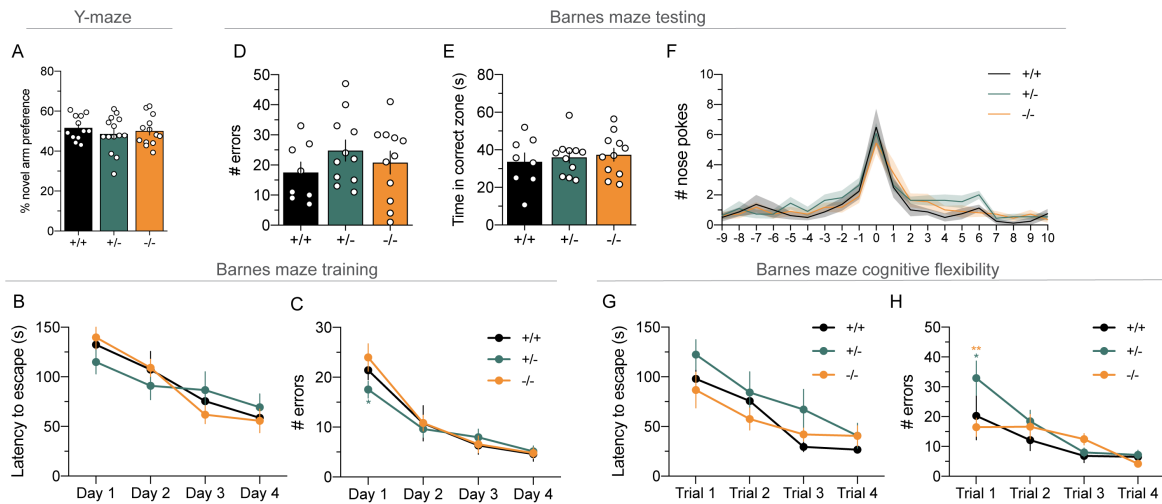


Figure 6.7 | Cyt-1 mutant mice have unaltered working and reference memory, and cognitive flexibility.

(A) Working memory expressed as percentage for novel arm preference in the Y-maze is normal in Cyt-1 mutant mice ($-/-$; orange) compared to heterozygote ($+/-$; green) and wildtype ($+/+$; black) littermates ($n=12-14/\text{genotype}$; one-way ANOVA). (B-G) Spatial reference memory in the Barnes maze of Cyt-1 mutant mice is comparable to heterozygote and wild-type littermates during (B,C) initial training over four days, (D-F) testing on day five and (G) adapting to a new target location. (B) Latency to escape during training. (C) Number of errors committed during training. (D) Number of errors during testing. (E) Time spent in the correct quadrant/zone during testing. (F) Nose pokes in individual holes during testing (0 – target, 10 – opposite). (G) Latency to escape and (H) number of errors after moving target to a new position (cognitive flexibility; $n=8-11/\text{genotype}$; two-way ANOVA except for D,E one-way ANOVA, * in B Tukey's multiple comparison test, Day 1 $+/-$ vs. $-/-$ $*p=0.0327$, **, ** in H Tukey's multiple comparison test, Trial 1 $+/-$ vs. $+/+$ $*p=0.0472$, $-/-$ vs. $+/-$ $**p=0.0027$).

6.4.6 Cyt-1 is enriched in the medial habenula, but does not regulate habenula-associated behaviors

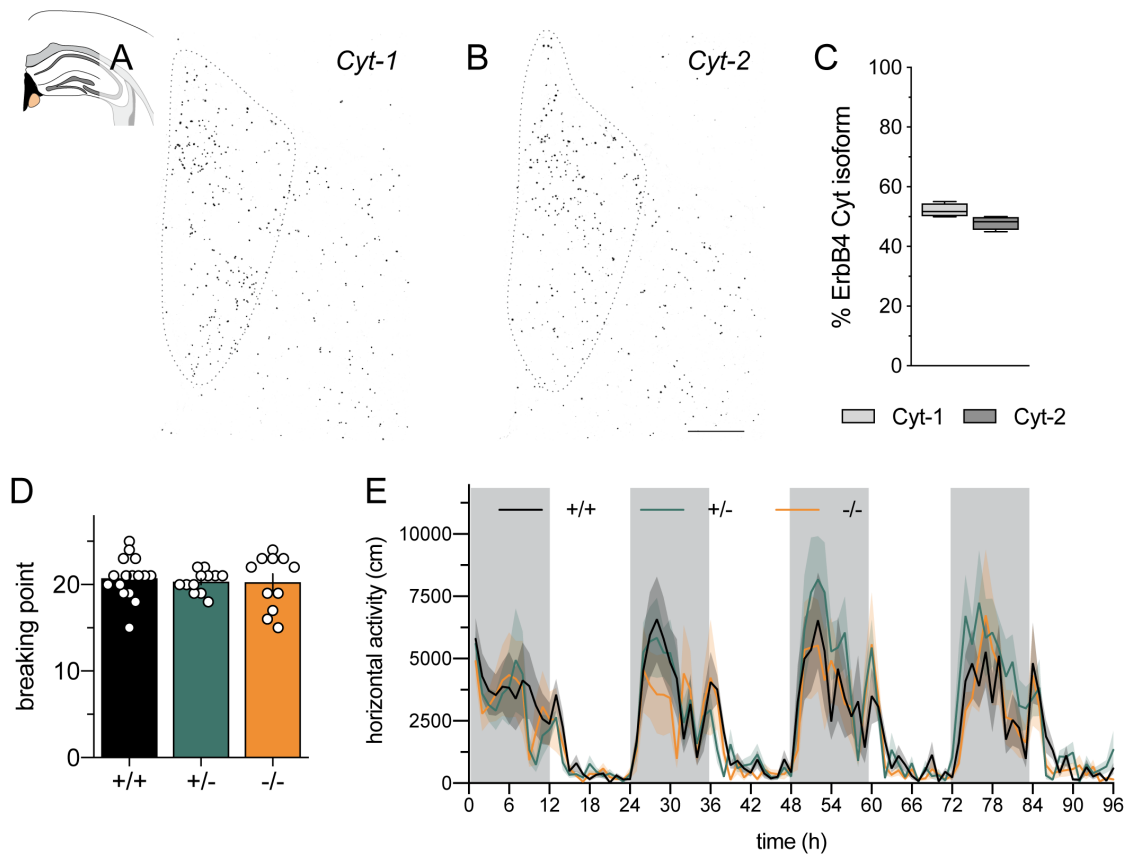


Figure 6.8 | Cyt expression in the medial habenula and habenula-regulated behaviors.

(A,B) Representative expression of Cyt-1 and Cyt-2 ErbB4 variants in the medial habenula (mHab) analyzed by exon-junction-specific ISH on sections of C57BL/6J mice. (C) Quantitative analysis of Cyt splice variant expression in the ventral tegmental area and substantia nigra compacta ($n=4$, Mann-Whitney test, $p=0.0571$). (D) Reward-seeking behavior of Cyt-1 mutant (orange) heterozygote (green) and control (black) littermates in the operant task (progressive ratio; $n=11-16$ /genotype, one-way ANOVA, $F(2,36)=0.1657$, $p=0.8479$). (E) Homecage activity was assessed over three days (grey boxes indicate dark cycle; $n=5-8$ /genotype, two-way ANOVA, $F(190,1575)=0.6117$, $p>0.9999$). Scale bar $100\mu\text{m}$.

Our efforts characterizing the function of Cyt-1 ErbB4 receptors based on phenotypes previously described to be altered in ErbB4 KO mice did not reveal any developmental, neurochemical or behavioral phenotypes in Cyt-1 mutant mice. Therefore, we next sought to analyze behaviors regulated by brain areas with particular enrichment of Cyt-1 expression. We identified high expression of Cyt-1 transcripts in the medial habenula (mHab; Fig. 6.8A-C) that was previously reported to have notable ErbB4 expression⁵⁶. Cyt-1 expression slightly exceeds Cyt-2 expression in this area ($52.1 \pm 1.2\%$ Cyt-1, $47.9 \pm 1.2\%$ Cyt-2, Mann-Whitney

test, $p=0.0571$). Then, we addressed reward-seeking behavior in *Cyt-1* mutant mice and littermates that previously were described to be regulated by the habenulo-interpeduncular pathway³⁶⁷. Reward-seeking and motivation was tested in food-deprived *Cyt-1* mutant mice in an operant task using a progressive ratio for reward delivery. The breaking-point, i.e. the cycle number/ number of rewards obtained when mice give up to work (nose poke) for a reward due to the increasing difficulty (nose pokes required) to receive a reward, did not differ between genotypes (Fig. 6.8D; $+/+$ 20.75 ± 0.60 , $+/-$ 20.33 ± 0.36 , $-/-$ 20.27 ± 0.96), suggesting similar motivation and willingness to work for food. Of note, *ErbB4* mutant mice have recently been tested to be more willing to work for palatable food (Skirzewski et al., in preparation).

General locomotor activity in hamsters increased after the transection of the fasciculus retroflexus, the major output of the medial habenula³⁶⁸. We therefore assessed general locomotor activity in the homecage of *Cyt-1* mutant mice. Locomotor activity over three days during light and dark cycle was not altered in *Cyt-1* mutant mice (Fig. 6.8E). Of note, heterozygote mutants traveled more distance when compared to homozygote mutants across all time points (two-way ANOVA, Tukey's multiple comparisons test, main column effect $+/+$ vs. $+/-$ $p=0.2037$, $+/+$ vs. $-/-$ $p=0.3049$, $+/-$ vs. $-/-$ $**p=0.0093$). In sum, although *Cyt-1* is the predominant *Cyt* variant expressed in the medial habenula, habenula-regulated reward-seeking/motivation and homecage activity are unaltered in *Cyt-1* mutant mice.

6.4.7 Gene expression analysis reveals changes in transcription factors regulating development

The absence of phenotypes in *Cyt-1* homozygote mutant mice, despite the prevalence of *Cyt-1* transcript in many brain areas (~40%), is unanticipated. It is plausible that during development a compensation occurred, and the system adapted to the loss of *Cyt-1* resulting in little or no phenotypes. Therefore, to elucidate potential compensatory mechanisms, we performed gene expression analysis by RNA sequencing from the VTA and the dorsal Hpp of *Cyt-1* mutant mice, heterozygote and control littermates. Consistent with initial TaqMan analyses (see Fig. 6.1E-H), no *Cyt-1* transcript was detected in *Cyt-1* mutant mice, *Cyt-1* transcript was reduced about 50% in heterozygote compared to control littermates, JM splicing was unaltered, and *ErbB3* and *ErbB4* expression levels were not changed. Differential gene expression analyses revealed that gene expression in the dorsal Hpp of the *Cyt-1* mutant or the

heterozygote mutant is comparable to control littermates, in line with no observed hippocampal-related developmental or behavioral changes in *Cyt-1* mutants.

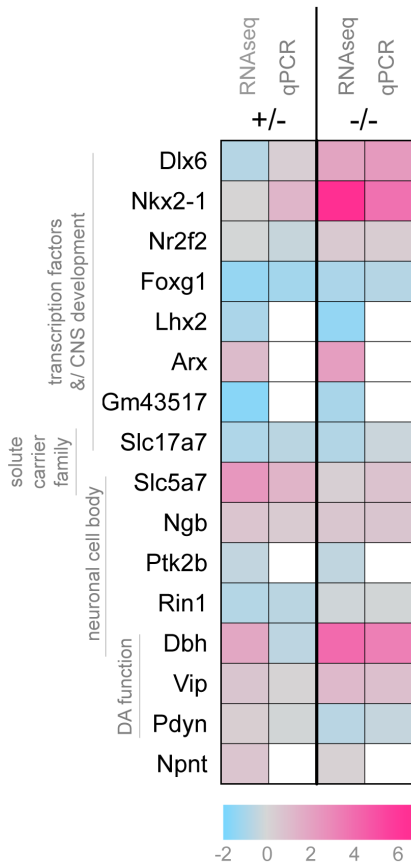


Figure 6.9 | Gene expression analysis in the VTA of *Cyt-1* mutant mice.

Gene expression analyses by whole genome RNA sequencing (RNAseq, n=3/genotype) and TaqMan quantitative PCR (qPCR, n=4) in the VTA of heterozygote (+/-) and homozygote (-/-) *Cyt-1* mutant mice relative to control littermates. Plotted log₂-fold change for all genes identified differentially expressed (adjusted p>0.05) in RNAseq. Gene ontology analyses and gene families are indicated. One box equals 3-4 animals, white boxes – expression not analyzed by qPCR.

In the VTA, however, we identified few genes (total of 16 genes) with small but significant differences in expression (adjusted p<0.05) between the three genotypes (Fig. 6.9). Among others two genes from the solute carrier family, vesicular glutamate transporter 1 (*Slc17a7*), choline transporter 1 (*Slc5a7*), several homeobox genes (*Nkx2-1*, *Lhx2*, *Dlx6*, *Arx*) and genes related to dopamine functions (*Dbh* (dopamine beta-hydroxylase), *Vip* (vasoactive intestinal peptide), *Pdyn* (Prodynorphin)) were identified. Gene expression was found to be both increased and decreased in homozygote and heterozygote mutants compared to control littermates and standard TaqMan qPCR showed similar trends and changes for a subset of genes analyzed (Fig. 6.9). Heterozygote mutants showed expression levels similar to controls (*Nkx2-1*, *Dlx6*, *Nr2f2*, *Dbh*, *Pdyn*), homozygote mutants (*Slc17a7*, *Lhx2*, *Foxg1*, *GM43517*, *Ptk2b*, *Ngb*) or intermediate expression (*Vip*, *Arx*). Interestingly, expression of *Slc5a7* (choline transporter 1), *Npnt* (Nephronectin) and *Rin1* (Ras and Rab interactor 1) was only altered in

heterozygote, but not homozygote mutant mice reminiscent of the changes in dopamine levels observed in the mPFC. Moreover, the forkhead box protein G1 (Foxg1), a FOXO class transcription factor was described downstream to ErbB4 signaling and the protein-tyrosine kinase 2-beta (Ptk2b) interacts with ErbB4³². Both were decreased in heterozygote and homozygote Cyt-1 mutants. Gene ontology analysis demonstrates significant enrichment of sequence-specific DNA binding (i.e. transcription factors; $p=0.0022$), the neuronal cell body in general ($p=0.0136$), and different developmental processes for instance axon guidance ($p=0.0216$), neuron migration ($p=0.0072$), forebrain neuron generation ($p=0.0150$), GABAergic interneuron differentiation ($p=0.0496$) and development of the cerebral cortex ($p=0.0024$) and the globus pallidus ($p=0.0045$). Taken together, gene expression in Cyt-1 mutant mice is unaltered in the dorsal Hpp, but transcription factors associated with neurodevelopment are differentially expressed between Cyt-1 mutant mice and their heterozygote and control littermates, suggesting a potential developmental compensation of the system for the loss of Cyt-1.

In conclusion, we addressed for the first-time isoform-specific function of ErbB4 receptors *in vivo* by generating Cyt-1-specific mutant mice. An array of conducted developmental, neurochemical, behavioral and expression studies suggest that ErbB4 Cyt-1 receptors are largely dispensable for CNS development and function. Transcriptomic analyses however suggest that the system might have adapted for the germline loss of Cyt-1. Therefore it will be interesting to investigate adult loss of function approaches (tamoxifen-inducible Cre recombinase or viral injection of Cre recombinase) to elucidate if Cyt-1 receptors regulate adult brain function, as the adult ablation of ErbB4 has recently been shown to regulate animal behavior¹¹⁸.

6.5 Discussion

To address the role of ErbB4 splice variants altered in postmortem schizophrenia patients, we generated the first splice variant-specific ErbB4 mutant mouse by removing the cytoplasmic Cyt-1 exon. Despite the prevalence of Cyt-1 in the brain (~40%) and essentiality of ErbB4 Cyt-1 to activate PI3K/Akt downstream signaling¹⁹¹, Cyt-1 mutant mice that lack Cyt-1 throughout development do not show schizophrenia-related developmental, neurochemical or behavioral impairments unlike different ErbB4 mutants lacking all splice

variants^{61, 68, 79, 118, 142, 234}. Surprisingly, Cyt-1 heterozygote but not homozygote mutant mice showed mild phenotypes. We conclude that ErbB4 Cyt-1 receptors are largely dispensable developmental functions of ErbB4¹¹⁸ and/or the loss of Cyt-1 was compensated as also supported by our transcriptomic analyses. Therefore, it will be interesting to see if Cyt-1-containing receptors play a crucial role in adult brain functions regulated by ErbB4¹¹⁸.

6.5.1 Mild phenotypes in heterozygote Cyt-1 mutant mice

Interestingly, heterozygote but not homozygote Cyt-1 mutants have elevated basal extracellular dopamine levels in the mPFC (Fig. 6.6F). Cyt-1 heterozygote mutants also show small differences in GABAergic interneuron density in cortical layer I (Fig. 6.4K), are slightly hypoactive in a novel environment (Fig. 6.5A), *hyperactive in a familiar environment* (Fig. 6.8E), commit less errors during the initial day of training in the Barnes maze (Fig. 6.7C), but are less flexible to adapt to a new paradigm (Fig. 6.7H). Strikingly, male but not female heterozygote mutants have an increased startle response and PPI. Gender differences in acoustic startle response and PPI were previously described in mice, rats and humans³⁶⁹⁻³⁷¹. Consistent with a heterozygote-specific phenotype, gene expression analyses revealed genes that are only altered in heterozygote Cyt-1 mutants (Fig. 6.9).

Allele-biased expression of ErbB4 has been suggested in humans³⁷². However, our Cyt transcript analyses suggest that both ErbB4 alleles are contributing similar amounts of ErbB4 transcripts in mice (Fig. 6.1D,E) and allelic expression would explain the phenotype in the heterozygote mutant, but not the absence of phenotype in the homozygote mutant. Heterozygote advantage or overdominance as a result of selective breeding in livestock and pets has been described in a handful of genes but is usually associated with disease in the homozygous mutants³⁷³. In the case of protein dimerization, homo- and heterodimers may differ in their stability and signaling³⁷⁴, but Cyt-1 and Cyt-2 homo- and heterodimers should occur both in the control as well as in the heterozygote mutant.

Interestingly, heterozygote-specific phenotypes were previously described for mutations of dopamine-related genes³⁷⁵⁻³⁷⁷. Heterozygote dopamine transporter (DAT) mutant mice for instance show increased exploration and less anxiety than their WT and homozygote littermates³⁷⁶. Heterozygote mutations in the dopamine receptor D4 (D4DR) result in reduced locomotor activity and in increased impulsivity, whereas homozygote mutants are normal³⁷⁵.

³⁷⁷. These effects were suggested to depend on compensatory mechanism that are effective upon absolute ablation, but not when expression levels are only reduced³⁷⁵. In line with this hypothesis, it is feasible that compensation can occur when Cyt-1 is absent (Cyt-1 $-/-$) but is prevented by residual Cyt-1 in the heterozygote mutant (Cyt-1 $+/-$). One possible mechanism would be through transcriptional regulation that has been shown to be different between Cyt-1 and Cyt-2 isoforms²¹¹.

6.5.2 Developmental loss of Cyt-1 may be compensated

In contrast, homozygote ErbB4 Cyt-1 mutant mice, in which Cyt-1 transcripts were ablated in the early development under the control of the EIIa promoter, do not have abnormal behaviors or alterations in prefrontal extracellular dopamine levels. Moreover, GABAergic development in Cyt-1 mutant mice is normal, although Cyt-1 has been previously suggested to regulate GABAergic interneuron migration²²¹. While, it is possible that ErbB4 Cyt-1 isoforms and its downstream mediate signaling through PI3K/Akt or proteins containing a WW-binding domain do not play a role throughout development, several line of evidence suggest that the lack of phenotype in Cyt-1 mutant mice is due to compensatory mechanisms that accounted for the loss of Cyt-1 throughout development. Heterozygote mutant mice exhibit mild phenotypes and transcriptomic analyses unveiled changes in developmental transcription factors (Fig. 6.9). Compensation could occur through ErbB4 Cyt-2 receptors which do not possess the ability to directly activate PI3K unlike Cyt-1 receptors, but can dimerize with ErbB3 receptors to activate PI3K^{191, 206}. However, first, transcript levels of ErbB3 are unaltered in Cyt-1 mutant mice (Fig. 6.1H) and second, ErbB3 is absent from neurons^{50, 51} e.g. GABAergic and dopaminergic neurons which are the primary cells to express ErbB4, mediate NRG/ErbB4 signaling and regulate animal behavior^{30, 60, 79, 142, 234}. Besides, it has become clear that PI3K/Akt and MAPK-mediated pathways extensively cross-react. They regulate the same substrates and MAPK signaling positively regulates PI3K/Akt/mTOR³⁷⁸, providing another possible explanation how PI3K and downstream signaling could be activated by ErbB4 Cyt-2 receptors in the absence of Cyt-1-containing receptors. At this point, it however remains unclear if and how the system adapts to the developmental deletion of Cyt-1.

Wang et al. (2018) have recently shown, that the ablation of ErbB4 in the postnatal brain causes similar deficits in behavior and neurotransmission compared to the loss of ErbB4 throughout development. Importantly, abnormalities in GABAergic neurotransmission and behaviors caused by the germline loss of ErbB4 can be enhanced by the postnatal reintroduction of ErbB4¹¹⁸. Therefore, it will be interesting to investigate if Cyt-1 ErbB4 receptors regulate adult brain function using acute loss of function approaches circumventing a potential compensation through developmental processes.

6.5.3 ErbB4 splice variants in schizophrenia

Polymorphisms in the *ErbB4* gene have been linked to an increased risk for schizophrenia. While changes to the expression levels of total ErbB4 transcript and receptor are controversial, described as unchanged²¹⁸ or increased²²², four independent studies have identified increased expression of the otherwise minor JMa and Cyt-1 transcripts in the DLPFC of schizophrenia patients, with a concomitant reduction in JMb and Cyt-2 transcripts^{28, 218, 222-224}. And ErbB4 polymorphisms were identified to correlate with increased Cyt-1 and PI3KCD expression^{223, 224}. Since the identification of NRG1 and ErbB4 as risk factors for schizophrenia, noticeable progress has been made in understanding the regulation of CNS circuits by NRG/ErbB4 signaling. However, to our knowledge no study has been dedicated to the understanding of the role of ErbB4 Cyt splice variants *in vivo*. The here described Cyt-1 mutant mice, suggest that the developmental loss of ErbB4 Cyt-1 receptors does not generate behavioral phenotypes related to psychiatric disorders unlike the deletion of all ErbB4 transcripts¹⁴². We are still at the beginning of understanding the function of ErbB4 isoforms and *in vivo* studies dedicated to the acute postnatal loss of Cyt-1 to circumvent potential developmental compensation and the other three main splice variants Cyt-2, JMa and JMb will be necessary to better understand each ErbB4 isoforms' unique function. This ultimately might advance the possibility for splice variant-specific treatment of psychiatric disorders using monoclonal antibodies or splice switching oligonucleotides^{216, 217}.



Discussion & Future Directions

The aim of my thesis was to better understand the expression and functions of ErbB4 isoforms in the central nervous system. The work presented in this dissertation, indeed supports the hypothesis that ErbB4 splice variants differ in their spatiotemporal expression and between cell types in the brain (*Aim 1*). Moreover, subcellular targeting of ErbB4 differs in two neuronal cell populations, namely GABAergic and dopamine neurons; however appears to be independent of the ErbB4 isoform expressed (*Aim 2*). Lastly, evidence for unique biological roles of Cyt-1 ErbB4 receptors could not be presented, as the extensive molecular, developmental, anatomical, neurochemical, behavioral and transcriptomic analyses of isoform-specific (homozygote) Cyt-1 mutant mice did not exhibit altered phenotypes (*Aim 3*). In conclusion, this dissertation provides an extensive characterization of ErbB4 splice variant expression in the brain and provides first insights into the biology of distinct ErbB4 isoforms in the CNS that warrant further investigation.

7.1 Expression and subcellular targeting of ErbB4 isoforms

Although ErbB4 variants are altered in postmortem brains of schizophrenia patients^{28, 218, 222, 223}, little was known about ErbB4 isoform expression and function in the brain. The expression of ErbB4 variants has only been addressed in a few well-studied brain areas and studies largely disregarded signal distribution or cellular expression^{59, 67, 213, 218, 219}, as sensitive tools to analyze short splice variants were not available. Therefore, in this dissertation, I first generated and extensively validated tools to perform and quantitatively analyze a novel ultrasensitive isoform-specific ISH approach (Chapter 3 & 4). This not only allows for the investigation of ErbB4 isoforms, but will also make rapid quantification of any splice variant

or even SNPs beyond ErbB4 and the brain possible. Moreover, the automated freely available quantification pipeline is useful for a variety of fluorescent dot/puncta quantification including multiplex ISH analyses or synapse quantitation. Using next-generation RNA sequencing, I conducted the first whole transcript splice variant analysis to unambiguously identify ErbB4 splice variants expressed in the brain. Although no novel splice variants were detected, I provided first evidence for the expression of the rare variants JMc, JMd and del.3 in the adult mouse brain, previously only described during development, in disease, and the human brain^{193, 230, 232} (Fig. 2.2). Using the developed ISH tools, I then went on to study the expression of the four main ErbB4 variants (JMa, JMb, Cyt-1, Cyt-2) that account for ~99% of all ErbB4 transcripts in the CNS. In this thesis, I describe the spatial expression of ErbB4 variants across many brain areas, advancing our understanding of ErbB4 isoforms in the CNS. Briefly, in most brain regions (Ctx, Hpp, Rtn, VTA) JMb and Cyt-2 variants are predominant, comprising about 80-90% and 60-80% of ErbB4 transcripts, respectively. My work is first to also characterize brain areas that are enriched by JMa and Cyt-1 transcripts. For instance, JMa is the sole JM variant expressed in the choroid plexus with JMb transcripts completely absent; slightly more Cyt-1 than Cyt-2 was detected in the medial habenula; and both JMa and Cyt-1 are the major ErbB4 isoforms in the thalamus, the corpus callosum, as well as in other white matter areas (hippocampal fimbria, data not quantified; Chapter 4 & 6). I also uncovered temporal regulation of the expression of ErbB4 splice variants during development. Both JMa and Cyt-1 variants are expressed at higher levels during early embryonic development and gradually decrease in the postnatal brain (Fig. 6.3; JM data not shown).

Interestingly, owing to the single-cell resolution of the ISH approach, I identified differences in ErbB4 variants between cell types. While JMb ErbB4 is predominant in cortical and hippocampal GABAergic interneurons and GABAergic corpus callosal interstitial cells, JMa is the sole juxtamembrane variant expressed in mature oligodendrocytes and oligodendrocyte precursor cells, as well as in the choroidal epithelium (Fig. 4.6, Suppl. Fig. 4.13). The unique capability of cleavable JMa receptors to regulate transcription⁴⁸ enables a diverse signaling capacity even if expressed at low levels. In fact, in preliminary immunohistochemical experiments, I was not able to detect ErbB4 protein in any of these cells. However, NRG/ErbB4 signaling has been previously suggested to regulate BBB permeability^{305, 306} and oligodendrocyte progenitor migration¹⁰⁵, maturation¹⁰⁶ and some

aspects of myelination¹⁰⁴. Therefore, my findings raise the question if these processes are kinase-mediated or rather depend on the transcriptional regulation by the ICD of ErbB4. Chromatin immunoprecipitation sequencing (ChIPseq) of cultured oligodendrocytes or isolated choroidal tissue could give valuable insights into genes potentially modulated by ErbB4 but was beyond the scope of this study. On the other hand, JMa transcripts are increased in the postmortem DLPFC of schizophrenia patients^{28, 218, 222, 223}. It was assumed that these changes mainly occur in GABAergic interneurons or more specifically in PV-expressing interneurons²¹⁸. However, given the enrichment of JMa transcripts in cells of the oligodendrocyte lineage, that are also present in the DLPFC, we must revisit this idea and analyze *ErbB4* splice variant changes in schizophrenic brains with methods that allow the distinction of cell types (single-cell RNA sequencing or exon-specific ISH). Oligodendroglia were previously described to be involved in the pathophysiology of schizophrenia¹⁰⁹; and it is crucial to elucidate for our comprehension of the disease in which cell type ErbB4 splice variant alterations occur, as this could have different biological implications.

Although this thesis provides a detailed expression analysis of ErbB4 isoforms, a few interesting questions remain unresolved. First, despite unique signaling properties of each of the four isoforms (JMa/Cyt-1, JMa/Cyt-2, JMb/Cyt-1, JMb/Cyt-2), it is unclear how splice variants at the two splice sites in the juxtamembrane and cytoplasmic region are combined. Indirect evidence from cell type-specific analyses suggests that all four possible combinations are expressed in the brain, but direct evidence and exact ratios of these combinations remain to be presented. Long-read RNA sequencing spanning both alternative splice sites could give valuable insight^{246, 247}. Second, the regulation of alternative splicing of ErbB4 constitutes a fascinating research direction. Splicing is regulated by regulatory factors that bind to *cis* regulatory splicing elements in intronic regions of the pre-mRNA and either enhance or suppress the inclusion of an alternative exon in mature mRNA transcripts²⁴. Isoform analyses in Cyt-1 mutant mice suggest that the disruption of Cyt splicing does not affect JM splicing (Fig. 6.1). Independent alternative splicing at the two loci seems reasonable given the distance (1189bp); however, no information is available on the regulation of ErbB4 splicing. It would be very interesting to address how exon inclusion differs in cell types that are characterized by distinct isoform expression (e.g. oligodendrocytes, choroidal epithelium vs. GABAergic interneurons). One possible approach would be to analyze regulatory proteins bound to ErbB4

transcripts. A variety of different techniques are available to capture RNA binding proteins and analyze downstream by mass spectrometry³⁷⁹. The identification of splicing regulation could be even of potential therapeutic value, as ErbB4 splicing is dysregulated in schizophrenia^{28, 218, 222, 223}. SNPs in the intron 12 and surrounding exon 3 have been previously associated with increased JMa and Cyt-1 transcript levels, respectively²²³. Although aberrant splicing was reported for many schizophrenia candidate genes and splicing alterations were previously suggested as potential underlying pathology for schizophrenia, molecular mechanisms remain largely unknown^{25, 289, 380}. Third, although I analyzed splice variant expression at a cellular level, only one transcript at the time could be visualized, leaving the question open if different juxtamembrane and cytoplasmic variants are co-expressed in a single cell. While this work was ongoing, a new version of exon-specific ISH (Duplex BaseScope, ACD) was released, that permits theoretically the analysis of two splice variants at the same time. However, the assay is purely chromogenic and, in my hands, resulted in lower signal-to-noise compared to the fluorescent detection that ultimately precluded the successful co-detection of two low-abundance isoforms (e.g. Cyt-1 and Cyt-2). Technically challenging and costly single-cell RNA approaches such as single-cell RNA sequencing, microfluidic based RT-PCR or emerging Patch-Seq, that additionally conveys morphological and electrophysiological information, would be insightful in this regard^{243, 381, 382}. Single-cell RNA approaches or RNA sequencing from purified cell populations also could give interesting information about population-specific ErbB4 splice variant expression²⁴⁸ similar to the already unrevealed cell type-specific JM expression between glia and neurons (Fig. 4.6). Of particular interest is the expression of ErbB4 splice variants in subclasses of interneurons or dopaminergic neurons³⁸³⁻³⁸⁵. Neuronal subgroups, that I was blind to in my studies, could differ in their isoform composition which could be intriguing with regard to divergent localization and receptor functions.

Here, I presented first time evidence for the existence of ErbB4 on axons of dopaminergic neurons (Fig. 5.1). Axonal/ presynaptic localization of ErbB4 on dopaminergic projections is contrary to the established dogma of somatodendritic localization of the receptor in most GABAergic interneurons⁵⁸ (see also Fig. 5.3) and has important implication for local (somatodendritic) versus distal (axonal) functions of ErbB4. For instance, ErbB4 on dopaminergic fibers in distal target areas such as the hippocampus can modulate locally

extracellular dopamine levels, γ -oscillations and synaptic plasticity^{138, 234, 322} on a faster time scale than when mediated through distal soma and dendrites in the mesencephalon¹⁸⁵. Despite previous reports on differential neurite targeting of isoforms, among others NRG1 isoforms^{39, 324, 325}, my data does not support the hypothesis of different subcellular localizations of ErbB4 isoforms, as all four ErbB4 isoforms were confined to the somatodendritic compartment when overexpressed in cultured hippocampal PV+ interneurons (Fig. 5.3). While suggesting a very strict restriction of ErbB4 in PV+ basket cells, this does not exclude the possibility of isoform-specific neurite targeting in other cell types such as PV+ Chandelier interneurons (previously suggested to be characterized by presynaptic ErbB4 accumulation^{60, 68, 69, 123}) and dopaminergic neurons, and therefore requires further investigation. The question whether the expression of ErbB4 variants differs among subpopulations of dopamine neurons (e.g. in the VTA and SNc) is of particular interest considering the recently discovered opposing dopamine alterations in different target areas. In NRG2 and ErbB4 KO mice, basal extracellular dopamine levels are increased in the dorsal striatum and decreased in the mPFC and dHpp (the latter only analyzed in ErbB4 KO mice)¹³⁵ (Skirzewski et al., *in preparation*). Interestingly, it is entirely unclear why in ErbB4 mice that only lack ErbB4 in Th+ (dopamine) neurons, dopamine imbalances occur in the opposite direction²³⁴. Regardless, taken together, this suggests that nigrostriatal and mesocorticolimbic dopamine pathways might be differentially regulated by ErbB4. This of course raises the question as to whether ErbB4 is targeted to different compartments or microdomains³⁸⁶ of SNc and VTA dopamine neurons and thus modulates these two dopaminergic populations in distinct ways. By immunohistochemistry, we could so far not unambiguously identify ErbB4 expression on dopaminergic fibers of either the SNc or VTA (L. Erben & I. Karavanova *unpublished data*). Divergence in targeting to the axon or axonal microdomains³⁸⁶ could be regulated by a difference in ErbB4 isoform expression between SNc and VTA dopamine neurons, alongside the potential unique downstream signaling pathways and functions that each isoform exerts. Preliminary analyses comparing ErbB4 variant expression in the SNc and VTA, however, did not suggest any obvious differences in isoform expression. Finally, the differences in altered dopamine levels in striatal and cortical projection areas might not be intrinsic to the dopamine neuron itself but regulated on the input, output and the circuit level. Differences exist for instance in the presence of ErbB4+ neurons in the projecting areas. Cortical and hippocampal interneurons express high levels of ErbB4, while

ErbB4+ GABAergic interneurons are sparse in the dorsal striatum (caudate putamen)⁵⁷. On the other hand, VTA dopamine neurons are inhibited by ErbB4+ GABAergic interneurons in the VTA³⁸⁷. This could potentially also explain why extracellular dopamine concentrations are altered contradistinctively in Th-Cre; ErbB4^{fl/fl} mice compared to NRG2 and ErbB4 KO mice that affect not only dopaminergic neurons but also GABAergic (and in the case of NRG2 also glutamatergic) neurons. The aforementioned imbalances in NRG and ErbB4 mutant mice are particularly interesting as schizophrenia patients suffer from similar dysregulations, hypodopaminergia in cortical areas versus hyperdopaminergia in the striatum^{19, 184}. Further studies to comprehend the pathophysiology behind this imbalance and the involvement of ErbB4 will be necessary.

7.2 ErbB4 isoform function *in vivo*

In order to address the function of ErbB4 *in vivo*, we generated the first isoform-specific ErbB4 mutant mouse that specifically lacks Cyt-1 variants. Cyt-1 ErbB4 receptors were of particular interest to us, as they possess the unique capability to directly activate PI3K/Akt signaling and both Cyt-1, as well as PI3K/Akt, have previously been described to be altered in schizophrenia patients^{28, 224, 388}. Despite Cyt-1 comprising almost half of ErbB4 receptor transcripts, homozygote Cyt-1 mutant mice surprisingly show no phenotypes in our extensive neurodevelopmental analyses regarding GABAergic interneuron density, neurochemical assessment of extracellular dopamine levels in the mPFC and behavioral tests addressed (open field, elevated plus maze, PPI, Y-maze, Barnes maze, homecage activity, progressive ratio in operant task; Chapter 6). This could indicate that Cyt-1 and Cyt-2 ErbB4 receptors have redundant functions in the brain, although they were previously suggested to activate distinct downstream signaling and exert divergent functions in a variety of *in vitro* and *ex vivo* approaches^{213, 219-221}. In germline deletions like the EIIa-mediated ablation of Cyt-1, long-term adaption and compensation of the system to the loss of the gene, also needs to be considered. Several mechanisms have been previously characterized to account for genetic compensation or transcriptional adaption. In many cases related genes are upregulated and compensate for the loss³⁸⁹. However, at least at the RNA level, total ErbB4 expression remains unchanged in Cyt-1 mutant mice and the only other NRG-binding ErbB receptor, ErbB3, is unaltered (Fig. 6.1). Moreover, the transcriptome of Cyt-1 mutant mice is completely unchanged in the dorsal

hippocampus and whole genome RNA sequencing revealed only a dozen of altered genes in the mesencephalon (Fig. 6.7). Phenotypic discrepancies and compensatory mechanisms have been previously reported between knock-out and knock-down in mice and human models³⁸⁹. Similarly, compensation could be effective in homozygote Cyt-1 mutants, but not heterozygote Cyt-1 mutants resulting in mild phenotypes when Cyt-1 transcript levels are reduced but not absent. This could also be potentially interesting regarding ErbB4 variant changes in schizophrenia, as altered ratios were reported, but not the complete deficiency of one variant^{28, 218, 223}. Finally, global loss-of-functions can be compensated through embryonic development, whereas the conditional ablation at later time points result in phenotypes³⁸⁹. This is in line with the alterations of neurodevelopmental transcription factors that we observed in our transcriptomic analyses in the mesencephalon of Cyt-1 mutants (Fig. 6.7). Moreover, the adult ablation of ErbB4 recently has been shown to cause similar behavioral phenotypes with relevance to schizophrenia than the germline deletion¹¹⁸. Therefore, I am currently following up our study using adult and region-specific ablation methods that circumvent a possible compensation throughout development. First, I am in the process of generating tamoxifen-inducible Cre; Cyt-1^{fl/fl} mice to induce postnatal but global ablation of Cyt-1 transcripts as in¹¹⁸. Second, I am acutely deleting Cyt-1 transcripts by viral Cre recombinase injections into the VTA of adult Cyt-1^{fl/fl} mice, where we observed potential compensatory transcriptional changes. In order to elucidate adult brain function of Cyt-1 ErbB4 receptors, these mice will be subjected to similar behavioral and neurochemical analyses than the germline ablation.

Here, we analyzed the role of Cyt-1 in the brain by generating isoform-specific mutant mice. ErbB4 is also expressed in other tissues (e.g. heart, lung, kidney, ovary)²¹³. ErbB4 is essential for heart trabeculation and ErbB4 mutant embryo die midgestation (E10-E11) due to myocardial deficits¹⁵⁶. Although Cyt-1 comprises ~80% of ErbB4 transcripts in the heart²¹³ and Cyt-1 receptors are sufficient to rescue heart abnormalities in ErbB4 mutant mice¹⁵⁷, Cyt-1 mutant mice are viable and the Cyt-1 cassette therefore dispensable for heart trabeculation. Moreover, Cyt-1 receptors are described in the regulation of mammary gland development and carcinogenesis³⁴⁹. Splice-switching oligonucleotides suppressing Cyt-1 variants have been shown to decrease the growth of xenografted breast tumors²¹⁷. Cyt-1 transcripts are also associated with poor survival and tumor grade in serous ovarian cancer³⁵⁰. It therefore would be interesting to address phenotypes of Cyt-1 mutant mice in tissues other than the brain.

Besides Cyt-1 ErbB4 receptors, it also would be intriguing to study the *in vivo* functions of the other three main ErbB4 variants in the brain by generating similar isoform-specific mutant mice. Of particular interest could be JMa receptors, due to their unique transcriptional activity⁴⁸ and augmentation in postmortem schizophrenic tissue²¹⁸. Moreover, I characterized several cell types that exclusively express JMa variants. The successful generation of JMa or JMb mutant mice could be a challenge, as the exons encoding JMa and JMb are only separated by an 121bp intron, running the risk of interfering with regulatory sequences. Advances in generating mutant mice lines using CRISPR (Clustered Regulatory Interspaced Short Palindromic Repeats) at least can shorten generation time and the intron between the two JM exons harbors four potential PAM (protospacer adjacent motif) sequences with a specificity score greater than 80 (CRISPOR³⁹⁰) necessary for CRISPR/Cas9 editing. On the other hand, the generation of Cyt-2 mutants, i.e. forcing the spliceosome to always include the Cyt-1 exon could be achieved by removing the 1169bp intron between the Cyt-1 exon and the subsequent exon 27. In addition, more specific and local *in vivo* functions of ErbB4 could be addressed by overexpression, knockdown, isoform-specific antibodies or splice-switching oligonucleotides^{48, 216, 217}.

In sum, my dissertation work provides novel quantitative *in situ* hybridization tools to analyze cellular expression of splice variants. Using the developed approaches an exhaustive expression analysis of ErbB4 splice variants in the mouse brain was conducted that describes regional and cell type-specific differences in expression. Surprisingly, ErbB4 isoforms do not play a role in directing ErbB4 receptors to their target location on dendrites and axons of distinct neuronal cell types, and the detailed examination of the first isoform-specific Cyt-1 mutant mice did not uncover any phenotypes. Nevertheless, the presented work highlights the necessity for further isoform-specific studies to ultimately advance our understanding of ErbB4 variant-specific pathophysiological changes observed in schizophrenia.

8

Appendix

Acknowledgments

I would like to thank my mentor Dr. Andres Buonanno for giving me the opportunity to pursue my PhD research in his laboratory. It has been a privilege to witness and thrive from his years of experience. I am thankful for the innumerable training opportunities and support he has provided – most notably a three-week course at the Cold Spring Harbor Laboratory and a presentation at the NICHD principal investigators meeting. Andres has made a great contribution in making me the scientist that I am today, and I am certain that I will continue to grow from his extensive advice in my future career. I am thankful to Prof. Dr. Andreas Zimmer for accepting me as his student and dedicating his precious time to supervise me. I am further grateful to the Intramural Research Program at the National Institute of Child Health and Human Development (NICHD) for funding my PhD and, together with the Graduate Student Partnership Program (GPP), the Office of Intramural Training and Education (OITE) and the Foundation for Advanced Education in the Sciences (FAES) providing a great environment for my training. This work would not have been possible without the great core facilities and their staff, namely the Microscopy and Imaging Core (NICHD), the Light Imaging Facility (NINDS), the Rodent Behavior Core (NIMH), the Human Brain Core Collection (NIMH), the Molecular Genomics Core (NICHD), and the animal facility of the Porter Neuroscience Research Center. Thanks also to my collaborators at Advanced Cell Diagnostics.

Most importantly, I also would like to thank all current and former lab members for their continuous help and advice. Drs. Detlef Vullhorst, Irina Karavanova and Miguel Skirzewski are true role models that I look up to, and I learned so much from. I am grateful to Marie

Cronin, Ricardo Murphy and Arihant Chadda for their incredible help and dedication to our joint projects, and to Daniel Abebe for his relentless help with animal caretaking.

I also would like to thank my family and friends that supported me throughout my PhD. I am grateful to the new friends that I made alongside this journey, in science but also outside. Thanks to my best friends Marisa and Henrike for their weekly skype support across three time zones and truly understanding my dreams. I am very thankful to Pablo for sharing this PhD experience in a foreign country with me, his patience, motivation and love he has given me. Finally, I am grateful to my parents, grandmother and siblings for their unconditional love, bringing me up with a mindset that anything is achievable, believing in me and supporting me to go abroad even if it meant to sacrifice the time spent with each other.

Eidesstattliche Erklärung

Hiermit erkläre ich an Eides statt, dass die vorliegende Dissertation – abgesehen von den ausdrücklich bezeichneten Hilfsmitteln – persönlich, selbstständig und ohne Benutzung anderer als der angegebenen Hilfsmittel angefertigt wurde; die aus anderen Quellen direkt oder indirekt übernommen Daten und Konzepte unter Angabe der Quelle kenntlich gemacht sind; kein früherer Promotionsversuch unternommen worden ist; die vorgelegte Arbeit oder ähnliche Arbeiten nicht bereits anderweitig als Dissertation eingereicht worden ist bzw. sind; für die inhaltlich-materielle Erstellung der vorgelegten Arbeit keine fremde Hilfe, insbesondere keine entgeltliche Hilfe von Vermittlungs- bzw. Beratungsdiensten in Anspruch genommen wurde, sowie keinerlei Dritte vom Doktoranden unmittelbar oder mittelbar geldwerte Leistungen für Tätigkeiten erhalten haben, die im Zusammenhang mit dem Inhalt der vorgelegten Arbeit stehen.

Washington, den 17. April

Larissa Erben

List of abbreviations

AAV – adeno-associated virus	D2DR – dopamine receptor D2
ACD – Advanced Cell Diagnostics	DA – dopamine
ADAM – a disintegrin and metalloproteinase domain-containing protein	DABCO – 1,4-diazabicyclo[2.2.2]octane
AIS – axon initial segment	DAPI – 4',6-diamidino-2-phenylindole
Akt – protein kinase B	DAT – dopamine transporter
AMP – amplification solution	del.3 – exon 3 deletion
AMPA – α -amino-3-hydroxy-5-methyl-4-isoxazolepropionic acid	DEPC – diethyl pyrocarbonate
AMPAR – AMPA receptor	dHpp – dorsal hippocampus
ANOVA – analysis of variance	DIV – days in vitro
BACE1 – β -site amyloid precursor protein cleaving enzyme	DLPFC – dorsolateral prefrontal cortex
BBB – blood brain barrier	Dlx6 – distal-less homeobox 6
BSA – bovine serum albumin	DMEM – Dulbecco's modified eagle medium
C1/C2/C3 – channel 1/2/3	E – embryonic day
CA – Cornu ammonis	ECD – extracellular domain
CAMKII – Ca^{2+} /calmodulin-dependent protein kinase-II	EGF – epidermal growth factor
CC – corpus callosum	ErbB4 – avian erythroblastosis virus oncogene B4
CCK – cholecystokinin	ERT2 – tamoxifen-inducible estrogen receptor 2
cDNA – complementary DNA	FBS – fetal bovine serum
CNP – cyclic-nucleotide phosphodiesterase	FFPE – formalin-fixed paraffin-embedded
CNS – central nervous system	FUDR – floxuridine
Cp – choroid plexus	GABA – gamma-aminobutyric acid
CR – calretinin	GAD – glutamate decarboxylase
CSF – cerebrospinal fluid	GE – ganglionic eminence
Ctx – Cortex	GFP – green fluorescent protein
Cyt/CYT – cytoplasmic region	GluN2B – NMDA receptor subunit 2B
	GWAS – genome-wide association study
	HBSS – Hank's balanced salt solution
	HEK – human embryonic kidney

HEPES – 4-(2-hydroxyethyl)-1-piperazineethanesulfonic acid
 Hpp – hippocampus
 hSynI – human synapsin I
 ICD – intracellular domain
 Ig – immunoglobulin
 IHC – immunohistochemistry
 ISH – *in situ* hybridization
 JM – juxtamembrane
 KO – knock-out
 Kv – voltage-gated potassium channel
 LDS – lithium dodecyl sulfate
 LTP – long-term potentiation
 LUHMES – Lund Human Mesencephalic
 MAG – myelin-associated glycoprotein
 MAP2 – microtubule associated protein 2
 MAPK – mitogen-activated protein kinase
 MCS – multiple cloning site
 mEPSC – miniature excitatory postsynaptic current
 MGE – medial ganglionic eminence
 mGluR1 – metabotropic glutamate receptor 1
 mHab – medial habenula
 MHC – myosin heavy chain
 mIPSC – miniature inhibitory postsynaptic current
 mPFC – medial prefrontal cortex
 NBF – normal buffered formalin
 NG2 – neural/glial antigen 2
 NMDA – N-methyl-D-aspartate
 NMDAR – NMDA receptor
 NNF – no-net flux
 nNOS – neuronal nitric oxide synthetase
 NRG – Neuregulin
 OB – olfactory bulb
 OPC – oligodendrocyte precursor cell
 P – postnatal day
 PAEZ – pre-axonic exclusion zone
 PBS – phosphate buffered saline
 PDL – poly-D-lysine
 Pen – penicillin
 PFA – paraformaldehyde
 PFC – prefrontal cortex
 PI3K – phosphatidylinositol-3-kinase
 PKC – protein kinase C
 PNS – peripheral nervous system
 PPI – prepulse inhibition
 PSD – postsynaptic density
 PSD-95 – postsynaptic density protein 95
 PV – parvalbumin
 qPCR – quantitative polymerase chain reaction
 qRT-PCR – quantitative real-time polymerase chain reaction
 Raf – rapidly accelerated fibrosarcoma
 RIPA – radioimmunoprecipitation assay
 RMS – rostral migratory stream
 RNAseq – RNA sequencing
 ROI – region of interest
 RRID – Research Resource Identifier
 Rsc – retrosplenial cortex
 RT – room temperature
 RT-PCR – reverse transcription polymerase chain reaction
 Rtn – reticular thalamic nucleus
 SC – Schaffer collateral

Scz – schizophrenia
SEM – standard error of the mean
SNc – substantia nigra pars compacta
SNP – single nucleotide polymorphism
SOM – somatostatin
SSCtx – somatosensory cortex
STAT – signal transducer and activator of transcription
Strep – streptomycin
SVZ – subventricular zone
TACE – tumor necrosis factor α -converting enzyme
TBST – tris-buffered saline + Tween-20

TCA – thalamocortical axons
Th – tyrosine hydroxylase
Thal – thalamus
TM – transmembrane
UTR – untranslated region
vGLUT1/2 – vesicular glutamate transporter 1/2
VIP – vasoactive intestinal peptide
VTA – ventral tegmental area
WT – wild-type
YAP – Yes associated protein

List of figures

Figure 1.1 Soluble and transmembrane Neuregulins.	5
Figure 1.2 ErbB receptor family and canonical signaling pathways.	7
Figure 1.3 Regulation of neurodevelopment by NRG/ErbB4.	10
Figure 1.4 Regulation of cortical and hippocampal circuits by Neuregulin/ErbB4 signaling.	15
Figure 1.5 Alternative splicing of ErbB4 and isoform-specific downstream signaling.	23
Figure 2.1 Splicing scheme of ErbB4.	30
Figure 2.2 Example of end-point PCR analysis of the 3' end of the ErbB4 transcript.	35
Figure 2.3 Analysis of ErbB4 splice variants in the mouse brain by RNA sequencing.	36
Figure 3.1 Overview of protocols described in this article.	43
Figure 3.2 Short print-out protocol for RNAscope and BaseScope assays on fresh-frozen and paraffin sections as well as on adherent cell culture samples.	46
Figure 3.3 Multiplexing of the three channels in RNAscope.	46
Figure 3.4 Example for RNAscope on fresh-frozen section (Basic Protocol 1).	48
Figure 3.5 Quantitative analysis of an exemplary RNAscope experiment.	49
Figure 3.6 Example for RNAscope on FFPE sections (Alternate Protocol 1) and adherent cell culture (Alternate Protocol 2).	54
Figure 3.7 Exon-specific BaseScope experiment on FFPE sections (Basic Protocol 2).	58
Figure 3.8 Examples for chromogenic BaseScope detection (Basic Protocol 2) and ISH-IHC combination (Basic Protocol 3).	67
Figure 3.9 Quantification of multiplex fluorescent ISH signal (e.g., RNAscope) with CellProfiler.	72
Figure 4.1 Scheme summarizing ErbB4 isoforms and single-pair probe design.	85
Figure 4.2 Single-pair probes targeting unique exon junctions are specific and sensitive.	89
Figure 4.3 Detection levels for independent probes targeting distinct exon junctions are similar and differ markedly from background in ErbB4- $\Delta 2$ KOs.	90
Figure 4.4 JMb- and CYT-2-containing transcripts are the major ErbB4 isoforms expressed in adult hippocampus.	92
Figure 4.5 Pattern of ErbB4 JMa and CYT-1 isoform expression in the corpus callosum differ markedly from other brain areas.	93
Figure 4.6 Oligodendrocytes and GABAergic neurons in the corpus callosum express different ErbB4 juxtamembrane isoforms.	94
Figure 4.7 Distinct patterns of ErbB4 JM and CYT isoforms in the grey and white matter are conserved between humans and mice.	96
Figure 4.8 Visualization of exon-specific and multiplex ISH signal by fluorescent and chromogenic dyes in hippocampal GABAergic interneurons.	105
Figure 4.9 TaqMan qRT-PCR analysis of ErbB4 isoforms in the adult mouse hippocampus (Hpp) and corpus callosum (CC).	106
Figure 4.10 ErbB4 isoform expression pattern in the retrosplenial cortex and the thalamic reticular nucleus are similar to the hippocampus.	107
Figure 4.11 As in the corpus callosum, JMa and CYT-1 isoforms are the major ErbB4 variants expressed in the thalamus.	108

Figure 4.12	Detection of low-abundant transcripts is increased when using multiple probe pairs.	109
Figure 4.13	In the choroid plexus, ErbB4 JMa is the predominant juxtamembrane splice variant.	111
Figure 5.1	ErbB4 mRNA and protein is expressed in soma and axons of midbrain dopaminergic neurons.	126
Figure 5.2	ErbB4 does not interact with DAT, and DAT expression is not altered in ErbB4 knock-out (KO) mice.	128
Figure 5.3	Subcellular targeting of ErbB4 isoforms in hippocampal PV interneurons.	130
Figure 6.1	Generation and validation of isoform-specific ErbB4 Cyt-1 knock-out mice by transcript analyses.	147
Figure 6.2	Expression of ErbB4 Cyt variants in hippocampal and cortical interneurons.	149
Figure 6.3	Expression of Cyt transcripts during development.	150
Figure 6.4	GABAergic interneurons in the hippocampus and primary somatosensory cortex are unaltered in Cyt-1 mutant mice.	151
Figure 6.5	Schizophrenia-related behaviors are unchanged in Cyt-1 mutant mice.	153
Figure 6.6	ErbB4 Cyt variants in the ventral tegmental area (VTA).	154
Figure 6.7	Cyt-1 mutant mice have unaltered working and reference memory, and cognitive flexibility.	156
Figure 6.8	Cyt expression in the medial habenula and habenula-regulated behaviors.	157
Figure 6.9	Gene expression analysis in the VTA of Cyt-1 mutant mice.	159

List of tables

Table 2.1	Primer pairs for end-point PCR	33
Table 3.1	Software to Analyze ISH Signal.	71
Table 4.1	Exon junction-specific single-pair probes for the detection of distinct ErbB4 isoforms	87
Table 4.2	TaqMan probes	103
Table 4.3	Quantification and statistical analysis of ErbB4 expression in the medial habenula (mHab) and the hippocampus (Hpp) using pan ErbB4 single-pair probes.	111
Table 4.4	Quantification and statistical analysis of ErbB4 expression in the adult hippocampus (Hpp) using isoform-specific single-pair probes.	112
Table 4.5	Quantification and statistical analysis of ErbB4 isoform expression in various adult brain region using isoform-specific single-pair probes.	113
Table 4.6	Histogram distribution of number of cells with same amount of dots in hippocampus of WT and ErbB4- Δ 2 KO mice.	114
Table 4.7	ErbB4 isoform expression in human cingulate cortex and corpus callosum.	114
Table 4.8	Quantification and statistical analysis of ErbB4 expression in the hippocampus (Hpp) comparing single-pair probes to probes using 20 pairs.	115
Table 4.9	Quantification and statistical analysis of ErbB4 JMa expression in the hippocampus (Hpp) comparing probes using one or two probe pairs, respectively.	115
Table 4.10	Quantification and statistical analysis of ErbB4 splice variants in the choroid plexus (Cp).	116

Reprints and Permissions

Permission from the publishers has been obtained to include published content in this dissertation.

1) Erben & Buonanno (2019) *Detection and Quantification of Multiple RNA Sequences Using Emerging Ultrasensitive Fluorescent In Situ Hybridization Techniques. Curr Protoc Neurosci, 87(1).*

Wiley's Self-Archiving Policy: Authors of articles published in Wiley journals are permitted to self-archive the submitted (preprint) version of the article at any time, and may self-archive the accepted (peer-reviewed) version after an embargo period.

“Permission is granted for you to use the material requested for your thesis/dissertation subject to the usual acknowledgements (author, title of material, title of book/journal, ourselves as publisher) and on the understanding that you will reapply for permission if you wish to distribute or publish your thesis/dissertation commercially.” – obtained from Paisley Chesters, permission co-ordinator at Wiley, on 04/09/2019

2) Erben et al. (2018) *A novel ultrasensitive in situ hybridization approach to detect short sequences and splice variants with cellular resolution. Mol Neurobiol, 55(7):6169-6181.*



RightsLink®

SPRINGER NATURE

Title: A Novel Ultrasensitive In Situ Hybridization Approach to Detect Short Sequences and Splice Variants with Cellular Resolution
Author: Larissa Erben, Ming-Xiao He, Annelies Laeremans et al
Publication: Molecular Neurobiology
Publisher: Springer Nature
Date: Jan 1, 2017
Copyright © 2017, The Author(s)

Creative Commons

This is an open access article distributed under the terms of the [Creative Commons CC BY](https://creativecommons.org/licenses/by/4.0/) license, which permits unrestricted use, distribution, and reproduction in any medium, provided the original work is properly cited.

You are not required to obtain permission to reuse this article.

To request permission for a type of use not listed, please contact [Springer Nature](https://www.springer.com/permissions)

To order reprints of this content, please contact Springer Nature by e-mail at reprintswarehouse@springernature.com, and you will be contacted very shortly with a quote.

This article is licensed under the Creative Commons Attribution 4.0 (<http://creativecommons.org/licenses/by/4.0/>) which permits unrestricted use, distribution, modification and reproduction in any medium. Chapter 4 represents an extended version of the

article which was edited to fit the format of this dissertation. Added sections are highlighted in dark grey italics.

3) *Skirzewski et al. (2018) ErbB4 signaling in dopaminergic axonal projections increases extracellular dopamine levels and regulates spatial/working memory behavior. Mol Psychiatry (23), 2227-2237.*



RightsLink®

SPRINGER NATURE

Title: ErbB4 signaling in dopaminergic axonal projections increases extracellular dopamine levels and regulates spatial/working memory behaviors
Author: M Skirzewski et al
Publication: Molecular Psychiatry
Publisher: Springer Nature
Date: Jul 20, 2017
Copyright © 2017, Springer Nature

Creative Commons

The request you have made is considered to be non-commercial/educational. As the article you have requested has been distributed under a Creative Commons license (Attribution-Noncommercial), you may reuse this material for non-commercial/educational purposes without obtaining additional permission from Springer Nature, providing that the author and the original source of publication are fully acknowledged (please see the article itself for the license version number). You may reuse this material without obtaining permission from Springer Nature, providing that the author and the original source of publication are fully acknowledged, as per the terms of the license. For license terms, please see <http://creativecommons.org/>

Copyright for content of original publications in Molecular Psychiatry (Springer Nature) remains with the Author that has the right to reproduce the article in whole or parts in any printed volume (book or thesis) of which they are the author.

References

1. Lewis, D.A. & Lieberman, J.A. Catching up on schizophrenia: natural history and neurobiology. *Neuron* **28**, 325-334 (2000).
2. Lewis, D.A. & Sweet, R.A. Schizophrenia from a neural circuitry perspective: advancing toward rational pharmacological therapies. *J Clin Invest* **119**, 706-716 (2009).
3. Avramopoulos, D. Recent Advances in the Genetics of Schizophrenia. *Mol Neuropsychiatry* **4**, 35-51 (2018).
4. Greenwood, T.A., Light, G.A., Swerdlow, N.R., Radant, A.D. & Braff, D.L. Association analysis of 94 candidate genes and schizophrenia-related endophenotypes. *PLoS One* **7**, e29630 (2012).
5. DiLalla, L.F., McCrary, M. & Diaz, E. A review of endophenotypes in schizophrenia and autism: The next phase for understanding genetic etiologies. *Am J Med Genet C Semin Med Genet* **175**, 354-361 (2017).
6. *American Psychiatric Association: Diagnostic and Statistical Manual of Mental Disorders* (American Psychiatric Association, Arlington, 2013).
7. Haller, C.S., Padmanabhan, J.L., Lizano, P., Torous, J. & Keshavan, M. Recent advances in understanding schizophrenia. *F1000Prime Rep* **6**, 57 (2014).
8. Tsuang, M.T., Stone, W.S. & Faraone, S.V. Genes, environment and schizophrenia. *Br J Psychiatry Suppl* **40**, s18-24 (2001).
9. Harrison, P.J. & Weinberger, D.R. Schizophrenia genes, gene expression, and neuropathology: on the matter of their convergence. *Mol Psychiatry* **10**, 40-68; image 45 (2005).
10. Schizophrenia Working Group of the Psychiatric Genomics, C. Biological insights from 108 schizophrenia-associated genetic loci. *Nature* **511**, 421-427 (2014).
11. Lewis, D.A. & Levitt, P. Schizophrenia as a disorder of neurodevelopment. *Annu Rev Neurosci* **25**, 409-432 (2002).
12. Kapur, S. & Remington, G. Atypical antipsychotics: new directions and new challenges in the treatment of schizophrenia. *Annu Rev Med* **52**, 503-517 (2001).
13. Leucht, S., *et al.* Comparative efficacy and tolerability of 15 antipsychotic drugs in schizophrenia: a multiple-treatments meta-analysis. *Lancet* **382**, 951-962 (2013).
14. Miyamoto, S., Duncan, G.E., Marx, C.E. & Lieberman, J.A. Treatments for schizophrenia: a critical review of pharmacology and mechanisms of action of antipsychotic drugs. *Mol Psychiatry* **10**, 79-104 (2005).
15. Laruelle, M., Kegeles, L.S. & Abi-Dargham, A. Glutamate, dopamine, and schizophrenia: from pathophysiology to treatment. *Ann N Y Acad Sci* **1003**, 138-158 (2003).
16. Goto, Y. & Grace, A.A. The dopamine system and the pathophysiology of schizophrenia: a basic science perspective. *Int Rev Neurobiol* **78**, 41-68 (2007).
17. Coyle, J.T. Glutamate and schizophrenia: beyond the dopamine hypothesis. *Cell Mol Neurobiol* **26**, 365-384 (2006).
18. Selten, M., van Bokhoven, H. & Nadif Kasri, N. Inhibitory control of the excitatory/inhibitory balance in psychiatric disorders. *F1000Res* **7**, 23 (2018).
19. Weinstein, J.J., *et al.* Pathway-Specific Dopamine Abnormalities in Schizophrenia. *Biol Psychiatry* **81**, 31-42 (2017).
20. McCutcheon, R.A., Abi-Dargham, A. & Howes, O.D. Schizophrenia, Dopamine and the Striatum: From Biology to Symptoms. *Trends Neurosci* **42**, 205-220 (2019).
21. Gonzalez-Burgos, G. & Lewis, D.A. GABA neurons and the mechanisms of network oscillations: implications for understanding cortical dysfunction in schizophrenia. *Schizophr Bull* **34**, 944-961 (2008).
22. Woo, T.U., Walsh, J.P. & Benes, F.M. Density of glutamic acid decarboxylase 67 messenger RNA-containing neurons that express the N-methyl-D-aspartate receptor subunit NR2A in the anterior cingulate cortex in schizophrenia and bipolar disorder. *Arch Gen Psychiatry* **61**, 649-657 (2004).
23. Buonanno, A. The neuregulin signaling pathway and schizophrenia: from genes to synapses and neural circuits. *Brain Res Bull* **83**, 122-131 (2010).
24. Licatalosi, D.D. & Darnell, R.B. Splicing regulation in neurologic disease. *Neuron* **52**, 93-101 (2006).
25. Morikawa, T. & Manabe, T. Aberrant regulation of alternative pre-mRNA splicing in schizophrenia. *Neurochem Int* **57**, 691-704 (2010).
26. Glatt, S.J., Cohen, O.S., Faraone, S.V. & Tsuang, M.T. Dysfunctional gene splicing as a potential contributor to neuropsychiatric disorders. *Am J Med Genet B Neuropsychiatr Genet* **156B**, 382-392 (2011).
27. Stefansson, H., *et al.* Neuregulin 1 and susceptibility to schizophrenia. *Am J Hum Genet* **71**, 877-892 (2002).

28. Silberberg, G., Darvasi, A., Pinkas-Kramarski, R. & Navon, R. The involvement of ErbB4 with schizophrenia: association and expression studies. *Am J Med Genet B Neuropsychiatr Genet* **141B**, 142-148 (2006).
29. Benzel, I., *et al.* Interactions among genes in the ErbB-Neuregulin signalling network are associated with increased susceptibility to schizophrenia. *Behav Brain Funct* **3**, 31 (2007).
30. Mei, L. & Nave, K.A. Neuregulin-ERBB signaling in the nervous system and neuropsychiatric diseases. *Neuron* **83**, 27-49 (2014).
31. Mostaid, M.S., *et al.* Neuregulin-1 and schizophrenia in the genome-wide association study era. *Neurosci Biobehav Rev* **68**, 387-409 (2016).
32. Mei, L. & Xiong, W.C. Neuregulin 1 in neural development, synaptic plasticity and schizophrenia. *Nat Rev Neurosci* **9**, 437-452 (2008).
33. Chen, Y., Hancock, M.L., Role, L.W. & Talmage, D.A. Intramembranous valine linked to schizophrenia is required for neuregulin 1 regulation of the morphological development of cortical neurons. *J Neurosci* **30**, 9199-9208 (2010).
34. Walsh, T., *et al.* Rare structural variants disrupt multiple genes in neurodevelopmental pathways in schizophrenia. *Science* **320**, 539-543 (2008).
35. Buonanno, A. & Fischbach, G.D. Neuregulin and ErbB receptor signaling pathways in the nervous system. *Curr Opin Neurobiol* **11**, 287-296 (2001).
36. Iwakura, Y. & Nawa, H. ErbB1-4-dependent EGF/neuregulin signals and their cross talk in the central nervous system: pathological implications in schizophrenia and Parkinson's disease. *Front Cell Neurosci* **7**, 4 (2013).
37. Falls, D.L. Neuregulins: functions, forms, and signaling strategies. *Exp Cell Res* **284**, 14-30 (2003).
38. Birchmeier, C. ErbB receptors and the development of the nervous system. *Exp Cell Res* **315**, 611-618 (2009).
39. Vullhorst, D., Ahmad, T., Karavanova, I., Keating, C. & Buonanno, A. Structural Similarities between Neuregulin 1-3 Isoforms Determine Their Subcellular Distribution and Signaling Mode in Central Neurons. *J Neurosci* **37**, 5232-5249 (2017).
40. Vullhorst, D., *et al.* A negative feedback loop controls NMDA receptor function in cortical interneurons via neuregulin 2/ErbB4 signalling. *Nat Commun* **6**, 7222 (2015).
41. Meyer, D., *et al.* Isoform-specific expression and function of neuregulin. *Development* **124**, 3575-3586 (1997).
42. Cho, H.S., *et al.* Structure of the extracellular region of HER2 alone and in complex with the Herceptin Fab. *Nature* **421**, 756-760 (2003).
43. Guy, P.M., Platko, J.V., Cantley, L.C., Cerione, R.A. & Carraway, K.L., 3rd. Insect cell-expressed p180erbB3 possesses an impaired tyrosine kinase activity. *Proc Natl Acad Sci U S A* **91**, 8132-8136 (1994).
44. Rai, S.N., *et al.* The Role of PI3K/Akt and ERK in Neurodegenerative Disorders. *Neurotox Res* **35**, 775-795 (2019).
45. Yarden, Y. The EGFR family and its ligands in human cancer. signalling mechanisms and therapeutic opportunities. *Eur J Cancer* **37 Suppl 4**, S3-8 (2001).
46. Mitchell, R.M., *et al.* ErbB4 reduces synaptic GABAA currents independent of its receptor tyrosine kinase activity. *Proc Natl Acad Sci U S A* **110**, 19603-19608 (2013).
47. Ni, C.Y., Murphy, M.P., Golde, T.E. & Carpenter, G. gamma -Secretase cleavage and nuclear localization of ErbB-4 receptor tyrosine kinase. *Science* **294**, 2179-2181 (2001).
48. Sardi, S.P., Murtie, J., Koirala, S., Patten, B.A. & Corfas, G. Presenilin-dependent ErbB4 nuclear signaling regulates the timing of astrogenesis in the developing brain. *Cell* **127**, 185-197 (2006).
49. Carpenter, G. Nuclear localization and possible functions of receptor tyrosine kinases. *Curr Opin Cell Biol* **15**, 143-148 (2003).
50. Steiner, H., Blum, M., Kitai, S.T. & Fedi, P. Differential expression of ErbB3 and ErbB4 neuregulin receptors in dopamine neurons and forebrain areas of the adult rat. *Exp Neurol* **159**, 494-503 (1999).
51. Pinkas-Kramarski, R., *et al.* Differential expression of NDF/neuregulin receptors ErbB-3 and ErbB-4 and involvement in inhibition of neuronal differentiation. *Oncogene* **15**, 2803-2815 (1997).
52. Gerecke, K.M., Wyss, J.M., Karavanova, I., Buonanno, A. & Carroll, S.L. ErbB transmembrane tyrosine kinase receptors are differentially expressed throughout the adult rat central nervous system. *J Comp Neurol* **433**, 86-100 (2001).
53. Abe, Y., Namba, H., Zheng, Y. & Nawa, H. In situ hybridization reveals developmental regulation of ErbB1-4 mRNA expression in mouse midbrain: implication of ErbB receptors for dopaminergic neurons. *Neuroscience* **161**, 95-110 (2009).
54. Yau, H.J., Wang, H.F., Lai, C. & Liu, F.C. Neural development of the neuregulin receptor ErbB4 in the cerebral cortex and the hippocampus: preferential expression by interneurons tangentially migrating from the ganglionic eminences. *Cereb Cortex* **13**, 252-264 (2003).

55. Kornblum, H.I., Yanni, D.S., Easterday, M.C. & Seroogy, K.B. Expression of the EGF receptor family members ErbB2, ErbB3, and ErbB4 in germinal zones of the developing brain and in neurosphere cultures containing CNS stem cells. *Dev Neurosci* **22**, 16-24 (2000).
56. Lai, C. & Lemke, G. An extended family of protein-tyrosine kinase genes differentially expressed in the vertebrate nervous system. *Neuron* **6**, 691-704 (1991).
57. Bean, J.C., *et al.* Genetic labeling reveals novel cellular targets of schizophrenia susceptibility gene: distribution of GABA and non-GABA ErbB4-positive cells in adult mouse brain. *J Neurosci* **34**, 13549-13566 (2014).
58. Vullhorst, D., *et al.* Selective expression of ErbB4 in interneurons, but not pyramidal cells, of the rodent hippocampus. *J Neurosci* **29**, 12255-12264 (2009).
59. Neddens, J., *et al.* Conserved interneuron-specific ErbB4 expression in frontal cortex of rodents, monkeys, and humans: implications for schizophrenia. *Biol Psychiatry* **70**, 636-645 (2011).
60. Fazzari, P., *et al.* Control of cortical GABA circuitry development by Nrg1 and ErbB4 signalling. *Nature* **464**, 1376-1380 (2010).
61. Wen, L., *et al.* Neuregulin 1 regulates pyramidal neuron activity via ErbB4 in parvalbumin-positive interneurons. *Proc Natl Acad Sci U S A* **107**, 1211-1216 (2010).
62. Yin, D.M., *et al.* Regulation of spine formation by ErbB4 in PV-positive interneurons. *J Neurosci* **33**, 19295-19303 (2013).
63. Neddens, J. & Buonanno, A. Selective populations of hippocampal interneurons express ErbB4 and their number and distribution is altered in ErbB4 knockout mice. *Hippocampus* **20**, 724-744 (2010).
64. Batista-Brito, R., *et al.* Developmental Dysfunction of VIP Interneurons Impairs Cortical Circuits. *Neuron* **95**, 884-895 e889 (2017).
65. Huang, Y.Z., *et al.* Regulation of neuregulin signaling by PSD-95 interacting with ErbB4 at CNS synapses. *Neuron* **26**, 443-455 (2000).
66. Garcia, R.A., Vasudevan, K. & Buonanno, A. The neuregulin receptor ErbB-4 interacts with PDZ-containing proteins at neuronal synapses. *Proc Natl Acad Sci U S A* **97**, 3596-3601 (2000).
67. Longart, M., Chatani-Hinze, M., Gonzalez, C.M., Vullhorst, D. & Buonanno, A. Regulation of ErbB-4 endocytosis by neuregulin in GABAergic hippocampal interneurons. *Brain Res Bull* **73**, 210-219 (2007).
68. Del Pino, I., *et al.* Erbb4 deletion from fast-spiking interneurons causes schizophrenia-like phenotypes. *Neuron* **79**, 1152-1168 (2013).
69. Tai, Y., Janas, J.A., Wang, C.L. & Van Aelst, L. Regulation of chandelier cell cartridge and bouton development via DOCK7-mediated ErbB4 activation. *Cell Rep* **6**, 254-263 (2014).
70. Yang, J.M., *et al.* erbb4 Deficits in Chandelier Cells of the Medial Prefrontal Cortex Confer Cognitive Dysfunctions: Implications for Schizophrenia. *Cereb Cortex* (2018).
71. Cao, S.X., *et al.* ErbB4 deletion in noradrenergic neurons in the locus coeruleus induces mania-like behavior via elevated catecholamines. *Elife* **7** (2018).
72. Fox, I.J. & Kornblum, H.I. Developmental profile of ErbB receptors in murine central nervous system: implications for functional interactions. *J Neurosci Res* **79**, 584-597 (2005).
73. Ozaki, M., Sasner, M., Yano, R., Lu, H.S. & Buonanno, A. Neuregulin-beta induces expression of an NMDA-receptor subunit. *Nature* **390**, 691-694 (1997).
74. Rio, C., Rieff, H.I., Qi, P., Khurana, T.S. & Corfas, G. Neuregulin and erbB receptors play a critical role in neuronal migration. *Neuron* **19**, 39-50 (1997).
75. Bernstein, H.G., *et al.* Localization of neuregulin-1alpha (heregulin-alpha) and one of its receptors, ErbB-4 tyrosine kinase, in developing and adult human brain. *Brain Res Bull* **69**, 546-559 (2006).
76. Thompson, M., *et al.* Widespread expression of ErbB2, ErbB3 and ErbB4 in non-human primate brain. *Brain Res* **1139**, 95-109 (2007).
77. Zheng, Y., *et al.* Expression of ErbB4 in substantia nigra dopamine neurons of monkeys and humans. *Prog Neuropsychopharmacol Biol Psychiatry* **33**, 701-706 (2009).
78. Marin, O. & Rubenstein, J.L. Cell migration in the forebrain. *Annu Rev Neurosci* **26**, 441-483 (2003).
79. Flames, N., *et al.* Short- and long-range attraction of cortical GABAergic interneurons by neuregulin-1. *Neuron* **44**, 251-261 (2004).
80. Li, H., Chou, S.J., Hamasaki, T., Perez-Garcia, C.G. & O'Leary, D.D. Neuregulin repellent signaling via ErbB4 restricts GABAergic interneurons to migratory paths from ganglionic eminence to cortical destinations. *Neural Dev* **7**, 10 (2012).
81. Bartolini, G., *et al.* Neuregulin 3 Mediates Cortical Plate Invasion and Laminar Allocation of GABAergic Interneurons. *Cell Rep* **18**, 1157-1170 (2017).

82. Martini, F.J., *et al.* Biased selection of leading process branches mediates chemotaxis during tangential neuronal migration. *Development* **136**, 41-50 (2009).
83. Fisahn, A., Neddens, J., Yan, L. & Buonanno, A. Neuregulin-1 modulates hippocampal gamma oscillations: implications for schizophrenia. *Cereb Cortex* **19**, 612-618 (2009).
84. Lois, C., Garcia-Verdugo, J.M. & Alvarez-Buylla, A. Chain migration of neuronal precursors. *Science* **271**, 978-981 (1996).
85. Anton, E.S., *et al.* Receptor tyrosine kinase ErbB4 modulates neuroblast migration and placement in the adult forebrain. *Nat Neurosci* **7**, 1319-1328 (2004).
86. Ghashghaei, H.T., *et al.* The role of neuregulin-ErbB4 interactions on the proliferation and organization of cells in the subventricular zone. *Proc Natl Acad Sci U S A* **103**, 1930-1935 (2006).
87. Zhang, H., He, X., Mei, Y. & Ling, Q. Ablation of ErbB4 in parvalbumin-positive interneurons inhibits adult hippocampal neurogenesis through down-regulating BDNF/TrkB expression. *J Comp Neurol* **526**, 2482-2492 (2018).
88. Gerecke, K.M., Wyss, J.M. & Carroll, S.L. Neuregulin-1beta induces neurite extension and arborization in cultured hippocampal neurons. *Mol Cell Neurosci* **27**, 379-393 (2004).
89. Lopez-Bendito, G., *et al.* Tangential neuronal migration controls axon guidance: a role for neuregulin-1 in thalamocortical axon navigation. *Cell* **125**, 127-142 (2006).
90. Lemke, G. Neuregulin-1 and myelination. *Sci STKE* **2006**, pe11 (2006).
91. Birchmeier, C. & Bennett, D.L. Neuregulin/ErbB Signaling in Developmental Myelin Formation and Nerve Repair. *Curr Top Dev Biol* **116**, 45-64 (2016).
92. Michailov, G.V., *et al.* Axonal neuregulin-1 regulates myelin sheath thickness. *Science* **304**, 700-703 (2004).
93. Taveggia, C., *et al.* Neuregulin-1 type III determines the ensheathment fate of axons. *Neuron* **47**, 681-694 (2005).
94. Vartanian, T., Goodearl, A., Viehover, A. & Fischbach, G. Axonal neuregulin signals cells of the oligodendrocyte lineage through activation of HER4 and Schwann cells through HER2 and HER3. *J Cell Biol* **137**, 211-220 (1997).
95. Garratt, A.N., Voiculescu, O., Topilko, P., Charnay, P. & Birchmeier, C. A dual role of erbB2 in myelination and in expansion of the schwann cell precursor pool. *J Cell Biol* **148**, 1035-1046 (2000).
96. Miyamoto, Y., *et al.* Neuregulin-1 type III knockout mice exhibit delayed migration of Schwann cell precursors. *Biochem Biophys Res Commun* **486**, 506-513 (2017).
97. Chen, S., *et al.* Neuregulin 1-erbB signaling is necessary for normal myelination and sensory function. *J Neurosci* **26**, 3079-3086 (2006).
98. Flores, A.I., *et al.* Akt-mediated survival of oligodendrocytes induced by neuregulins. *J Neurosci* **20**, 7622-7630 (2000).
99. Canoll, P.D., *et al.* GGF/neuregulin is a neuronal signal that promotes the proliferation and survival and inhibits the differentiation of oligodendrocyte progenitors. *Neuron* **17**, 229-243 (1996).
100. Sussman, C.R., Vartanian, T. & Miller, R.H. The ErbB4 neuregulin receptor mediates suppression of oligodendrocyte maturation. *J Neurosci* **25**, 5757-5762 (2005).
101. Fernandez, P.A., *et al.* Evidence that axon-derived neuregulin promotes oligodendrocyte survival in the developing rat optic nerve. *Neuron* **28**, 81-90 (2000).
102. Calaora, V., *et al.* Neuregulin signaling regulates neural precursor growth and the generation of oligodendrocytes in vitro. *J Neurosci* **21**, 4740-4751 (2001).
103. Taveggia, C., *et al.* Type III neuregulin-1 promotes oligodendrocyte myelination. *Glia* **56**, 284-293 (2008).
104. Brinkmann, B.G., *et al.* Neuregulin-1/ErbB signaling serves distinct functions in myelination of the peripheral and central nervous system. *Neuron* **59**, 581-595 (2008).
105. Ortega, M.C., *et al.* Neuregulin-1/ErbB4 signaling controls the migration of oligodendrocyte precursor cells during development. *Exp Neurol* **235**, 610-620 (2012).
106. Makinodan, M., Rosen, K.M., Ito, S. & Corfas, G. A critical period for social experience-dependent oligodendrocyte maturation and myelination. *Science* **337**, 1357-1360 (2012).
107. Schmucker, J., *et al.* erbB3 is dispensable for oligodendrocyte development in vitro and in vivo. *Glia* **44**, 67-75 (2003).
108. Fields, R.D. A new mechanism of nervous system plasticity: activity-dependent myelination. *Nat Rev Neurosci* **16**, 756-767 (2015).
109. Davis, K.L., *et al.* White matter changes in schizophrenia: evidence for myelin-related dysfunction. *Arch Gen Psychiatry* **60**, 443-456 (2003).
110. Hakak, Y., *et al.* Genome-wide expression analysis reveals dysregulation of myelination-related genes in chronic schizophrenia. *Proc Natl Acad Sci U S A* **98**, 4746-4751 (2001).

111. Hoistad, M., *et al.* Linking white and grey matter in schizophrenia: oligodendrocyte and neuron pathology in the prefrontal cortex. *Front Neuroanat* **3**, 9 (2009).
112. Georgieva, L., *et al.* Convergent evidence that oligodendrocyte lineage transcription factor 2 (OLIG2) and interacting genes influence susceptibility to schizophrenia. *Proc Natl Acad Sci U S A* **103**, 12469-12474 (2006).
113. Zuliani, R., *et al.* Genetic variants in the ErbB4 gene are associated with white matter integrity. *Psychiatry Res* **191**, 133-137 (2011).
114. Rico, B. & Marin, O. Neuregulin signaling, cortical circuitry development and schizophrenia. *Curr Opin Genet Dev* **21**, 262-270 (2011).
115. Hahn, C.G., *et al.* Altered neuregulin 1-erbB4 signaling contributes to NMDA receptor hypofunction in schizophrenia. *Nat Med* **12**, 824-828 (2006).
116. Ting, A.K., *et al.* Neuregulin 1 promotes excitatory synapse development and function in GABAergic interneurons. *J Neurosci* **31**, 15-25 (2011).
117. Yang, J.M., *et al.* Development of GABA circuitry of fast-spiking basket interneurons in the medial prefrontal cortex of erbB4-mutant mice. *J Neurosci* **33**, 19724-19733 (2013).
118. Wang, H., *et al.* Genetic recovery of ErbB4 in adulthood partially restores brain functions in null mice. *Proc Natl Acad Sci U S A* **115**, 13105-13110 (2018).
119. Krivosheya, D., *et al.* ErbB4-neuregulin signaling modulates synapse development and dendritic arborization through distinct mechanisms. *J Biol Chem* **283**, 32944-32956 (2008).
120. Janssen, M.J., Leiva-Salcedo, E. & Buonanno, A. Neuregulin directly decreases voltage-gated sodium current in hippocampal ErbB4-expressing interneurons. *J Neurosci* **32**, 13889-13895 (2012).
121. Chang, Q. & Fischbach, G.D. An acute effect of neuregulin 1 beta to suppress alpha 7-containing nicotinic acetylcholine receptors in hippocampal interneurons. *J Neurosci* **26**, 11295-11303 (2006).
122. Li, K.X., *et al.* Neuregulin 1 regulates excitability of fast-spiking neurons through Kv1.1 and acts in epilepsy. *Nat Neurosci* **15**, 267-273 (2011).
123. Woo, R.S., *et al.* Neuregulin-1 enhances depolarization-induced GABA release. *Neuron* **54**, 599-610 (2007).
124. Chen, Y.J., *et al.* ErbB4 in parvalbumin-positive interneurons is critical for neuregulin 1 regulation of long-term potentiation. *Proc Natl Acad Sci U S A* **107**, 21818-21823 (2010).
125. Tan, Z., *et al.* Dynamic ErbB4 Activity in Hippocampal-Prefrontal Synchrony and Top-Down Attention in Rodents. *Neuron* **98**, 380-393 e384 (2018).
126. Nusser, Z., Sieghart, W., Benke, D., Fritschy, J.M. & Somogyi, P. Differential synaptic localization of two major gamma-aminobutyric acid type A receptor alpha subunits on hippocampal pyramidal cells. *Proc Natl Acad Sci U S A* **93**, 11939-11944 (1996).
127. Pierri, J.N., Chaudry, A.S., Woo, T.U. & Lewis, D.A. Alterations in chandelier neuron axon terminals in the prefrontal cortex of schizophrenic subjects. *Am J Psychiatry* **156**, 1709-1719 (1999).
128. Konopaske, G.T., Sweet, R.A., Wu, Q., Sampson, A. & Lewis, D.A. Regional specificity of chandelier neuron axon terminal alterations in schizophrenia. *Neuroscience* **138**, 189-196 (2006).
129. Guan, Y.F., *et al.* Neuregulin 1 protects against ischemic brain injury via ErbB4 receptors by increasing GABAergic transmission. *Neuroscience* **307**, 151-159 (2015).
130. Barros, C.S., *et al.* Impaired maturation of dendritic spines without disorganization of cortical cell layers in mice lacking NRG1/ErbB signaling in the central nervous system. *Proc Natl Acad Sci U S A* **106**, 4507-4512 (2009).
131. Li, B., Woo, R.S., Mei, L. & Malinow, R. The neuregulin-1 receptor erbB4 controls glutamatergic synapse maturation and plasticity. *Neuron* **54**, 583-597 (2007).
132. Chen, Y.J., *et al.* Type III neuregulin-1 is required for normal sensorimotor gating, memory-related behaviors, and corticostriatal circuit components. *J Neurosci* **28**, 6872-6883 (2008).
133. Cahill, M.E., *et al.* Neuregulin1 signaling promotes dendritic spine growth through kalirin. *J Neurochem* **126**, 625-635 (2013).
134. Glantz, L.A. & Lewis, D.A. Decreased dendritic spine density on prefrontal cortical pyramidal neurons in schizophrenia. *Arch Gen Psychiatry* **57**, 65-73 (2000).
135. Yan, L., *et al.* Neuregulin-2 ablation results in dopamine dysregulation and severe behavioral phenotypes relevant to psychiatric disorders. *Mol Psychiatry* **23**, 1233-1243 (2018).
136. Lisman, J., Yasuda, R. & Raghavachari, S. Mechanisms of CaMKII action in long-term potentiation. *Nat Rev Neurosci* **13**, 169-182 (2012).
137. Kwon, O.B., Longart, M., Vullhorst, D., Hoffman, D.A. & Buonanno, A. Neuregulin-1 reverses long-term potentiation at CA1 hippocampal synapses. *J Neurosci* **25**, 9378-9383 (2005).
138. Kwon, O.B., *et al.* Neuregulin-1 regulates LTP at CA1 hippocampal synapses through activation of dopamine D4 receptors. *Proc Natl Acad Sci U S A* **105**, 15587-15592 (2008).

139. Pitcher, G.M., Beggs, S., Woo, R.S., Mei, L. & Salter, M.W. ErbB4 is a suppressor of long-term potentiation in the adult hippocampus. *Neuroreport* **19**, 139-143 (2008).
140. Iyengar, S.S. & Mott, D.D. Neuregulin blocks synaptic strengthening after epileptiform activity in the rat hippocampus. *Brain Res* **1208**, 67-73 (2008).
141. Ma, L., *et al.* Ligand-dependent recruitment of the ErbB4 signaling complex into neuronal lipid rafts. *J Neurosci* **23**, 3164-3175 (2003).
142. Shamir, A., *et al.* The importance of the NRG-1/ErbB4 pathway for synaptic plasticity and behaviors associated with psychiatric disorders. *J Neurosci* **32**, 2988-2997 (2012).
143. Kato, T., *et al.* Transient exposure of neonatal mice to neuregulin-1 results in hyperdopaminergic states in adulthood: implication in neurodevelopmental hypothesis for schizophrenia. *Mol Psychiatry* **16**, 307-320 (2011).
144. Hou, X.J., Ni, K.M., Yang, J.M. & Li, X.M. Neuregulin 1/ErbB4 enhances synchronized oscillations of prefrontal cortex neurons via inhibitory synapses. *Neuroscience* **261**, 107-117 (2014).
145. Kawata, M., Morikawa, S., Shiosaka, S. & Tamura, H. Ablation of neuropsin-neuregulin 1 signaling imbalances ErbB4 inhibitory networks and disrupts hippocampal gamma oscillation. *Transl Psychiatry* **7**, e1052 (2017).
146. Wilson, T.W., *et al.* Cortical gamma generators suggest abnormal auditory circuitry in early-onset psychosis. *Cereb Cortex* **18**, 371-378 (2008).
147. Kwon, J.S., *et al.* Gamma frequency-range abnormalities to auditory stimulation in schizophrenia. *Arch Gen Psychiatry* **56**, 1001-1005 (1999).
148. Gu, Y., *et al.* Neuregulin-Dependent Regulation of Fast-Spiking Interneuron Excitability Controls the Timing of the Critical Period. *J Neurosci* **36**, 10285-10295 (2016).
149. Sun, Y., *et al.* Neuregulin-1/ErbB4 Signaling Regulates Visual Cortical Plasticity. *Neuron* **92**, 160-173 (2016).
150. Hensch, T.K. Critical period plasticity in local cortical circuits. *Nat Rev Neurosci* **6**, 877-888 (2005).
151. Grieco, S.F., Holmes, T.C. & Xu, X. Neuregulin directed molecular mechanisms of visual cortical plasticity. *J Comp Neurol* **527**, 668-678 (2019).
152. van den Buuse, M. Modeling the positive symptoms of schizophrenia in genetically modified mice: pharmacology and methodology aspects. *Schizophr Bull* **36**, 246-270 (2010).
153. Arguello, P.A. & Gogos, J.A. Cognition in mouse models of schizophrenia susceptibility genes. *Schizophr Bull* **36**, 289-300 (2010).
154. O'Tuathaigh, C.M., Kirby, B.P., Moran, P.M. & Waddington, J.L. Mutant mouse models: genotype-phenotype relationships to negative symptoms in schizophrenia. *Schizophr Bull* **36**, 271-288 (2010).
155. Meyer, D. & Birchmeier, C. Multiple essential functions of neuregulin in development. *Nature* **378**, 386-390 (1995).
156. Gassmann, M., *et al.* Aberrant neural and cardiac development in mice lacking the ErbB4 neuregulin receptor. *Nature* **378**, 390-394 (1995).
157. Tidcombe, H., *et al.* Neural and mammary gland defects in ErbB4 knockout mice genetically rescued from embryonic lethality. *Proc Natl Acad Sci U S A* **100**, 8281-8286 (2003).
158. Duffy, L., Cappas, E., Scimone, A., Schofield, P.R. & Karl, T. Behavioral profile of a heterozygous mutant mouse model for EGF-like domain neuregulin 1. *Behav Neurosci* **122**, 748-759 (2008).
159. Duffy, L., Cappas, E., Lai, D., Boucher, A.A. & Karl, T. Cognition in transmembrane domain neuregulin 1 mutant mice. *Neuroscience* **170**, 800-807 (2010).
160. Karl, T., Duffy, L., Scimone, A., Harvey, R.P. & Schofield, P.R. Altered motor activity, exploration and anxiety in heterozygous neuregulin 1 mutant mice: implications for understanding schizophrenia. *Genes Brain Behav* **6**, 677-687 (2007).
161. Moy, S.S., *et al.* Deficient NRG1-ERBB signaling alters social approach: relevance to genetic mouse models of schizophrenia. *J Neurodev Disord* **1**, 302-312 (2009).
162. O'Tuathaigh, C.M., *et al.* Schizophrenia-related endophenotypes in heterozygous neuregulin-1 'knockout' mice. *Eur J Neurosci* **31**, 349-358 (2010).
163. O'Tuathaigh, C.M., *et al.* Sexually dimorphic changes in the exploratory and habituation profiles of heterozygous neuregulin-1 knockout mice. *Neuroreport* **17**, 79-83 (2006).
164. Rimer, M., Barrett, D.W., Maldonado, M.A., Vock, V.M. & Gonzalez-Lima, F. Neuregulin-1 immunoglobulin-like domain mutant mice: clozapine sensitivity and impaired latent inhibition. *Neuroreport* **16**, 271-275 (2005).
165. Hayes, L.N., *et al.* Neuregulin 3 Knockout Mice Exhibit Behaviors Consistent with Psychotic Disorders. *Mol Neuropsychiatry* **2**, 79-87 (2016).
166. Loos, M., *et al.* Neuregulin-3 in the mouse medial prefrontal cortex regulates impulsive action. *Biol Psychiatry* **76**, 648-655 (2014).

167. Lu, Y., *et al.* Maintenance of GABAergic activity by neuregulin 1-ErbB4 in amygdala for fear memory. *Neuron* **84**, 835-846 (2014).
168. O'Tuathaigh, C.M.P., *et al.* Specialized Information Processing Deficits and Distinct Metabolomic Profiles Following TM-Domain Disruption of Nrg1. *Schizophr Bull* **43**, 1100-1113 (2017).
169. Kato, T., *et al.* Phenotypic characterization of transgenic mice overexpressing neuregulin-1. *PLoS One* **5**, e14185 (2010).
170. Deakin, I.H., *et al.* Behavioural characterization of neuregulin 1 type I overexpressing transgenic mice. *Neuroreport* **20**, 1523-1528 (2009).
171. Deakin, I.H., *et al.* Transgenic overexpression of the type I isoform of neuregulin 1 affects working memory and hippocampal oscillations but not long-term potentiation. *Cereb Cortex* **22**, 1520-1529 (2012).
172. Luo, X., He, W., Hu, X. & Yan, R. Reversible overexpression of bace1-cleaved neuregulin-1 N-terminal fragment induces schizophrenia-like phenotypes in mice. *Biol Psychiatry* **76**, 120-127 (2014).
173. Yin, D.M., *et al.* Reversal of behavioral deficits and synaptic dysfunction in mice overexpressing neuregulin 1. *Neuron* **78**, 644-657 (2013).
174. Role, L.W. & Talmage, D.A. Neurobiology: new order for thought disorders. *Nature* **448**, 263-265 (2007).
175. Bjarnadottir, M., *et al.* Neuregulin1 (NRG1) signaling through Fyn modulates NMDA receptor phosphorylation: differential synaptic function in NRG1+/- knock-outs compared with wild-type mice. *J Neurosci* **27**, 4519-4529 (2007).
176. Thuret, S., *et al.* The neuregulin receptor, ErbB4, is not required for normal development and adult maintenance of the substantia nigra pars compacta. *J Neurochem* **91**, 1302-1311 (2004).
177. Zhang, L., *et al.* Neurotrophic and neuroprotective effects of the neuregulin glial growth factor-2 on dopaminergic neurons in rat primary midbrain cultures. *J Neurochem* **91**, 1358-1368 (2004).
178. Carlsson, T., *et al.* Systemic administration of neuregulin-1beta1 protects dopaminergic neurons in a mouse model of Parkinson's disease. *J Neurochem* **117**, 1066-1074 (2011).
179. Depboylu, C., Rosler, T.W., de Andrade, A., Oertel, W.H. & Hoglinger, G.U. Systemically administered neuregulin-1beta1 rescues nigral dopaminergic neurons via the ErbB4 receptor tyrosine kinase in MPTP mouse models of Parkinson's disease. *J Neurochem* **133**, 590-597 (2015).
180. Roy, K., *et al.* Loss of erbB signaling in oligodendrocytes alters myelin and dopaminergic function, a potential mechanism for neuropsychiatric disorders. *Proc Natl Acad Sci U S A* **104**, 8131-8136 (2007).
181. Newell, K.A., Karl, T. & Huang, X.F. A neuregulin 1 transmembrane domain mutation causes imbalanced glutamatergic and dopaminergic receptor expression in mice. *Neuroscience* **248**, 670-680 (2013).
182. Golani, I., Tadmor, H., Buonanno, A., Kremer, I. & Shamir, A. Disruption of the ErbB signaling in adolescence increases striatal dopamine levels and affects learning and hedonic-like behavior in the adult mouse. *Eur Neuropsychopharmacol* **24**, 1808-1818 (2014).
183. Nawa, H., Sotoyama, H., Iwakura, Y., Takei, N. & Namba, H. Neuropathologic implication of peripheral neuregulin-1 and EGF signals in dopaminergic dysfunction and behavioral deficits relevant to schizophrenia: their target cells and time window. *Biomed Res Int* **2014**, 697935 (2014).
184. Slifstein, M., *et al.* Deficits in prefrontal cortical and extrastriatal dopamine release in schizophrenia: a positron emission tomographic functional magnetic resonance imaging study. *JAMA Psychiatry* **72**, 316-324 (2015).
185. Yurek, D.M., Zhang, L., Fletcher-Turner, A. & Seroogy, K.B. Supranigral injection of neuregulin1-beta induces striatal dopamine overflow. *Brain Res* **1028**, 116-119 (2004).
186. Ledonne, A., *et al.* Neuregulin 1 signalling modulates mGluR1 function in mesencephalic dopaminergic neurons. *Mol Psychiatry* **20**, 959-973 (2015).
187. Namba, H., Okubo, T. & Nawa, H. Perinatal Exposure to Neuregulin-1 Results in Disinhibition of Adult Midbrain Dopaminergic Neurons: Implication in Schizophrenia Modeling. *Sci Rep* **6**, 22606 (2016).
188. Ledonne, A. & Mercuri, N.B. mGluR1-Dependent Long Term Depression in Rodent Midbrain Dopamine Neurons Is Regulated by Neuregulin 1/ErbB Signaling. *Front Mol Neurosci* **11**, 346 (2018).
189. Neddens, J., Vullhorst, D., Paredes, D. & Buonanno, A. Neuregulin links dopaminergic and glutamatergic neurotransmission to control hippocampal synaptic plasticity. *Commun Integr Biol* **2**, 261-264 (2009).
190. Elenius, K., *et al.* A novel juxtamembrane domain isoform of HER4/ErbB4. Isoform-specific tissue distribution and differential processing in response to phorbol ester. *J Biol Chem* **272**, 26761-26768 (1997).
191. Elenius, K., *et al.* Characterization of a naturally occurring ErbB4 isoform that does not bind or activate phosphatidylinositol 3-kinase. *Oncogene* **18**, 2607-2615 (1999).
192. Erben, L., He, M.X., Laeremans, A., Park, E. & Buonanno, A. A Novel Ultrasensitive In Situ Hybridization Approach to Detect Short Sequences and Splice Variants with Cellular Resolution. *Mol Neurobiol* **55**, 6169-6181 (2018).

193. Tan, W., Dean, M. & Law, A.J. Molecular cloning and characterization of the human ErbB4 gene: identification of novel splice isoforms in the developing and adult brain. *PLoS One* **5**, e12924 (2010).
194. Rio, C., Buxbaum, J.D., Peschon, J.J. & Corfas, G. Tumor necrosis factor-alpha-converting enzyme is required for cleavage of erbB4/HER4. *J Biol Chem* **275**, 10379-10387 (2000).
195. Cheng, Q.C., Tikhomirov, O., Zhou, W. & Carpenter, G. Ectodomain cleavage of ErbB-4: characterization of the cleavage site and m80 fragment. *J Biol Chem* **278**, 38421-38427 (2003).
196. Lu, Y.M., *et al.* Calpain-Dependent ErbB4 Cleavage Is Involved in Brain Ischemia-Induced Neuronal Death. *Mol Neurobiol* **53**, 2600-2609 (2016).
197. Lee, H.J., *et al.* Presenilin-dependent gamma-secretase-like intramembrane cleavage of ErbB4. *J Biol Chem* **277**, 6318-6323 (2002).
198. Jones, F.E. HER4 intracellular domain (4ICD) activity in the developing mammary gland and breast cancer. *J Mammary Gland Biol Neoplasia* **13**, 247-258 (2008).
199. Williams, C.C., *et al.* The ERBB4/HER4 receptor tyrosine kinase regulates gene expression by functioning as a STAT5A nuclear chaperone. *J Cell Biol* **167**, 469-478 (2004).
200. Zhu, Y., *et al.* Coregulation of estrogen receptor by ERBB4/HER4 establishes a growth-promoting autocrine signal in breast tumor cells. *Cancer Res* **66**, 7991-7998 (2006).
201. Aqeilan, R.I., *et al.* WW domain-containing proteins, WWOX and YAP, compete for interaction with ErbB-4 and modulate its transcriptional function. *Cancer Res* **65**, 6764-6772 (2005).
202. Omerovic, J., *et al.* Ligand-regulated association of ErbB-4 to the transcriptional co-activator YAP65 controls transcription at the nuclear level. *Exp Cell Res* **294**, 469-479 (2004).
203. Komuro, A., Nagai, M., Navin, N.E. & Sudol, M. WW domain-containing protein YAP associates with ErbB-4 and acts as a co-transcriptional activator for the carboxyl-terminal fragment of ErbB-4 that translocates to the nucleus. *J Biol Chem* **278**, 33334-33341 (2003).
204. Nakajo, H., *et al.* Role for tyrosine phosphorylation of SUV39H1 histone methyltransferase in enhanced trimethylation of histone H3K9 via neuregulin-1/ErbB4 nuclear signaling. *Biochem Biophys Res Commun* (2019).
205. Naresh, A., *et al.* The ERBB4/HER4 intracellular domain 4ICD is a BH3-only protein promoting apoptosis of breast cancer cells. *Cancer Res* **66**, 6412-6420 (2006).
206. Gambarotta, G., *et al.* ErbB4 expression in neural progenitor cells (ST14A) is necessary to mediate neuregulin-1beta1-induced migration. *J Biol Chem* **279**, 48808-48816 (2004).
207. Sundvall, M., *et al.* Isoform-specific monoubiquitination, endocytosis, and degradation of alternatively spliced ErbB4 isoforms. *Proc Natl Acad Sci U S A* **105**, 4162-4167 (2008).
208. Feng, S.M., *et al.* The E3 ubiquitin ligase WWP1 selectively targets HER4 and its proteolytically derived signaling isoforms for degradation. *Mol Cell Biol* **29**, 892-906 (2009).
209. Li, Y., Zhou, Z., Alimandi, M. & Chen, C. WW domain containing E3 ubiquitin protein ligase 1 targets the full-length ErbB4 for ubiquitin-mediated degradation in breast cancer. *Oncogene* **28**, 2948-2958 (2009).
210. Zeng, F., Xu, J. & Harris, R.C. Nedd4 mediates ErbB4 JM-a/CYT-1 ICD ubiquitination and degradation in MDCK II cells. *FASEB J* **23**, 1935-1945 (2009).
211. Wali, V.B., *et al.* Convergent and divergent cellular responses by ErbB4 isoforms in mammary epithelial cells. *Mol Cancer Res* **12**, 1140-1155 (2014).
212. Kainulainen, V., *et al.* A natural ErbB4 isoform that does not activate phosphoinositide 3-kinase mediates proliferation but not survival or chemotaxis. *J Biol Chem* **275**, 8641-8649 (2000).
213. Veikkolainen, V., *et al.* Function of ERBB4 is determined by alternative splicing. *Cell Cycle* **10**, 2647-2657 (2011).
214. Hollmen, M. & Elenius, K. Potential of ErbB4 antibodies for cancer therapy. *Future Oncol* **6**, 37-53 (2010).
215. Di Marcotullio, L., Ferretti, E., De Smaele, E., Screpanti, I. & Gulino, A. Suppressors of hedgehog signaling: Linking aberrant development of neural progenitors and tumorigenesis. *Mol Neurobiol* **34**, 193-204 (2006).
216. Hollmen, M., Maatta, J.A., Bald, L., Sliwkowski, M.X. & Elenius, K. Suppression of breast cancer cell growth by a monoclonal antibody targeting cleavable ErbB4 isoforms. *Oncogene* **28**, 1309-1319 (2009).
217. Nielsen, T.O., Sorensen, S., Dagnaes-Hansen, F., Kjems, J. & Sorensen, B.S. Directing HER4 mRNA expression towards the CYT2 isoform by antisense oligonucleotide decreases growth of breast cancer cells in vitro and in vivo. *Br J Cancer* **108**, 2291-2298 (2013).
218. Chung, D.W., *et al.* Dysregulated ErbB4 Splicing in Schizophrenia: Selective Effects on Parvalbumin Expression. *Am J Psychiatry* **173**, 60-68 (2016).

219. Fregnan, F., Gnani, S., Macri, L., Perroteau, I. & Gambarotta, G. The four isoforms of the tyrosine kinase receptor ErbB4 provide neural progenitor cells with an adhesion preference for the transmembrane type III isoform of the ligand neuregulin 1. *Neuroreport* **25**, 233-241 (2014).
220. Fornasari, B.E., *et al.* Neuregulin1 alpha activates migration of neuronal progenitors expressing ErbB4. *Mol Cell Neurosci* **77**, 87-94 (2016).
221. Rakic, S., *et al.* Cdk5 phosphorylation of ErbB4 is required for tangential migration of cortical interneurons. *Cereb Cortex* **25**, 991-1003 (2015).
222. Joshi, D., Fullerton, J.M. & Weickert, C.S. Elevated ErbB4 mRNA is related to interneuron deficit in prefrontal cortex in schizophrenia. *J Psychiatr Res* **53**, 125-132 (2014).
223. Law, A.J., Kleinman, J.E., Weinberger, D.R. & Weickert, C.S. Disease-associated intronic variants in the ErbB4 gene are related to altered ErbB4 splice-variant expression in the brain in schizophrenia. *Hum Mol Genet* **16**, 129-141 (2007).
224. Law, A.J., *et al.* Neuregulin 1-ErbB4-PI3K signaling in schizophrenia and phosphoinositide 3-kinase-p110delta inhibition as a potential therapeutic strategy. *Proc Natl Acad Sci U S A* **109**, 12165-12170 (2012).
225. Chong, V.Z., *et al.* Elevated neuregulin-1 and ErbB4 protein in the prefrontal cortex of schizophrenic patients. *Schizophr Res* **100**, 270-280 (2008).
226. Chung, D.W., Chung, Y., Bazmi, H.H. & Lewis, D.A. Altered ErbB4 splicing and cortical parvalbumin interneuron dysfunction in schizophrenia and mood disorders. *Neuropsychopharmacology* **43**, 2478-2486 (2018).
227. Carpenter, A.E., *et al.* CellProfiler: image analysis software for identifying and quantifying cell phenotypes. *Genome Biol* **7**, R100 (2006).
228. Wang, L., *et al.* Brain Development and Akt Signaling: the Crossroads of Signaling Pathway and Neurodevelopmental Diseases. *J Mol Neurosci* **61**, 379-384 (2017).
229. Sanchez-Alegria, K., Flores-Leon, M., Avila-Munoz, E., Rodriguez-Corona, N. & Arias, C. PI3K Signaling in Neurons: A Central Node for the Control of Multiple Functions. *Int J Mol Sci* **19** (2018).
230. Gilbertson, R., *et al.* Novel ERBB4 juxtamembrane splice variants are frequently expressed in childhood medulloblastoma. *Genes Chromosomes Cancer* **31**, 288-294 (2001).
231. Gilmour, L.M., *et al.* Expression of erbB-4/HER-4 growth factor receptor isoforms in ovarian cancer. *Cancer Res* **61**, 2169-2176 (2001).
232. Zeng, N., *et al.* Real-time quantitative polymerase chain reaction (qPCR) analysis with fluorescence resonance energy transfer (FRET) probes reveals differential expression of the four ERBB4 juxtamembrane region variants between medulloblastoma and pilocytic astrocytoma. *Neuropathol Appl Neurobiol* **35**, 353-366 (2009).
233. Madisen, L., *et al.* A robust and high-throughput Cre reporting and characterization system for the whole mouse brain. *Nat Neurosci* **13**, 133-140 (2010).
234. Skirzewski, M., *et al.* ErbB4 signaling in dopaminergic axonal projections increases extracellular dopamine levels and regulates spatial/working memory behaviors. *Mol Psychiatry* **23**, 2227-2237 (2018).
235. Bruce, L.L., Kornblum, H.I. & Seroogy, K.B. Comparison of thalamic populations in mammals and birds: expression of ErbB4 mRNA. *Brain Res Bull* **57**, 455-461 (2002).
236. Trapnell, C., Pachter, L. & Salzberg, S.L. TopHat: discovering splice junctions with RNA-Seq. *Bioinformatics* **25**, 1105-1111 (2009).
237. Dobin, A., *et al.* STAR: ultrafast universal RNA-seq aligner. *Bioinformatics* **29**, 15-21 (2013).
238. Liao, Y., Smyth, G.K. & Shi, W. featureCounts: an efficient general purpose program for assigning sequence reads to genomic features. *Bioinformatics* **30**, 923-930 (2014).
239. Robinson, J.T., *et al.* Integrative genomics viewer. *Nat Biotechnol* **29**, 24-26 (2011).
240. Ovcharenko, I., Nobrega, M.A., Loots, G.G. & Stubbs, L. ECR Browser: a tool for visualizing and accessing data from comparisons of multiple vertebrate genomes. *Nucleic Acids Res* **32**, W280-286 (2004).
241. Houseley, J. & Tollervy, D. Apparent non-canonical trans-splicing is generated by reverse transcriptase in vitro. *PLoS One* **5**, e12271 (2010).
242. Tardaguila, M., *et al.* SQANTI: extensive characterization of long-read transcript sequences for quality control in full-length transcriptome identification and quantification. *Genome Res* (2018).
243. Arzalluz-Luque, A. & Conesa, A. Single-cell RNAseq for the study of isoforms-how is that possible? *Genome Biol* **19**, 110 (2018).
244. Hsu, S.N. & Hertel, K.J. Spliceosomes walk the line: splicing errors and their impact on cellular function. *RNA Biol* **6**, 526-530 (2009).
245. Oh, S.W., *et al.* A mesoscale connectome of the mouse brain. *Nature* **508**, 207-214 (2014).
246. Rhoads, A. & Au, K.F. PacBio Sequencing and Its Applications. *Genomics Proteomics Bioinformatics* **13**, 278-289 (2015).

247. Boldogkoi, Z., Moldovan, N., Balazs, Z., Snyder, M. & Tombacz, D. Long-Read Sequencing - A Powerful Tool in Viral Transcriptome Research. *Trends Microbiol* (2019).
248. Zhang, Y., *et al.* An RNA-sequencing transcriptome and splicing database of glia, neurons, and vascular cells of the cerebral cortex. *J Neurosci* **34**, 11929-11947 (2014).
249. Young, W.S., Song, J. & Mezey, E. Hybridization Histochemistry of Neural Transcripts. *Curr Protoc Neurosci* **82**, 1.3.1-1.3.27 (2018).
250. Wang, F., *et al.* RNAscope: a novel in situ RNA analysis platform for formalin-fixed, paraffin-embedded tissues. *J Mol Diagn* **14**, 22-29 (2012).
251. Baker, A.M., *et al.* Robust RNA-based in situ mutation detection delineates colorectal cancer subclonal evolution. *Nat Commun* **8**, 1998 (2017).
252. Del Castillo, P., Llorente, A.R. & Stockert, J.C. Influence of fixation, exciting light and section thickness on the primary fluorescence of samples for microfluorometric analysis. *Basic Appl Histochem* **33**, 251-257 (1989).
253. Dowson, J.H. The evaluation of autofluorescence emission spectra derived from neuronal lipopigment. *J Microsc* **128**, 261-270 (1982).
254. Schnell, S.A., Staines, W.A. & Wessendorf, M.W. Reduction of lipofuscin-like autofluorescence in fluorescently labeled tissue. *J Histochem Cytochem* **47**, 719-730 (1999).
255. Gerfen, C.R. Basic neuroanatomical methods. *Curr Protoc Neurosci* **Chapter 1**, Unit 1.1 (2003).
256. Zeller, R. Fixation, embedding, and sectioning of tissues, embryos, and single cells. *Curr Protoc Pharmacol* **Appendix 3**, 3D (2001).
257. Guo, X., *et al.* Quantitative Analysis of Alternative Pre-mRNA Splicing in Mouse Brain Sections Using RNA In Situ Hybridization Assay. *J Vis Exp* (2018).
258. Zhu, Y., *et al.* Novel Junction-specific and Quantifiable In Situ Detection of AR-V7 and its Clinical Correlates in Metastatic Castration-resistant Prostate Cancer. *Eur Urol* **73**, 727-735 (2018).
259. Anderson, C.M., *et al.* Visualizing Genetic Variants, Short Targets, and Point Mutations in the Morphological Tissue Context with an RNA In Situ Hybridization Assay. *J Vis Exp* (2018).
260. Haring, M., *et al.* Neuronal atlas of the dorsal horn defines its architecture and links sensory input to transcriptional cell types. *Nat Neurosci* **21**, 869-880 (2018).
261. Tan, J. & Yang, L. Long noncoding RNA VPS9D1-AS1 overexpression predicts a poor prognosis in non-small cell lung cancer. *Biomed Pharmacother* **106**, 1600-1606 (2018).
262. De Sa Nogueira, D., Merienne, K. & Befort, K. Neuroepigenetics and addictive behaviors: Where do we stand? *Neurosci Biobehav Rev* (2018).
263. Guillaumet-Adkins, A., *et al.* Epigenetics and Oxidative Stress in Aging. *Oxid Med Cell Longev* **2017**, 9175806 (2017).
264. Johnson, M.B. & Walsh, C.A. Cerebral cortical neuron diversity and development at single-cell resolution. *Curr Opin Neurobiol* **42**, 9-16 (2017).
265. Ayata, P., *et al.* Epigenetic regulation of brain region-specific microglia clearance activity. *Nat Neurosci* **21**, 1049-1060 (2018).
266. Cembrowski, M.S., *et al.* Dissociable Structural and Functional Hippocampal Outputs via Distinct Subiculum Cell Classes. *Cell* **173**, 1280-1292 e1218 (2018).
267. Shrestha, B.R., *et al.* Sensory Neuron Diversity in the Inner Ear Is Shaped by Activity. *Cell* **174**, 1229-1246 e1217 (2018).
268. Advanced Cell Diagnostics Troubleshooting Guide.
269. Holt, C.E. & Schuman, E.M. The central dogma decentralized: new perspectives on RNA function and local translation in neurons. *Neuron* **80**, 648-657 (2013).
270. Sahoo, P.K., Smith, D.S., Perrone-Bizzozero, N. & Twiss, J.L. Axonal mRNA transport and translation at a glance. *J Cell Sci* **131** (2018).
271. Li, H., Illenberger, J.M., McLaurin, K.A., Mactutus, C.F. & Booze, R.M. Identification of Dopamine D1-Alpha Receptor Within Rodent Nucleus Accumbens by an Innovative RNA In Situ Detection Technology. *J Vis Exp* (2018).
272. Wang, E.T., *et al.* Alternative isoform regulation in human tissue transcriptomes. *Nature* **456**, 470-476 (2008).
273. Iijima, T., Hidaka, C. & Iijima, Y. Spatio-temporal regulations and functions of neuronal alternative RNA splicing in developing and adult brains. *Neurosci Res* **109**, 1-8 (2016).
274. Kang, H.J., *et al.* Spatio-temporal transcriptome of the human brain. *Nature* **478**, 483-489 (2011).
275. Cull-Candy, S., Brickley, S. & Farrant, M. NMDA receptor subunits: diversity, development and disease. *Curr Opin Neurobiol* **11**, 327-335 (2001).

276. Miller, K., Kolk, S.M. & Donoghue, M.J. EphA7-ephrin-A5 signaling in mouse somatosensory cortex: developmental restriction of molecular domains and postnatal maintenance of functional compartments. *J Comp Neurol* **496**, 627-642 (2006).
277. Onwuli, D.O. & Beltran-Alvarez, P. An update on transcriptional and post-translational regulation of brain voltage-gated sodium channels. *Amino Acids* **48**, 641-651 (2016).
278. David, C.J. & Manley, J.L. Alternative pre-mRNA splicing regulation in cancer: pathways and programs unhinged. *Genes Dev* **24**, 2343-2364 (2010).
279. Hashimoto, R., *et al.* Expression analysis of neuregulin-1 in the dorsolateral prefrontal cortex in schizophrenia. *Mol Psychiatry* **9**, 299-307 (2004).
280. Kao, W.T., *et al.* Common genetic variation in Neuregulin 3 (NRG3) influences risk for schizophrenia and impacts NRG3 expression in human brain. *Proc Natl Acad Sci U S A* **107**, 15619-15624 (2010).
281. Law, A.J., *et al.* Neuregulin 1 transcripts are differentially expressed in schizophrenia and regulated by 5' SNPs associated with the disease. *Proc Natl Acad Sci U S A* **103**, 6747-6752 (2006).
282. Tan, W., *et al.* Molecular cloning of a brain-specific, developmentally regulated neuregulin 1 (NRG1) isoform and identification of a functional promoter variant associated with schizophrenia. *J Biol Chem* **282**, 24343-24351 (2007).
283. Weickert, C.S., Tiwari, Y., Schofield, P.R., Mowry, B.J. & Fullerton, J.M. Schizophrenia-associated HapICE haplotype is associated with increased NRG1 type III expression and high nucleotide diversity. *Transl Psychiatry* **2**, e104 (2012).
284. Wong, J., *et al.* Promoter specific alterations of brain-derived neurotrophic factor mRNA in schizophrenia. *Neuroscience* **169**, 1071-1084 (2010).
285. Gibbons, A.S., Thomas, E.A. & Dean, B. Regional and duration of illness differences in the alteration of NCAM-180 mRNA expression within the cortex of subjects with schizophrenia. *Schizophr Res* **112**, 65-71 (2009).
286. Nakata, K., *et al.* DISC1 splice variants are upregulated in schizophrenia and associated with risk polymorphisms. *Proc Natl Acad Sci U S A* **106**, 15873-15878 (2009).
287. Aberg, K., Saetre, P., Jareborg, N. & Jazin, E. Human QKI, a potential regulator of mRNA expression of human oligodendrocyte-related genes involved in schizophrenia. *Proc Natl Acad Sci U S A* **103**, 7482-7487 (2006).
288. Jenkins, A.K., *et al.* Neurexin 1 (NRXN1) splice isoform expression during human neocortical development and aging. *Mol Psychiatry* **21**, 701-706 (2016).
289. Kaalund, S.S., *et al.* Contrasting changes in DRD1 and DRD2 splice variant expression in schizophrenia and affective disorders, and associations with SNPs in postmortem brain. *Mol Psychiatry* **19**, 1258-1266 (2014).
290. Kristiansen, L.V., Beneyto, M., Haroutunian, V. & Meador-Woodruff, J.H. Changes in NMDA receptor subunits and interacting PSD proteins in dorsolateral prefrontal and anterior cingulate cortex indicate abnormal regional expression in schizophrenia. *Mol Psychiatry* **11**, 737-747, 705 (2006).
291. Kunii, Y., *et al.* Revisiting DARPP-32 in postmortem human brain: changes in schizophrenia and bipolar disorder and genetic associations with t-DARPP-32 expression. *Mol Psychiatry* **19**, 192-199 (2014).
292. Sartorius, L.J., *et al.* Expression of a GRM3 splice variant is increased in the dorsolateral prefrontal cortex of individuals carrying a schizophrenia risk SNP. *Neuropsychopharmacology* **33**, 2626-2634 (2008).
293. Zhao, C., *et al.* Two isoforms of GABA(A) receptor beta2 subunit with different electrophysiological properties: Differential expression and genotypical correlations in schizophrenia. *Mol Psychiatry* **11**, 1092-1105 (2006).
294. Norton, N., *et al.* Evidence that interaction between neuregulin 1 and its receptor erbB4 increases susceptibility to schizophrenia. *Am J Med Genet B Neuropsychiatr Genet* **141B**, 96-101 (2006).
295. Pardiñas, A.F., *et al.* Common schizophrenia alleles are enriched in mutation-intolerant genes and maintained by background selection. *bioRxiv* (2016).
296. Taylor, A.M., *et al.* Axonal mRNA in uninjured and regenerating cortical mammalian axons. *J Neurosci* **29**, 4697-4707 (2009).
297. Rocco, B.R., Sweet, R.A., Lewis, D.A. & Fish, K.N. GABA-Synthesizing Enzymes in Calbindin and Calretinin Neurons in Monkey Prefrontal Cortex. *Cereb Cortex* **26**, 2191-2204 (2016).
298. Deng, Y., *et al.* Direct visualization of membrane architecture of myelinating cells in transgenic mice expressing membrane-anchored EGFP. *Genesis* **52**, 341-349 (2014).
299. Hughes, E.G., Kang, S.H., Fukaya, M. & Bergles, D.E. Oligodendrocyte progenitors balance growth with self-repulsion to achieve homeostasis in the adult brain. *Nat Neurosci* **16**, 668-676 (2013).
300. Tamamaki, N., *et al.* Green fluorescent protein expression and colocalization with calretinin, parvalbumin, and somatostatin in the GAD67-GFP knock-in mouse. *J Comp Neurol* **467**, 60-79 (2003).

301. Yun, M.E., Johnson, R.R., Antic, A. & Donoghue, M.J. EphA family gene expression in the developing mouse neocortex: regional patterns reveal intrinsic programs and extrinsic influence. *J Comp Neurol* **456**, 203-216 (2003).
302. Junttila, T.T., *et al.* Identification of patients with transitional cell carcinoma of the bladder overexpressing ErbB2, ErbB3, or specific ErbB4 isoforms: real-time reverse transcription-PCR analysis in estimation of ErbB receptor status from cancer patients. *Clin Cancer Res* **9**, 5346-5357 (2003).
303. Kastin, A.J., Akerstrom, V. & Pan, W. Neuregulin-1-beta1 enters brain and spinal cord by receptor-mediated transport. *J Neurochem* **88**, 965-970 (2004).
304. Rosler, T.W., *et al.* Biodistribution and brain permeability of the extracellular domain of neuregulin-1-beta1. *Neuropharmacology* **61**, 1413-1418 (2011).
305. Wu, L., *et al.* Neuregulin1-beta decreases interleukin-1beta-induced RhoA activation, myosin light chain phosphorylation, and endothelial hyperpermeability. *J Neurochem* **136**, 250-257 (2016).
306. Lok, J., *et al.* Neuregulin-1 effects on endothelial and blood-brain-barrier permeability after experimental injury. *Transl Stroke Res* **3 Suppl 1**, S119-124 (2012).
307. Lok, J., *et al.* Neuregulin-1 signaling in brain endothelial cells. *J Cereb Blood Flow Metab* **29**, 39-43 (2009).
308. Qian, H., *et al.* ErbB4 Preserves Blood-Brain Barrier Integrity via the YAP/PIK3CB Pathway After Subarachnoid Hemorrhage in Rats. *Front Neurosci* **12**, 492 (2018).
309. Bovetti, S., *et al.* Differential expression of neuregulins and their receptors in the olfactory bulb layers of the developing mouse. *Brain Res* **1077**, 37-47 (2006).
310. Birnbaum, R., *et al.* Investigation of the prenatal expression patterns of 108 schizophrenia-associated genetic loci. *Biol Psychiatry* **77**, e43-51 (2015).
311. Birnbaum, R., Jaffe, A.E., Hyde, T.M., Kleinman, J.E. & Weinberger, D.R. Prenatal expression patterns of genes associated with neuropsychiatric disorders. *Am J Psychiatry* **171**, 758-767 (2014).
312. Colantuoni, C., *et al.* Age-related changes in the expression of schizophrenia susceptibility genes in the human prefrontal cortex. *Brain Struct Funct* **213**, 255-271 (2008).
313. Harris, L.W., *et al.* Gene expression in the prefrontal cortex during adolescence: implications for the onset of schizophrenia. *BMC Med Genomics* **2**, 28 (2009).
314. Mighdoll, M.I., Tao, R., Kleinman, J.E. & Hyde, T.M. Myelin, myelin-related disorders, and psychosis. *Schizophr Res* **161**, 85-93 (2015).
315. Takahashi, N., Sakurai, T., Davis, K.L. & Buxbaum, J.D. Linking oligodendrocyte and myelin dysfunction to neurocircuitry abnormalities in schizophrenia. *Prog Neurobiol* **93**, 13-24 (2011).
316. Guillozet-Bongaarts, A.L., *et al.* Altered gene expression in the dorsolateral prefrontal cortex of individuals with schizophrenia. *Mol Psychiatry* **19**, 478-485 (2014).
317. Tao, R., *et al.* GAD1 alternative transcripts and DNA methylation in human prefrontal cortex and hippocampus in brain development, schizophrenia. *Mol Psychiatry* (2017).
318. Fung, S.J., *et al.* Expression of interneuron markers in the dorsolateral prefrontal cortex of the developing human and in schizophrenia. *Am J Psychiatry* **167**, 1479-1488 (2010).
319. Volk, D.W., Sampson, A.R., Zhang, Y., Edelson, J.R. & Lewis, D.A. Cortical GABA markers identify a molecular subtype of psychotic and bipolar disorders. *Psychol Med* **46**, 2501-2512 (2016).
320. Lewis, D.A. Inhibitory neurons in human cortical circuits: substrate for cognitive dysfunction in schizophrenia. *Curr Opin Neurobiol* **26**, 22-26 (2014).
321. Rosen, Z.B., Cheung, S. & Siegelbaum, S.A. Midbrain dopamine neurons bidirectionally regulate CA3-CA1 synaptic drive. *Nat Neurosci* **18**, 1763-1771 (2015).
322. Andersson, R.H., *et al.* Neuregulin and dopamine modulation of hippocampal gamma oscillations is dependent on dopamine D4 receptors. *Proc Natl Acad Sci U S A* **109**, 13118-13123 (2012).
323. Christie, S.B. & De Blas, A.L. GABAergic and glutamatergic axons innervate the axon initial segment and organize GABA(A) receptor clusters of cultured hippocampal pyramidal cells. *J Comp Neurol* **456**, 361-374 (2003).
324. Ozaita, A., Martone, M.E., Ellisman, M.H. & Rudy, B. Differential subcellular localization of the two alternatively spliced isoforms of the Kv3.1 potassium channel subunit in brain. *J Neurophysiol* **88**, 394-408 (2002).
325. Strack, S., Kini, S., Ebner, F.F., Wadzinski, B.E. & Colbran, R.J. Differential cellular and subcellular localization of protein phosphatase 1 isoforms in brain. *J Comp Neurol* **413**, 373-384 (1999).
326. Tushev, G., *et al.* Alternative 3' UTRs Modify the Localization, Regulatory Potential, Stability, and Plasticity of mRNAs in Neuronal Compartments. *Neuron* **98**, 495-511 e496 (2018).

327. Taliaferro, J.M., *et al.* Distal Alternative Last Exons Localize mRNAs to Neural Projections. *Mol Cell* **61**, 821-833 (2016).
328. Ciolli Mattioli, C., *et al.* Alternative 3' UTRs direct localization of functionally diverse protein isoforms in neuronal compartments. *Nucleic Acids Res* **47**, 2560-2573 (2019).
329. Scholz, D., *et al.* Rapid, complete and large-scale generation of post-mitotic neurons from the human LUHMES cell line. *J Neurochem* **119**, 957-971 (2011).
330. Hensch, T.K. & Quinlan, E.M. Critical periods in amblyopia. *Vis Neurosci* **35**, E014 (2018).
331. Bentley, M. & Banker, G. The cellular mechanisms that maintain neuronal polarity. *Nat Rev Neurosci* **17**, 611-622 (2016).
332. Lu, X., Kim-Han, J.S., Harmon, S., Sakiyama-Elbert, S.E. & O'Malley, K.L. The Parkinsonian mimetic, 6-OHDA, impairs axonal transport in dopaminergic axons. *Mol Neurodegener* **9**, 17 (2014).
333. Lipton, D.M., Maeder, C.I. & Shen, K. Rapid Assembly of Presynaptic Materials behind the Growth Cone in Dopaminergic Neurons Is Mediated by Precise Regulation of Axonal Transport. *Cell Rep* **24**, 2709-2722 (2018).
334. Volpicelli-Daley, L.A. Effects of alpha-synuclein on axonal transport. *Neurobiol Dis* **105**, 321-327 (2017).
335. Woodward, W.R. Axonal transport of [3H] GABA and [3H] glutamate in excitatory and inhibitory neurons innervating lobster exoskeletal musculature. *J Neurobiol* **15**, 49-65 (1984).
336. Maday, S., Twelvetrees, A.E., Moughamian, A.J. & Holzbaur, E.L. Axonal transport: cargo-specific mechanisms of motility and regulation. *Neuron* **84**, 292-309 (2014).
337. Guedes-Dias, P., *et al.* Kinesin-3 Responds to Local Microtubule Dynamics to Target Synaptic Cargo Delivery to the Presynapse. *Curr Biol* **29**, 268-282 e268 (2019).
338. Zander, J.F., *et al.* Synaptic and vesicular coexistence of VGLUT and VGAT in selected excitatory and inhibitory synapses. *J Neurosci* **30**, 7634-7645 (2010).
339. Fattorini, G., *et al.* VGLUT1 and VGAT are sorted to the same population of synaptic vesicles in subsets of cortical axon terminals. *J Neurochem* **110**, 1538-1546 (2009).
340. Zhang, S., *et al.* Dopaminergic and glutamatergic microdomains in a subset of rodent mesoaccumbens axons. *Nat Neurosci* **18**, 386-392 (2015).
341. Britt, D.J., Farias, G.G., Guardia, C.M. & Bonifacino, J.S. Mechanisms of Polarized Organelle Distribution in Neurons. *Front Cell Neurosci* **10**, 88 (2016).
342. Gaven, F., Marin, P. & Claeysen, S. Primary culture of mouse dopaminergic neurons. *J Vis Exp*, e51751 (2014).
343. Leviel, V. Dopamine release mediated by the dopamine transporter, facts and consequences. *J Neurochem* **118**, 475-489 (2011).
344. Garcia-Olivares, J., *et al.* Gbetagamma subunit activation promotes dopamine efflux through the dopamine transporter. *Mol Psychiatry* **22**, 1673-1679 (2017).
345. Vaughan, R.A. & Foster, J.D. Mechanisms of dopamine transporter regulation in normal and disease states. *Trends Pharmacol Sci* **34**, 489-496 (2013).
346. Nason, M.W., Jr., Adhikari, A., Bozinoski, M., Gordon, J.A. & Role, L.W. Disrupted activity in the hippocampal-accumbens circuit of type III neuregulin 1 mutant mice. *Neuropsychopharmacology* **36**, 488-496 (2011).
347. Maatta, J.A., *et al.* Proteolytic cleavage and phosphorylation of a tumor-associated ErbB4 isoform promote ligand-independent survival and cancer cell growth. *Mol Biol Cell* **17**, 67-79 (2006).
348. Fujiwara, S., *et al.* The localization of HER4 intracellular domain and expression of its alternately-spliced isoforms have prognostic significance in ER+ HER2- breast cancer. *Oncotarget* **5**, 3919-3930 (2014).
349. Wali, V.B., *et al.* Overexpression of ERBB4 JM-a CYT-1 and CYT-2 isoforms in transgenic mice reveals isoform-specific roles in mammary gland development and carcinogenesis. *Breast Cancer Res* **16**, 501 (2014).
350. Paatero, I., *et al.* CYT-1 isoform of ErbB4 is an independent prognostic factor in serous ovarian cancer and selectively promotes ovarian cancer cell growth in vitro. *Gynecol Oncol* **129**, 179-187 (2013).
351. Bae, J.A., *et al.* Elevated Coexpression of KITENIN and the ErbB4 CYT-2 Isoform Promotes the Transition from Colon Adenoma to Carcinoma Following APC loss. *Clin Cancer Res* **22**, 1284-1294 (2016).
352. Munk, M., *et al.* The HER4 isoform JM-a/CYT2 relates to improved survival in bladder cancer patients but only if the estrogen receptor alpha is not expressed. *Scand J Clin Lab Invest* **73**, 503-513 (2013).
353. Nielsen, T.O., Poulsen, S.S., Journe, F., Ghanem, G. & Sorensen, B.S. HER4 and its cytoplasmic isoforms are associated with progression-free survival of malignant melanoma. *Melanoma Res* **24**, 88-91 (2014).
354. Fregnan, F., *et al.* Eps8 involvement in neuregulin1-ErbB4 mediated migration in the neuronal progenitor cell line ST14A. *Exp Cell Res* **317**, 757-769 (2011).
355. Liu, P., Jenkins, N.A. & Copeland, N.G. A highly efficient recombineering-based method for generating conditional knockout mutations. *Genome Res* **13**, 476-484 (2003).

356. Nagasawa, H., Miyamoto, M. & Fujimoto, M. [Reproductivity in inbred strains of mice and project for their efficient production (author's transl)]. *Jikken Dobutsu* **22**, 119-126 (1973).
357. Erben, L. & Buonanno, A. Detection and Quantification of Multiple RNA Sequences Using Emerging Ultrasensitive Fluorescent In Situ Hybridization Techniques. *Curr Protoc Neurosci*, e63 (2019).
358. Love, M.I., Huber, W. & Anders, S. Moderated estimation of fold change and dispersion for RNA-seq data with DESeq2. *Genome Biol* **15**, 550 (2014).
359. Reimand, J., Kull, M., Peterson, H., Hansen, J. & Vilo, J. g:Profiler--a web-based toolset for functional profiling of gene lists from large-scale experiments. *Nucleic Acids Res* **35**, W193-200 (2007).
360. Friend, D.M., *et al.* Basal Ganglia Dysfunction Contributes to Physical Inactivity in Obesity. *Cell Metab* **25**, 312-321 (2017).
361. Paxinos, G.a.F., K.B.J. *The Mouse Brain in Stereotaxic Coordinates* (Academic Press, San Diego, 2001).
362. Hernandez, L., Stanley, B.G. & Hoebel, B.G. A small, removable microdialysis probe. *Life Sci* **39**, 2629-2637 (1986).
363. Berridge, K.C. & Robinson, T.E. Parsing reward. *Trends Neurosci* **26**, 507-513 (2003).
364. Bartolini, G., Ciceri, G. & Marin, O. Integration of GABAergic interneurons into cortical cell assemblies: lessons from embryos and adults. *Neuron* **79**, 849-864 (2013).
365. Frick, K.M., Burlingame, L.A., Arters, J.A. & Berger-Sweeney, J. Reference memory, anxiety and estrous cyclicity in C57BL/6NIA mice are affected by age and sex. *Neuroscience* **95**, 293-307 (2000).
366. Tucker, L.B., Fu, A.H. & McCabe, J.T. Performance of Male and Female C57BL/6J Mice on Motor and Cognitive Tasks Commonly Used in Pre-Clinical Traumatic Brain Injury Research. *J Neurotrauma* **33**, 880-894 (2016).
367. Xu, C., *et al.* Medial Habenula-Interpeduncular Nucleus Circuit Contributes to Anhedonia-Like Behavior in a Rat Model of Depression. *Front Behav Neurosci* **12**, 238 (2018).
368. Paul, M.J., Indic, P. & Schwartz, W.J. A role for the habenula in the regulation of locomotor activity cycles. *Eur J Neurosci* **34**, 478-488 (2011).
369. Ison, J.R. & Allen, P.D. Pre- but not post-menopausal female CBA/CaJ mice show less prepulse inhibition than male mice of the same age. *Behav Brain Res* **185**, 76-81 (2007).
370. Lehmann, J., Pryce, C.R. & Feldon, J. Sex differences in the acoustic startle response and prepulse inhibition in Wistar rats. *Behav Brain Res* **104**, 113-117 (1999).
371. Kumari, V. Sex differences and hormonal influences in human sensorimotor gating: implications for schizophrenia. *Curr Top Behav Neurosci* **8**, 141-154 (2011).
372. Lin, M., *et al.* Allele-biased expression in differentiating human neurons: implications for neuropsychiatric disorders. *PLoS One* **7**, e44017 (2012).
373. Hedrick, P.W. Heterozygote advantage: the effect of artificial selection in livestock and pets. *J Hered* **106**, 141-154 (2015).
374. Lemmon, M.A. Ligand-induced ErbB receptor dimerization. *Exp Cell Res* **315**, 638-648 (2009).
375. Young, J.W., Powell, S.B., Scott, C.N., Zhou, X. & Geyer, M.A. The effect of reduced dopamine D4 receptor expression in the 5-choice continuous performance task: Separating response inhibition from premature responding. *Behav Brain Res* **222**, 183-192 (2011).
376. Kalueff, A.V., Ren-Patterson, R.F. & Murphy, D.L. The developing use of heterozygous mutant mouse models in brain monoamine transporter research. *Trends Pharmacol Sci* **28**, 122-127 (2007).
377. Ananth, M., Hetelekides, E.M., Hamilton, J. & Thanos, P.K. Dopamine D4 receptor gene expression plays important role in extinction and reinstatement of cocaine-seeking behavior in mice. *Behav Brain Res* **365**, 1-6 (2019).
378. Mendoza, M.C., Er, E.E. & Blenis, J. The Ras-ERK and PI3K-mTOR pathways: cross-talk and compensation. *Trends Biochem Sci* **36**, 320-328 (2011).
379. Jazurek, M., Ciesiolka, A., Starega-Roslan, J., Bilinska, K. & Krzyzosiak, W.J. Identifying proteins that bind to specific RNAs - focus on simple repeat expansion diseases. *Nucleic Acids Res* **44**, 9050-9070 (2016).
380. Jaffe, A.E., *et al.* Developmental and genetic regulation of the human cortex transcriptome illuminate schizophrenia pathogenesis. *Nat Neurosci* **21**, 1117-1125 (2018).
381. Fuccillo, M.V., *et al.* Single-Cell mRNA Profiling Reveals Cell-Type-Specific Expression of Neurexin Isoforms. *Neuron* **87**, 326-340 (2015).
382. Cadwell, C.R., *et al.* Electrophysiological, transcriptomic and morphologic profiling of single neurons using Patch-seq. *Nat Biotechnol* **34**, 199-203 (2016).
383. Zeisel, A., *et al.* Brain structure. Cell types in the mouse cortex and hippocampus revealed by single-cell RNA-seq. *Science* **347**, 1138-1142 (2015).

384. Tiklova, K., *et al.* Single-cell RNA sequencing reveals midbrain dopamine neuron diversity emerging during mouse brain development. *Nat Commun* **10**, 581 (2019).
385. Munoz-Manchado, A.B., *et al.* Diversity of Interneurons in the Dorsal Striatum Revealed by Single-Cell RNA Sequencing and PatchSeq. *Cell Rep* **24**, 2179-2190 e2177 (2018).
386. Liu, C., Kershberg, L., Wang, J., Schneeberger, S. & Kaeser, P.S. Dopamine Secretion Is Mediated by Sparse Active Zone-like Release Sites. *Cell* **172**, 706-718 e715 (2018).
387. Creed, M.C., Ntamati, N.R. & Tan, K.R. VTA GABA neurons modulate specific learning behaviors through the control of dopamine and cholinergic systems. *Front Behav Neurosci* **8**, 8 (2014).
388. Matsuda, S., *et al.* Roles of PI3K/AKT/GSK3 Pathway Involved in Psychiatric Illnesses. *Diseases* **7** (2019).
389. El-Brolosy, M.A. & Stainier, D.Y.R. Genetic compensation: A phenomenon in search of mechanisms. *PLoS Genet* **13**, e1006780 (2017).
390. Haeussler, M., *et al.* Evaluation of off-target and on-target scoring algorithms and integration into the guide RNA selection tool CRISPOR. *Genome Biol* **17**, 148 (2016).